DESIGN AND OPTIMIZATION OF CONDENSER AND CENTRIFUGE UNITS FOR ENHANCEMENT OF A BATCH VACUUM FRYING SYSTEM

A Thesis

by

AKHILESH PANDEY

Submitted to the Office of Graduate Studies of
Texas A&M University
in partial fulfillment of the requirements for the degree of

MASTER OF SCIENCE

December 2009

Major Subject: Biological and Agricultural Engineering

DESIGN AND OPTIMIZATION OF CONDENSER AND CENTRIFUGE UNITS FOR ENHANCEMENT OF A BATCH VACUUM FRYING SYSTEM

A Thesis

by

AKHILESH PANDEY

Submitted to the Office of Graduate Studies of
Texas A&M University
in partial fulfillment of the requirements for the degree of

MASTER OF SCIENCE

Approved by:

Chair of Committee,	Rosana Moreira
Committee Members,	M. Elena Castell-Perez
	Maria Barrufet
Head of Department,	Gerald Riskowski

December 2009

Major Subject: Biological and Agricultural Engineering

ABSTRACT

Design and Optimization of Condenser and Centrifuge Units for Enhancement of a Batch Vacuum Frying System.

(December 2009)

Akhilesh Pandey, B.Tech, Mahatma Gandhi University

Chair of Advisory Committee: Dr. Rosana Moreira

A batch vacuum frying system, which processes fruits and vegetables, includes a frying pan, a surface-condenser, and a vacuum pump. With health and safety issues in mind, this research focused on developing a modified surface-condenser to prevent cavitation of the vacuum pump. The final oil-content was reduced by centrifugal de-oiling of the product under vacuum, which make the product healthier than what is currently available.

The de-oiling mechanism consists of a centrifuge with a motor attached to the basket shaft, rotating up to 750 rpm (63 g units). The condenser consists of a (counter-flow) spiral-coil heat exchanger (SHE) connected to a refrigeration system that uses R404a refrigerant.

De-oiling for 40 s at 300 and 750 RPM removed up to 67% and 72% of the chip's surface oil, respectively. At 750 RPM for 10 s, 40 s, and 60 s the oil-content was reduced by 38%, 44%, and 51%, respectively.

The convective heat transfer coefficient (h) of the frying oil was determined at 120°C and 140°C using the lumped capacitance method. The h-values were 217±13 W/m^{2}K (120°C) and 258±37 W/m^{2}K (140°C) using a copper-ball thermocouple. The h-values increased to 3.6 times during the boiling period.

COMSOL™ Multiphysics was used to model the heat transfer in the vacuum fryer pan. Based on the simulation results, a 1.5 cm thick insulation material was installed in the fryer to reduce the energy losses.

The refrigeration system operates at T_{evap} = -26°C and T_{cond} = 50°C with 26°C sub-cooling. Sensitivity analysis showed that the system Coefficient of Performance (COP) was about 3.87 at these conditions and compressor power requirement (CPR) was 74 W (85% efficiency) when frying 30 g of potatoes slices. The best results were obtained at T_{evap} = -10°C and T_{cond} = 40°C with 26°C sub-cooling and superheat of 5°C. The predicted COP was 4 and the CPR 70 W.

The ice-formation on coils reduced the condensation rate. Reducing the refrigerant temperature to -10°C (from -26°C) reduced the condensation rate by 30%.

These results show a more effective vacuum frying system for high-quality fruits and vegetables than the system previously used.

DEDICATION

I dedicate this thesis to my Mother and Father.

ACKNOWLEDGEMENTS

From the formative stages of this thesis, to the final draft, I owe an immense debt of gratitude to my chair, Dr. Rosana Moreira, and my committee members, Dr. Elena Castell and Dr. Maria Barrufet, for their guidance and support throughout the course of this research.

Thanks also go to my friends and the department faculty and staff for making my time at Texas A&M University a great experience. I also want to extend my gratitude to the Agricultural Engineering shop facility, especially Richard, for helping me out in the fabrication work. I would also like to thank Alex, Carla, Carmen, Ezekiel, Isin, Jongsoon, Mauricio, Paulo, Taehoon and Yolanda for being such good friends as well as colleagues and for always being available for helping me in my doubts.

Finally, thanks to my mother and father for their encouragement, my brother, Nikhil, for his help in computer programming and my girl friend, Pranalika, for bolstering me in difficult times of my research.

NOMENCLATURE

2-D	Two dimensional
3-D	Three dimensional
A	Area, m^2
atm	Atmospheric pressure
BMA	Braunschweigische maschinenbauanstalt AG (BMA AG) in Braunschweig, Germany. BMA AG
℃	Degree celsius
C_p	Specific heat, [kJ/kgK]
db	Dry basis, [% d.b]
FEM	Finite element method
GUI	Graphic user interface
kg	Kilo gram
kPa	Kilo pascal
LRVP	Liquid ring vacuum pump
m	Meter
MC	Moisture content, [% w.b.]
min	Minutes
MPa	Mega pascal
N	Newton
ø	Diameter, m

OC	Oil content
P	Pressure, kPa
P&ID	Process and instrumentation diagram
psi	Pounds per square inch
rad	Radian
Rev	Revolutions
RPM	Revolutions per minute
t	Time, s
$T_{\text{ball-probe}}$	Ball probe temperature, ^{o}C
$T_{\text{comp, cond}}$	Temperature between compressor and condenser, ^{o}C
$T_{\text{cond, cap}}$	Temperature between air cooled condenser and capillary tube, ^{o}C
$T_{\text{cond-in}}$	Condenser inlet temperature, ^{o}C
$T_{\text{cond-out}}$	Condenser outlet temperature, ^{o}C
T_{pc}	Temperature at the center of potato chips, ^{o}C
$T_{\text{pre-cond}}$	Temperature at pre-condenser entrance, ^{o}C
$T_{\text{ref, in}}$	Refrigerant inlet temperature, ^{o}C
$T_{\text{ref, out}}$	Refrigerant outlet temperature, ^{o}C
$T_{\text{steam-hose}}$	Temperature in vacuum hose between condenser and vacuum fryer pan, ^{o}C
T_{evap}	Temperature inside evaporator at the refrigerant coil entrance, ^{o}C
VDC	DC voltage
VFS	Vacuum fryer simulator

W	Watt
wb	Wet basis
WIPO	World Intellectual Property Organization, Geneva, Switzerland

TABLE OF CONTENTS

Page

CHAPTER Page

CHAPTER Page

Page

LIST OF FIGURES

FIGURE Page

FIGURE Page

FIGURE Page

FIGURE Page

FIGURE Page

FIGURE Page

LIST OF TABLES

TABLE Page

CHAPTER I

INTRODUCTION

Deep-fat frying is one of the oldest methods of food preparation. It is defined as a process of cooking and drying through contact with hot oil, and it involves simultaneous heat and mass transfer. In deep-fat frying of foods, the temperature of the heated oil, the frying time, and the fryer type (batch or continuous; atmospheric, vacuum, or high-pressure) are factors that affect the process. The chemical composition of the frying oils, the physical and physicochemical changes of the food, and the presence of additive and contaminants also influence the frying process (Moreira et al., 1999).

Frying technology is important to many sectors of the food industry: suppliers of oils and ingredients, food service (hotel, restaurant, and institution) operators, food industries (snack, fully fried, and par-fried foods), and manufacturers of frying equipment. The amount of food fried and oils used at both the industrial and commercial levels are vast (Moreira et al., 1999).

Deep-fat frying of foods usually is carried out under atmospheric conditions at temperatures ranging from 165^{o}C to 190ºC. If the process is not well designed and operated, excessive darkening or scorching of the product can occur, even before the product is completely cooked. Additionally, continued use of the frying oil can produce decomposition products, which may produce adverse health effects.

Today, consumers are looking for healthy products with good taste. The food industry has produced fried products using non hydrogenated oil, non saturated fat, and

---

This thesis follows the style of *Journal of Food Engineering*.

no trans-fats. Some of these new products (sweet-potato chips, apple chips, blue potato chips) are fried under vacuum yielding less oil absorption (so they taste less greasy) with higher retention of their natural color and flavors.

Vacuum frying is defined as the frying process that is carried out under pressures well below atmospheric levels, preferably below 50 Torr (6.65 kPa). In the low pressure, the boiling point of the water in the foods is lowered. Therefore, vacuum frying can operate at much lower temperatures (< 100^{o}C) than atmospheric fryers and still produce crispy, low oil, and colorful products. A couple of companies in Asia (Japan, Thailand, Taiwan) have developed such a system for the process of fruits (apples, pineapples, grapes, bananas, guavas, mangoes, peaches, etc.) and vegetables (sweet potatoes, potatoes, pumpkins, carrots, etc.) into chips and fried fish and shell-fish (octopus and cattle fish).

A majority of commercial frying systems are batch types with capacity from 50 to 100 kg/hr of potato chips. The concept of continuous vacuum frying was developed by Florigo (H&H Industry Systems BMA, The Netherlands) in the early 1970s to produce high quality french fries. Today, BMA automatic continuous vacuum fryers are used mainly to produce fruit chips and very delicate snack products (Moreira et al., 1999). The capacity of this unit is about 350 kg/hr of potato chips.

Food process engineering is a quantitative science that consists of design and optimization of processes. A process may be thought of as a sequence of operations that takes place in one or more sets of equipment, giving rise to a series of chemical,

biological, and physical changes in the feed material and resulting in a useful and desirable product (Smith, 2002).

Food engineering begins from a stage where a new food product is developed through specialized processing operations; all currently sold food products have been developed using multiple unit operations at a smaller laboratory scale. After the product has been approved for mass production in the food industry, a mass production scale-up procedure is prepared. The scale-up procedure includes numerous unit operations of process engineering and accounts for energy and mass balances. These unit operations are carried out by specifically designed prototypes or enhancements in current machines, which should meet the processing requirements of the product.

One of the main characteristics of vacuum frying units is the de-oiling mechanism. It is used to de-oil the product before it is removed from the vacuum so the surface oil is not absorbed by the product during the pressurization process. De-oiling mechanisms are generally centrifuges, which are installed in a special vacuum dome attached to the vacuum fryer (BMV, Woerden, The Netherlands). Another important piece of equipment in a vacuum frying system is the condensing unit, which is used to condense the water vapor from the product before it reaches the vacuum pump, which could damage it.

Therefore, this research primarily focuses on the design of an efficient condenser and a centrifuge unit for de-oiling the product (in this case potato chips) in a lab-scale vacuum frying system. The specific objectives of this research were the following:

1. To build and install a centrifuge unit to de-oil the fried product (potato chips) under vacuum conditions
2. To build and install a refrigerated condensing unit
3. To install a data acquisition system to collect experimental data (oil temperature, product temperature, etc.) and control the condensing and centrifuge units
4. To simulate the heat transfer in the frying system using COMSOL™ software
5. To simulate the condensing unit using FRIGOSIM™ software
6. To perform sensitivity analysis

The lab-scale vacuum fryer was tested with potato chips fried under different times, temperatures, and batch sizes. Thermocouples were used to measure the product and oil temperatures, as well as the temperatures around the condensing unit. The de-oiling mechanism was tested at different times and rotation speeds. The amount of water vapor condensed by the refrigerant unit was measured to evaluate the system efficiency. Temperatures inside the potato chips were monitored during the process to model the heat and mass transfer mechanisms involved in vacuum frying. The convective heat transfer coefficient was calculated using the lumped-capacitance approach. Finally, the product moisture content and oil content were measured for different temperatures and product thickness, and for all the conditions described above.

CHAPTER II

LITERATURE REVIEW

A processed food product undergoes numerous unit operations depending on the final desired product. Among the available operations of processing food products, deep-fat frying (such as fruit and vegetable-based snacks) has been very successful in the consumer market. The most popular fried snack, the potato chips has always been the top selling product in the snack category with $6,393.7 million worth of sales for year 2007 (Gupta, 2009). George Crum was the first person to serve potato crisps in his restaurant in Saratoga, New York. These chips gained popularity among the locals and were popularly known as Saratoga chips. Gradually these chips became an integral part of everyday restaurant menus around the world (Jones and Obrien, 1991).

The first potato chips came into existence while creating thin slices for french fries in 1854. These thin slices became extremely popular as a side dish among people and still is a must-have in any restaurant as it blends well with different fast foods (burgers, sandwiches, quesadillas, etc.). During frying of potato chips, the right frying temperature, accurate frying time and final texture are of the highest importance (Moreira et al., 1999). For decades research has been carried out to produce the perfectly crisp potato chip. Several new techniques of frying have been introduced to provide better and more uniform quality. Deep-fat frying as an independent business began in the late 1890s mainly for manufacturing potato chips (Banks, 2007).

2.1. Deep-fat frying

Deep-fat frying is defined as the process of cooking and dehydration of food in a hot oil medium. While frying potato slices (with 70 to 75% initial moisture content) (USDA/ARS, 2007) in wet conditions, oil uptake increases up to 35 to 40% wet basis (w.b.) and moisture content reduces to 1 to 2% w.b. Several types of equipment are used to fry potato chips, categorized under two basic methods: continuous frying or batch frying. These two frying methods are differentiated based on five factors (1) technique of loading and unloading chips in the oil; (2) capacity of the vessel and product output; (3) frying time/product throughput time; (4) maximum frying temperature; and (5) heat source. The other categorization of fryers is based on the technique involved for frying potato chips.

Deep-fat frying can be accomplished under three different pressure conditions: atmospheric pressure, low pressure (vacuum), and high pressure. Under atmospheric (open) frying, the temperature of the oil is usually between 160^{o}C and 200^{o}C (Moreira et al., 1999). Vacuum frying is carried out at pressures below atmospheric levels, preferably below 6.65 kPa. When the pressure is lowered, the boiling point of the oil and the moisture of the foods are lowered as well (Garayo and Moreira, 2002). Reducing the boiling point of oil gives way to the following advantages: (1) reducing the oil content of the product; (2) preserving color and flavor; and (3) maintaining good oil quality with less degradation (Shyu and Hwang, 2001). This process of vacuum frying can be a feasible alternative method to produce chips with lower oil content and high quality color and texture (Garayo and Moreira, 2002).

Figure 2-1 displays the use of different deep-fat fryers in the commercial food industry (restaurants), research and development (laboratory), and for home use.

Deep-fat fryers are designed to accommodate application and the type of food product to be fried. Richard et al., (1993) recommended designing "a fryer that fries just one product with full efficiency rather than to design a fryer that fries multiple products with less efficiency". Therefore, a fryer or similar food processing equipment is always designed with product in mind. All fryers follow one basic design, a vat or vessel filled with oil in which the product is submerged for frying. The heat source can be gas, electricity, or fuel oil with infrared assisted designs (Moreira et al., 1999). Infrared assisted designs are relatively new and still under developmental phase. The product is generally lowered inside a basket or conveyed on a moving belt in batch and continuous fryers respectively. All deep-fat fryers can be categorized as batch or continuous type.

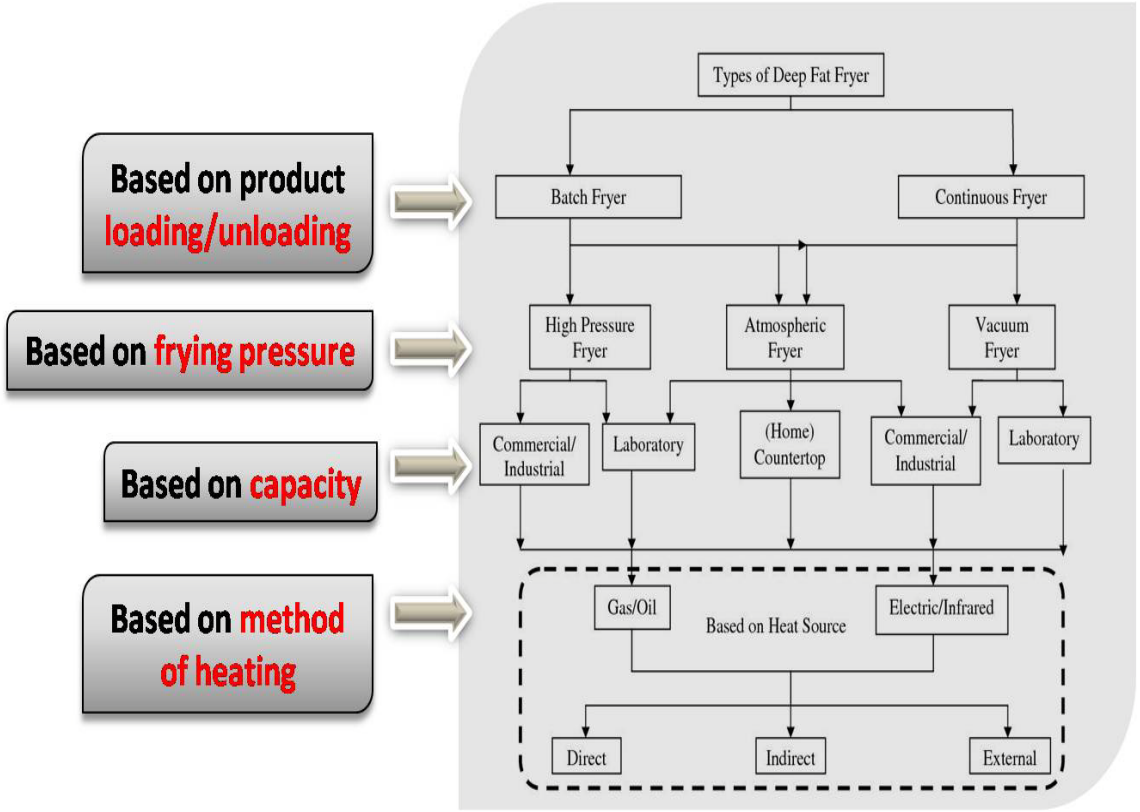

Figure 2-1. Types of deep-fat fryers.

2.2. Types of deep-fat fryers

2.2.1. Batch fryers

Batch fryers, as the name implies, fry one batch of product at a time. They are of different types: countertops with capacity of 8 to 11 liters or high capacity/efficiency fryers with capacity of 17 to 28 liters. Countertops are generally used in homes, while high efficiency batch fryers are employed in commercial (McDonalds, KFC, etc.) food services as well as industries (Frito Lay, Pringles, etc.). Application of a batch fryer is limited to frying small loads of product. Since product capacity is limited, the use of batch fryers is limited in heavy industrial frying use.

All types of fryers such as vacuum batch fryers, pressure batch fryers, and atmospheric (open) batch fryers are available for batch frying. Pressure batch fryers, which can be electric or gas fired, are used mainly in frying higher density products such as chicken pieces and require shorter frying time. Pressure also enhances uniformity in color and moisture distribution in the product. The capacity of the pressure batch fryers ranges from 11 to 25 liters. The operating pressure is from 9 to14 psi for some fryers, and 28 to 32 psi in others (Moreira et al., 1999).

2.2.2. Continuous fryers

The first continuous fryer (atmosphere) was made by Mcbeth Freeman of J.D. Ferry Co. to produce potato chips (Banks, 2007). The continuous frying equipment is widely adapted for industrial use in mass production of different type of products. The capacity may vary from 250 to 25,000 kg/hour. The continuous fryers have multi-zone frying sections/divisions. The raw product is carried from one section to other with the help of conveyor belts. These conveyor belts are designed such that the moving speed of the belt can be set for different frying times and products. Often a submerged conveyor follows the product conveyor system to hold the product being fried to move along inside the long vat of continuous fryers.

A continuous vacuum fryer is rarely used in industrial applications, but is catching on around the world for economical reasons. Continuous fryers are designed for methods used to fry products such as surface fried (dough nuts), immersion fried (pellets), partially floating (chips), and non-floating (french fries) (Richard et al., 1993).

2.3. Types of heat source

In a direct heating system, the heat source can be a fire-in-tube heater in which hot fuel gas flows in the tubes while transferring heat to oil. The process of indirect heating occurs when oil is heated away from main frying vessel and a continuous flow is maintained for large fryers. A heat exchanger similar to a direct heating system provides heat to the oil pumped into the fryer. This enhances uniform distribution of heated oil and lessens the number of cold zones in the fryer. External heat sources employ heat exchangers in which oil is pumped inside the tubes and an external source of heat such as gas, fuel oil or electricity provides heating (Moreira et al., 1999).

Infrared lamps are used to assist in the process of frying by heating the product through radiant energy. According to Oztopa et al. (2007), use of microwaves during frying enhances the moisture removal rate of potato chips. They heated oil in the microwave to bring it to the frying temperature and fried chips in that oil, focusing on the optimal frying setting for three different power levels (400 W, 550 W, and 700 W) and oils (hazelnut, sunflower, and corn oil). The results were best at 550 W of microwave power for 2.5 min of frying time.

Microwaves have also been used efficiently as a pre-frying treatment. Gamble and Rice (1987) used microwaves, hot air, and freeze drying as pre-fry drying techniques. The results successfully showed the reduction in oil content, lighter color, and shorter frying time when using microwave or hot air drying as a pre frying treatment in potato chips.

2.4. Vacuum fryers

Vacuum frying is carried out at pressures below atmospheric level, usually less than 6.65 kPa or 50 Torr. Vacuum fryers require lower oil temperature ($T_{oil} < 140^{o}C$) for frying as the boiling point of water vapor is lowered (Garayo and Moreira, 2002).

Potato chips are not the only products being used for vacuum frying; fruits and vegetables such as carrots, green beans, mangoes, squash, taro, sweet potatoes, red sweet potatoes, and radishes are also vacuum fried on a large scale in the food industry (Da Silva and Moreira, 2008). Since the frying temperature is well below $160^{o}C$, the product quality is retained when fried under a vacuum. Conventional deep-fat frying may cause excessive darkening of the product. Traditional frying also causes higher acrylamide (a carcinogenic substance/polymer) formation adversely affecting the health of people consuming these products (Granda, 2005). To avoid harm and to maintain product quality, vacuum frying is the most popular means for frying fruits and vegetables.

Vacuum fryers are available for batch and continuous applications. The very first continuous vacuum fryer was developed in Europe by Florigo Inc., The Netherland. It was developed in the 1970s for producing high quality french fries. Today, the capacity of a vacuum fryer ranges from 350 kg/hour to 1500 kg/hour. It is mainly used for non blanched products (BMA, The Netherland).

Vacuum fryers have proven efficacy for high quality, less oil absorption and maintaining natural color and flavor. Therefore, they are widely used in processing fruits and vegetables and in the delicate extruded snacks market (Moreira et al., 1999).

2.5. Vapor condensation

Vapor condensation is the most important unit operation required to prevent steam from reaching the vacuum pump by condensing it. The condenser is a device used to change the phase of vapor into liquid. Many industries require a condenser for a variety of operations in chemical and petroleum processing, including distillation, refrigeration and power generation (Serth, 2007).

2.5.1. Modes of condensation

According to Hewitt et al. (1994), condensation can occur in multiple modes, such as:

1. *Film-wise condensation* – In this type of condensation a thin, continuous liquid film forms on a flat plate surface. This type of condensation also occurs in tubes on either side and is the most common consideration for solving any condensation problem.
2. *Homogeneous condensation* – The condensation that occurs in bulk with immediate pressure or temperature changes is called *homogeneous condensation*. The reverse phenomenon takes place in a cavitation problem related to vacuum pump impeller damage. This liquid evaporates rapidly and explosively with a sudden change in the pressure at the outlet of the vacuum pumps.
3. *Drop-wise condensation* – During drop-wise condensation, the drops are formed by condensate vapors where the condensing surface has poor wetting characteristics. The collection of small drops tends to grow bigger on the surface

and starts to move in the direction of gravity. The droplet contact angle and surface roughness play the most important roles in drop-wise condensation.

4. *Immiscible liquid condensation* – When a mixture of vapor condenses, two separate condensate phases are formed in a process called *immiscible liquid condensation*. The heat transfer characteristics of these condensate fluids may vary, and the design of the condenser requires special consideration for handling condensates.

2.5.2. Vapor condensers

Condensers are basically heat exchangers that are designed to remove heat from the gaseous feed to change its phase from vapor to liquid or solid. Condensers are used in the final stages of evaporation systems and mainly in vacuum producing systems (Minton, 1986). There are two types of condensers: direct-contact condensers and surface type condensers.

2.5.2.1. Direct-contact vapor condensers

In these units the vapor condenses when directly in contact with the cooling medium. This eliminates the requirements for heat transfer surfaces. The condensate may be lost as it is mixed with the cooling medium. Cold water is mainly used in such condensers, although condensate vapors when mixed within the cooling medium prohibits its use in vacuum process systems. Many direct-contact condensers also use spray nozzles to mix the inlet vapor feed with coolant. This provides rapid heat transfer between feed and coolant. Direct-contact condensers are mainly used in the last effect of

a multi-stage steam generation system. This limits their ability to be used in sophisticated processes of volatile compound (VOC) distillation/separation (Pita, 1984).

2.5.2.2. Surface condensers

Surface condensers have a suitable heat transfer surface to condense vapors by transferring heat by conduction. A coolant at low temperatures flows on one side and hot vapors on the other. Unlike the direct-contact condensers, the cooling fluid and condensate remain totally separate in surface condensers. This also allows use of surface condensers in cryogenics and very low temperature applications.

The surface condensers are of many types depending on the heat exchanger design (Minton, 1986). They are: shell and tube, plate type, shell and coil, air-cooled, and evaporative cooled (refrigerated condenser).

All these types can be a horizontal system or a vertical system, depending upon the application and usage of the condenser. Also, the feed can flow either from the shell side or the tube side of the condenser. The design considerations for condensers vary according to the type of applications. The main configuration is based upon tube side flow and shell side flow. Hot fluids or coolant may flow through the tube side.

In evaporative cooled (refrigerated condenser) design, a refrigeration condensing unit provides the necessary cold fluid in the condenser. It can be divided into three types: low temperature condensing unit, medium temperature condensing unit, and high temperature condensing unit.

Condensing steam at vacuum pressure around 1.33 kPa requires reduction in the steam's temperature below its saturation or dew point temperature. The most suitable option is a low temperature condensing unit that reaches temperatures for this purpose.

2.6. De-oiling

The oil absorption mechanism is a complex process. According to Moreira et al. (1997), oil absorption is a surface phenomenon that happens as the product is removed from the fryer (atmospheric) due to temperature difference between the product and ambient temperatures (T_{pc} and T_{amb} respectively). The change in temperature causes an increase in capillary pressure in the product pores, which causes the oil to flow into the open pore spaces.

In the case of vacuum frying, most of the oil absorption takes place during the depressurization (vacuum to atmospheric) step. Therefore, this type of frying system requires a mechanism to remove the oil from the product's surface before the fryer is pressurized.

One such mechanism is the use of a centrifuge that rotates at a certain velocity that helps remove most of the products surface oil. De-oiling is also carried out with methods other than centrifugation. A research patent for (atmospheric frying) (Baker et al. 1997), describes a de-oiling apparatus that puts tortilla chips in direct contact with super-heated steam at temperatures ranging from about 149°C to 171°C, with impinging velocities between about 488 m/min and 670 m/min in a controlled atmospheric condition of reduced oxygen to remove oil from the potato chips. The processed chips have oil content below 25% w.b. and moisture content of about 3.5% w.b. The processed

chips are post dried to reduce the moisture content from 3.5% to less than 2% w.b. This process works on tortilla chips and potato chips (Caixeta et al., 2002) with similar results and methodology.

In commercial oil removal techniques for potato chips, vertical placement of potato chips is ensured by certain mechanical means. During centrifugation, the centrifugal force acts perpendicular to the surface of the chips and separates the oil directly from the porous surface. This technique is an improvement over horizontal or lateral placement of chips being fried. In laterally placed chips, the oil moves towards one side of the product instead of completely leaving the surface of the chips.

Other methods of reducing oil content in fried chips include pre-frying operations such as blanching, pre-drying, and dehydration and coating of the surface of the product to ensure less oil content in the final product. But these methods indirectly affect the final quality of the food product. In the blanching method, the chips are treated in water solutions of calcium chloride or citric acid (28% and 15% oil content reduction) (Rimac-Brncic et al., 2004). Garcia et al., (2002) produced potato chips with 40% reduction in oil uptake by immersing and coating the chips in methylcellulose and hydroxypropylmethylcellulose before frying.

Marisol et al. (2007) studied the effect of oil absorption and distribution with different pre-treatments and oil temperatures during atmospheric deep-fat frying. They concluded that in frying potato slices at 180^{o}C, 62% of oil remained on the surface of the chips without entering the microstructure. For shorter frying times of potato slices, the oil was entrapped in intercellular spaces, while for longer frying times, it reached the

crust and cell microstructure. Many other studies concluded that oil distribution can also be located in the interior voids, and high amounts of oil may be entrapped in blisters on the surface of the potato chips during frying (Gamble and Rice, 1987).

The de-oiling process becomes more important during vacuum frying because of the pressurization process. The chips do have increased oil content following vacuum frying and depressurization because of the rapid change in pressure (vacuum to atmospheric). According to Da Silva, Moreira and Gomes (2009), de-oiling is one of the most important unit operation steps in vacuum deep-fat frying to ensure best quality products.

2.6.1. Centrifugal separation

Centrifugal separation of an immiscible liquid/solid, liquid/liquid, or solid/solid phase depends upon the effect of gravity on the product/media. Every material has its own specific gravity, which on application of rotational force (centrifugal force outwards) may part depending on its material specific gravity.

Therefore, the net force on the oil at the product surface is a balance between gravity and centrifugal force. The centrifugal force increases with increase in angular momentum or the rotational speed. The distance from the rotational axis plays a very important role in the development of the gravitational forces. When the centrifugal force becomes higher than the gravitational force, the component with different specific gravity separates from the media (Earle and Earle, 2004). The axis for placement of a product (vertical/horizontal) is an important criterion for oil removal efficiency.

The centrifugal force on a particle rotating in circular motion is:

$$F_c = m \times r \times \omega^2 \quad [2\text{-}1]$$

where, F_c is the centrifugal force [N] acting on the particle to maintain it in the circular path, r is the radius [m] of the path, m is the mass [kg] of the particle, and ω is the angular velocity [rad/s] of the particle. Since $\omega = v/r$, where v is the tangential velocity [m/s] of the particle, Equation 2-1 can be written as:

$$F_c = \frac{m \times v^2}{r} \quad [2\text{-}2]$$

Rotational speeds are normally expressed in revolutions per minute, so that Equation 2-1 can also be written, as $\omega = 2\pi N/60$:

$$F_c = m \times r \times \left(\frac{2\pi N}{60} \right)^2 \quad [2\text{-}3]$$

$$F_c = 0.011 \times m \times r \times N^2 \quad [2\text{-}4]$$

where N is the rotational speed in [rev/min].

Equation 2-4 is compared with the gravitational force, and $F_c = F_g$, then

$$F_g = m \times g \quad [2\text{-}5]$$

$$m \times g = 0.011 \times m \times r \times N^2 \quad [2\text{-}6]$$

$$g = 0.011 \times r \times N^2 \quad [2\text{-}7]$$

The centrifugal force is often expressed for comparative purposes as so many "g" (Earle and Earle, 2004).

Cooking oil has very low specific gravity in comparison to the chips and remains mostly on the surface after frying. The freshly fried chips are at high temperature and pressure; therefore, oil is not absorbed inside them until the vacuum fryer vessel is depressurized and the chips cool down (Moreira et al., 1999). A method using a de-oiling centrifuge relies on surface oil.

2.7. Computer software and data acquisition for frying process

Many of the past research studies effectively show the use of data acquisition and monitoring internal processes during frying. The latest research studies also include finite element methods (FEM) for design and optimization of various internal processes and equipment (Banga et al., 1993).

Modeling the frying process and determining the heat transfer coefficient depend greatly upon the temperature profile of the process. Farkas et al. (1996) used thermocouples for determining temperature profiles during frying for infinite slabs (restructured potato slices). These temperature profiles were used in development of predictive equations. Yildiza et al. (2007) successfully determined effective heat and mass transfer coefficients for frying french fries at 150^{o}C, 170^{o}C and 190^{o}C (atmospheric fryer). According to their research the heat transfer coefficient decreases with increase in oil temperature, and the mass transfer coefficient increases with an increase in temperature.

Use of FEM for process modeling using the FEMLAB/COMSOL™ multi-physics tool had been a great breakthrough in understanding coupled heat and mass transfer variables in a process. The FEM plays an important role in the optimization of

heat transfer inside the vacuum fryer vessel. Halder and Datta (2008) successfully used COMSOL^{TM} as a modeling tool for development of a program for predicting food safety and quality.

A previous COMSOL^{TM} based model developed by Halder et al. (2006) consisted of development of a multi phase porous media model that predicts various quality parameters such as oil absorption, crust formation, phase equilibrium conditions during cooking process methods such as frying, baking and similar dehydration applications.

Different types of software are available for modeling plants such as refrigeration and thermal process facilities. These software have in-built components such as heat exchangers, compressors, pumps, and fluid libraries that can be readily used for simulation of a large and small systems.

Similar research studies have been carried out in the field of food process optimization and design for modeling heat transfer in porous media and design of food equipment such as heat exchangers and extruders. Therefore, use of data acquisition techniques, computer modeling, and simulation holds tremendous potential for improvement and implementation of pilot scale studies of food processes.

CHAPTER III

MATERIALS AND METHODS

3.1. Laboratory vacuum fryer system setup - original system

The laboratory vacuum fryer (Figure 3-1) located at the food engineering lab, Department of Biological and Agricultural Engineering, Texas A&M University, was used in this study. The vacuum fryer consists of an (a) aluminum vessel (kettle) with a lid that can be closed to form vacuum inside it. This pan has an induction heating element at the bottom to heat the oil at suitable temperatures monitored by a thermostat. The maximum temperature that the ring shaped (ø = 0.0889 m) induction heating filament can generate is 140^{o}C for an oil capacity of 6.5 liters.

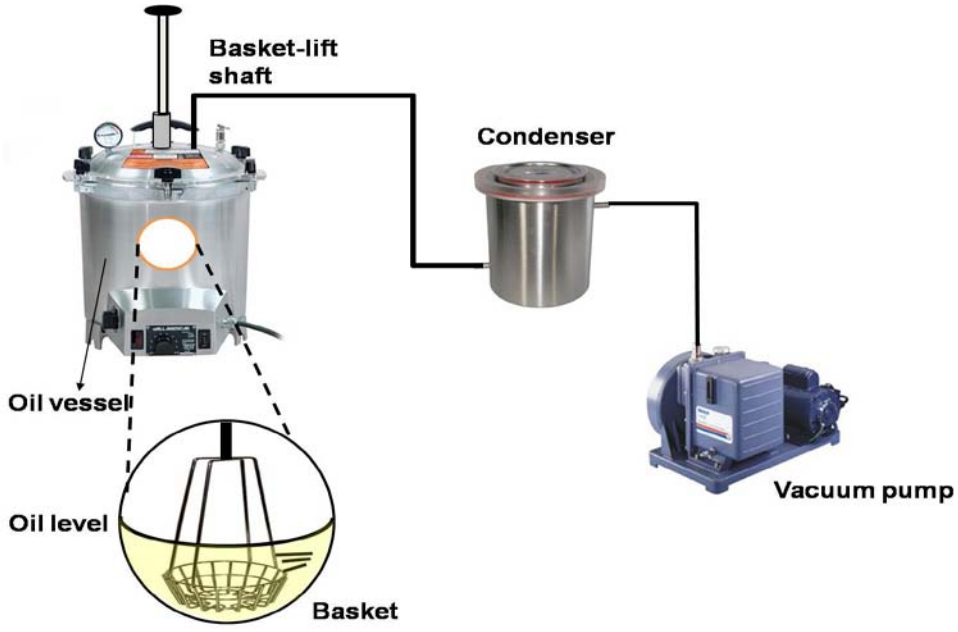

Figure 3-1. Schematic of a vacuum frying system.

A motion feed-through shaft moves to and fro for immersing the fryer basket in the oil without loss of vacuum. The shaft moves on a set of pressure gaskets made of Buna-N.

The main property of the Buna-N design is to form a tight seal against the inner walls of the washers and the shaft (Kurt J. Lesker, Clairton, PA); (b) a vacuum pump attached to a (c) condenser, where vapor from the chips completely condenses to liquid before it reaches the vacuum pump. A liquid ring vacuum pump (LRVP) (Model 1402 Welch Scientific Co., Skokie, Illinois) was used to provide ultra-high vacuum gauge pressure of 1.33 kPa in the vacuum frying system (see specifications in Appendix D).

The condenser is a concentric cylinder steam heat exchanger/trap (dry ice/liquid nitrogen trap, Welch Scientific Co., Skokie, Illinois). The center well has a capacity of 2.8 liters, which is filled with a 50/50 ratio of dry ice and ethanol (95%). The slurry is formed at around -78.6^{o}C, which is sufficient to condense any water vapor entering the condenser and trap it from going to the vacuum pump.

A quick disconnect valve (QC4-B400, Swagelok, Solon, OH) is used to disconnect the vacuum pump from the condenser when not in use. Figure 3-2 shows the aluminum vessel/pan used for vacuum frying.

Figure 3-2. Aluminum vacuum frying pan.

3.2. Modified vacuum fryer system setup - modified system

The main objective was to automate the whole vacuum frying process, making it more efficient and user friendly by installation of new components. Thus, some basic modifications were made to the vacuum frying system setup described before (Figure 3-1), including: (Figures 3-3 and 3-4):

a. The condenser unit.

b. The de-oiler unit.

c. The control unit

d. The data acquisition system.

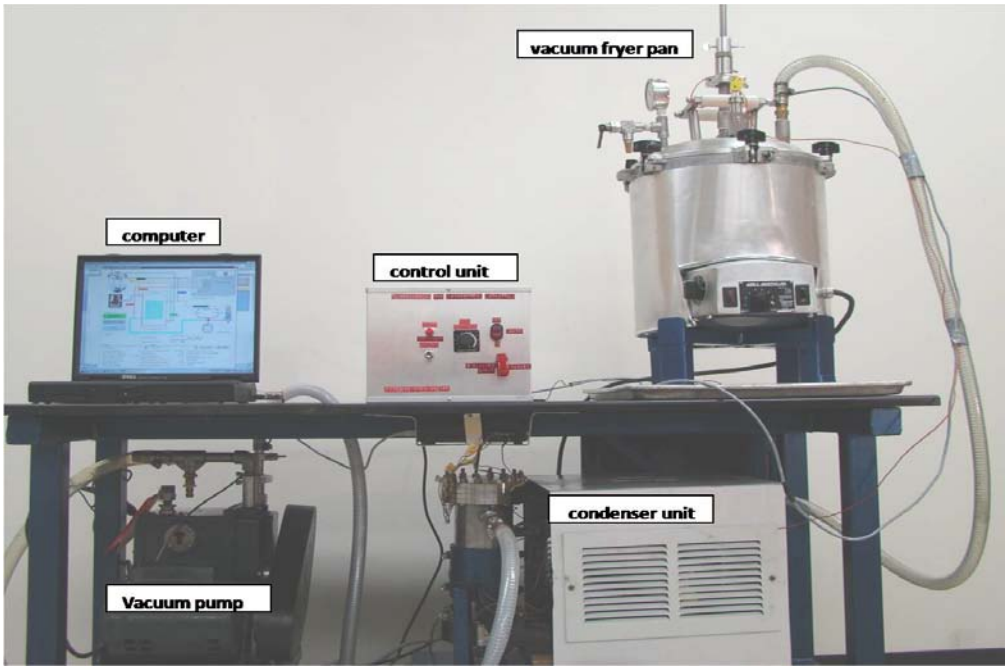

Figure 3-3. Modified vacuum frying system setup.

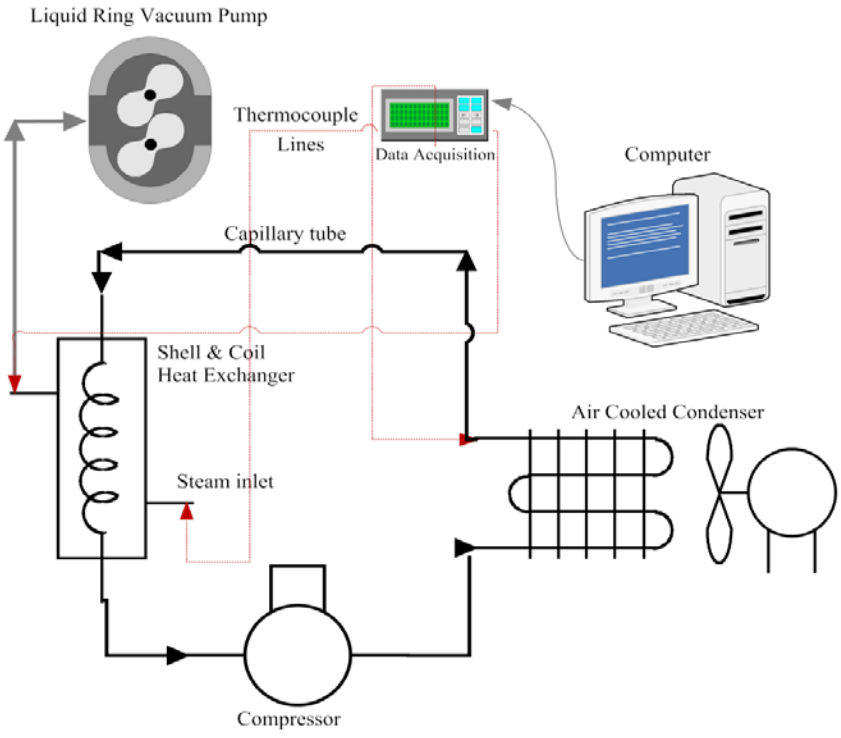

Figure 3-4. Schematic of modified vacuum frying system setup.

3.2.1. Condenser unit

A condenser unit/steam trap was installed between the vacuum pump and the fryer vessel to prevent water vapor from entering the vacuum pump mechanism.

The modified system used the principle of condensation with the help of a refrigerated heat exchanger between refrigerant and steam. This modified condenser setup uses a shell-and-coil-type heat exchanger (Figure 3-5). The steam flows from the shell side and refrigerant R-404A flows from the coil or tube side of the heat exchanger (Figure 3-6). The heat from the hot steam is transferred to the refrigerant rapidly with a phase change from the saturated vapor phase to the liquid phase. The purpose of the introduction of a refrigerated condensing unit to condense process water vapor is to allow automated control of the vacuum frying process.

This research study includes a shell and coil type heat exchanger for condensing water vapors from the vacuum fryer. The shell and coil type design (Figure 3-5) provides larger surface area in smaller volume of condenser (Coulson et al., 1983). In a vertical shell side condenser design, vapors enter at the bottom and move up, passing through the coolant carrying coils.

The refrigerated condenser is designed such that its capacity is higher than the incoming steam's latent heat. This causes vapors to condense by transferring heat through the surface of the coil. The condensate drops to the bottom of the condenser, where it can be removed by a condensate discharge valve. The material used for this purpose complies with ASTM standard materials for heat exchanger design; i.e., copper for tubes and grade 306 stainless steel for the shell.

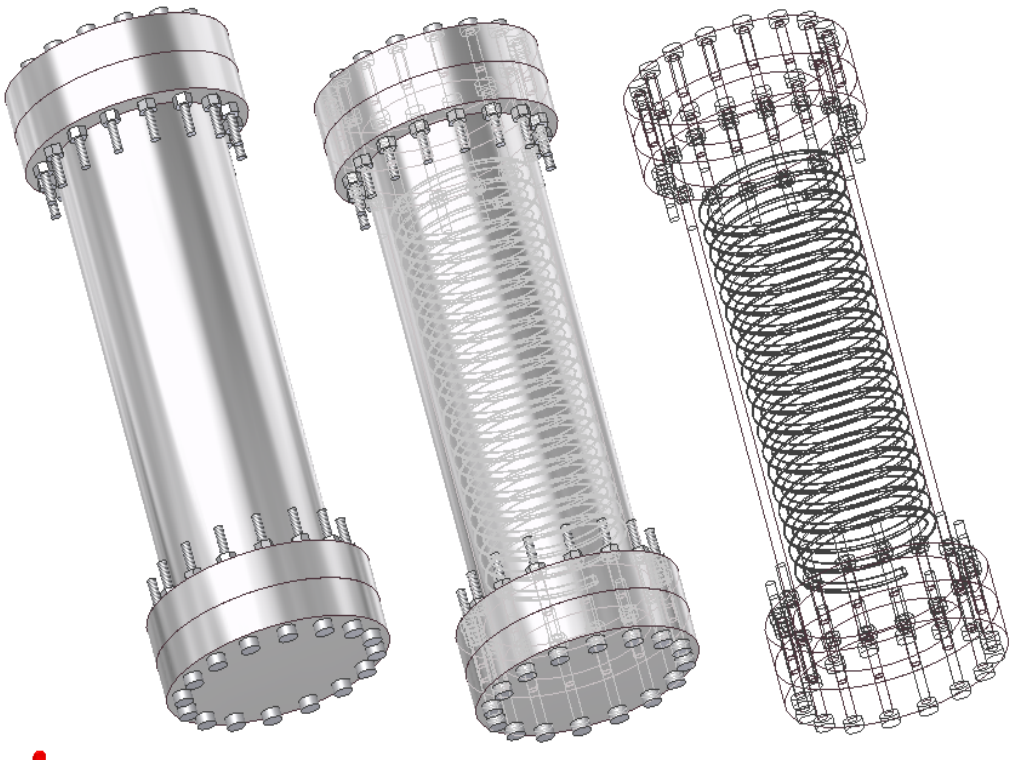

Figure 3-5. The 3D isometric visualization of the shell and coil heat exchanger design.

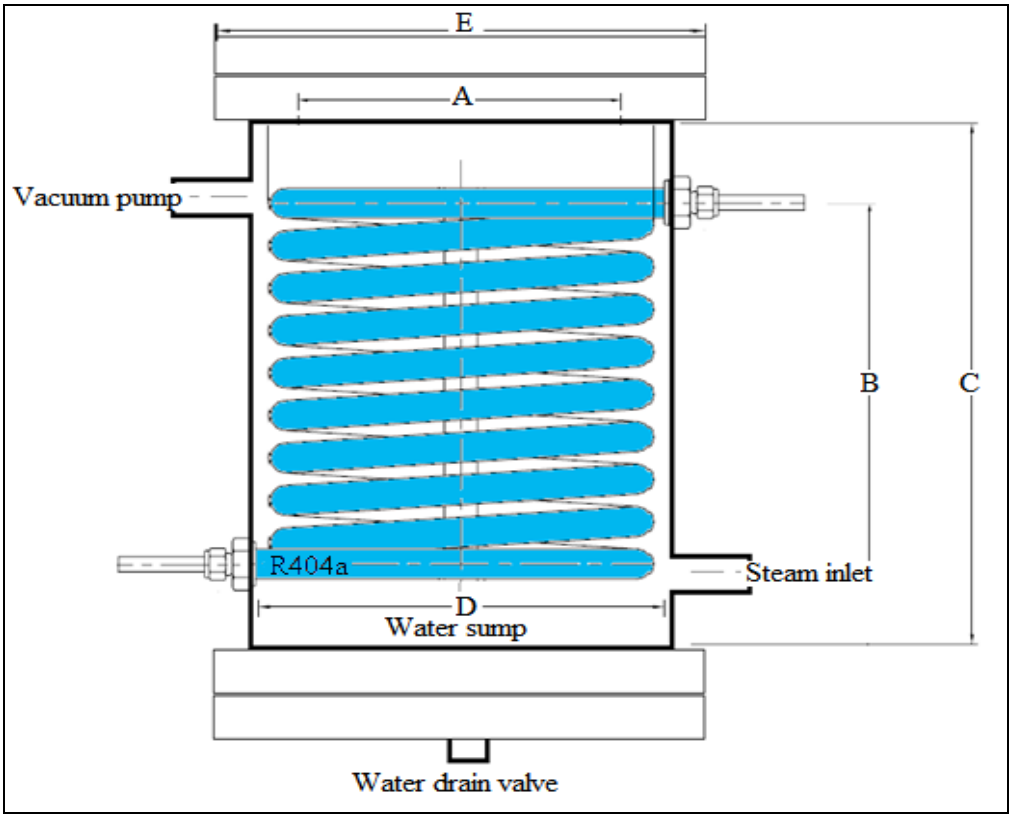

Figure 3-6. Steam condenser heat exchanger (shell and coil) schematic.

Dimensions for Figure 3-6 are:

A = 0.09525 m coil inner diameter

B = 0.254 m height

C = 0.3048 m height

D = 0.1016 m condenser inner diameter

E = 0.1524 m flange fittings

Tube length = 6.09 m

Length of shell [L_{sh}] = 0.3048 m

Outside diameter of tube [$D_{o,\,s}$] = 0.007163 m

Inside diameter of Tube [$D_{i,\,s}$] = 0.00635 m

Inside diameter of coil [$D_{i,\,c}$] = 0.081229 m

Outside diameter of coil [$D_{o,\,c}$] = 0.094742 m

Number of turns of coil [N_c] = 18

Diameter of shell [D_{sh}] = 0.1016 m

Table 3-1 compares the concentric cylinder heat exchanger/steam trap and the refrigerated shell-and-coil condenser. Figure 3-7 shows the stainless steel condenser shell.

Table 3-1. Comparison of the concentric cylinder steam-trap with refrigerated shell-and-tube heat exchanger.

Steam Trap	**Refrigeration Unit**
• Steam trap reaches -78.6^{o}C final temperature.	• R-404a carrying coil reaches -15^{o}C final temperature.
• Ice alcohol slurry should be replaced after every 2-3 frying experiments.	• No need of revival, just turn on and off.
• Low initial purchase cost, higher running cost.	• Low initial cost, low running cost
• Heat transfer surface made of stainless steel with low thermal conductivity, k = 134 W/mK, (surface area = 0.0659 m^3).	• Heat transfer surface is copper with high thermal conductivity, k = 401 W/mK, (surface area = 0.0843 m^3).
• Ice formation greatly reduces heat transfer since condenser cannot be cooled after each cycle.	• Condenser ice melts as soon as the experiment completes and depressurization takes place.
• Vacuum grease is required on removal of center well for water draining.	• Water drains when the drainage valve is opened.
• No way of mounting temperature probes inside the condenser.	• Temperature probes pre-mounted on all the inlets and outlets of heat exchanger.
• No allowance for future upgrades.	• Future upgrades and enhancements possible.
• Successfully condenses water vapors during vacuum frying of potato slices.	• Successfully condenses water vapors during vacuum frying of potato slices.

Figure 3-7. Stainless steel condenser shell.

3.2.1.1. Cavitation problem

Inside the liquid ring vacuum pump, the compression of the gas occurs in one impeller stage. Water or some other incompressible fluid (oil), called the pump liquid, is introduced to the liquid ring vacuum pump. As the impeller rotates, a ring of liquid is formed inside the pump casing from centrifugal force. This action draws the gaseous stream into the pump through the inlet port. The gas is compressed by the liquid ring, exiting the first stage through a smaller area discharge port and into the second stage of the pump.

The second stage is volumetrically smaller and does the final compression of the gas. The gas then exits the pump usually at atmospheric pressure, along with the pump

oil. Cavitation is the only major problem in using a condenser in vacuum frying. This problem arises when any uncondensed water vapor enters the vacuum pump, which results in suction cavitation.

Suction cavitation (Figure 3-8) occurs when the pump suction is under a low pressure/high vacuum condition where the liquid turns into a vapor at the eye of the pump impeller. This vapor is carried over to the discharge side of the pump where it no longer has vacuum and is compressed back into a liquid by the discharge pressure. This imploding action occurs violently and attacks the face of the impeller.

An impeller that has been operating under a suction cavitation condition can have large and small chunks of material removed from its face, causing the impeller to look like a sponge. Both cases will cause premature failure of the pump, often due to bearing failure. Suction cavitation is often identified by a sound like gravel or marbles in the pump casing (Skelton, 1999).

Figure 3-8. Suction cavitation eats up and makes the impeller blade look sponge-like at edges (Skelton, 1999).

3.2.1.2. Operation of condenser unit

The initial condenser setup required changing the dry ice every time the system was operated (Table 3-1). Therefore, a refrigerated unit was designed consisting of a condensing unit and a shell-and-coil heat exchanger to condense the water vapor with equal or improved efficiency, similar to a dry ice based system. The refrigeration unit can also be turned on based on the duration of frying; thereby making it more energy efficient than using the dry ice based system.

The condenser unit operates as shown in Figure 3-9. It consists of a 1/3 HP Copeland compressor (Emerson Climate Technologies, Ohio, USA), an air-cooled condenser, a filter drier, and a capillary tube. The evaporator of the refrigeration system is the shell-and-coil heat exchanger where the actual phase change takes place. Shell-and-coil type heat exchangers are basically used in water coolers and vapor/vapor or vapor/liquid separators. These heat exchangers are preferred for their use in condensation applications.

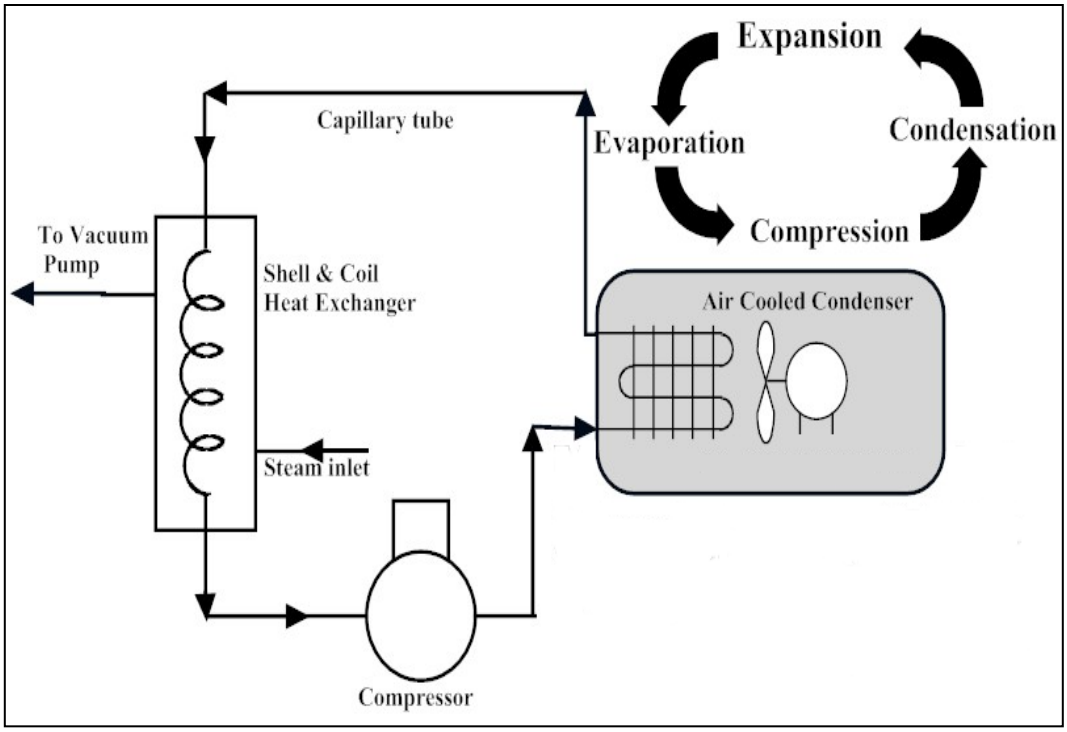

Figure 3-9. Refrigerated condenser unit with its four parts: condenser, evaporator (heat exchanger), capillary tube, and compressor.

The refrigeration system follows the reverse Carnot cycle as the basis of the principle of refrigeration:

- The compressor does work (compresses) the refrigerant, increasing its pressure at constant entropy.
- The high-pressure refrigerant goes through the condenser, where it becomes a liquid.
- The liquid passes through a capillary tube to reduce the pressure.
- The refrigerant evaporates in a low-pressure environment.
- The evaporated refrigerant then goes back into the compressor and the cycle repeats itself.

The boiling point of the refrigerant vapor rises when it goes through the compressor. This rise in pressure liquefies the refrigerant at higher temperatures. The refrigerant at high pressure and liquid form is ready to evaporate as soon as the pressure is lowered.

A capillary tube carries the refrigerant at high pressure and releases it in a larger tube where sudden expansion causes the refrigerant pressure and temperature to drop. The pressure before the capillary tube (expansion valve) can be as high as 1 or 2 MPa (high side), while on the evaporator side it is only 0.15 to 0.20 MPa (low side).

Inside the evaporator the refrigerant expands so quickly that it pulls the heat away from the evaporation surface to the boiling point of the refrigerant, which usually ranges from -20^{o}C to -150^{o}C for different types of refrigerants used in the system. In this research, R-404a refrigerant, which has a boiling point of -46.5^{o}C (SUVA R404a) was used to condense the water vapor into liquid (phase change). See Appendix E for detailed information on R404a.

3.2.1.3. Pre-condenser

The steam flows in the system through a small pre-condenser that is air cooled with the help of small fan and goes to the main refrigerated condenser. The pre-condenser is a spiral copper tube; a fan rotates in the center of these tubes to cool down the incoming water vapors. It increases the residence time of steam in the condenser system before reaching the main condenser and therefore increases the capacity of the system from 10 to 15%.

3.2.2. The de-oiler unit

The centrifugation step was carried out directly after frying. The vacuum was not broken during the centrifugation, since de-pressurizing the chamber would create a gradient between ambient pressure and inside the pores of the chips. This pressure gradient causes the oil collected on the surface of the chips to be suctioned inside the pores. The centrifugal de-oiling unit provides a more efficient process and a good quality product with less oil content than the traditional frying system.

3.2.2.1. Operation of the de-oiler unit

The principle of centrifugation is based upon Newton's third law that states "every action has an equal and opposite reaction." Any object rotating eccentrically outwards on a curved path (centripetal force) faces a force just in the opposite direction called as reactive centrifugal force because the object wants to move in the outward direction but is fixed on the path with mechanical means. Therefore, two inter-mixed objects may experience an outward force inside a rotating basket. If the mixture contains different specific gravities, each object will tend to move in the direction of force in accordance with its specific gravity. For example, potato chips possess surface oil after frying. When they are rotated at high speed inside the basket, the surface oil is removed. This is because oil's specific gravity (~ 0.9) is much less than that of the potato chips.

The de-oiler consists of a small AC motor mounted on the basket shaft (Figures 3-10 and 3-11). This AC motor rotates the free moving basket at the desired speed from 45 to 750 RPM (0.2 g-force to 63 g-force) with the help of a 2:1 reduction gear drive. The de-oiling was performed immediately after the chips were fried and removed from

the oil (by lifting the basket). The rotary control switch was set on the desired speed and the centrifuge switch was turned on, causing the product to rotate eccentrically inside and providing the centrifugal force sufficient for de-oiling. The centrifugal force generated through this rotation caused the oil to spill out from the product's surface and crevices. Potato chips were tested through this methodology in the laboratory, and good results were obtained.

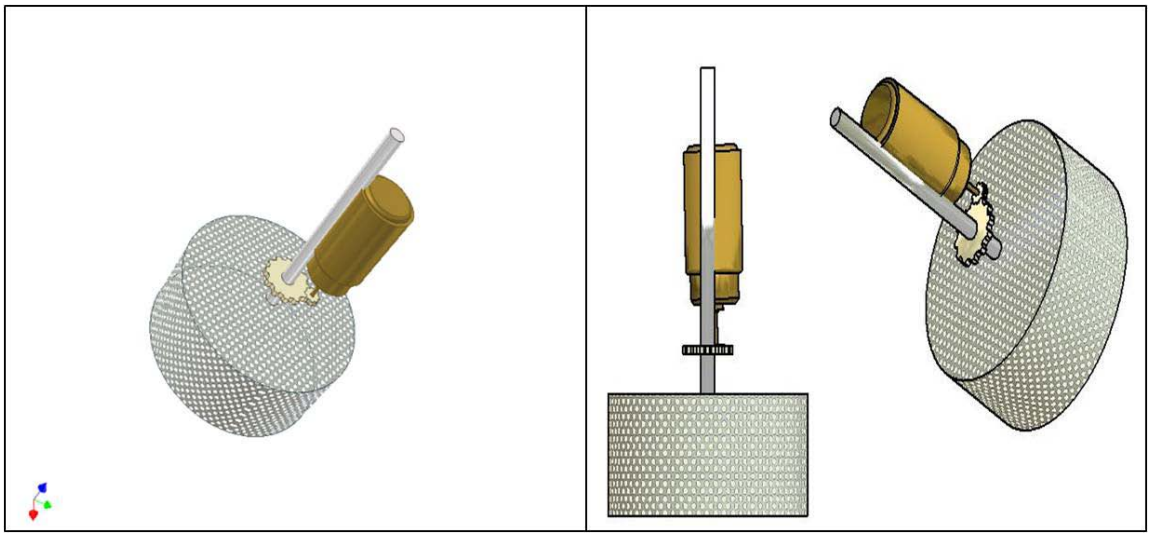

Figure 3-10. A 3-D isometric view and schematic for basket centrifuge assembly with 2:1 gear ratio (max RPM=750 or 63 g-force at the basket).

The speed controller used is an ES02 (Oriental Motor, Torrance, CA) AC solid-state speed control unit. The results obtained at different rotational speeds helped in calibration of the equipment and in improving the quality of the de-oiled chips. The motor (2IK6RA-CWE, Oriental Motor, Torrance, CA) chosen for the de-oiling operation is a fully enclosed "Type B" winding. The motor was designed to bear shell

temperatures up to 90^{o}C and winding temperature of 130^{o}C. This makes the motor suitable for operation in a vacuum system at high temperature.

3.2.3. Control system

The system to control operation of both de-oiler and condenser units was designed. It comprises various electrical and electronic components to provide a switch-based interface for controlling various operations during frying.

It is divided into two separate parts, (1) to control the speed of the de-oiler motor and provide conditioned power supply (230 V/50 Hz) to the AC speed controller ES02 unit; (2) for automatic control of the condenser unit using a 12 V relay circuitry to form a switch that activates the condensing unit automatically when the frying vessel lid is closed.

Figure 3-11. Centrifuge control unit and vacuum vessel and basket rotation mechanism (left) and de-oiler system (right).

The speed controller can be used to set desired speeds for rotating the basket when the power switch is turned on after setting the speed control knob. The speed controller receives power from a regulated 230 VAC (250 W grounded step-up converter) power supply unit and in turn powers the AC speed control motor. The other part acts as a simple relay switch that is powered by a 12 VDC transformer. An auto and a manual switch can activate the relay circuit. When the auto switch is turned on, the relay is powered up, and the circuit completes when the lid is closed on the frying vessel. Turning on the manual switch bypasses the relay circuit and turns on the condensing unit. A snubber circuit, capacitors and fuse components are mounted to complete the system and avoid any losses or electrical shock in the case of a power surge.

3.2.4. Data acquisition methodology

The vacuum fryer control unit has a program that relies upon a data acquisition system to provide data readings from the thermocouples and generates other calculations for heat and mass transfer during vacuum frying of potato chips. The vacuum fryer simulator requires the following components to work.

a. Data acquisition system (OMB-DAQ 54)
b. Thermocouple temperature sensors
c. Graphical user interface (GUI) computer program (VBA)
d. A computer with a Microsoft Windows-based operating system

3.2.4.1. Data acquisition system

The data acquisition system by Omega Engineering Inc., OMB DAQ 54 (Omega Engineering, Stamford, CT, USA), works on the principle of analog-to-digital

conversion. A controller directly collects the data in the form of voltage through thermocouples. This data is further interpreted by the controller with a particular frequency. The scan rate is dependent upon the frequency of the data collection. Every millisecond, the system takes the signal in the form of voltages and then converts it into a basic temperature reading. This program is easy to use with the help of a GUI (Graphic User Interface).

The data acquisition system used for this research can take readings from up to 5 thermocouples simultaneously. It can be connected to a personal computer using a universal serial bus (USB) cable. Once the reading is obtained, it usually stores it into a buffer memory until the user asks it to save the data permanently. This is also known as data logging.

Figure 3-12 shows the control box designed to accommodate all the switches and controls for operating the condenser and centrifuge.

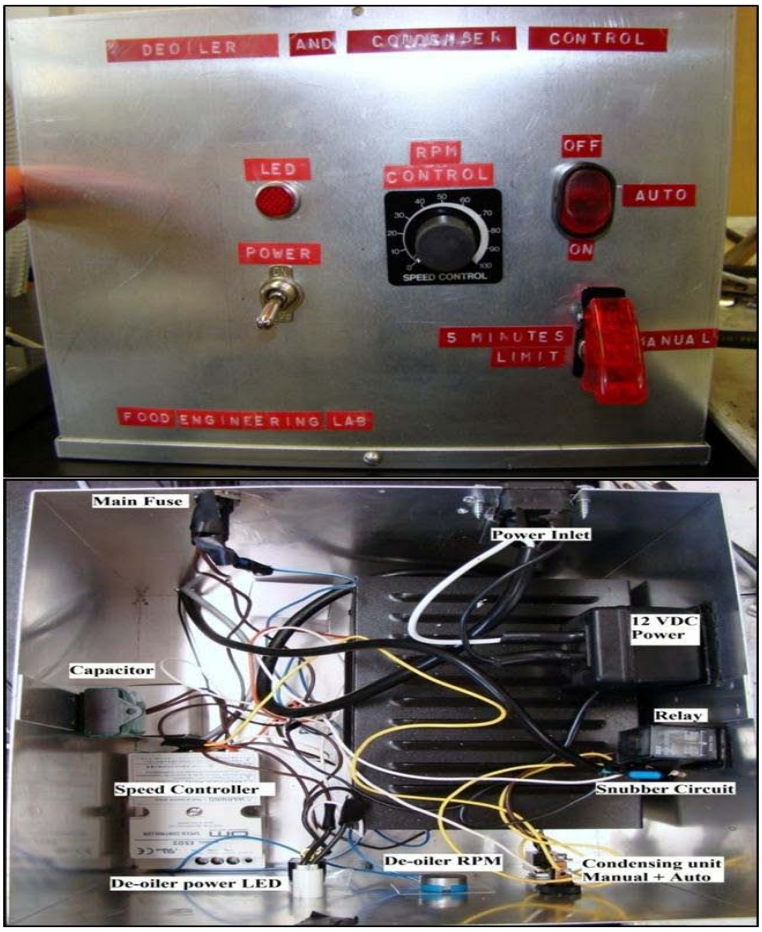

Figure 3-12. The controller design for condenser and de-oiler unit: controls view (top); assembly view (bottom).

3.2.4.2. Thermocouple temperature sensors

Thermoelectric effects can be harnessed for heating and cooling as well as for instrumentation purposes. A thermocouple makes use of one aspect of the thermoelectric effect to measure temperatures, the voltage produced between two different wires with junctions at different temperatures. A thermocouple must consist of two wires of different compositions. The most popular combination is copper and constantan, an alloy of copper and nickel. The wires are joined at the ends to make two junctions. One of the

wires is then cut so that a voltmeter can be placed in the circuit to measure the voltage between the two junctions. This voltage will depend on the temperature difference between the two junctions (Pollock, 1991).

The thermocouple temperature sensors are generally used at places where rapid changes in temperature have to be determined. The two different types of metal, having different compositions, will have different densities of electrons. The electrons will tend to diffuse from the higher to the lower densities. Both of these electron densities depend on the temperature, so if the two junctions are at different temperatures, the diffusion of electrons will proceed at different rates at each junction. The net result is a motion of the electrons that creates voltage between the two junctions. The thermocouples basically are a combination of metals between Seebeck and Peltier series. These metals are used to form a cold junction and a hot junction when joined from both ends. A voltage potential difference is created when relative temperature is used (Pollock, 1991).

In this research, a Type K thermocouple was used because its range (-200°C to +1200°C) is ideal for use in analysis of the vacuum frying process. These types of thermocouples are easily available in different shapes and sizes. The Type K thermocouple is made of Chromel-Alumel™ alloy, where the Chromel™ (Hoskins Manufacturing Company) is constituted of 90% nickel and 10% chromium, and the Alumel™ (Hoskins Manufacturing Company) is made of approximately 95% nickel, 2% manganese, 2% aluminum, and 1% silicon.

The three major thermocouples used in the process for monitoring the temperature of condenser inlet, condenser outlet, and refrigerant outlet are general Type

K beaded thermocouples, while the thermocouples used inside the vacuum frying vessel were customized according to the process. The application requires one thermocouple to acquire ambient temperature inside the fryer. This was done through a 0.0508 m long, 0.0007874 m wide thermocouple probe, while the other thermocouple was 0.4752 m long thread-like, and only 0.000254 m wide. It should be inserted directly inside the potato chips during the temperature measurement. These thermocouples are readily removable and were inserted inside the vacuum fryer with the help of a Type K twin-pair thermocouple feed-through. This configuration and placement strategy of the thermocouples will allow the user to determine the temperatures every second (minimum) during the process. The temperatures were then further used in different formulas to find the required heat and mass transfer parameters of vacuum frying.

The relationship between the temperature difference and the output voltage of a thermocouple is non-linear and is approximated by polynomial:

$$\Delta T = \sum_{n=0}^{N} a_n v^n \qquad [3\text{-}1]$$

where N ranges between 0 to between 5 and 9, and v is the potential difference [Voltage].

The vacuum fryer control unit employs five different thermocouples and a provision to use a sixth thermocouple in place of the $T_{\text{ref, in}}$ thermocouple. This allows the user to collect data from six different places during the vacuum frying process. The calculation for the thermocouple provides temperature that is also used by the simulator to determine other heat and mass transfer parameters:

1. $T_{ref,\ in}$- This thermocouple is a Type K, bead-type thermocouple mounted between the capillary tube and the evaporator coil entrance. It was placed outside the condenser refrigerant inlet line and covered by thermal insulation. The refrigerant shows regular temperatures of -15^{o}C.
2. T_{amb}- A Type K probe thermocouple 2 inch long and 0.0008128 m in diameter was mounted inside the fryer vessel to determine the ambient temperature during the frying session. The thermocouple is grounded and stainless sheathed for protection from oil. The normal temperatures during the frying process reach 95 to 100^{o}C caused by the radiant heat of oil of about 60 to 65^{o}C and the heat of steam vapor of about 24 to 25^{o}C.
3. $T_{cond,\ out}$ - The condenser outlet temperature is the temperature of highest importance for efficient working of the refrigerated condenser system. This temperature should be constant during the frying process. Any rise in this thermocouple's temperature would imply leakage of steam from the condenser towards the vacuum pump. This thermocouple reading was closely monitored, and it successfully remained under the saturation temperature of steam at 1.33 kPa vacuum pressure until 70 g of mass load of potato slices was fried.
4. $T_{cond,\ in}$- This thermocouple is installed on the condenser inlet inside the pipe after the pre-condenser and main condenser. The usual temperatures for this thermocouple vary from 22 to 25^{o}C. This is because water boils at around 24.55^{o}C in 1.33 kPa vacuum pressure.

5. $T_{ref,\ out}$- This monitors the refrigerant outlet temperature and is mounted in a similar way outside the refrigerated condenser on the suction line of the condenser. This temperature should be monitored to understand the basic properties and behavior of refrigerant R-404a in the system.
6. T_{pc}- This stands for the thermocouple used to monitor temperature inside the potato chip. This is a very thin hair-like thermocouple just 0.000254 m wide and 0.4752 m long. The thermocouple reaches an average temperature of 110 to 120^{o}C during frying.
7. $T_{comp,\ cond}$- This thermocouple is a Type K, bead-type thermocouple mounted across the refrigerant carrying tube between the compressor and condenser. The compressor compresses the refrigerant, causing a huge change in enthalpy and phase. The temperature measurement was of critical importance at this point to study the performance of the compressor in the refrigeration system.
8. $T_{cond,\ cap}$- This thermocouple is also a Type K, bead-type thermocouple mounted between the condenser and capillary tube. It records the temperature of the refrigerant coming out of the air-cooled condenser. The change of temperature from the air-cooled condenser outlet to the refrigeration condensing unit can be seen with increased load conditions. This thermocouple helped in evaluation of heat transfer coefficients for refrigeration cycle design. It also helped in evaluating the air-cooled condenser performance of the refrigeration system.

9. $T_{steam\ hose}$- The temperature of steam directly after it leaves the fryer vessel changes and comes down to the temperature at which the steam exists in vacuum (1.33 kPa) around 24 to 25^{o}C (Garayo, 2001). This temperature was important to record because ambient temperature of the system T_{amb} rises to about 90^{o}C during frying. A Type K, bead-type thermocouple was used for this purpose.
10. $T_{pre,\ cond}$- This temperature was recorded with the help of a Type K, bead-type thermocouple to understand the performance of an air-cooled pre-condenser. The difference in temperature of $T_{pre,\ cond}$ and $T_{cond,\ in}$ helps in understanding the efficiency of the pre-condenser in the steam condenser unit.
11. $T_{ball,\ probe}$- A copper and aluminum ball-type, Type E thermocouple was used to determine the convective heat transfer coefficient between the product and oil.

3.2.4.3. The GUI computer program

The vacuum fryer simulator is a customized user interface for vacuum frying potato chips. It can perform calculations for oil temperatures of 120^{o}C, 130^{o}C and 140^{o}C. The vacuum fryer simulator (VFS) provides the user a process and instrumentation diagram in a GUI by showing the real-time data during the vacuum frying process. It also saves and opens the existing user settings. The VFS simulator consists of three sections. First, it displays and allows changing the way the data acquisition system may acquire the data. This means that the user can choose the number of thermocouples he or she wants to run, the interval of the data being collected, and the

time or counts it must execute from the start. The program was designed such that it resets the counter every time the process is halted. Second, it links the reading of the thermocouple to the parameter simulator "pc monitor module" to show most of the heat and mass transfer parameters in real time. At the end of the process, it can draw a reference table for all the data it has acquired during the process. It can also draw a graph between any two parameters (*x*-axis and *y*-axis) chosen by the user during and after the simulation start up.

The third part is the user input parameters in the "pc monitor module" that allows the user to tell the program about the amount of chips fried through the "initial weight" input box. It also allows setting the temperature of oil at which the experiments have to be carried out. Finally, it gives the different process parameters (temperatures, time, etc) with the help of user-defined data and real-time temperature readings.

The thermocouples collect temperature readings from different parts in the whole process; namely, temperature of the potato chip (center) (T_{pc}), ambient temperature inside the vacuum frying vessel (T_{amb}), temperature at the condenser inlet ($T_{cond,\ in}$), temperature at the condenser outlet ($T_{cond,\ out}$), and temperature of the refrigerant outlet ($T_{ref,\ out}$).

This strategic placement of thermocouples provides continuous temperature reading with respect to time. Figure 3-13 is a GUI for the vacuum fryer control unit program. Appendix C shows the complete code for the design of the graphic user interface.

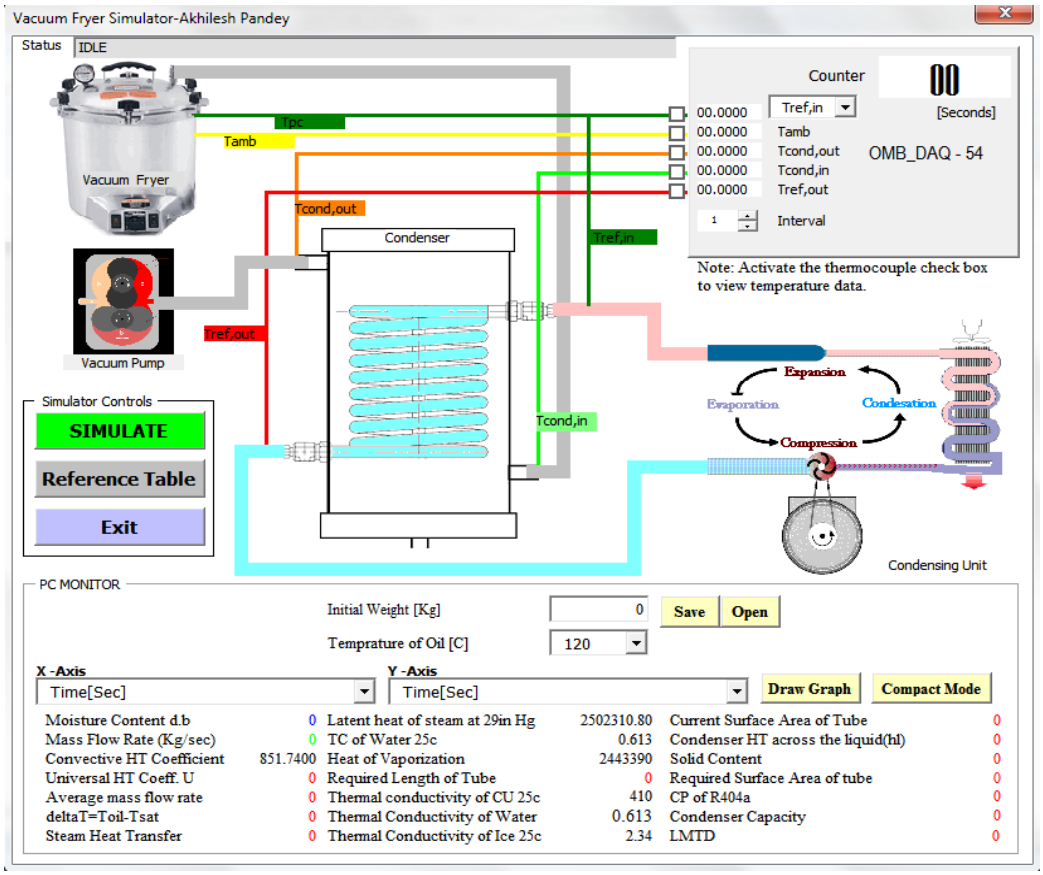

Figure 3-13. The GUI for vacuum fryer simulator program.

3.3. Experimental data for optimization of the system

After the design and installation of the condenser and the de-oiling unit were completed, potato slices were used as subjects for experimental optimization. The experiments were carried out by frying three different mass loads of potato slices (30 g, 50 g, and 70 g) at two oil temperatures (120^{o}C and 140^{o}C) at different time durations. The initial and final changes in moisture content, oil content variation with different de-oiling speeds and durations, effect of varying product loads on the condenser unit were evaluated by analyzing the acquired data. A process and instrumentation diagram (P&ID) program on Visual Basic Editor (MS Excel) was designed to collect and

generate temperature history data for determining parameters for both real-time and theoretical process profiles.

The data acquired was used to run the system at optimal settings by establishing a correlation between the best combinations of operational strategies from the vacuum fryer to the condenser to the centrifuge unit. This also helped to better understand the whole vacuum frying process.

3.3.1. Moisture content of raw potato slices

The moisture content of raw potatoes must be determined before frying to provide an understanding of total amount of moisture passing through the condensing system. For potatoes, average moisture content varies around 70% to 75% w.b. (USDA/ARS, 2007). Potato tubers have considerable variability in initial moisture content from potato to potato. To account for this variability, the initial moisture content of each potato was measured before the slices were fried. The initial moisture content was determined by drying samples of 3 g of the potato (slices) to a constant mass for 72 hours at 105 °C (AACC, 1986). The test was carried out in triplicate.

The moisture content on a wet basis is defined as:

$$M.C._{wb} = \frac{W_{wet} - W_{dry}}{W_{wet}} \qquad [3\text{-}2]$$

and on a dry basis;

$$M.C._{db} = \frac{W_{wet} - W_{dry}}{W_{dry}} \qquad [3\text{-}3]$$

where W is the weight [kg] of the potato slices.

3.3.2. Moisture content of potato chips

Potato chips were finely ground with a mortar and pestle after frying. Moisture content of the chips was determined by weight loss after drying 3 g samples of finely ground chips in a convection oven at 105°C for 24 hours (AACC, 1986). This test was performed in triplicate. Moisture content in wet and dry basis was calculated using Equation (3-2) and (3-3), respectively.

3.3.3. Specific gravity of raw potatoes

Various methods are used to determine specific gravity of raw potatoes, which is highly variable and may range between 1.050 and 1.106 (Snack Food Association, 1991). According to Gould (1995), specific gravity can be measured by finding the ratio of weight of a given sample of potatoes to that in pure water. For every 0.005 increase in specific gravity, an additional pound of chips can be obtained per 100 pounds of potatoes. Lulai and Orr (1979) found that yield of chip increased and chips oil content decreased linearly as the specific gravity value reached closer to 1.110. Specific gravity was calculated by weighing the raw potatoes on a scale; further, the potatoes were dipped in a 1,000 ml capacity hydrometer test tube (Lucas and Rooney, 2001). The change in volume (ml) of water was observed and noted before and after the immersion.

$$S.G. = \frac{w_{air}}{w_{air} - w_{water}} \qquad [3\text{-}4]$$

where w_{air} and w_{water} is weight [kg] of potatoes in air and water, respectively.

3.3.4. Oil content of potato chips

Total oil content (OC) of potato chips was determined by using the Soxtec System HT (Pertorp, Inc., Silver Spring, MD) extraction unit with petroleum ether (AACC, 1986). The test was performed for a 3 g sample of finely ground chips in triplicate, and oil content determined as:

$$O.C.[\%] = \frac{W_i - W_f}{W_i} \times 100 \qquad [3\text{-}5]$$

where W_i is the initial and W_f is the final weight of the potato slices.

The experiments related to optimization of the condenser were designed to analyze maximum load capacity of the system as well as to understand the performance and behavior of the condenser in various experimental conditions. The basic heat exchanger performance was evaluated by checking the amount of steam it condenses during vacuum frying. To do that, several heat transfer parameters were needed.

3.3.5. Convective heat transfer coefficient (*h*) between the oil and the surface of the potato chips

The convective heat transfer coefficient of the oil was determined at 120 and 140^{o}C using the lumped capacity method, LCM, (Incropera et al., 2006) for heat transfer in a copper sphere (25.4 mm diameter) with a thermocouple (Type-E) located in its geometric center. Time-temperature data were recorded by a data acquisition system as the transducer was lowered into the frying oil.

The LCM essentially assumes that the temperature within the object is uniform through the duration of the heating process. This is accomplished by using a material

with a very high value of the thermal conductivity (k) i.e., a metal; so that the Biot number $Bi = \left(\frac{hD_{copper}}{k_{copper}} \right)$ is lower than 0.1.

Thus, the changes in the center temperature with time of a copper sphere submerged in the frying oil (k_{copper} = 401 W/mK) heated up to 120°C or 140°C, is described by the following equation (Incropera et al., 2006):

$$\frac{T - T_\infty}{T_i - T_\infty} = \exp\left[-\frac{hA_s}{\rho V C_p} t \right] \qquad [3\text{-}6]$$

where, T_i is the initial temperature of the spherical ball probe [°C], T_∞ is the temperature of the frying oil [°C], A_s is the area of the copper spherical ball probe [0.002027 m^2], ρ is the density of the copper probe [8954 kg/m^3], V_c is the volume of the spherical ball probe [8.50×10^{-6} m^3], t is the heating time [s], C_p is the specific heat [383 J/kg.K] and, h is the convective heat transfer coefficient [W/m^2K] of the spherical copper probe.

The convective heat transfer coefficient can then be calculated by Equation 3-7 by fitting the experimental data using non-linear regression.

$$T(t) = (T_i - T_\infty) \times \exp\left[-\frac{hA_s}{\rho V C_p} t \right] + T_\infty \qquad [3\text{-}7]$$

3.4. Condenser simulation and design calculations

The sample calculations for the design of the heat exchanger were conducted automatically in the software used for data acquisition of temperature profiles from the thermocouples. The following values for temperature were used for the first step in sample calculations.

At time t = 210 s, the beginning of frying, (Table B-3, Appendix B):

$T_{ref,\ in}$ = -14.9352°C

T_{amb} = 51.389°C

$T_{cond,\ out}$ = -5.9248°C

$T_{cond,\ in}$ = 20.8097°C

$T_{ref,\ out}$ = -25.5412°C

Condenser Dimensions (from actual design, Figure 3-6):

- Outside diameter of tube [$D_{o,\ s}$] = 0.007163 m
- Inside diameter of tube [$D_{i,\ s}$] = 0.00635 m
- Inside diameter of coil [$D_{i,\ c}$] = 0.081229 m
- Outside diameter of coil [$D_{o,\ c}$] = 0.094742 m
- Length of coil [L_c] = 6.09 m
- Number of turns of coil [N_c] = 18
- Diameter of shell [D_{sh}] = 0.1016 m
- Length of shell [L_{sh}] = 0.3048 m

To calculate the condenser area for the coil (refrigerant section) and the shell (steam section) components, the unit was simplified as a concentric cylinder as sketched in Figure 3-14.

3.4.1. Calculation of total area of coil/tube side (refrigerant) system

$$A_{coil} = \pi \times (D_{o,c} - D_{i,c}) \times L_c = 0.0130 m^2 \qquad [3\text{-}8]$$

3.4.2. Calculation of total area of shell side annulus (steam) system

$$A_{an} = \pi \times (D_{sh}) \times L_{sh} = 0.0980 m^2 \quad [3\text{-}9]$$

Therefore, total area of steam inside the condenser is:

$$A_{steam} = A_{coil} - A_{an} = 0.0845 m^2 \quad [3\text{-}10]$$

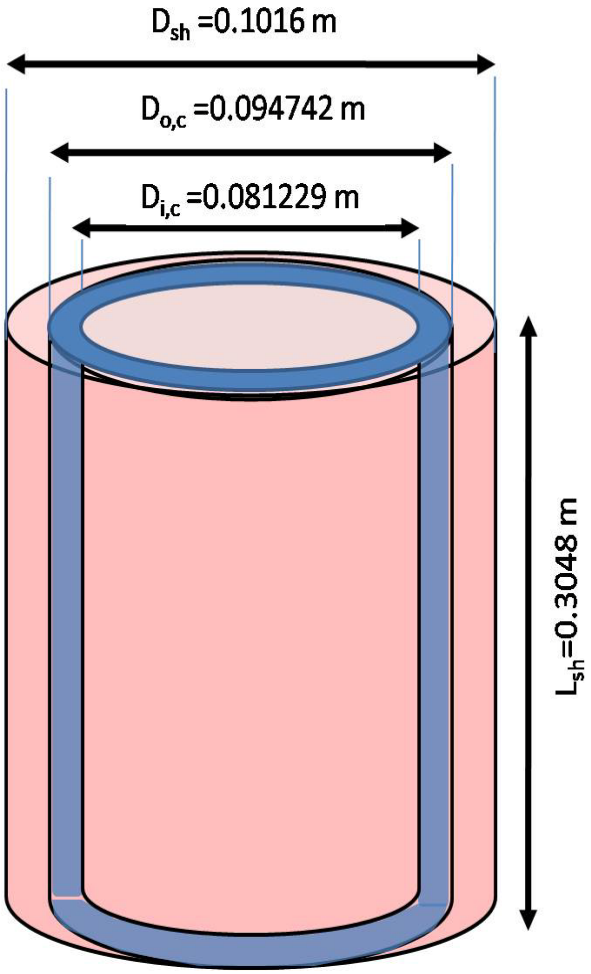

Figure 3-14. Schematic of the condenser unit used to calculate the surface areas for the steam and refrigerant sections.

3.4.3. Calculation of the saturation temperature of steam

The primary requirement was to check the condenser capacity by running an initial experiment. Different mass loads of 30 g, 50 g, and 70 g of potato chips were fried until the temperature of the condenser was close to the saturation temperature of steam at vacuum gauge pressure, $P_g \approx 29.53$ in-Hg or to an absolute pressure $P_{\text{abs}} = 1.33$ kPa.

The saturation temperature for steam in a vacuum at $P \approx 1.33$ kPa was calculated by using the Antoine equation (Steinmann and Eck, 2006; Reid et al., 1987):

$$T_{sat} = \frac{B}{A - \log[P_{sat}]} - C \qquad [3\text{-}11]$$

where the parameter values for water between $99^{o}\text{C} \leq T \leq 374^{o}\text{C}$ are $A = 8.14019$, $B = 1810.94$ and $C = 244.485^{o}\text{C}$, and P is in [mmHg].

Hence, saturation pressure [mmHg] can be calculated as:

$$P_{sat} = 10^{A - \frac{B}{C+T}} \qquad [3\text{-}12]$$

At a vacuum pressure of $P_{abs} \approx 1.33$ kPa ($P_{\text{g}} = 29.53$ in-Hg) or 10 mm-Hg (10 Torr), the saturation temperature was calculated as:

$$T_{sat} = \frac{1810.94}{8.14019 - \log[10]} - 244.485 = 9.1413^{o}C \qquad [3\text{-}13]$$

A close observation was required to monitor the condenser outlet temperature to ensure the maximum capacity of the system. The experiment works on the principle that any portion of water vapor that the condenser is not able to condense goes into the vacuum pump. The condenser outlet thermocouple will show a rapid rise in temperature reading from the hot steam, allowing detection of the maximum mass load that can be

condensed. The steam leakage risks were minimized by mounting an inline desiccator with color changing Dririte® beads. A fine metal mesh was installed before the vacuum pump inlet to prevent any desiccant beads from getting into the vacuum pump. As soon as the steam leakage was detected, the vacuum hose could be disconnected from the vacuum pump with the help of a quick disconnect valve. The maximum capacity was ensured and determined well below the saturation temperature of steam to provide necessary operational allowance limits.

Another experiment was related to determination of the efficiency of the condenser by collecting the amount of water condensed after each frying session. The amount of water removed from the condenser was directly compared with the initial and final moisture present in the potato chips being fried. Finally, the temperature inside the chips was determined to allow calculation of heat and mass transfer during the vacuum frying process.

3.4.4. Moisture content of potato slices as function of time

The moisture loss of potato slices fried at different loads was calculated with the moisture diffusion equation for an infinite flat plate (Brooker et al., 1992):

$$MC_{db} = (M_i - M_e) \times \left(\frac{8}{\pi^2} \right) \times \exp\left(\frac{-\pi^2 \times D_e \times t}{4 \times a^2} \right) + M_e \qquad [3\text{-}14a]$$

where $MC_{d.b}$ is the moisture content on a decimal dry basis [decimal d.b.], M_i is the initial moisture content [decimal, d.b.], M_e is the equilibrium moisture content [decimal, d.b.], t is the frying time [s], and a is the thickness of the potato slice [m], and D_e is the effective diffusion coefficient [m/s].

The Arrhenius-type equation can be used to account for temperature effect (Brooker et al., 1992), $D_e = A \times \exp\left(\frac{E_a}{R \times T_{abs}}\right)$ [m/s] with A = constant, E_a = activation energy [kmol/kJ], R the gas constant [kJ/kmol K], and T_{abs} the absolute temperature [K].

The changes in moisture content with time were determined experimentally for different frying temperatures (120°C, 130°C, and 140°C), and Equation 3-14b was used for calculations. With the help of the initial frying load, the equations were directly used by the vacuum fryer simulator in analytical form to show changes in moisture content of potato chips. The initial weight and diffusion coefficient were required to estimate the change in moisture content, which can be shown in real time on the PC monitor module of the VFS program interface.

In this study, the change in moisture content with time was calculated using the following equation (Granda, 2005):

$$MC_{db} = 2.34698 \times \exp\left[\left(-5412.61 \times \exp\left(-\frac{5086.15}{T_{abs}}\right)\right) \times t\right] + 0.0167 \qquad [3\text{-}14b]$$

3.4.5. Solid content of potato chips

The total solids content of the potatoes does not during frying. It is calculated in the software when the user inputs the amount of frying load being fried during an experiment. Therefore, the total solids in the frying load will be constant:

$$TSC = W_i \times (1 - MC_{wb}) \qquad [3\text{-}15]$$

where W_i is the initial weight of the potato slice load input by the user and MC_{wb} is the moisture content of potato slices in wet basis.

3.4.6. Mass flow rate of moisture leaving the potato slices

When steam evaporates from the potato chips during frying, it is suctioned by the vacuum pump out of the system. The steam passes through the evaporator at a certain rate that must be known to calculate the mass transferred through the system. The mass of moisture evaporating from the chips per second can be measured and multiplied by the total solids content; the rate can be calculated as:

$$\dot{m} = TSC \times \left(MC_{i,db} - MC_{f,db}\right) \quad [3\text{-}16]$$

where $\dot{m}$ is the moisture flow rate [kg/s], $MC_{\mathrm{i,db}}$ and $MC_{\mathrm{f,db}}$ are initial moisture and final moisture content in dry basis, respectively.

3.4.7. Total steam condensing load

The measurement of cooling load is very important for understanding the capacity of the system. The data was recorded by calculation of load generated by the product in the form of water vapor. The water vapor that needs to be cooled or condensed is highest at the start and will decrease as the freezing progresses. The cooling load can be calculated by the given formula (Incropera et al., 2006):

$$q = \dot{m} \times \Delta h \quad [3\text{-}17]$$

where the mass flow rate of water vapor can be calculated from Equation 3-16.

The change in enthalpy is given as:

$$\Delta h = \dot{m} \times [h_{fg} + h_{fs} + C_{p,steam} \times \Delta T_{steam} + C_{p,water} \times \Delta T_{water} + C_{p,ice} \times \Delta T_{ice}] \quad [3\text{-}18]$$

where the latent heat of vaporization, h_{fg} [kJ/kg] can be calculated as:

$$h_{fg} = 2.792 \times 10^4 \times \left(P_s^{-0.002049}\right) - 25410 \quad [3\text{-}19]$$

and the latent heat of fusion, h_{ls}, is 334 kJ/kg, the $C_{p,ice}$ is 2.11 kJ/kg (at 1.33 kPa), the specific heat of steam and water, $C_{p,steam}$ and $C_{p,water}$ [kJ/kgK] can be calculated as:

$$C_{p,steam} = 1.854 + 0.0004965 \times T_{cond,in} + 4.044 \times 10^{-6} \times T_{cond,in}^2 + 8.247 \times 10^{-8} T_{cond,in}^3$$
$$C_{p,water} = 4.211 - 0.00147 \times T_{cond,in} + 1.497 \times 10^{-5} \times T_{cond,in}^2$$

[3-20]

where P is the water vapor pressure [kPa] and $T_{cond,\,in}$ is the steam inlet temperature [^{o}C], $\Delta T_{steam} = (T_{sat} - T_{cond,in})$, $\Delta T_{water} = (T_{sat} - 0.01)$, and $\Delta T_{ice} = (T_{evap} - 0.01)$. Equations 3-19 and 3-20 were developed by fitting polynomial curves to the steam table data (Incropera et al., 2006).

3.4.8. Heat transfer coefficient for the refrigerant inside the condenser coils - preliminary

In a surface condenser, the water vapor (hot fluid) in the shell side condenses on interaction with the helical tube carrying the refrigerant (R404a). The refrigerant convective heat transfer coefficient can be calculated by using the following correlation for heat transfer in coils (Bai et al., 1999):

$$Nu \times \mathrm{Pr}^{-0.4} = \frac{1}{41} \mathrm{Re}^{5/6} \left(\frac{D_{i,s}}{D_{o,s}} \right)^{1/12} \left[1 + \frac{0.061}{\left(\mathrm{Re} \left(\frac{d_{i,c}}{d_{o,c}} \right)^{2.5} \right)^{1/6}} \right] \qquad [3\text{-}21]$$

where Nu = Nusselt number and Re = Reynolds number, which can be calculated as (Incropera et al., 2006):

$$\mathrm{Re} = \frac{4 \times \dot{m}_{ref}}{\pi \times \left(D_{o,s} - D_{i,s}\right) \times \mu_{ref}} \qquad [3\text{-}22]$$

For a mass flow rate of 0.00277 kg/s (manufacturer's data) where, viscosity μ_{ref} [Pa.s] can be calculated as a function of temperature (Dupont™ SUVA® R404a, 2009):

$$\mu_{ref} = \frac{180.7 - 2.46 \times T_{ref,in} + 0.0202 \times T_{ref,in}^2 - 1.3 \times 10^{-4} \times T_{ref,in}^3}{10^6} = 0.000222 \text{ Pa.s} \qquad [3\text{-}23]$$

The Prandtl number is given by:

$$\mathrm{Pr} = \frac{C_{p\,ref} \times \mu_{ref}}{k_{ref}} = 3.502 \qquad [3\text{-}24]$$

where C_{p} [kJ/kgK], the heat capacity of the R404a, can be calculated as a function of temperature (ASHRAE, 2006):

$$Cp_{ref} = 1.345 + 0.004435 \times T_{ref,in} + 6.91 \times 10^{-5} \times T_{ref,in}^2 + 2.113 \times 10^{-6} \times T_{ref,in}^3 = 1.287 \text{ kJ/kgK} \qquad [3\text{-}25]$$

Similarly, the thermal conductivity of R404a can be calculated as a function of temperature (Dupont™ SUVA® R404a, 2009):

$$k_{\mathrm{ref}} = \frac{76.7 - 0.333 \times T_{\mathrm{ref,in}} + 1.38 \times 10^{-4} \times T_{\mathrm{ref,in}}^2 - 1.06 \times 10^{-5} \times T_{\mathrm{ref,in}}^3}{10^3} = 0.082 \text{ W/mK} \qquad [3\text{-}26]$$

Therefore, the heat transfer coefficient, h [W/m^{2}K], of R-404a in a spiral coil tube can be given as:

$$h_{ref} = \frac{k_{ref} \times Nu}{D_{i,s}} = 160 \text{ W/m}^2\text{K} \quad [3\text{-}27]$$

where the Nusselt number was calculated as Nu = 12.42.

3.4.9. Heat transfer coefficient for steam and thickness of ice formation - preliminary

Condensation of water vapor on the surface of the evaporator coil is an important consideration for future design of condensers for vacuum frying system. A simplified heat transfer model can be used to determine the ice production rate at the wall of the condenser tube (spiral). Heat is conducted through the copper and ice layer, and then convected through the steam mixture. The heat removal rate from the steam by the refrigerant drives the ice formation. The thickness of the ice changes with time and add resistance via increase in the frost layer thus reducing the heat exchange efficiency.

The appropriate thickness and porosity of the frost must be matched to experimental data to determine a frost formation modeling methodology.

The heat transfer, q [W], through the coil and frost can be modeled as (Incropera et al., 2006):

$$q = \frac{\Delta T}{\frac{1}{2\pi r_{steam} h_{steam} L} + \frac{\ln(r_{ice} / r_{cop2})}{2\pi k_{ice} L} + \frac{\ln(r_{cop2} / r_{cop1})}{2\pi k_{cop} L}} \quad [3\text{-}28]$$

where ΔT the temperature gradient (T_{steam}-T_{refrig}), h the convective heat transfer coefficient [W/m^{2}K], k the thermal conductivity [W/mK], and r the radius [m]. Note that $k_{ice}^{'} \approx (1 - porosity)^2 \times k_{ice}$ (Anderson et al., 2001).

Therefore, the mass rate of ice [kg/s] formation can be calculated as:

$$\dot{m}_{ice} = \frac{q}{h_{fg} + h_{fs} + C_{p,steam}\Delta T_{steam} + C_{p,water}\Delta T_{water} + C_{p,ice}\Delta T_{ice}} \quad [3\text{-}29]$$

where h_{fg} and h_{fs} are the latent heat of vaporization and fusion [kJ/kg], respectively. The thickness of ice [m] produced can be calculated as:

$$d_{ice} = \frac{\Delta t \times \dot{m}_{ice}}{\rho_{ice} \times A} \quad [3\text{-}30]$$

where ρ_{ice} is the density of the ice [kg/m^3].

The h_{steam} may be calculated by assuming that the steam flow rate, once it leaves the potato slices, depends on the pump air displacement value (5.6 CFM = 2.93 m/s inside the condenser). So for flow across a cylinder, the following empirical equations can be used to calculate the convective heat transfer coefficient for steam, which include convection and condensation (Incropera et al., 2006; Singh and Heldman, 2001):

$$\mathrm{Re} = \frac{\rho_{steam} \times v_{steam} \times D_c}{\mu_{steam}} \quad [3\text{-}31]$$

$$Nu = \frac{h_{conv} \times D_c}{k_{steam}} = 0.989 \times \mathrm{Re}_D^{0.33}\ \mathrm{Pr}^{1/3} \quad [3\text{-}32]$$

$$h_{cond} = 0.729 \times \left[\frac{g \times \rho_l \times (\rho_l - \rho_v) \times k_l^3 \times h_{fg}^{'}}{\mu_l \times (T_{sat} - T_s) \times D} \right]^{1/4} \quad [3\text{-}33]$$

where Re is the Reynolds number (~ 0.4 to 4.0) and Pr is the Prandtl number; g is the gravity acceleration [9.8 m/s^2], T_s is surface temperature [C] and $h_{fg}^{'} = h_{fg} + 0.68 \times C_{p,l}(T_{sat} - T_s)$ [kJ/kg]. The subscripts l and v denote liquid and vapor, respectively. The values for the convection and condensation heat transfer coefficients for steam should be in the order of ~ 5 and 10,000 W/m^{2}K, respectively.

With a known convective heat transfer coefficient for steam, an experimental data can be used to fit the model to determine the appropriate k'_{ice} from the porosity of the ice.

3.5. Mathematical modeling of condenser process simulation

The condenser system comprises of a refrigeration unit with a secondary fluid-to-refrigerant evaporator (shell-and-coil heat exchanger). This evaporator/heat exchanger acts as a condenser in the vacuum frying process. To study the condenser components, the mathematical calculations for sizing the system and estimation of process parameters was carried out. The refrigeration condenser system uses the following components:

1. Compressor (1/3HP, Copeland™, model AFE11C3E-IAA-103)
2. Condenser (Copeland™, air-cooled)
3. Capillary tube
4. Heat exchanger (shell-and-coil)

3.5.1. Compressor sizing

The reciprocating Copeland™ 1/3 horse power compressor comes as a part of the M4FL0033 condensing unit (United Refrigeration, Houston, TX). The following performance data were provided from the manufacturer for performance calculation of the overall system (Table 3-2).

Pressure ratio (*PR*), which can be defined as the ratio of compression gas pressures at inlet (P_1) and outlet (P_2) points of the compressor (Bloch, 2006):

$$PR = \frac{P_2}{P_1} \qquad [3\text{-}34]$$

Volumetric Efficiency, which can be defined as the ratio of the actual delivered induced gas volume to the swept volume of the cylinder (Bloch, 2006):

$$\eta_v = 1 - \frac{V_i}{V_s} \times \left(PR^{1/n} - 1 \right) \qquad [3\text{-}35]$$

where V_i is induced volume [m^3] and V_s is swept volume [m^3], and n is the polytropic exponent or index.

Table 3-2. Reciprocating compressor mechanical and performance data provided by manufacturer (Copeland™ Compressor model AFE11C3E-IAA-103).

Compressor Data	**Value***	**Type**
Number of cylinders	1	Mechanical Data
Bore Size [m] (in)	0.02649 (1.043)	
Stroke [m] (in)	0.01592 (0.627)	
Displacement [m^3/rev] (in^3/rev)	8.7834 x 10^{-6} (0.536)	
Displacement [m^3/min] (ft^3/hr)	0.3072 (65.10125)	
Evaporator Temperature [^oC] (^oF)	-23.3 (-10)	Performance Data
Condenser Temperature [^oC] (^oF)	48.9 (120)	
Return Gas Temperature [^oC] (^oF)	4.4 (40)	
Capacity [W](Btu/hr)	287 (980)	
Power [W]	380	
Current [A]	5.5	
EER [kJ/W-h] (Btu/W-h)	2.72 (2.6)	
Mass flow rate [kg/s] (lb/hr)	0.00277 (22)	
Ton of refrigerant	0.082	

*****Conversion for enthalpy – h[Btu/lb] = {h[kJ/kg]-h(ref)}*0.43021, h(ref) = 145.6 kJ/kg

The coefficient of performance (COP) is defined as the ratio of the useful effect or desired energy transfer accomplished by the evaporator to the work done by the compressor. COP becomes equal to the ratio of enthalpy change in the evaporator (h_2-h_1) and enthalpy increase during compression (h_3-h_2) (Khan and Zubair, 1999):

$$COP = \frac{h_2 - h_1}{h_3 - h_2} = \frac{3.314}{EER} \qquad [3\text{-}36]$$

where EER is energy efficiency ratio. Figure 3-15 illustrates an example of enthalpy values in the *P*-*h* diagram for R-404a showing a refrigeration cycle.

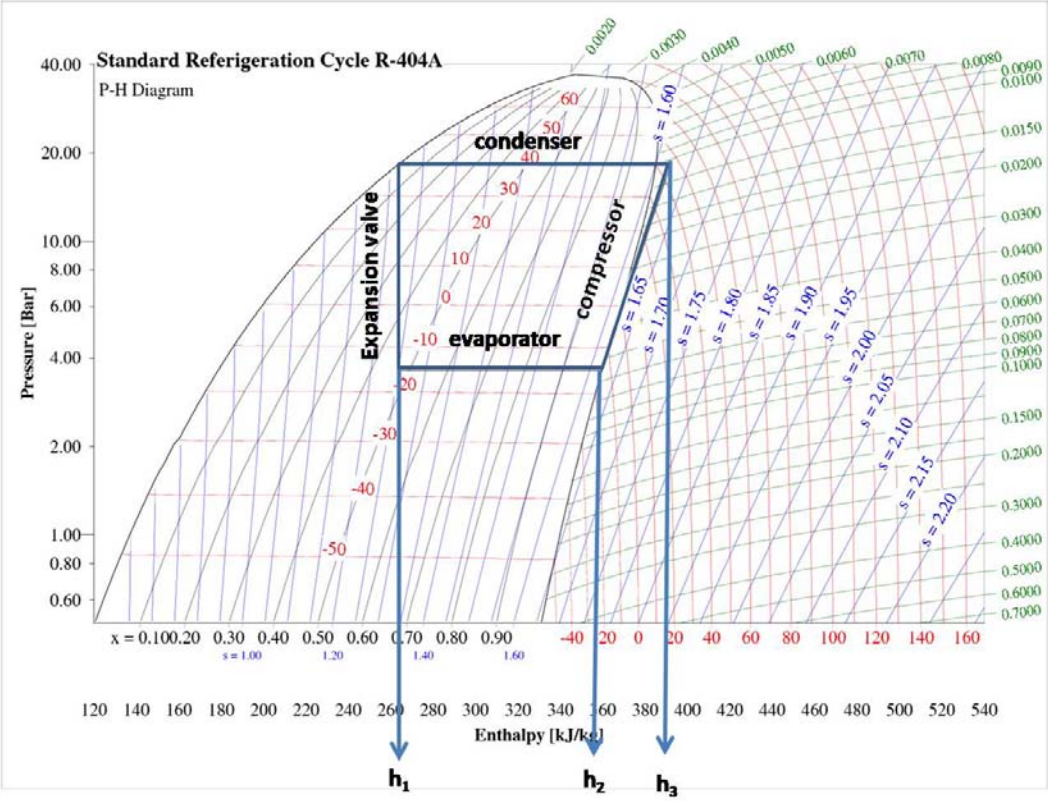

Figure 3-15. A pressure-enthalpy chart for a vapor-compression refrigerant cycle.

Isentropic efficiency is the efficiency of the compressor at constant entropy or without heat transfer. Therefore, isentropic efficiency of the system can be defined as a ratio of actual work (change in entropy) to the isentropic work (no change in entropy). It can be represented as:

$$\eta_{isen} = \frac{\left(h_{g,isen} - h_{g,suc}\right) \times \dot{m}_{ref}}{W_{comp}} \qquad [3\text{-}37]$$

where W_{comp} is the compressor work [J].

3.5.2. Air-cooled condenser sizing

The air-cooled condenser cools down and condenses the refrigerant from high-temperature compressed vapor to low temperature liquid. It essentially works as the phase change heat exchanger, consisting of a large number of fins cooled by a motorized fan assembly. The manufacturer data for the air-cooled condenser was used to evaluate its performance.

The air volume flow rate of the fan is 220 CFM or 6.22 m^3/min, with a total heat exchange area of 0.0167 m^2. The refrigerant mass flow density was calculated by dividing the mass flow rate m_{R404a} (0.00277 kg/s) of the refrigerant by the total heat exchange area to give 0.166 kg/m^2.s. The refrigerant return gas temperature was 4.4^oC with -21^oC of sub cooling temperature. The air-cooled condenser performance capacity at an evaporator temperature of -26^oC and 41^oC condenser temperature was 355 W.

3.5.3. Capillary-tube line sizing

A capillary tube is basically a metering device used to restrict the flow of the refrigerant in a smaller diameter tube. After the refrigerant comes out of this small tube to the bigger tube of the evaporator, it expands rapidly, causing it to cool down and absorb the heat load on the evaporator coil. The capillary tube size was kept at 0.762 m in a 0.00254 m thick copper tube to meet low temperature application requirements (Wile, 1977).

3.6. Frigosim™ simulator

Frigosim™, a simulator designed by Thorbergsen Frigosoft Company, Norway, is a Windows-based simulation tool for design of refrigeration and heat pumps-based plants. The program provides insertion of both direct and indirect basis components and user-defined fluid parameters. The program then represents each component in graphical form as shown in Figure 3-16. Each component can be connected to each other. Line sizes and connection details can also be set. Every part of the system layout can be introduced with various control parameters and boundary conditions. Error tracking is also relatively fast with the help of graphical representations. The component parameters may have constant values or be a function of 2 to *n* different variables. A correlation between two parameters can also be fitted to find the required data.

In this research, for modeling in Frigosim™, various process variables were separately modeled along with equipment sizing calculations using a built-in material library for R-404a refrigerant data and defining while steam thermodynamic data through experimental values obtained during vacuum frying.

3.6.1. Model assumptions

The model was based on the following assumptions:

- No steam comes out of the main evaporator condenser ($\dot{m}_{cond,out} = 0$).
- The vacuum pump is a standard inverse pump working at a similar flow rate.
- The compressor is powered by an external motor rather than a built-in motor without loss.
- The mass flow rate of steam in the system varies with respect to the time-based correlation (Equation 3-16).
- The refrigeration cycle is close to ideal conditions using theoretical parameters and manufacturer's data.

Figure 3-16 shows the system layout in the frigosim calculation program for modeling the condenser refrigeration cycle.

3.7. Mathematical modeling of vacuum fryer

The mathematical modeling is analysis of the complex process of both heat and mass transfer during the process of vacuum frying. The complete analysis was done by design of the vacuum fryer vessel and condensing unit on COMSOL™ multiphysics and Frigosim™ respectively.

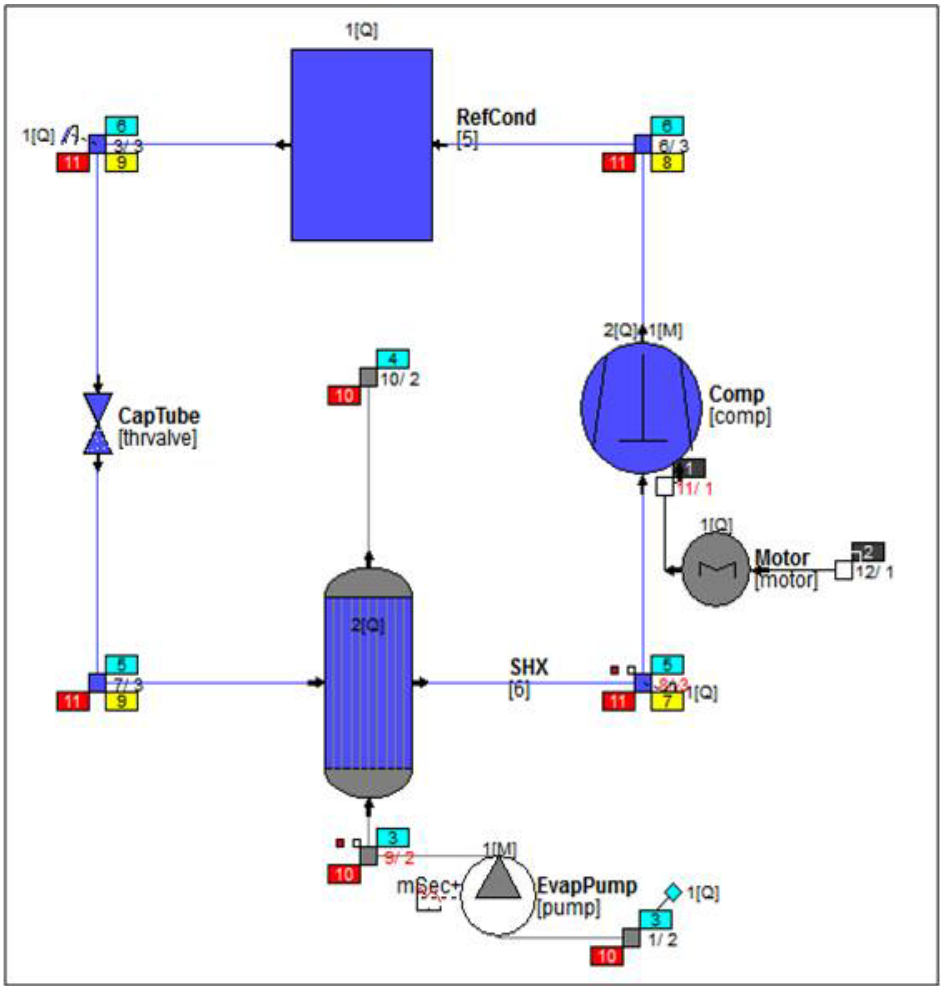

Figure 3-16. The system layout in the Frigosim^{TM} calculation program for refrigerated condenser system including vacuum pump with regulated vapor mass flow rate.

3.7.1. COMSOL™ simulation for heat transfer inside vacuum fryer

3.7.1.1. Introduction

The Finite element method FEM is used most commonly to solve complex heat and mass transfer problems. A stationary, steady-state analysis of heat transfer was required for simulating the vacuum frying pan and to better understand the heat transfer in different modes (i.e., conduction, convection, and radiation) inside the vacuum fryer

in stand-by position. The temperature distribution during heat transfer analysis consisted of a coil transferring heat to canola oil by convection and the canola oil to aluminum fryer wall by conduction at 120^{o}C. The main assumption was that heat transfer inside the frying vessel must consist of conduction, convection, and radiation for a coil temperature of 120^{o}C and vacuum pressure of 1.33 kPa. This model was designed as a first step to understand the temperature profile of the vacuum frying vessel after depressurizing at 1.33 kPa. This temperature profile helped in understanding the moisture loss in raw potato slices when kept in a vacuum before submerging them into hot oil for frying.

COMSOL™ multiphysics, Los Angeles, is a FEM modeling tool that provides user a GUI for designing/importing a 1-D, 2-D, or 3-D geometry object for analysis. COMSOL™ converted these geometries into various subdomains that can be discretized into nodes with different material properties. Finally, a problem was stated with various boundary conditions observed in the real time experiments. An important step before solving the problem is to create a mesh around the surface of the object and to divide each domain into various finite elements.

The FEM is a numerical method to solve problems in form of partial differential equations (PDEs). The basic characteristic of a FEM is the discretization of a mesh into a set of sub domains called as elements. A PDE is used to form a given relationship for each element in the continuum that on solving predicts various unknown parameters in an existing relationship.

Both the steady state and parametric analyses were performed for understanding the mode of heat transfer inside the vacuum frying vessel. The PDE heat transfer

equation, also known as the "heat equation" for all modes of heat transfer can be stated as (COMSOL™, 2005):

$$\rho C_p\left(\frac{\partial T}{\partial t}+(u\bullet\nabla)T\right)=-(\nabla\bullet q)+\tau:S-\frac{T}{\rho}\bigg|_p\left(\frac{\partial p}{\partial t}+(u\bullet\nabla)P\right)+Q \qquad [3\text{-}38]$$

where C_p is the specific heat capacity at constant pressure [J/(kg·K)], u is the velocity vector [m/s], T is absolute temperature [K], q is the heat flux by conduction [W/m^2], τ is the viscous stress tensor [Pa], S is the strain rate tensor [1/s], ρ is the density [kg/m^3] and P is pressure [Pa].

3.7.1.2. Constants used in the model

In the design of the 2-D and 3-D models, the constant values in Table 3-3 were used to specify different properties of the vacuum condition, ambient pressure, and temperature, and thermal properties of canola oil.

Table 3-3. Constants for various subdomains for the vacuum frying system.*

Parameter	Value	Description
P_{vacuum} [Pa]	$1.33x10^3$	Vacuum pressure
P_{amb} [Pa]	$1.00x10^5$	Ambient pressure
T_{amb} [^oC]	20	Ambient temperature
k_{oil} [W/mK]	0.180	Thermal conductivity of canola Oil
C_{poil} [J/kgK]	1910	Heat Capacity of canola Oil
ρ_{oil} [kg/m^3]	915	Density of canola Oil
Length-side [m]	0.3048	Length of fryer outer wall
Length-top-mid [m]	0.0762	Length of top lid mid section
Length-top-end [m]	0.0508	Length of top lid end section
Length-edges [m]	0.0254	Length of the lid and fryer edges
Length-bottom [m]	0.13	Length of the bottom (radius)

*Canola oil properties (Przybylski, n.d.).

3.7.1.3. Subdomain settings of the model

In 2-D axial symmetric diagram, five subdomains were formed from the 2-D fryer geometry imported from AutoCAD import module. The fryer model's physical properties were defined under various subdomains. A control volume of air (subdomain 1 in Figure 3-17) was formed around the vacuum fryer geometry to create a temperature and pressure gradient between fryer vessel and ambient conditions; free convection was allowed in this subdomain.

The air behaves as an ideal gas and the density Equation 3-39 and the specific heat ratio Equation 3-40 are calculated according to reference pressure and specific gas constant given by:

$$\rho = \frac{P + P_{ref}}{R_s T} \qquad [3\text{-}39]$$

$$\gamma = \frac{Cp}{Cp - R_s} \qquad [3\text{-}40]$$

where P is the actual pressure of the gas, P_{ref} is the reference pressure, and R_s is the specific gas constant.

The constants for this subdomain were defined in the COMSOL^{TM} program, as shown in Table 3-3. The material properties were taken from inbuilt library for air at 1 atm pressure. Similarly, subdomain 2, 4 for an aluminum vessel and tungsten coil was defined using COMSOL^{TM} library material properties. Subdomain 3 for canola oil was defined using constants as function of temperature in the subdomain settings with free convection.

Finally, subdomain 5 was introduced as library material air at 1 atm and pressure (P_{amb}) was used as function of temperature given as constant 1.33 kPa in Table 3-3. Figure 3-17 and Table 3-4 depict the subdomain governing equations for the 2-D axial symmetric model.

The parameters in Table 3-4 show various subdomain specific properties including temperature, pressure, material type, heat transfer mechanism and material related physical properties for each domain. The partial differential equations that govern the each sub domain consisting of parts specific to the modes of heat transfer.

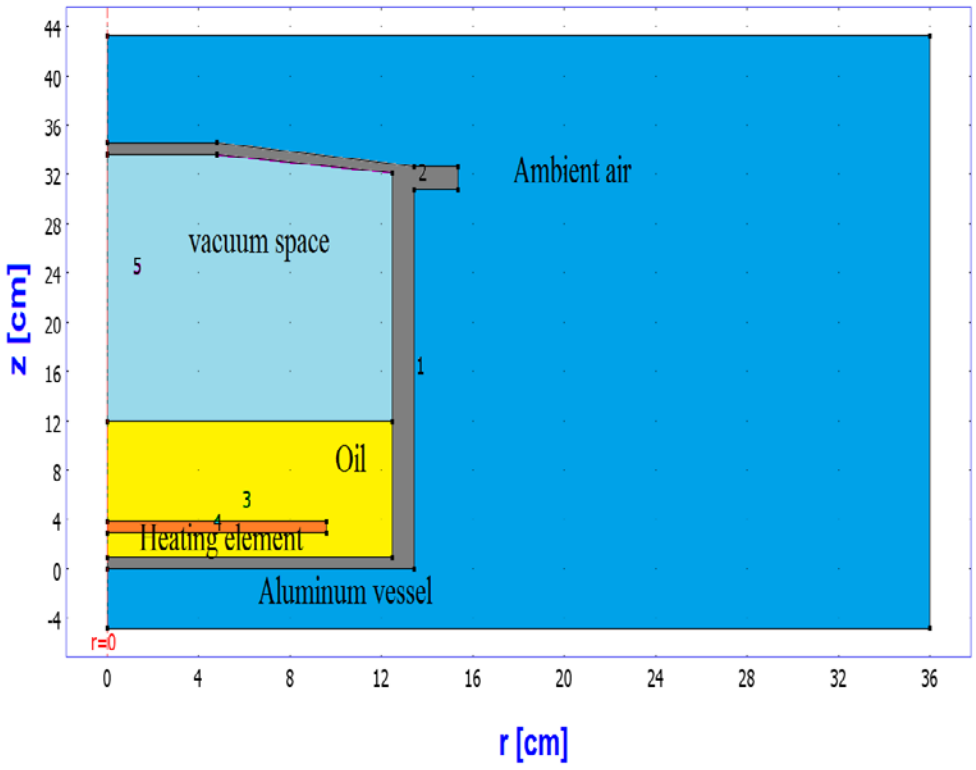

Figure 3-17. The various subdomains of the vacuum fryer in a 2-D axial symmetric model.

Table 3-4. Subdomain equations for the vacuum frying system.

Number	Subdomain Name	Subdomain governing PDE equations	Subdomain parameters
1	Ambient Air	$\nabla \cdot (-K\nabla \mathrm{T}) = \mathrm{Q} - \rho \mathrm{C_p} \mathrm{u} \cdot \nabla \mathrm{T} + \eta \left[\nabla \mathrm{u} + (\nabla \mathrm{u})^{\mathrm{T}} - \left(\frac{2}{3}\right)(\nabla \cdot \mathrm{u})\mathrm{I}\right] : \nabla \mathrm{u}$	• Ideal Gas • Viscous heating • Transparent • T_{ambient} • P_{ambient} • Convection
2	Aluminum vessel	$\nabla \cdot (-K\nabla \mathrm{T}) = \mathrm{Q}$	• Material: 1050 (UNS: A91050) • Opaque • Conduction
3	Canola Oil	$\nabla \cdot (-K\nabla \mathrm{T}) = \mathrm{Q} - \rho \mathrm{C_p} \mathrm{u} \cdot \nabla \mathrm{T} + \eta \left[\nabla \mathrm{u} + (\nabla \mathrm{u})^{\mathrm{T}} - \left(\frac{2}{3}\right)(\nabla \cdot \mathrm{u})\mathrm{I}\right] : \nabla \mathrm{u}$	• K_{oil} • Cp_{oil} • ρ_{oil} • Transparent • Liquid • Viscous heating • Convection
4	Copper sheathed (Tungsten Coil) tubular heating element	$\nabla \cdot (-K\nabla \mathrm{T}) = \mathrm{Q}$	• Heat source • Opaque • Q [W/m3] • Conduction
5	Vacuum Chamber	$\nabla \cdot (-K\nabla \mathrm{T}) = \mathrm{Q} - \rho \mathrm{C_p} \mathrm{u} \cdot \nabla \mathrm{T} + \eta \left[\nabla \mathrm{u} + (\nabla \mathrm{u})^{\mathrm{T}} - \left(\frac{2}{3}\right)(\nabla \cdot \mathrm{u})\mathrm{I}\right] : \nabla \mathrm{u}$	• P_{vacuum} • Transparent • Density function of pressure • Ideal gas • Radiation

3.7.1.4. Initial and boundary conditions

The boundary settings in COMSOL™ multiphysics were used for representing the problem, by stating the type of physics, in this case a heat transfer model. The heat transfer in this model followed a basic assumption that the coil (subdomain 4) is the primary source of heat, at 120^{o}C temperature.

The hot coil transfers heat directly to oil (liquid) through convection. This heat flux moves from the oil to fryer walls in various modes of conduction and radiation. The radiation takes place inside the frying vessel due to low vacuum pressure at 1.33 kPa. Radiation occurs in two different conditions between (surface and ambient) and between (surface to surface) conditions. Thus inside the closed fryer all the boundaries have radiation between surface to surface, whereas at the outer boundaries of the fryer there is surface to ambient type of radiation. The heat moves in the wall through conduction and then from vessel walls to the surrounding ambient air.

The air outside the vessel was at atmospheric (101.325 kPa) pressure. This air showed convection; heated air moved towards the fryer in an upward motion causing free natural convection of the air in the control volume. COMSOL™ multiphysics have built-in functions for calculation of convective heat transfer coefficient (h_{ave}) for natural laminar and turbulent flow on external vertical and horizontal walls of the aluminum vessel. Similarly, internal heat transfer coefficient library expressions were used for convection in air interacting with hot wall surfaces of the fryer inner walls.

The primary equation for heat transfer consists of conduction, convection, and radiation in the steady-state heat transfer system. The equation becomes the combined form of all the three modes of heat transfer given as:

$$-n_u \bullet \left(-k_u \nabla T_u + \rho_u C_{p_u} u_u T_u\right) - n_d \bullet \left(-k_d \nabla T_d + \rho_d C_{p_d} u_d T_d\right) = q_0 + h\left(T_{\inf} - T\right) + \varepsilon\sigma\left(T_{amb}^4 - T^4\right) \quad [3\text{-}41]$$

where subscripts *u* and *d* represents the normal to up and down sides of the boundary; *n* is the normal vector of the boundary, pointing out from the domain; *k* is the thermal conductivity and $T_{\inf}$ is reference bulk temperature.

In an axial symmetry, the total number of boundaries formed by the system were 27. In Figure 3-18, general boundary setting for boundaries 1, 3, 5, 7, 11, 13, and 15 represent the axial symmetry of the 2-D fryer geometry as:

$$r = 0 \quad [3\text{-}42]$$

Boundaries 2, 17, and 27 are thermal insulation across the control volume represented by:

$$q_0 = -n\left(-k\nabla T + \rho C_p u T\right) = 0 \quad [3\text{-}43]$$

The boundaries 10, 20, and 6 were set to a temperature of 393.15 K or 120^{o}C as the coil temperature prescribed at the boundary as Dirichlet type given by:

$$T = T_0 \quad [3\text{-}44]$$

Boundaries 4, 20, and 12 represented canola oil and were used to describe convective heat transfer from coil to the oil. Boundaries 12, 14, 18, and 22 were the key boundaries participating in the surface to surface radiation as part of same radiation

group 1. All the other boundaries were set to continuity in formation of the model that follows:

$$q = \varepsilon\sigma\left(T_{amb}^{4} - T^{4}\right) \qquad [3\text{-}45]$$

where ε is the emissivity and σ is the Stefan-Boltzmann constant = 5.68 x10^{-8} W/m^{2}K^4

The radiation boundary group was set to temperature boundary setting for surface to ambient radiation under group 2. The outer boundaries of the fryer wall were also considered to be participating in heat transfer by surface to ambient radiation.

Figure 3-18 depicts the boundary plot for the 2-D axis symmetric model of the fryer.

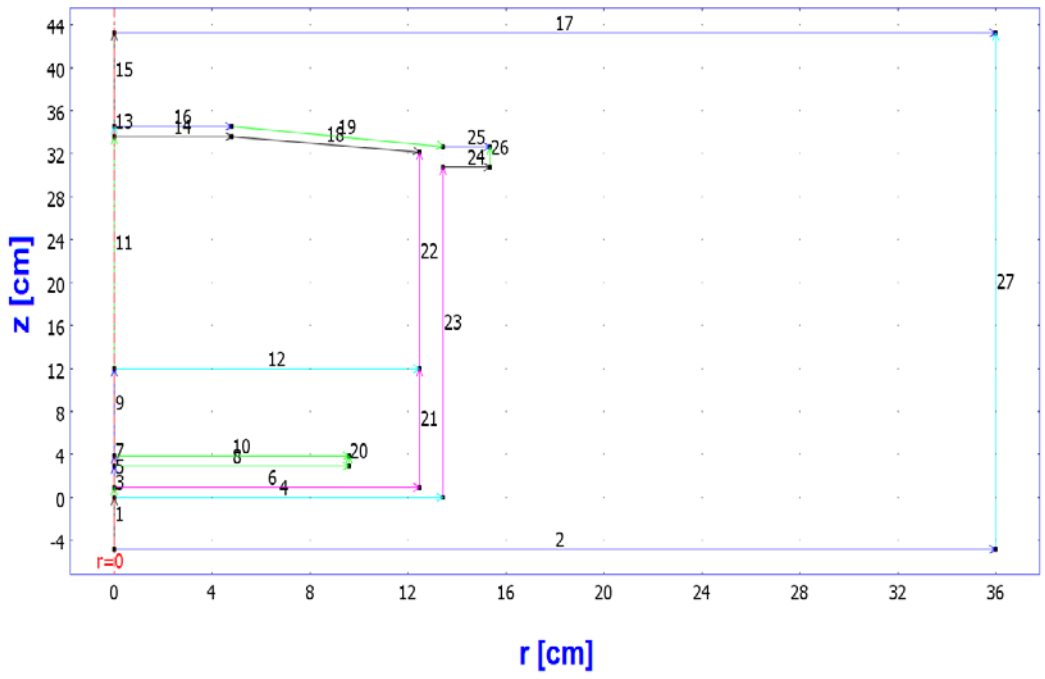

Figure 3-18. The boundary mode geometry of 2-D axis symmetric vacuum fryer.

3.7.1.5. Mesh mode

The model was meshed under fine-free mesh parameters. Table 3-5, shows the parameters used during mesh formation. Figure 3-19 depicts the mesh formed on the 2-D axis symmetric model. The mesh elements were shaped in triangular form by default and the total number of mesh elements was 2637 for a 2-D model.

Table 3-5. Mesh statistics parameters for vacuum frying vessel.

Mesh Statistics	**Parameters**
Number of degrees of freedom	5380
Number of mesh points	1372
Number of elements	2637
Triangular	2637
Quadrilateral	0
Number of boundary elements	227
Number of vertex elements	23
Minimum element quality	0.669
Element area ratio	0.08

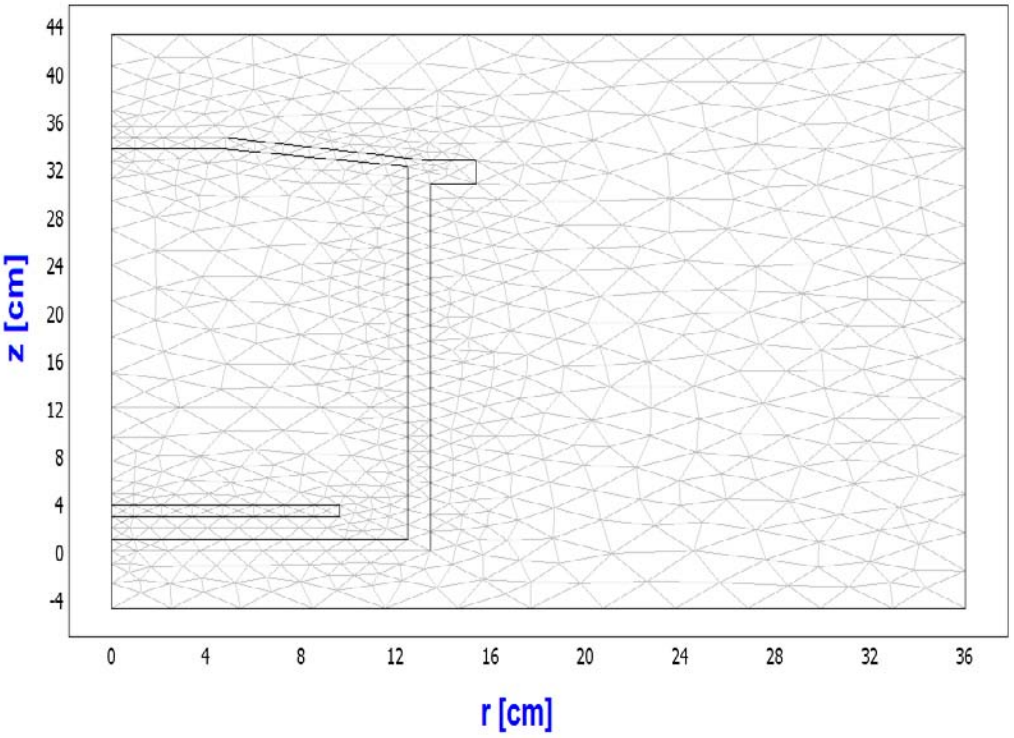

Figure 3-19. The meshed geometry of 2-D axis symmetric vacuum fryer.

3.7.1.6. 3-D model features

The 2-D axial symmetry was converted into 3-D by revolving the model around the *y*-axis. The 3-D model also allows better understanding of the heat transfer inside the vacuum fryer and will help in optimization of the fryer by using correct insulation to retain heat and increase the efficiency of the vacuum frying system. During formation of 3-D model, total 5 subdomains from working 2-D model were revolved to form a total of 76 boundaries. The 3-D fryer sketch, with all the components, used in the simulation is depicted in Figure 3-20.

Figure 3-20. The 3-D sketch of the vacuum fryer (showing the heater element and the basket with the motor) used in the simulation studies.

3.7.1.7. Subdomain and boundary mode

The 3-D fryer geometry followed the same subdomains across the revolution used for 2-D axial symmetric model although the number of boundaries increased to 76 (Figure 3-21) and were represented automatically by the 2-D axial symmetric model. The mesh setting was kept to normal and triangular by default.

The number of mesh elements were 2637 (Table 3-5) with higher degree of freedom than the 2-D model. Figure 3-22 represents the mesh diagram of the 3-D fryer vessel model.

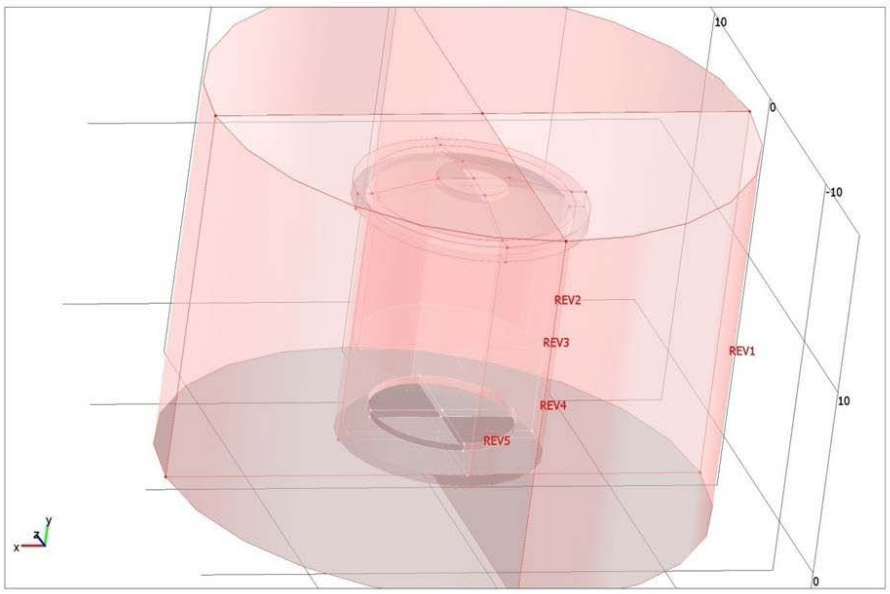

Figure 3-21. The 3-D revolution of the 2-D axial symmetric vacuum fryer vessel to obtain 3-D results.

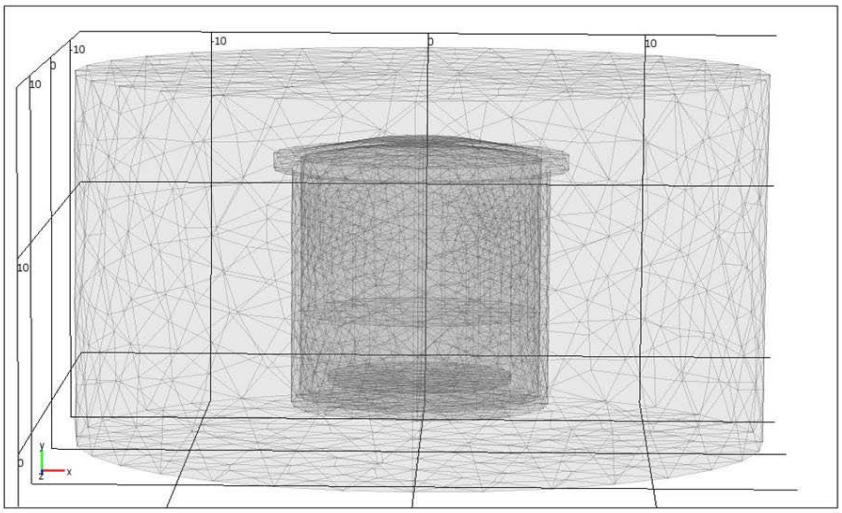

Figure 3-22. The mesh mode for 3-D model of vacuum fryer vessel in a control volume.

3.8. Microstructure analysis of potato chips

Environmental scanning electron microscopy (ESEM) was used to study the cross sectional and surface microstructure of potato chips at 120^{o}C and 140^{o}C oil temperatures in vacuum frying and 165^{o}C oil temperature in traditional frying. An Electroscan® ESEM-E3 microscope at Microscopy and Imaging Center, Texas A&M University was used for analysis of samples. A resolution of 50 μm was used at 15 kV voltages setting during sample examination. Each sample was divided into small pieces for cross-sectional and surface views.

The prepared samples were placed on an aluminum stub, covered by a conductive carbon tape, and loaded in the observation chamber. At desired resolution, the samples were analyzed at multiple points and best images were recorded. The selection criteria for best image depended upon the pore size distribution, structural discontinuities, and deterioration of starch from frying and mainly distribution of oil globules throughout the potato chips.

CHAPTER IV

RESULTS AND DISCUSSION

4.1. Condenser heat exchanger temperature history for frying potato chips (*P* = 1.33 kPa)

Figure 4-1 represents the temperature profile history for various thermocouples, collected by a data acquisition system (OMB-DAQ 54) during vacuum frying of potato chips. The figure shows average temperature readings (triplicate) of 30 g of potato chips fried at for 360 s. The time lapse (*x*-axis) during various operations was noted during frying. The average time for completing the following operations is shown in the Table 4-1. The temperature history of 9 different thermocouples was used for calculation of heat and mass transfer parameters in frying.

Table 4-1. Operations during frying and average time for completion.

Serial	Operation	Time [s]
1	Data logging started	20
2	Lid closed	52
3	Vacuum valve closed	60
4	Wait for refrigerant inlet temperature to reach -15^{o}C	210
5	Frying basket dipped in oil	210
6	Frying ends	570
7	Frying basket removed	578
8	Vacuum valve open	630
9	Pressurization	640
10	Lid open	655

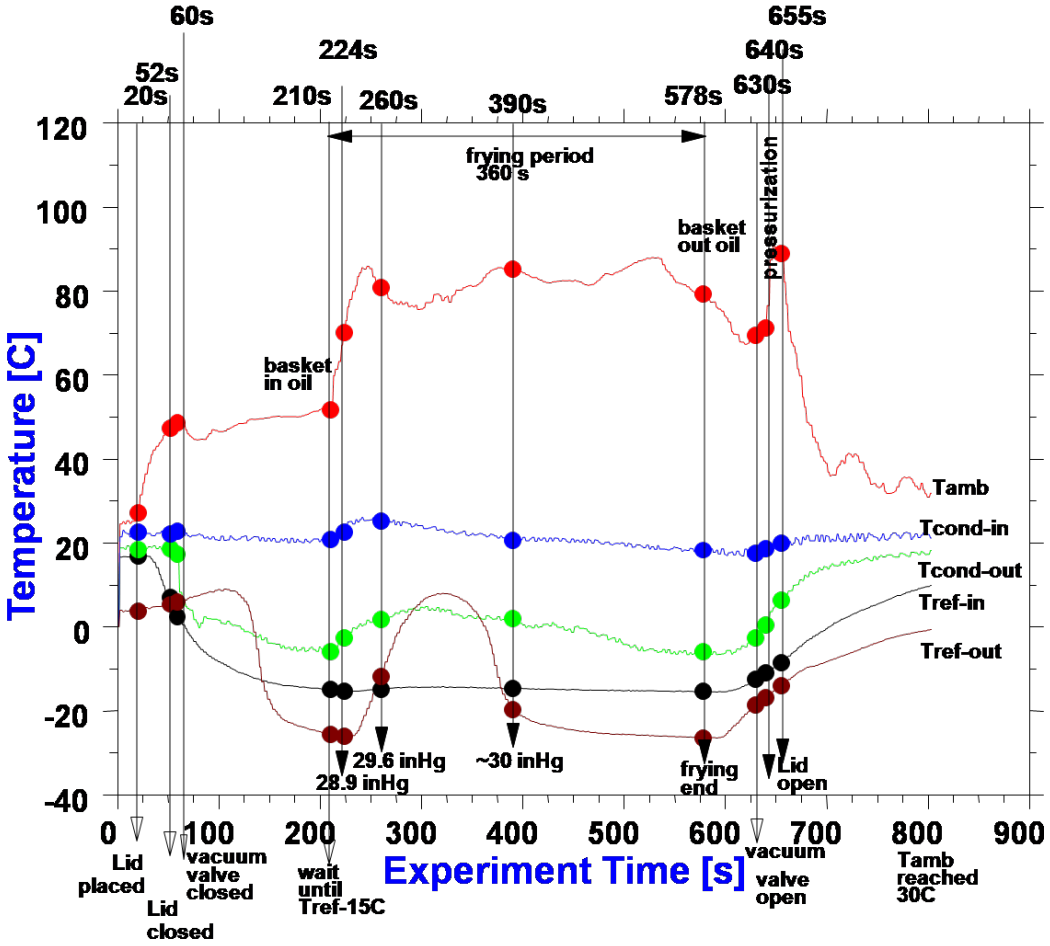

Figure 4-1. Temperature history for the vacuum frying system and condenser unit (T_{oil} = 120°C; P = 1.33 kPa; frying time = 360 s; potato slices = 30 g).

Figures on page 91 through 100 show the average temperature histories during vacuum frying of potato chips. In all the figures, each curve represents temperature history from thermocouples at different locations in the process. The vacuum gage pressure was also observed to identify changes in pressure during frying. The temperature histories were observed for different frying operation conditions. The temperature history profile for different thermocouples was recorded and is discussed below:

- T_{amb} or T_{vacuum} - The ambient temperature of the fryer head space showed a maximum rise of 90^{o}C during frying (Figure 4-1). At the beginning of the frying period the curve showed 21^{o}C to 22^{o}C (room temperature) before the fryer lid was placed on the frying vessel. On closing the fryer lid (52 s) an instant rise in temperature of this thermocouple was noted attaining 50^{o}C to 60^{o}C. On depressurizing the vessel by closing the vacuum valve (60 s) no changes were observed. This temperature rise was due to radiant heat from the hotter frying oil. A slight rise was recorded as the refrigerant ($T_{ref, in}$) reached -15^{o}C around 210 s and the fryer basket was dipped into the hot oil (T_{oil} = 120^{o}C). The vacuum gauge showed a drop in vacuum (from P_g of 29.5 in-Hg to 28.9 in-Hg or from P_{abs} of 1.33 kPa to 3.48 kPa) as soon as the frying basket was dipped into the oil and water vapor started to evaporate from the potato slices. The ambient temperature rose to around 85^{o}C (P_g increased to 29.53 in-Hg; P_{abs} = 1.33 kPa) within 20 s time of immersion. During the total frying time (360 s), the temperature deviation remained within ±5^{o}C limit.

This temperature was actually the temperature of steam and the radiant heat of hot oil and the inner walls of the frying vessel. After the frying was completed, the basket was removed from the oil (578 s), showing an instant drop in ambient temperature. After the de-oiling cycle, the vessel was pressurized by disconnecting the vacuum hose and opening the vacuum valve on the vessel (630 s). Pressurization showed a spike in temperature because of the increase in pressure in the vessel until the fryer lid was opened (655 s). The temperature slowly reached back to normal room temperature in ambient air (~25^{o}C).

- $T_{cond,\ in}$- The condenser inlet temperature was used as an indicator for calculation of log mean temperature difference (LMTD) of the steam condenser heat exchanger. Second, it helped in understanding the performance of the pre-condensing unit in the system. The temperature of steam varied between 1^{o}C and 2^{o}C, but mostly remained constant throughout the vacuum frying process at 24^{o}C to 25^{o}C.
- $T_{cond,\ out}$- The condenser outlet temperature was mainly recorded to determine any steam leakage through the steam condenser heat exchanger. During vacuum frying process the temperature fell to around 0^{o}C and remained constant with fluctuation of ±3^{o}C. The low temperature indicated a temperature well below the condensation temperature of steam at 1.33 kPa (T_{sat} = 9.14^{o}C) of vacuum, thereby suggesting that the steam condenser system was working properly without any leaks to the vacuum pump.

- $T_{ref, in}$- The refrigerant inlet temperature reached a mark of -15^{o}C operational temperature within 150 to 200 s of the vacuum frying process. This temperature always remained constant throughout the process until the condenser unit controls were switched off after the pressurization step was complete at 630 s.
- $T_{ref, out}$- The refrigerant outlet temperature showed an increase in temperature as soon as the frying basket was immersed into the oil starting at -25^{o}C (210 s). The peak of the rise reached just above 0^{o}C temperature due to superheating of the refrigerant. This denoted the way the refrigerant behaves when gaining heat from the steam through the condenser heat exchanger. After the steam coming into the condenser gradually (390 s) decreased, the temperature fell back to its normal operational value of -25^{o}C. This was also an indicator of evaporation during frying of potato slices and shows that steam mass flow rate decreased to an almost negligible value in 60 to 70 s of frying.
- $T_{comp, cond}$- This temperature represents the liquid line temperature in the condensing unit. The temperature of the compressed refrigerant reached a temperature of 40^{o}C after the condenser system was started. This temperature had little or no effect on the vacuum frying process and showed no changes during frying. This was because the compressor automatically adjusted the incoming refrigerant to a constant flow rate and cycle within the condensing unit.

- $T_{steam\ hose}$- The temperature of the vacuum hose connecting the frying vessel with the condenser system became free of radiant heat of oil and vessel walls. It was used to determine the actual temperature of steam travelling through the system just out of the frying vessel. This temperature remained constant throughout the process of frying at 24.55^{o}C to 25^{o}C. The initial steam coming out of the vacuum fryer travelled through the steam hose, thus being superheated from its saturation temperature at 1.33 kPa (T_{sat} = 9.14^{o}C). These readings were cross-verified with the steam tables; the temperature showed a perfect analog of steam existing at 9.14^{o}C at 1.33 kPa vacuum pressure.
- $T_{pre,\ cond}$- The pre-condenser performance was evaluated by recording temperature data at the entrance of the pre-condensing coil. This temperature was used to calculate the efficiency of the pre-condensing unit during vacuum frying. A comparison carried out between the main condenser inlet temperature and the pre-condenser inlet temperature is discussed in more detail later in this chapter. The peak temperature was about 35^{o}C possibly due to the higher rate of heat transfer during vacuum frying, but gradually it became similar to the condenser inlet temperature. A difference in values between these two temperatures was mathematically calculated to find the efficiency of the pre-condenser.
- $T_{cond,\ cap}$- The liquid line temperature of the condensing unit between the condenser and the capillary tube. This temperature was used to determine the working of condensing unit and refrigeration cycle. This temperature reached

a constant value of about 25°C after the condensing unit was started in Figure 4-3.

In the vacuum frying process, the water vapor liberated from the potato slices was suctioned towards the vacuum pump. The condenser system functions to store the water and condense vapors to liquid water before they reach the vacuum pump. Figure 4-4 shows the temperature data collected during the vacuum frying process. T_{vacuum} represents the temperature of space directly above the hot oil; this temperature was discussed in previous pages under T_{amb}.

The T_{vacuum} also consisted of high amount of radiant heat from hot oil at 140°C and 120°C heating up aluminum walls of frying vessel. $T_{steam\ hose}$ is the actual temperature at which the steam travels through the condenser system, around 24.55°C at 1.33 kPa vacuum. Due to pressure drop in the length of the steam hose connecting the fryer vessel with the condenser system, a drop of 3°C to 5°C was recorded between $T_{steam\ hose}$ and $T_{pre,\ cond}$ temperatures.

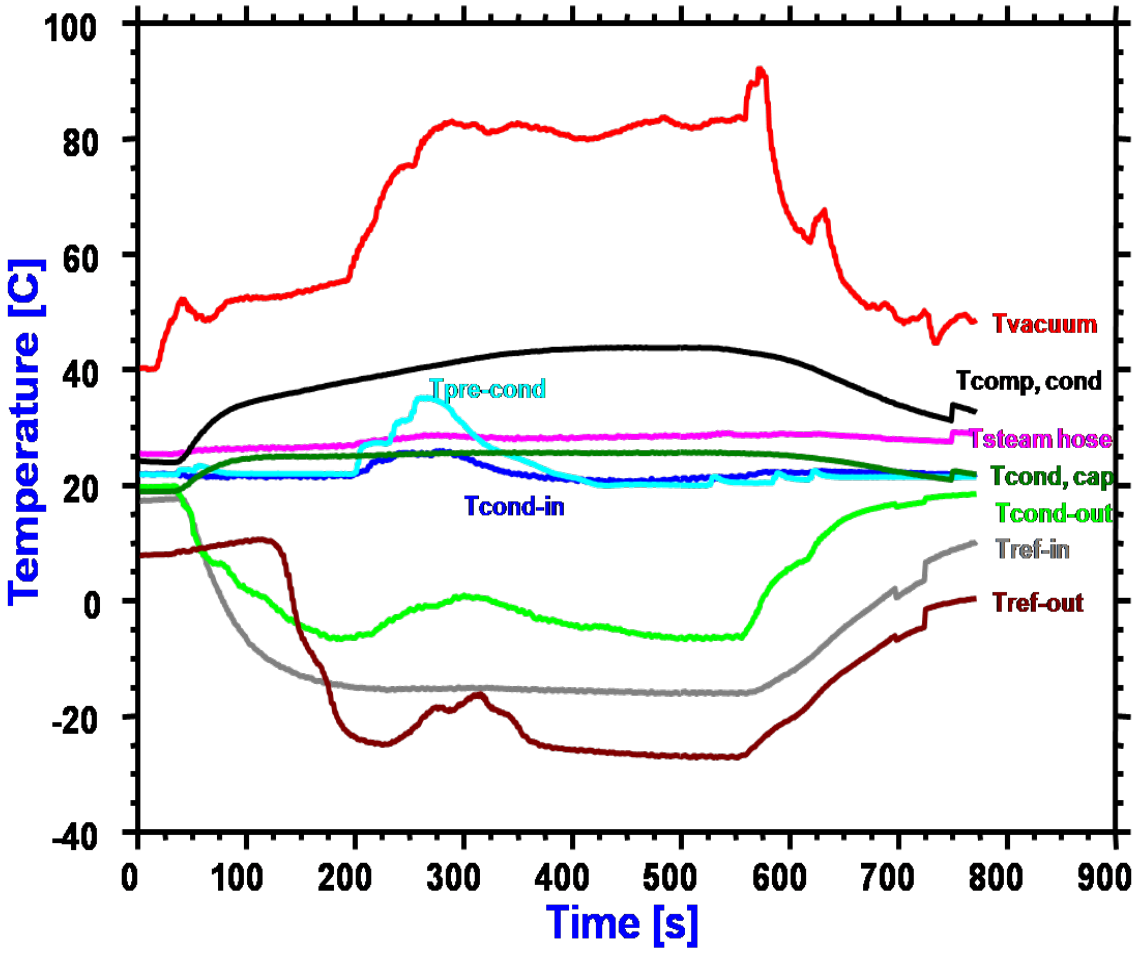

Figure 4-2. Temperature history for the vacuum frying system and condenser unit (T_{oil} = 120°C).

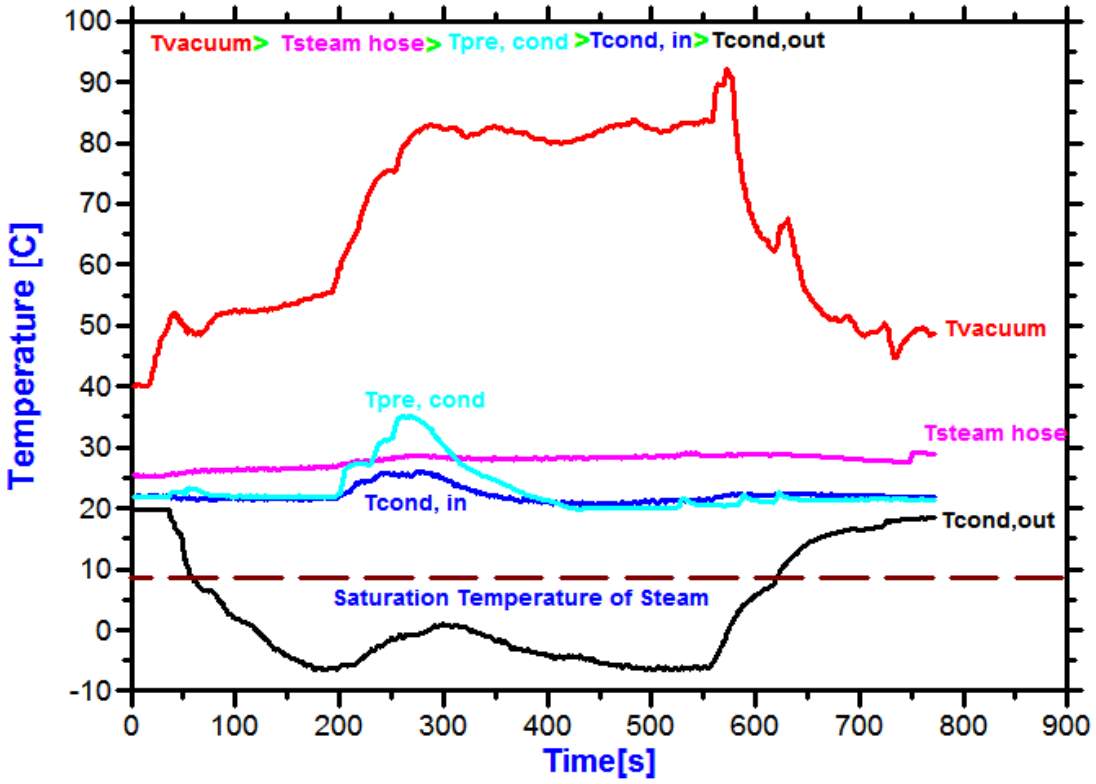

Figure 4-3. Temperature history for the steam leaving the vacuum frying system (T_{oil} = 120^{o}C).

A pre-condenser was used to reduce the load on the main condenser and thereby increase the performance of the condenser system. The temperature in the pre-condenser coil rose slightly above the steam hose temperature probably because of the copper coil being over-heated with the incoming steam and ambient air cooling load. The pre-condenser showed good performance efficiency, which is discussed in detail later in this chapter. During the vacuum frying for 360 s the temperature of the condenser inlet remained less than (9^{o}C to 10^{o}C max/1^{o}C to 2^{o}C min) the range of $T_{pre,\ cond}$ temperature. The main condenser performance could be evaluated if and only if the temperature of $T_{cond,\ out}$ never reached above the saturation temperature of steam line as shown in Figure 4-3. The condenser outlet temperature always remained below the mark of the saturation temperature line of steam at 9.14^{o}C. Thereby, showing that steam never reached the vacuum pump during the whole vacuum frying process.

4.2. Pre-condenser performance evaluation

The pre-condenser performance evaluation was done to understand the overall effect of using a pre-condenser in the main water vapor condensing line. Two thermocouples were mounted in the steam-travelling hose before and after the pre-condenser coil. During the vacuum frying process (360 s) a rise in temperature was noticed in the $T_{pre,\ cond}$ temperature. Comparing the temperature profiles by finding the difference in temperature ΔT showed that it varied from minimum 1^{o}C to 2^{o}C to 9^{o}C to 10^{o}C during the vacuum frying process. This difference successfully showed an increase in condenser system performance with a pre-condensing unit.

Figure 4-4 shows the difference in temperature between $T_{\text{pre, cond}}$ and $T_{\text{cond, in}}$ thermocouples. The temperature drop was a result of the pre-condenser design made with a helical copper tube cooled with air from a fan. During frying a maximum temperature drop of about 9^{o}C can be observed in Figure 4-4. Similarly, after completion of frying, the temperature gradient went in negative between two readings represented by $T_{\text{cond, in}} < T_{\text{pre, cond}}$ below the 0^{o}C mark.

4.3. Calculation of log mean temperature difference (LMTD)

Temperatures were recorded to find the log mean temperature difference (LMTD) as well as to calculate the heat and mass transfer coefficients and to understand the performance of the system (Figure 4-5). The LMTD is mainly used to determine the temperature driving force and is usually done on heat exchangers with constant thermal and flow properties with time (Figure 4-5).

$$LMTD = \frac{\left(T_{steam,in} - T_{evap,out}\right) - \left(T_{sat} - T_{evap,in}\right)}{\ln\left[\frac{\left(T_{steam,in} - T_{evap,out}\right)}{\left(T_{sat} - T_{evap,in}\right)}\right]} \qquad [4\text{-}1]$$

$$LMTD = \frac{\left(24.55 - (-26)\right) - \left(9.14 - (-26)\right)}{\ln\left[\frac{\left(24.55 - (-26)\right)}{\left(9.14 - (-26)\right)}\right]} = 42.38^{o}C \qquad [4\text{-}2]$$

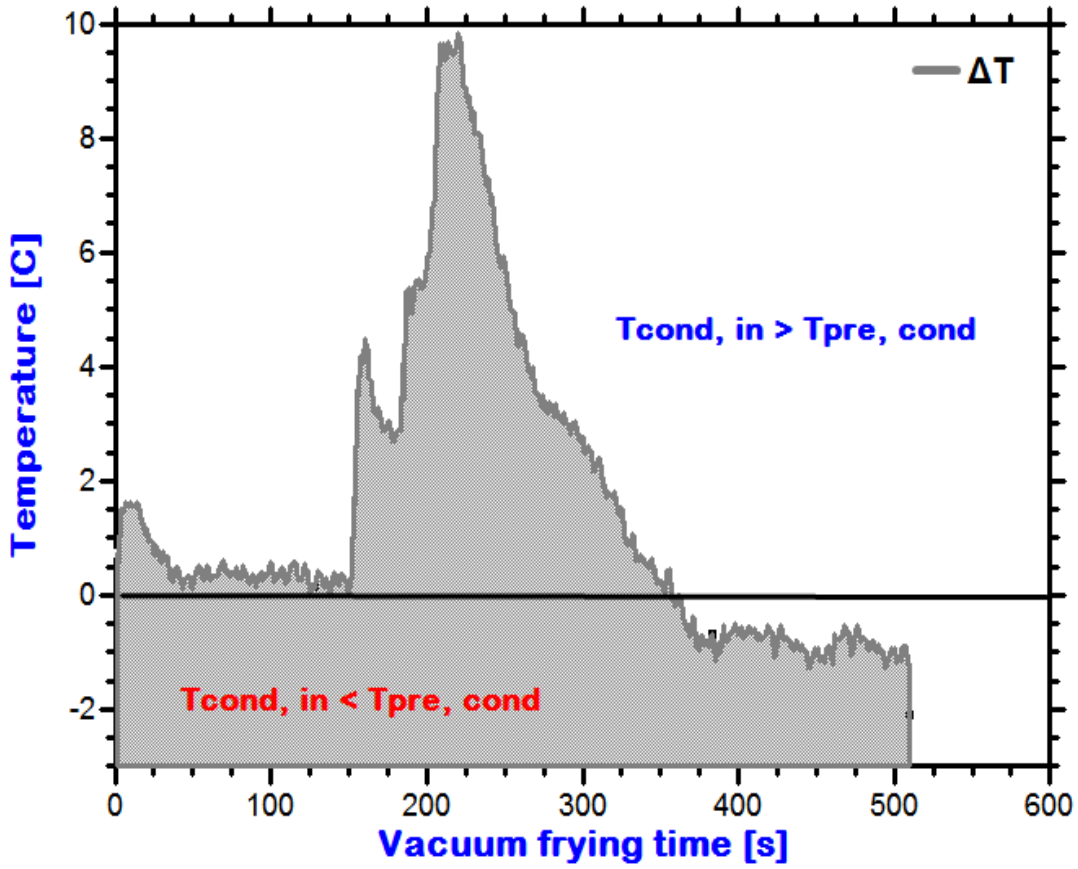

Figure 4-4. Pre-condenser efficiency history by difference in temperature between $T_{pre, cond}$ and $T_{cond, in}$ during vacuum frying at T_{oil} =120°C for 360 s frying time.

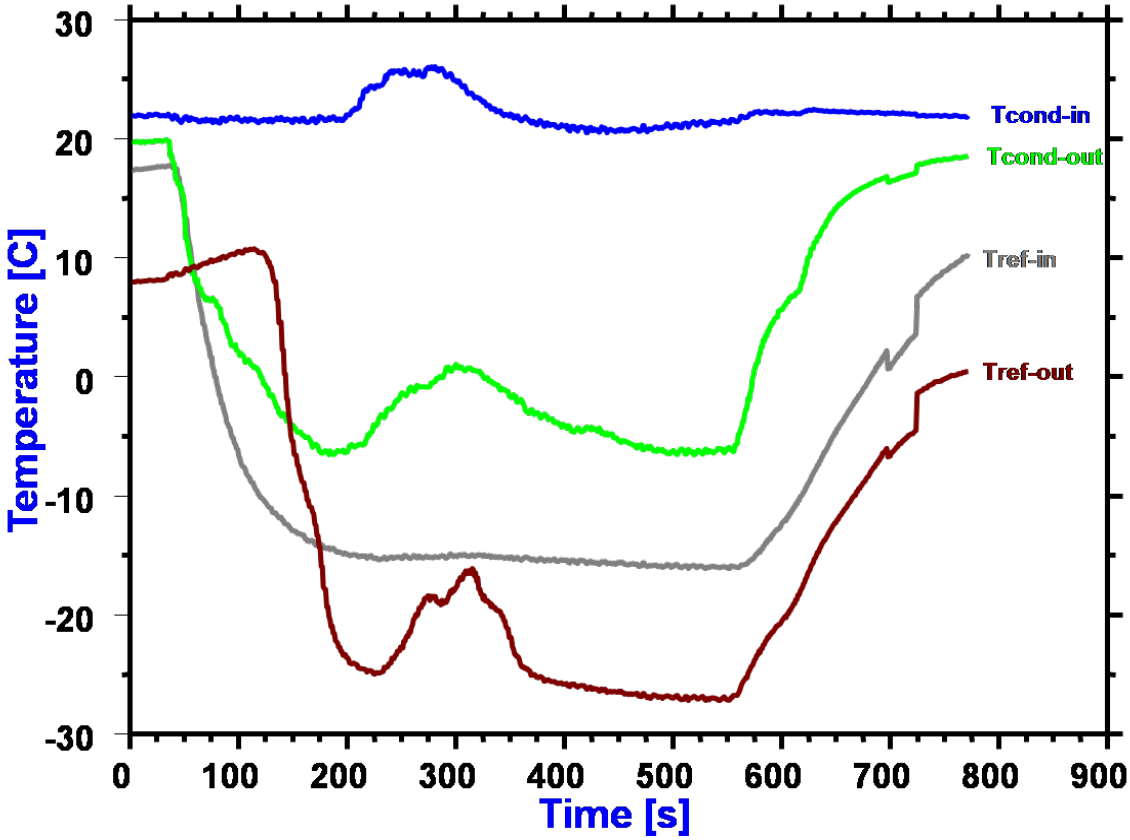

Figure 4-5. Temperature history for the steam and refrigerant entering and leaving the condenser unit (T_{oil} = 120°C).

As soon as the temperature of the refrigerant $T_{ref, in}$ reaches -15^{o}C (210 s) the vacuum frying begins (Figure 4-5). The water evaporated from the potato slices causes the temperature of the $T_{cond, in}$ and $T_{cond, out}$ to rise. In the process, heat was exchanged from the water vapor to the refrigerant, causing the $T_{ref, out}$ to rise. This profile can be easily understood by observing the LMTD for all temperatures. The larger the LMTD the more heat is transferred during the process.

Figure 4-6 shows the temperature profile in the system for frying at the temperature of 140^{o}C. The experiment was conducted at a higher temperature setting to increase the heat transfer coefficient between the oil and potato slices. The result showed increases in all temperature history profiles during the frying process. This also clarified the effect of increased mass flow rate of water vapor through the system and its effect on the condenser efficiency. According to Garayo and Moreira (2002), the convective heat transfer coefficient between the oil and the chips' surface increases with its temperature. This increase in temperature further caused faster evaporation of moisture from potato slices during frying thereby increasing the drying rate. Higher frying temperature also resulted in increased texture hardness in the final product (Garayo and Moreira, 2002).

Therefore, frying with higher oil temperature is directly proportional to the drying rate of potato slices. An increased drying rate was also verified by Figure 4-6, that depicts an increase in rapid temperature change in T_{amb} (T_{vacuum}) at oil temperature 140^{o}C(20^{o}C higher than T_{amb} at 120^{o}C oil temperature) reaching 100^{o}C maximum temperature. Similarly, $T_{pre\text{-}cond}$ reached 40^{o}C, 10^{o}C higher than $T_{pre\text{-}cond}$ at 120^{o}C. The condenser was successful in handling the product load at the oil temperatures of 140^{o}C.

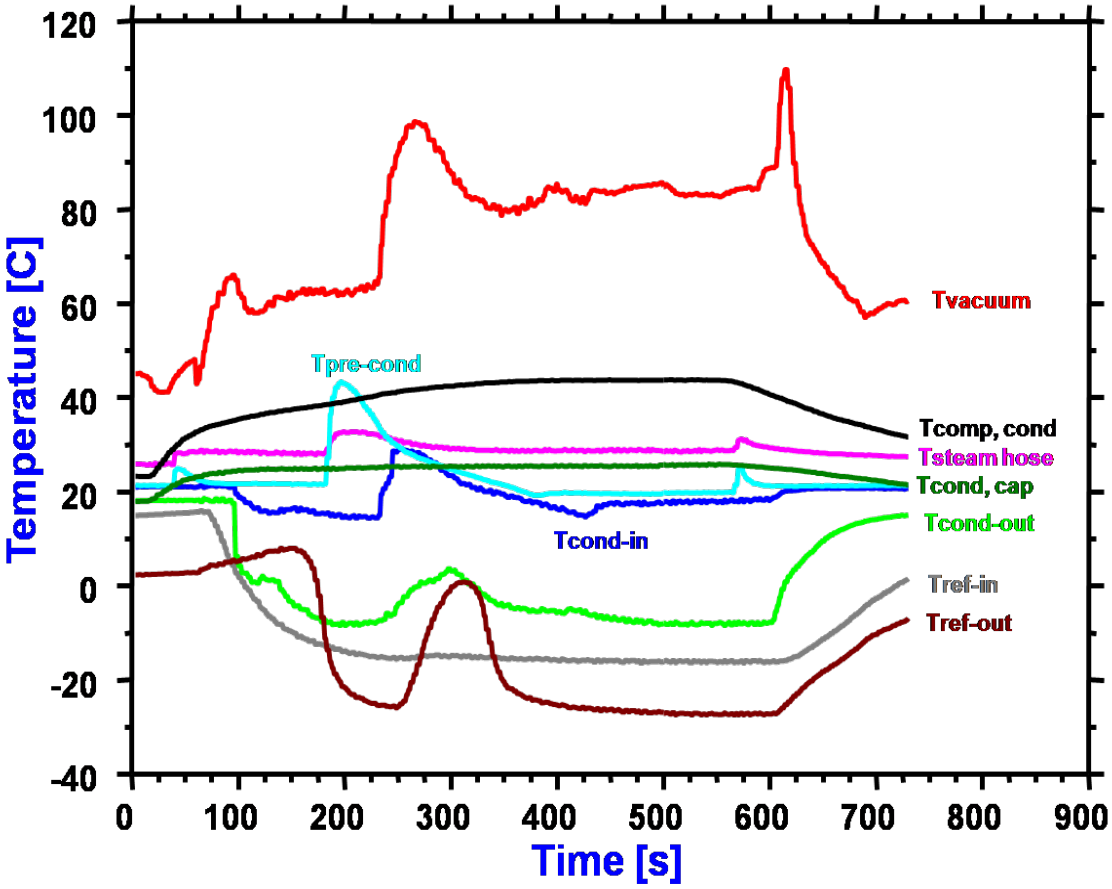

Figure 4-6. Temperature history for the vacuum frying system and condenser unit (T_{oil} = 140°C).

4.4. Effect of frying load on T_{vacuum}

For different frying loads an increase in the fryer head space (top space above the oil) temperature was recorded (Figure 4-7).The fryer head space temperature and frying time of potato slices at varying loads of 30 g, 50 g, and 70 g were compared at 120^{o}C frying oil temperature. No difference in the fryer top temperature was observed with increased load conditions. During the start of frying and after closing the vacuum fryer lid, the fryer top temperature rose to 50^{o}C irrespective of the product load in the frying basket. After that, a constant temperature was observed until the frying basket was immersed in the oil at 210 s. For potato loads of 30 g and 50 g, the immediate temperature rise in fryer top temperature was attributed to production of water vapor.

However, no significant differences were observed between loads and temperature rises. According to Moreira et al. (1999), the maximum moisture loss occurs in the first 10 s of frying, or the drying rate is the highest in the first 10 s. A slight drop in this temperature was observed until the frying was complete at 360 s. This temperature history for the fryer top temperature helped in understanding an increase in heat transfer and drying rate during vacuum frying of potato chips with various load conditions.

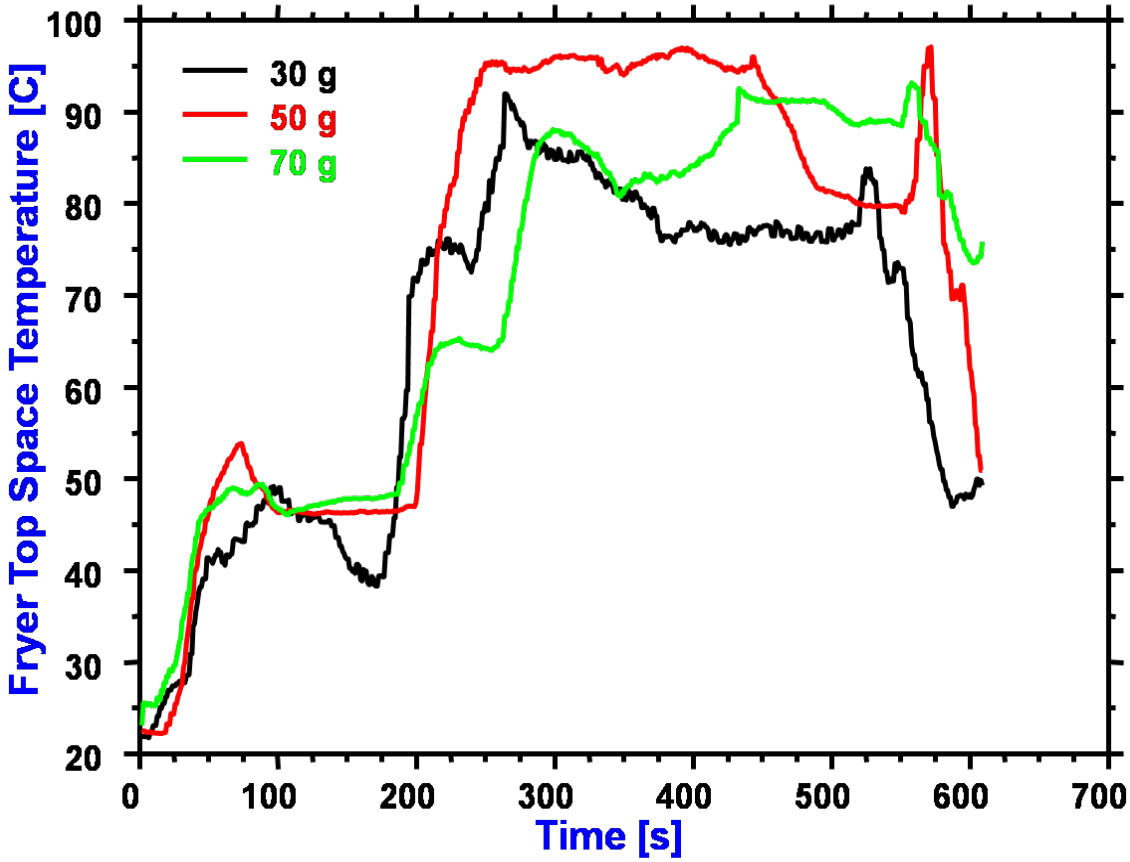

Figure 4-7. Temperature history for the top space in the vacuum fryer (T_{oil} = 120°C).

4.5. Moisture removed vs. water collected with varying product load

During the vacuum frying process, the water evaporated from the chips should completely condense in the main condenser stage. Figure 4-8 shows good agreement between the condensed water and the moisture evaporated from different frying loads of potato slices, although the variability decreased with an increase in product load from the 30 g, 50 g, and 70 g sample.

This variability existed probably because the condensed water before the main condenser stage was unable to overcome the surface tension from the inner walls of the heat exchanger system. But, when the product load was increased, the amount of water passing through the system became relatively higher, thereby increasing the amount of water collected through the main condenser. These water droplets gained sufficient weight to overcome the surface tension force and finally made it to the drainage valve. Therefore, the amount of water retrieved finally also increases with the increase in frying load.

Table 4-2 shows the initial and final moisture contents of the potato slices and the amount of water collected from the main condenser stage.

Table 4-2. Initial and final moisture content of potato chips and moisture removed during frying (T_{oil} = 120°C oil temperature; 360 s).

Potato chips drying load [g]	IMC[a] [% w.b.]	FMC[b] [% w.b.]	MR[c] [g]	MC[d] [g]
30	72.62±0.42	1.44±0.37	21.61±0.29	15.67±1.15
50	75.52±0.35	1.99±0.40	37.52±0.17	33.00±2.00
70	75.16±0.22	1.50±0.83	52.36±0.19	52.00±2.00

[a]IMC: Initial Moisture Content; [b]FMC: Final Moisture Content; [c]MR: Moisture Removed; [d]MC: Moisture Collected

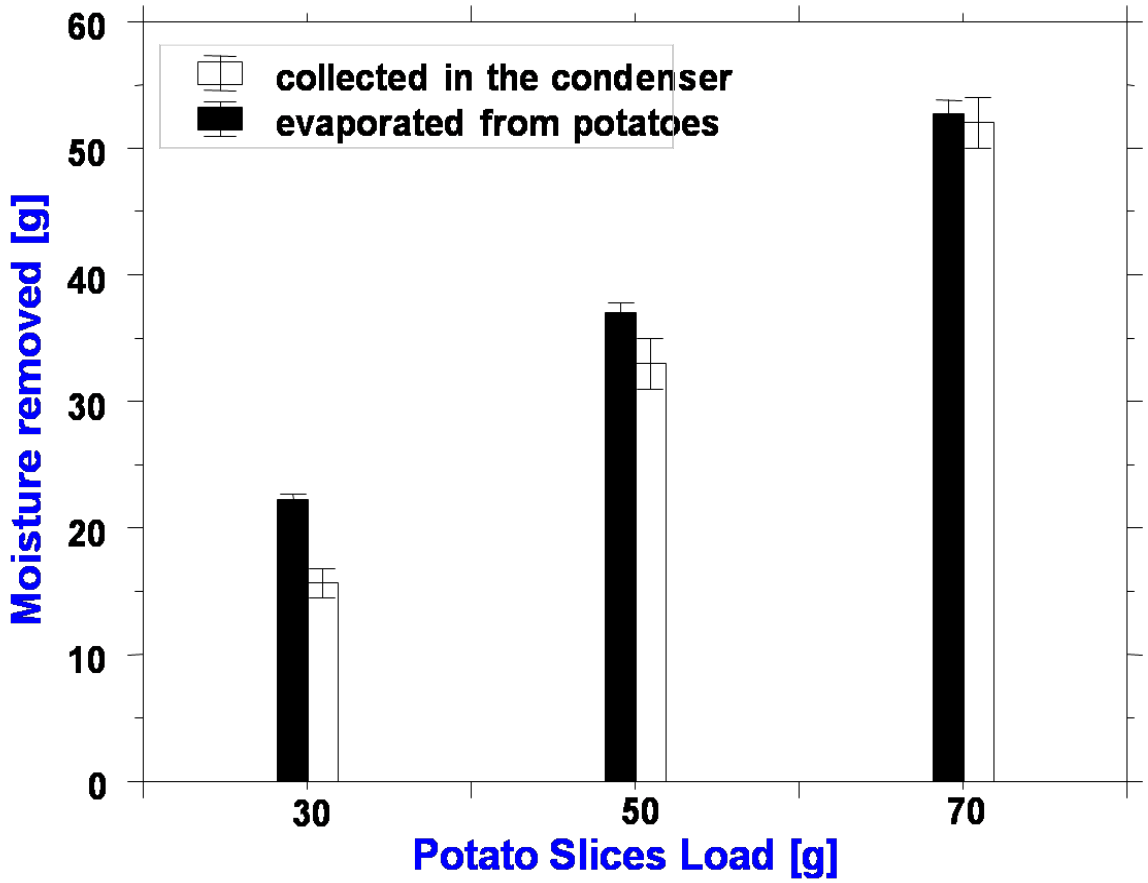

Figure 4-8. Moisture removed from potato chips and water collected at the bottom of the condenser unit during vacuum frying at 120°C for 360 s with different potato load.

4.6. Effect of centrifuge speed on the de-oiling process

The de-oiling of potato chips or similar products may be carried out with the help of different techniques and methods. In this research work the effect of centrifuging the potato chips in the fryer basket was studied to better understand the removal of surface oil. In the process of de-oiling of potato chips, centrifugal force plays the key role. According to Moreira et al. (1999), oil is absorbed in chips after frying is complete while the chips cool down. The main reason for oil absorption, in atmospheric frying, is the temperature gradient (ΔT) whereas, in vacuum frying, both temperature and pressure gradients (ΔT and ΔP) play an important role.

An experiment was conducted by securing the potato chips horizontally with a metal mesh and two different speed settings were chosen for chips fried at oil temperature of 120^{o}C at 300 RPM (12.2 g-force) and 750 RPM (63 g-force) for 40 s centrifuge time (Figure 4-9). At 0 RPM (control sample), the oil content with mesh was higher than without mesh. However, after centrifugation at 300 RPM and 40 s the oil content dropped to 15% w.b. with mesh and around 22% w.b. without mesh. At 750 RPM, a much lower drop in oil content was found from the 350 RPM setting with a slight reduction of 13% w.b. with mesh and 18% w.b. without mesh. The oil content decreased with increase in centrifuge time. In general, more oil is removed from the chips surface when centrifuged without mesh than with mesh. The minimum oil content (~15% w.b.) was obtained at 60 s of centrifuging at 750 RPM. Figure 4-10 illustrates the effect of centrifuge time at 750 RPM on the oil content of potato chips at 140^{o}C for 360 s at 1.33 kPa.

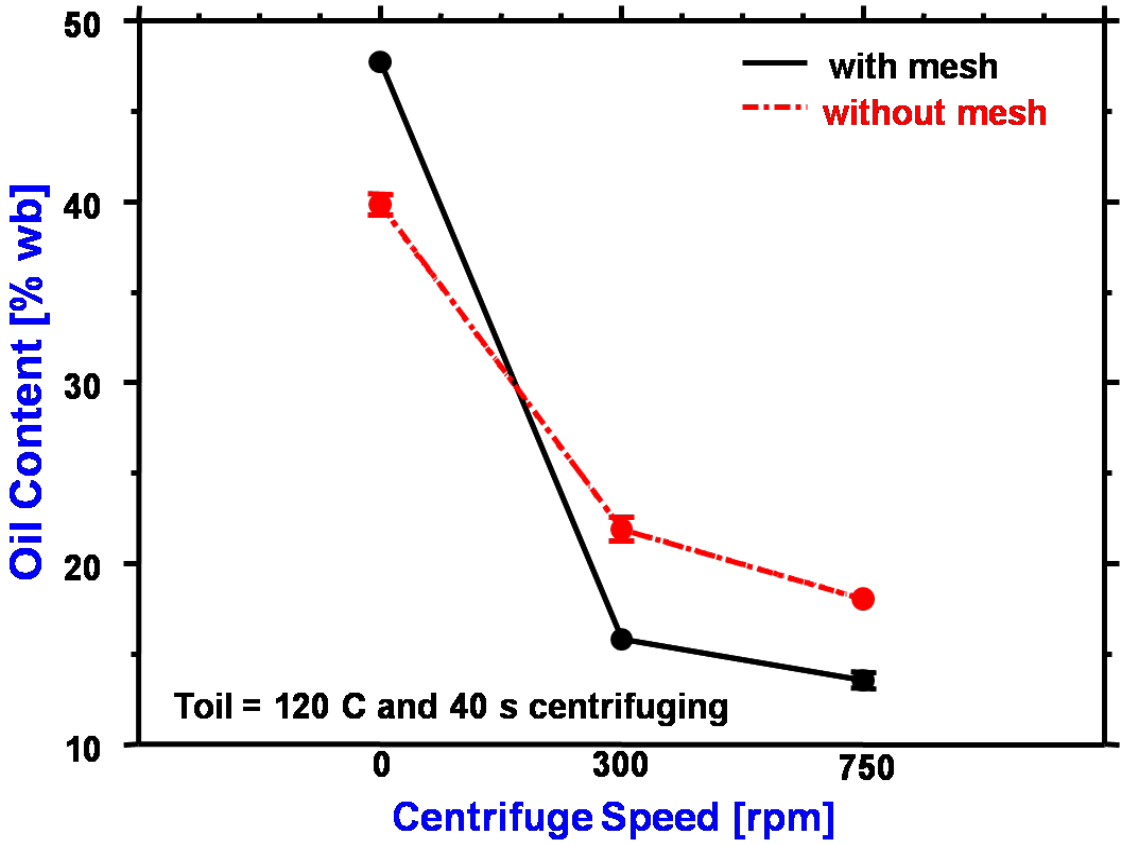

Figure 4-9. Oil content in potato chips versus centrifuge speed (40 s) with and without a mesh in the fryer basket (chips fried at 120^{o}C for 360 s at 1.33 kPa).

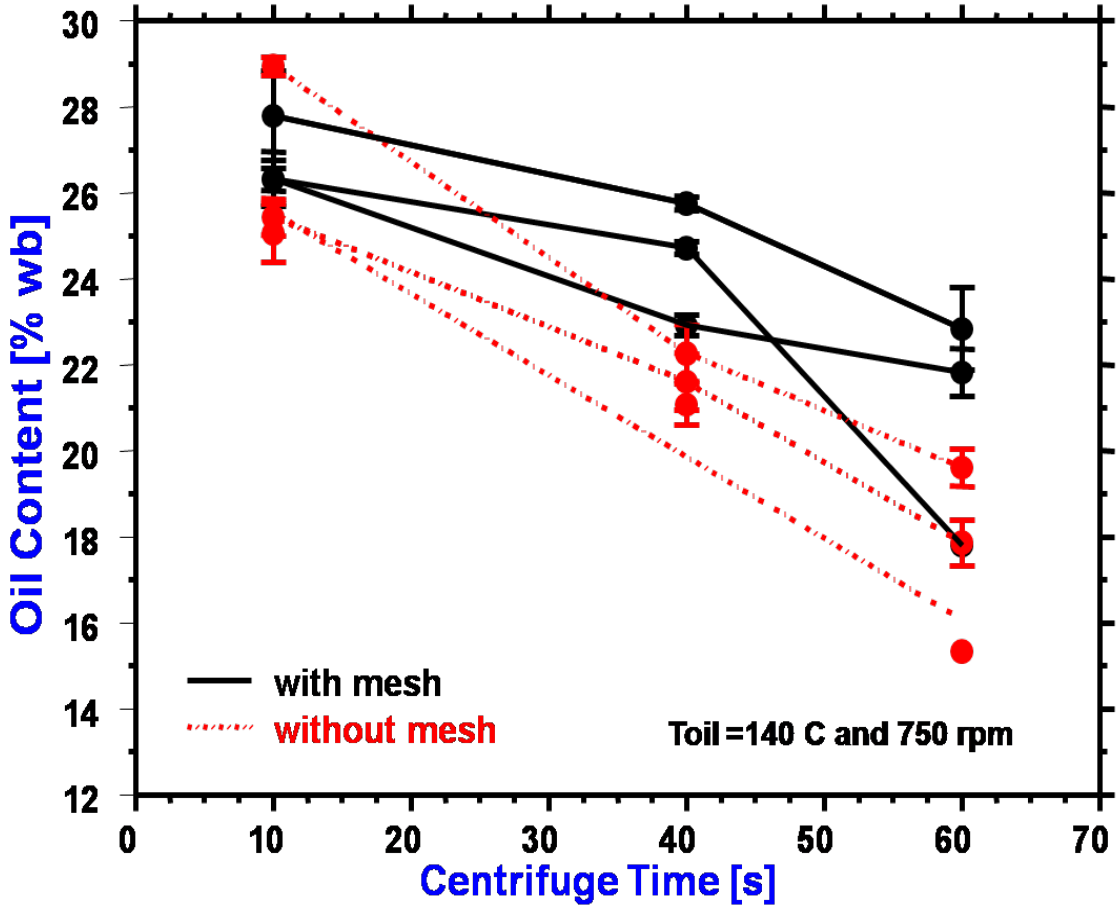

Figure 4-10. Oil content in potato chips versus centrifuge time at 750 RPM (63 g-force) with and without a mesh in the fryer basket (chips fried at 140°C for 360 s at 1.33 kPa).

4.7. Effect of rate of pressurization on the oil absorption in potato slices

Oil absorption in potato chips is primarily a complex phenomenon. In any food product, the primary structure acts as a porous medium that uptakes oil inside the capillaries due to temperature and pressure differentials. A study of tortilla chips for oil uptake by Tseng et al. (1996) concluded that only 20% of the final product's oil content absorbed during the period of frying and that about 64% is absorbed during the cooling period in a traditional fryer. The oil absorption is mainly related to the capillary pressure differences in porous media. According to Ufheil and Escher (1996), oil uptake is a surface phenomenon that forms an interfacial tension between surface oil and gas in the pores. When the chips cool down, this surface oil is suctioned into the capillaries and becomes absorbed in the chips.

In a similar manner, pressure differential plays an important role in uptake of oil in cases of vacuum frying. After completion of frying of potato slices in a vacuum fryer, the vessel must be depressurized for removal of chips. The major oil absorption takes place during this period of pressurization causing pressure gradient between capillaries and ambient conditions, which causes oil to move from the surface of the chips to within the product.

The experimental results show three different rates of pressurization of the vacuum fryer after completion of frying at 120^{o}C and 140^{o}C oil temperature and centrifugal de-oiling at 300 RPM and 750 RPM for 40 s. The results strongly correlate lesser oil uptake in potato chips with a decrease in pressurization rate.

The oil uptake during frying at 140^{o}C shows higher oil uptake than at 120^{o}C. This would be because of the chip's structure formation at 140^{o}C oil temperature, which produces more number of pores or increase in the pore size across the surface. Therefore, an increase in oil uptake occurs at higher frying temperatures (140^{o}C). In Figures 4-11 and 4-12, the relationship with centrifugation speeds of 300 RPM and 750 RPM shows the rate of surface oil removal before pressurizing.

Interesting to note is that at full (100% open) position of the release valve, the higher the centrifuge speed the lower the oil absorption by the potato chips for both frying oil temperatures of 120^{o}C and 140^{o}C. However, for the half release position (50% open) and the quarter release position (25% open) of the release valve, more surface oil was removed when the chips were centrifuged at the lower speed (350 RPM) than at higher speed (750 RPM). The oil content reached a minimum of approximately 14%w.b. when the chips were centrifuged at 750 RPM at 120^{o}C (for all pressurization rates) compared to 21% w.b. at 140^{o}C. The higher the frying temperature the higher the oil content for the 750 RPM centrifuge speed. Centrifuging the chips at 350 RPM, produced less oil content only when the fryer was pressurized at half and quarter positions of the release valve.

Table B-2 contains the experimental data collected for Figures 4-11 and 4-12.

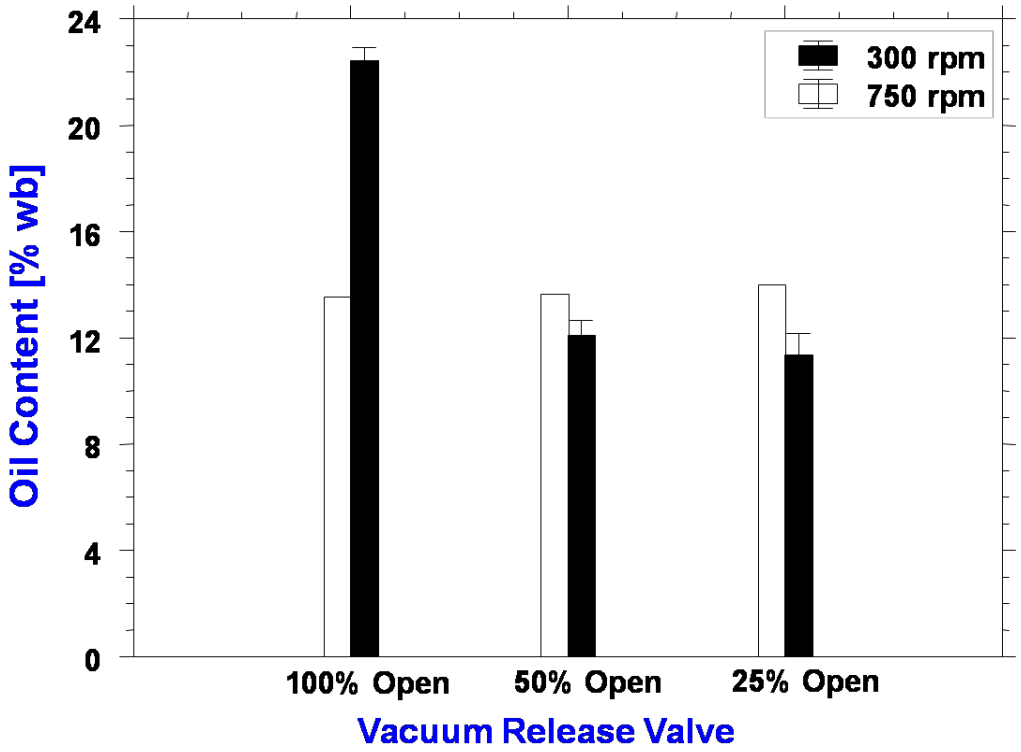

Figure 4-11. Oil content in potato chips versus vacuum release valve as a function of centrifuge speed of 300 RPM (8.89 g-force) and 750 RPM (63 g-force) for 40 s for chips fried at 120^{o}C for 360 s.

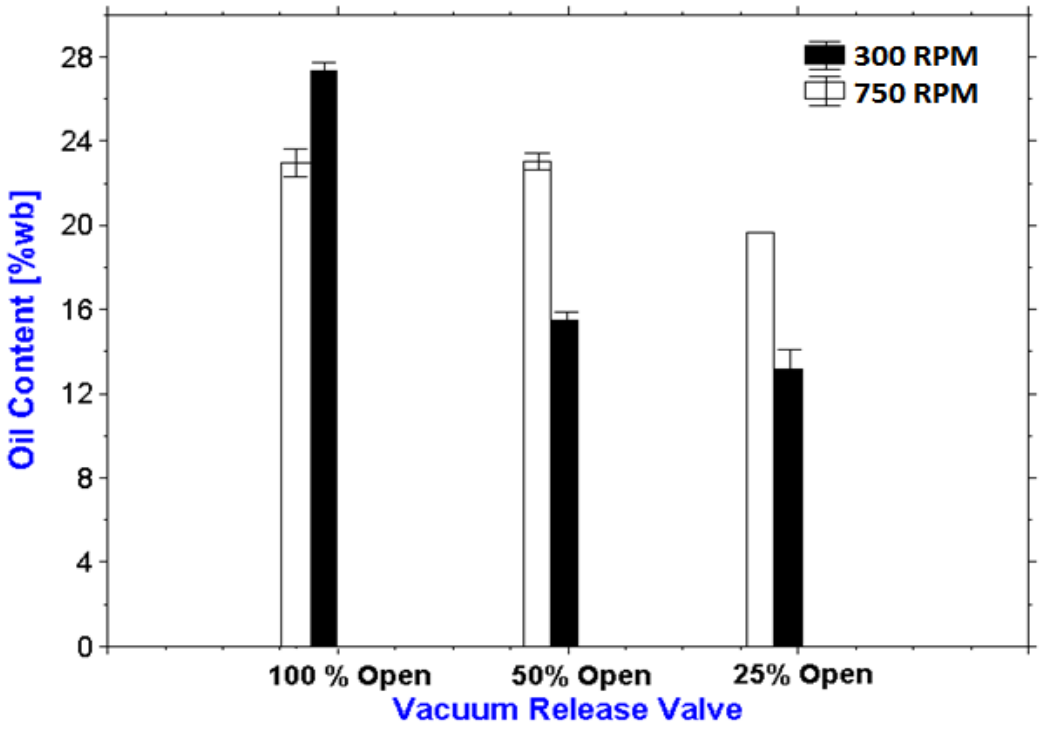

Figure 4-12. Oil content in potato chips versus vacuum release valve as function of centrifuge speed of 300 RPM (8.89 g-force) and 750 RPM (63 g-force) for 40 s for chips fried at 140^{o}C for 360 s.

4.8. Analysis of the convective heat transfer coefficient

Figure 4-13 shows the measured and the predicted temperature history at the center of the copper ball using the lumped capacity approach.

Raw potato slices consists of 70 to 90% moisture content wet basis, this moisture starts to evaporate rapidly during frying until all the unbound and free surface moisture is vaporized. The rate of moisture evaporation depends on the temperature of heating media (oil), and on the physical properties like geometry and size of the product.

The rate of moisture evaporating from the product may increase the convective heat transfer coefficient between the oil and the product surface due to turbulence present in oil during frying. Therefore, it is important to understand the effect of this rapid removal of moisture on the convective heat transfer coefficient during frying.

The convective heat transfer coefficient was analyzed with the help of special thermocouple arrangement and calculations were done by lumped capacitance approach at oil temperatures of 120^{o}C, 140^{o}C during vacuum frying and resulting convective heat transfer coefficient were obtained and compared to 165^{o}C oil temperature during traditional frying.

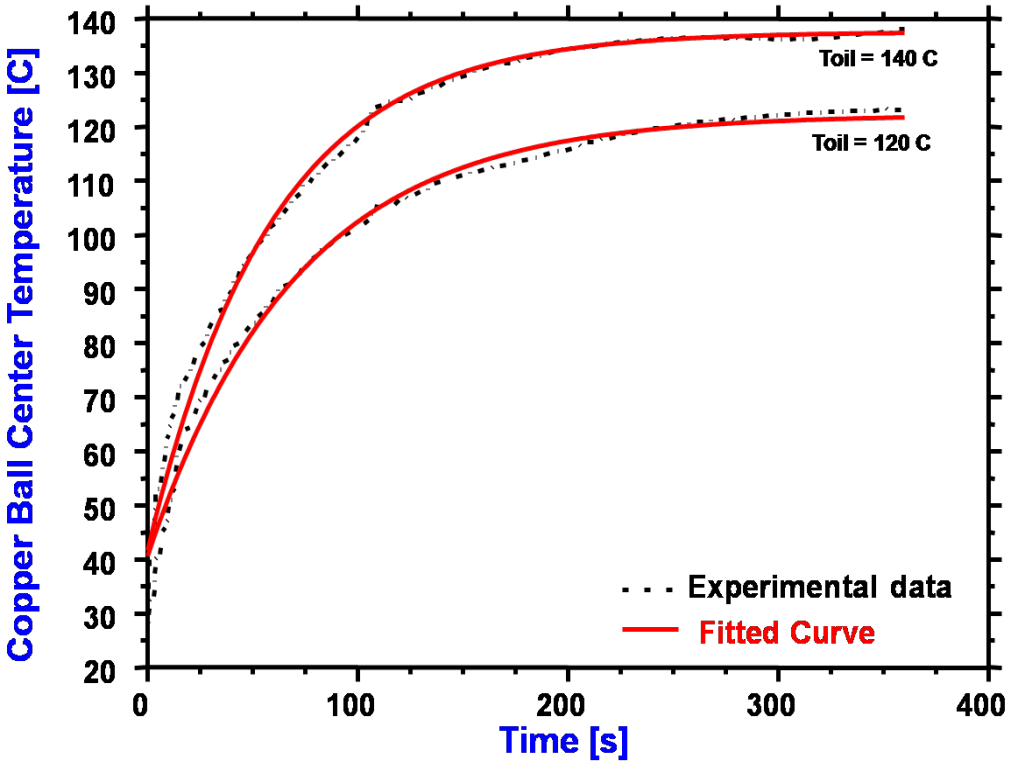

Figure 4-13. Temperature history at the center of a copper ball probe as a function of oil temperatures heated in a vacuum frying system (fitted curve using the lumped capacitance approach).

Figure 4-14 shows the temperature histories for a 70 g load of potato slices fried at 120^{o}C in a vacuum fryer. The spherical copper ball probe was adjusted such that it stood above the potato slice load inside the basket. During frying, the temperature of the ball probe with the potato slices load rose faster than that with the ball probe alone. It took only 50 s for the probe to reach the oil temperature when the probe was heated with potato load compared to about 200 s when the probe was heated alone.

A similar experiment was conducted at 140^{o}C (Figure 4-15). With a product load, the ball probe temperature showed a more rapid increase than with the ball probe alone. The observation strongly points towards turbulence in oil due to moisture bubbles from potato slice load. The ball probe with product load required only 50 s to reach the maximum temperature, while the ball probe alone required almost 200 s to reach a final constant temperature. The experimental data shows good agreement with the curve fitted with the lumped capacity approach.

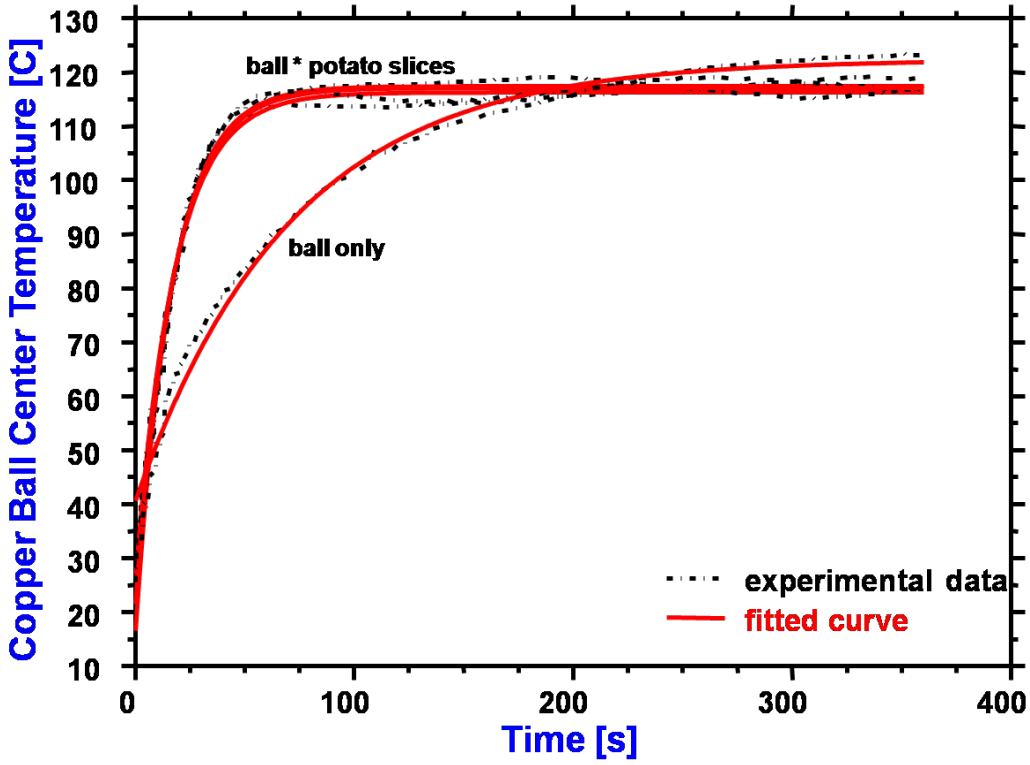

Figure 4-14. Temperature history at the center of a copper ball heated in frying oil at 120°C (under vacuum, P = 1.33 kPa) as a function of potato load (fitted curve using the lumped capacitance approach).

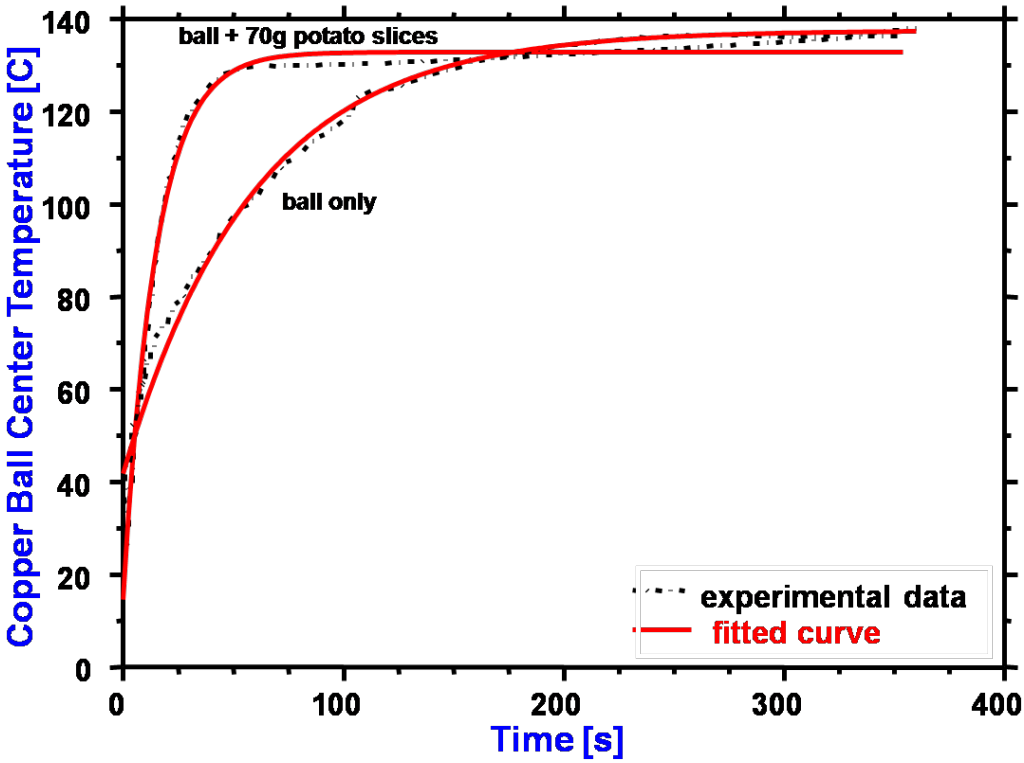

Figure 4-15. Temperature history at the center of a copper ball heated in frying oil at 140°C (under vacuum, P = 1.33 kPa) as a function of potato load (fitted curve using the lumped capacitance approach).

During vacuum frying (1.33 kPa), the turbulence in the oil is higher due to the pressure gradient in comparison to traditional frying (101.3 kPa). The moisture is removed faster due to suction from the vacuum pump and higher driving force, thereby increasing the heat transfer between frying oil and the copper ball probe. The experiment showed good agreement with the lumped capacitance approach.

A bench-top traditional fryer was used to observe the change in temperature in the copper probe with respect to time at 165^{o}C (Figure 4-16).

A similar phenomenon was noticed with and without a product load of 72 g potato slices, although in comparison to vacuum frying the temperature of the copper ball probe took 50 s to reach the frying oil temperature, while with the ball probe alone around 200 s was required for the probe to reach the frying oil temperature.

It can be concluded that frying at atmospheric pressure produced less turbulence in the frying oil on immersion of potato slices therefore heat transfer coefficient was low even at higher oil temperature.

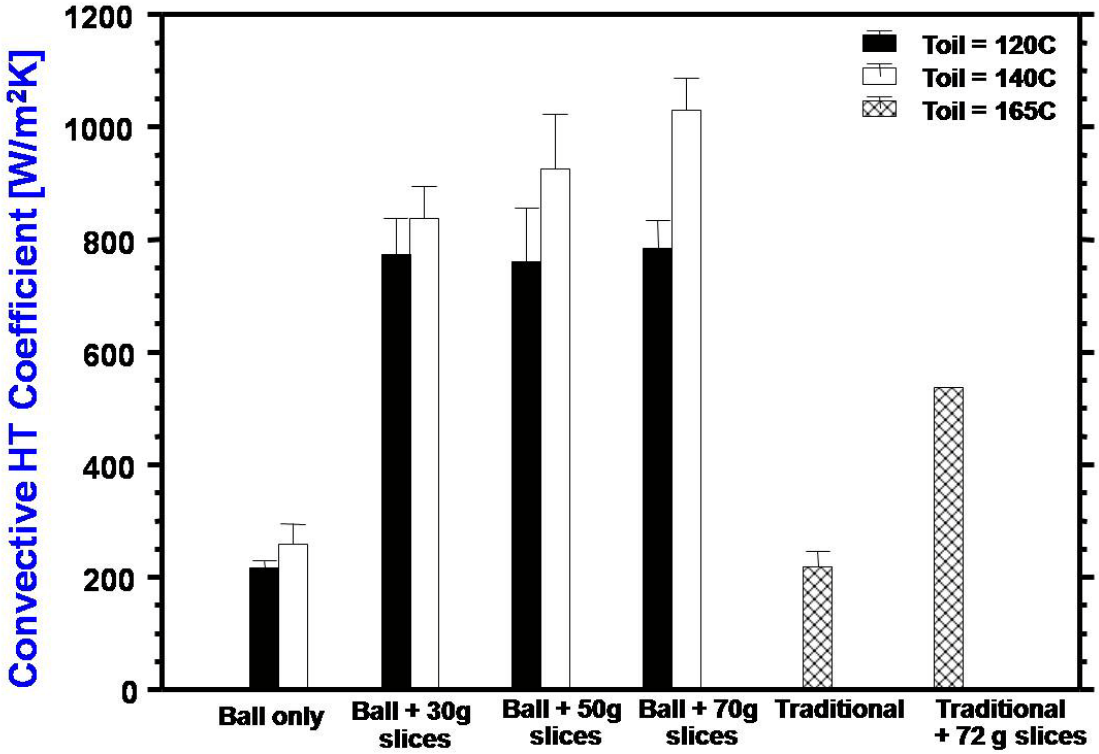

Figure 4-16. Temperature history at the center of a copper ball heated in frying oil at 165°C (under atmosphere P = 101.3 kPa) as a function of potato load (fitted curve using the lumped capacitance approach).

The convective heat transfer coefficient was also calculated as a function of different product loads of 30 g, 50 g, and 70 g at 120^{o}C and 140^{o}C oil temperature (Figure 4-17). A similar experiment was conducted for a traditional fryer with 72 g of potato slices at 165^{o}C oil temperature.

The convective heat transfer coefficient increased with the product load and oil temperature. For the ball probe only setting, the maximum convective heat transfer coefficient was 216.604 ± 12.985 W/m^{2}K at 120^{o}C and 258.125±36.382 W/m^{2}K at 140^{o}C oil temperature. An addition of 30 g of 2.6 mm-thick potato slices yielded calculated heat transfer coefficients of 773.60±63.63 W/m^{2}K at 120^{o}C and 837.19±57.53 W/m^{2}K at 140^{o}C oil temperature. Increasing the product load to 50 g of potato slices, the heat transfer coefficient attained a maximum value of 760.15±95.81 W/m^{2}K at 120^{o}C oil temperature and 924.30±98.28 W/m^{2}K at 140^{o}C oil temperature. For a 70 g product load a very little variation 783.74±49.47 W/m^{2}K was found at 120^{o}C oil temperature but the heat transfer coefficient rose to 1029.36±56.98 W/m^{2}K at 140^{o}C The traditional frying with a ball probe yielded a calculated value of the convective heat transfer coefficient of 218.15±27.88 W/m^{2}K at 165^{o}C oil temperature and 537 W/m^{2}K at 165^{o}C oil temperature with a 72 g of potato slice load (Figure 4-17, Table 4-3).

Therefore, it can be concluded that higher turbulence in the oil is observed when frying potato chips in vacuum than in atmospheric frying.

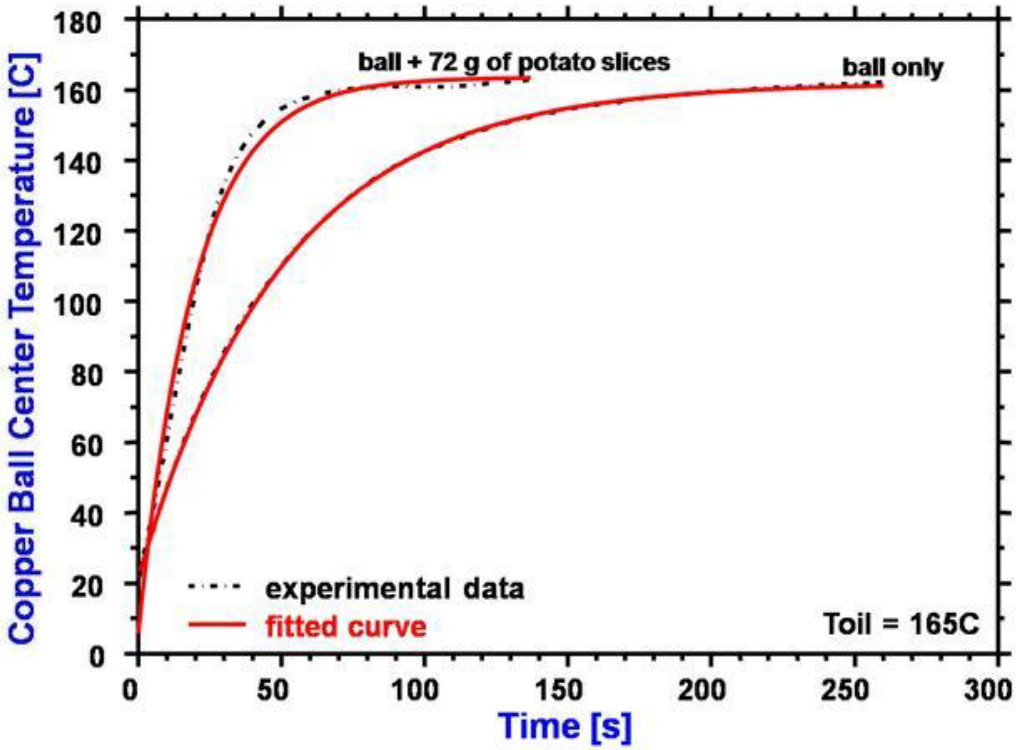

Figure 4-17.Convective heat transfer coefficient for vacuum and traditional fryers as a function of oil temperature and potato load (fitted curve using the lumped capacitance approach).

Table 4-3. Calculated values for the convective heat transfer coefficient for the vacuum and atmospheric fryers.

Experiment Type	**Predicted Convective Heat transfer Coefficient *h* [W/m^{2}K]**	
	Vacuum Frying	
	120^{o}C	140^{o}C
Ball only	216.60±12.99	258.13+36.38
Ball + 30 g slices	773.60+63.63	837.19+57.53
Ball + 50 g slices	760.15+95.81	924.30+98.28
Ball + 70 g slices	783.74+49.47	1029.36+56.98
	Atmospheric Frying 165^{o}C	
Ball only	218.15±27.88	
Ball + 72 g slices	537.00	

4.9. Temperature history at the center of potato slice during frying

A finite slab is the most commonly studied model for heat transfer in potato slices. A single potato slice of 2.6 mm thickness and 25.2 mm in diameter was fried in canola oil at 120^{o}C oil temperature (Figure 4-18). The potato slice was not immersed for the first 135 s to allow the vacuum fryer to get ready for the frying process. A slight variation in the temperature noticed in this period was studied in more detail.

After the start of frying period at 135 s, the chip was fried until it reached constant temperature of 120^{o}C, in equilibrium with the frying oil. During the start of the frying period, a temperature spike (max: 100.7^{o}C) was observed after 20 -30 s the chip was immersed in the hot oil. In less than 25 s, after that, the chips' temperature was reduced to 80^{o}C. This phenomenon can be explained by analogy with the Joule-

Thompson effect, i.e., a cooling effect due to evaporation of gas (water vapor) in a porous media (potato slices). During this process, the enthalpy remains constant, while the water vaporizes through the pore space, from high pressure to lower pressure, to cover the place of already evaporated surface water at the pore's outlet. When a thermocouple was placed at center of a potato slice being fried, the temperature of the water vapor in the pore space increased rapidly from ~20^{o}C to a maximum value of 100.7^{o}C. Consequently, the vapor pressure also increased to the saturated pressure at that temperature. As the outside pressure is lower than the pore space, a cooling effect is observed as measured by the thermocouple.

A constant temperature profile was noticed after that due to water vaporization from the potato slice (latent heat phase). This constant temperature of 80^{o}C started rising to that of the frying oil temperature as soon as most of the moisture had evaporated from the potato slices. After 300 to 305 s from the start of the process, the temperature showed a continuous rise until it reached the 120^{o}C frying oil temperature.

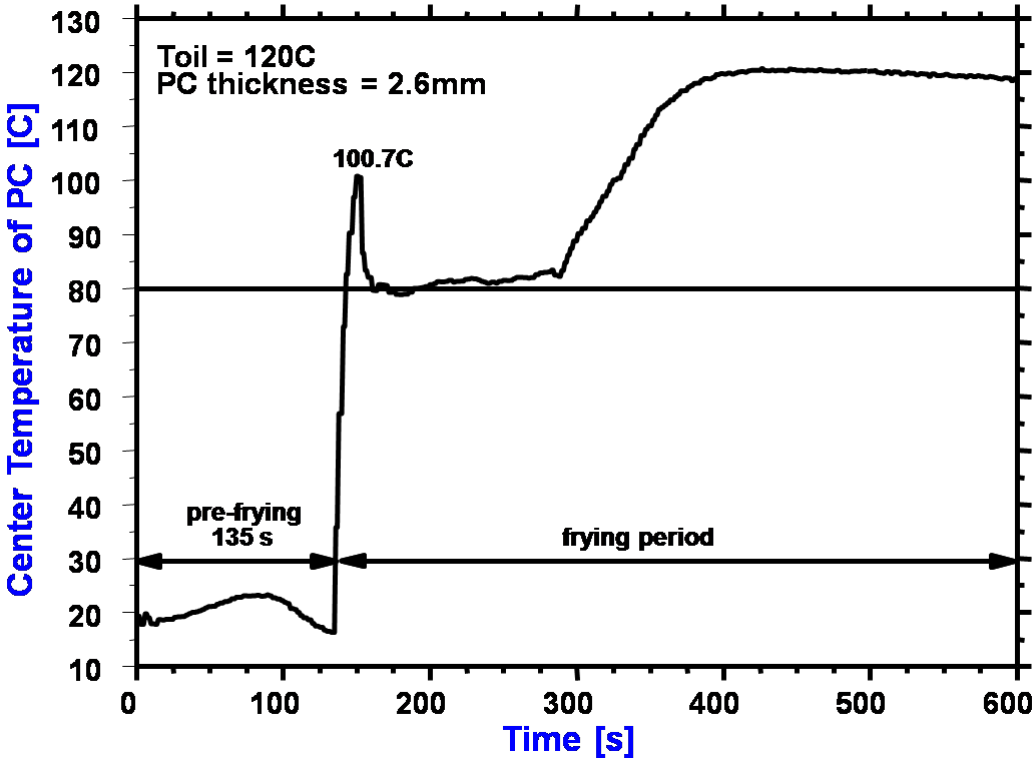

Figure 4-18.Temperature history at the center of a 2.6 mm potato slice fried at 120^{o}C for 360 s in a vacuum fryer (P=1.33 kPa).

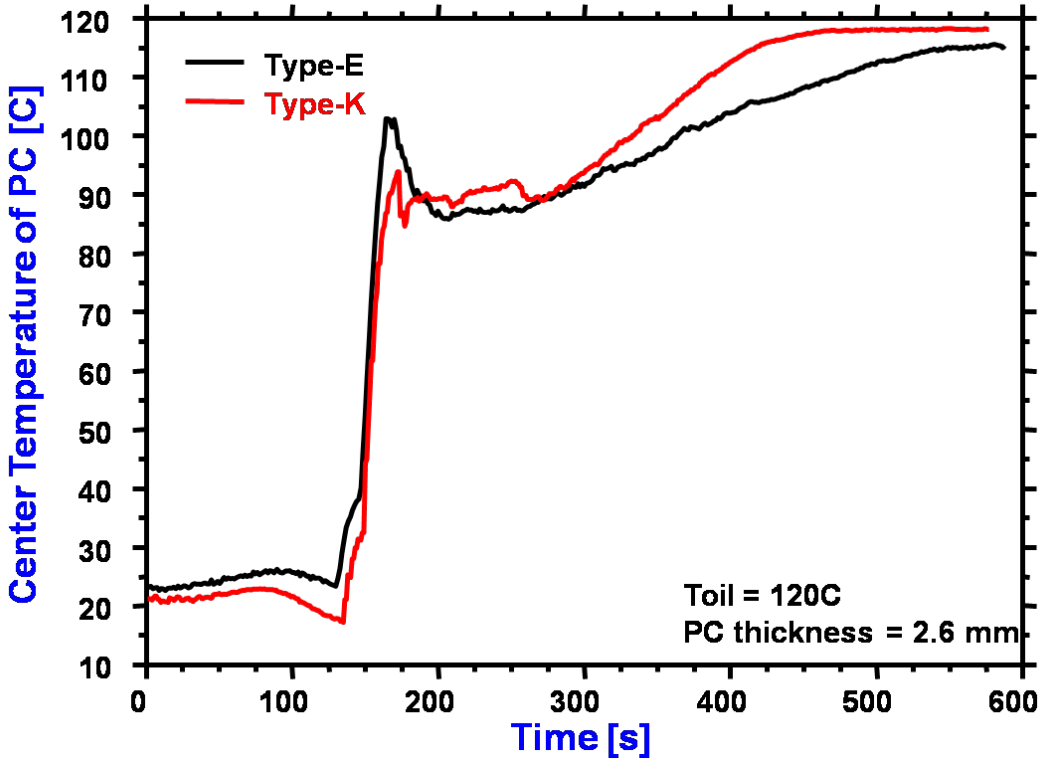

Figure 4-19.Temperature history at the center of a 2.6 mm potato slice fried at 120°C for 360 s in a vacuum fryer (P=1.33 kPa) using two different thermocouple types (and thicknesses).

Two different types of thermocouples were used at the same time to observe and validate any temperature history differences at the center of potato slices at 120^{o}C oil temperature during vacuum frying (Figure 4-19). The potato slices used were 2.6 mm in thickness and 25.2 mm in diameter, although a slight lag was seen with the Type K thermocouple in comparison to the Type E thermocouple, the Type E thermocouple showed the same profile as the Type K thermocouple.

The temperature at the center of the potato slice (2.6 mm thick; 25.2 mm diameter) was recorded in triplicate with respect to time at 140^{o}C oil temperature (Figure 4-20). A similar pattern was seen in comparison to the temperature history at 120^{o}C oil temperature (Figure 4-18). The process variability increased under high temperature resulting in more noisy data. The pre-frying period lasted for 150 s, dropping the temperature of slices to almost 16^{o}C from the room temperature of 20^{o}C inside the vacuum fryer vessel. A similar spike was noticed in all the frying experiments, with peaks lying between 95^{o}C to103^{o}C maximum temperatures.

The average constant temperature until all the moisture evaporated was around 90^{o}C for different experiments. A continuous rise in the temperature of the total frying process, started at 300 s. The temperature reached a constant value of about 140^{o}C frying oil temperature until completion of the 360 s total frying period.

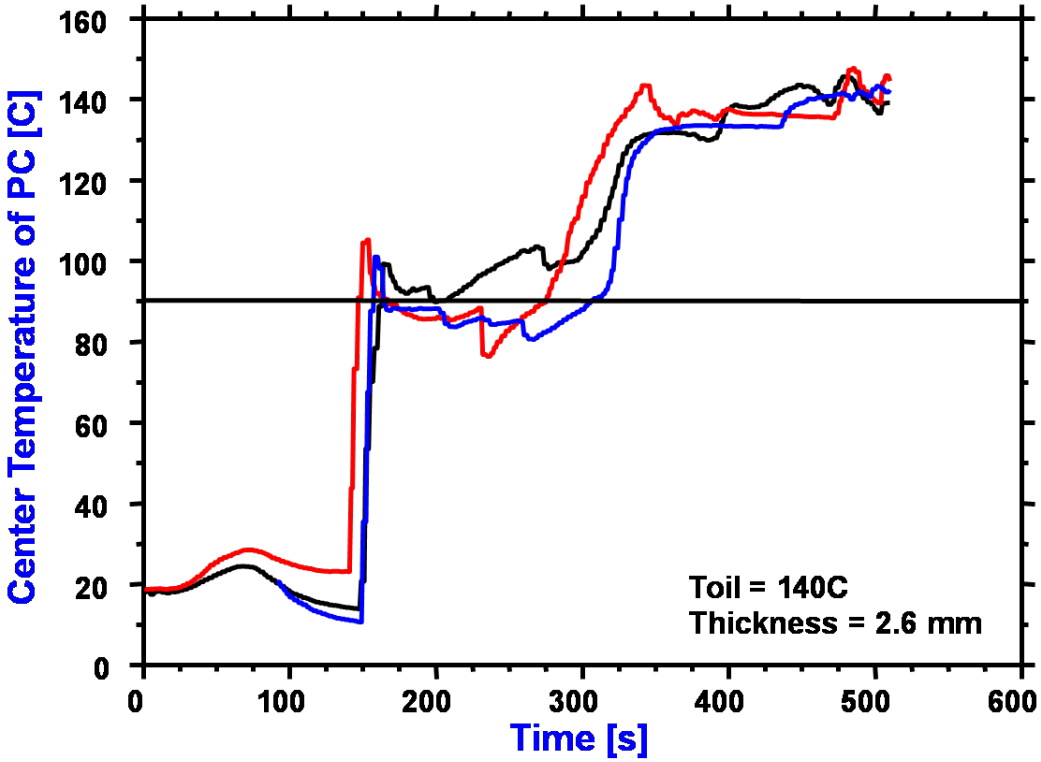

Figure 4-20.Temperature histories (triplicate) at the center of a 2.6 mm potato slice fried at 140°C for 360 s in a vacuum fryer (P=1.33 kPa).

Figure 4-21 shows the results for temperature history of the potato slices fried in traditional fryer at 165^{o}C oil temperature, maximum peak for the spike was 110^{o}C to115^{o}C higher than in vacuum frying due to a higher oil temperature. The spike slowly dropped to 100^{o}C average constant temperature in 25 s. After 250 s, the temperature started to rise again to attain 165^{o}C constant temperature, thus equilibrating with the oil temperature.

For the Type E thermocouple a pattern similar to vacuum frying was noticed, while the Type K thermocouple did not completely attain the final constant temperature until at the end of the frying period. The chips were fried for a longer period than in vacuum frying to achieve a constant temperature inside the potato chips. This kind of temperature profile is created because frying at atmospheric pressure (101.3 kPa) showed smoother glide than vacuum frying. The term *smoother glide* means less sudden variations in temperature profile because of the negligible pressure differential, in contrast to vacuum frying, which allows faster heat transfer at lower temperatures. Therefore, the primary spike during the frying cycle shows more sudden temperature variations during vacuum frying but less in traditional frying method.

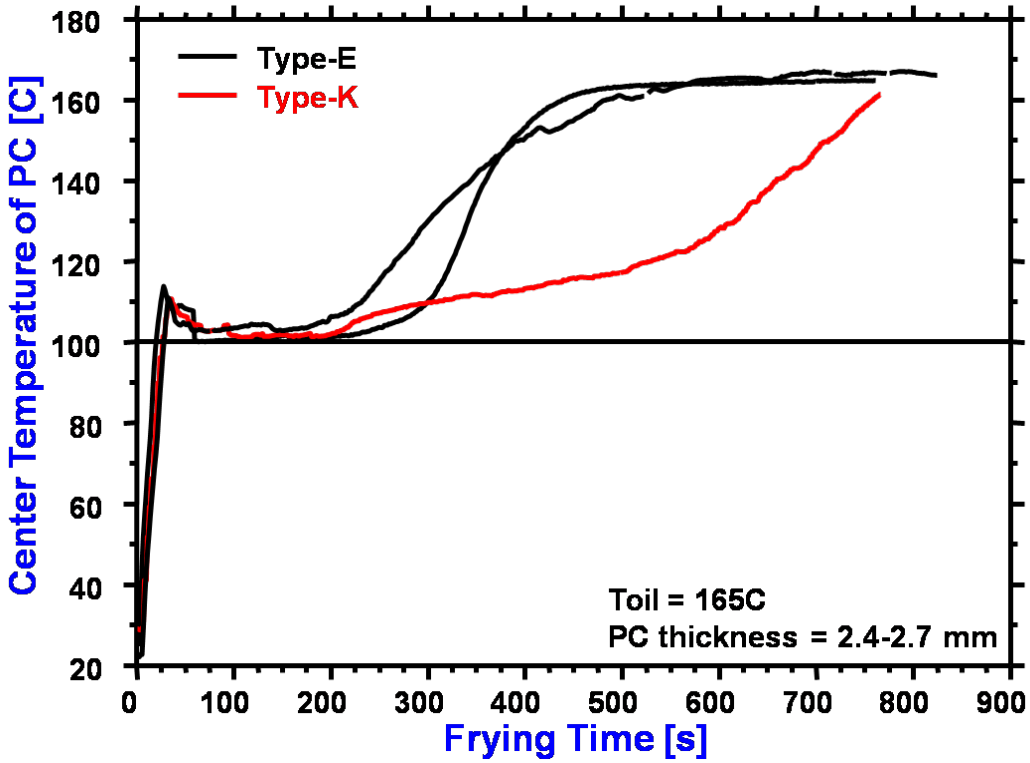

Figure 4-21.Temperature history at the center of a 2.6 mm potato slice fried at 165^{o}C for 360 s in a traditional fryer (P=101.03 kPa) using two different thermocouple types (and thicknesses).

4.10. Moisture loss and temperature drop in potato slices before immersing in the hot oil

The result shows the effect of pressure drop, which causes evaporation of moisture from the product. The potato slices center temperature was recorded and the samples were left above the hot oil at 120^{o}C for 600 s.

The vacuum pressure in the vacuum chamber decreases rapidly from atmosphere to 1.33 kPa in 120 s (2 min), i.e., from the time the chamber is depressurized at 80 s to 200 s. When it reaches to set pressure it starts to fluctuate around it. When the pressure is lower or equal to the saturation pressure at the local temperature, water evaporates. In the non-evaporating region where temperature distribution is only affected by diffusion heat transfer, the pressure and temperature distributions are essentially parabolic. In the evaporating region, the pressure and temperature distributions are related. The movement of evaporating front is along the thickness (*x*-direction) direction.

A small temperature rise, at the center of the slice, from 19^{o}C to 23^{o}C was observed in the first 80 s period. This is mainly because the radiant heat of the hot oil raised the center temperature of the potato slices until their surface moisture dried off. The cooling effect comes from water evaporating from the samples, and therefore evaporation and cooling of sample start from the surface. However, with decreasing the pressure, evaporation and cooling (evaporative cooling phenomenon) occur through the potato slice and temperature decreases together. Notice that after 80 s, the sample temperature started to fall rapidly and reached a value of below 10^{o}C inside the potato chips (in about 120 s). The total cooling time is dependent on the shape of the product,

porosity, pore size, the pore distribution within the samples, availability of free water in the pores and set pressure. Temperature of the potato slices should decrease from 25^{o}C (ambient temperature) to 9.14^{o}C at 1.33 kPa.

Weight loss occurred during depressurization of the fryer since the cooling effect directly comes from water evaporation from the sample. Weight losses of potato slices during depressurization are given in Table 4-4. Weight loss is closely related to final set pressure.

Over the first 150 s, moisture content was reduced by 12%. Similarly, over 200 and 400 s, the moisture decreased by 20%, respectively. A maximum drop of about 38% in moisture content was noticed for 600 s residence time of potato. Therefore, the moisture starts evaporating even before the chips were immersed in the oil during vacuum frying.

The sample temperature slightly increased after 200 s reaching a final value of 12^{o}C at 600 s. This increase in temperature is due to the vacuum frying temperature which causes an increase in the T_{sat} (superheated). Figure 4-22 shows the result for the pre-frying period during depressurization of the vacuum fryer chamber. Table 4-4 shows the moisture content change in potato slices during depressurization.

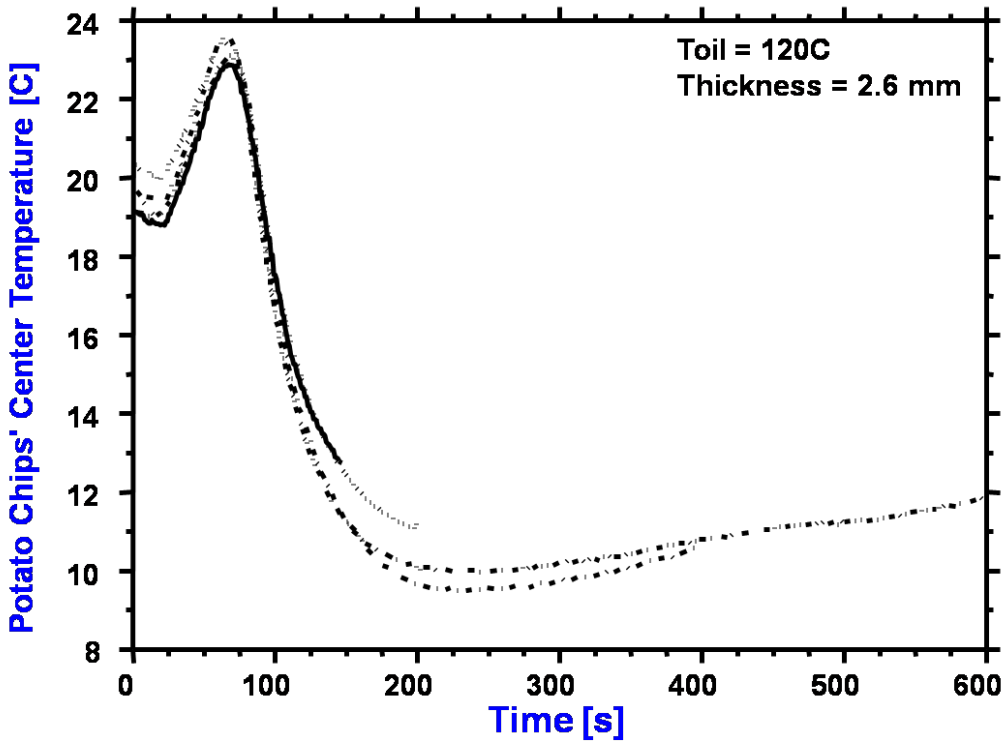

Figure 4-22.Temperature history at the center of a 2.6 mm potato slice during the depressurization period (T_{oil} = 120°C, P=1.33 kPa).

Table 4-4. Moisture content changes in potato slices during the depressurization period (frying oil at T_{oil} = 120°C).

Duration [s]	**IMC[a] [%w.b.]**	**FMC[b] [%w.b.]**	**MR[c] [g]**
150 s	71.74±0.28	68.98±1.10	0.44±0.20
200 s	74.59±0.31	70.02±0.22	0.76±0.02
400 s	77.47±1.30	73.27±2.26	0.78±0.16
600 s	77.27±0.64	67.76±1.20	1.47±0.12

[a]IMC = initial moisture content; [b]FMC = final moisture content; [c]MR = moisture removed (assuming 5 g per slice of potato)

4.11. Microstructure changes in potato chips during vacuum and traditional frying

Vacuum fried potato chips and traditionally fried potato slices showed visible micro-structural differences. Traditional frying of potato slices at 165^{o}C oil temperature for 360 s caused higher structural deterioration. The faster rates of heat and mass transfer caused greater destruction of microstructure at higher temperatures.

In four pictures, each for cross-section and surface view (Figures 4-23 to 4-28) for 120^{o}C, 140^{o}C, and 165^{o}C, oil temperature settings, the cross-section view (AI to AIV) provided more prominent structural differences than surface views (BI to BIV). At 120^{o}C oil temperature the potato slices fried for 360 s (Figures 4-23 and 4-24, A and B, I to IV) showed less structure damage and were similar to potato slices fried at 140^{o}C oil temperature (Figures 4-25 and 4-26, A and B, I to IV). This is because vacuum frying at lower oil temperature causes a steady rate of evaporation and less pore formation in the final product.

The starch lattice seems almost intact in vacuum fried chips; while in traditionally fried chips the starch structure became completely indistinguishable as to very large pores form throughout the microstructure. Therefore, it can be concluded that the slices fried at lower temperature (120^{o}C) were the smoothest in structural integrity. At 140^{o}C, the structure showed no visible difference in structural uniformity during vacuum frying, while at 165^{o}C (Figures 4-27 and 4-28), a highly porous and broken structure was noticed in traditionally (atmospheric) fried potato slices.

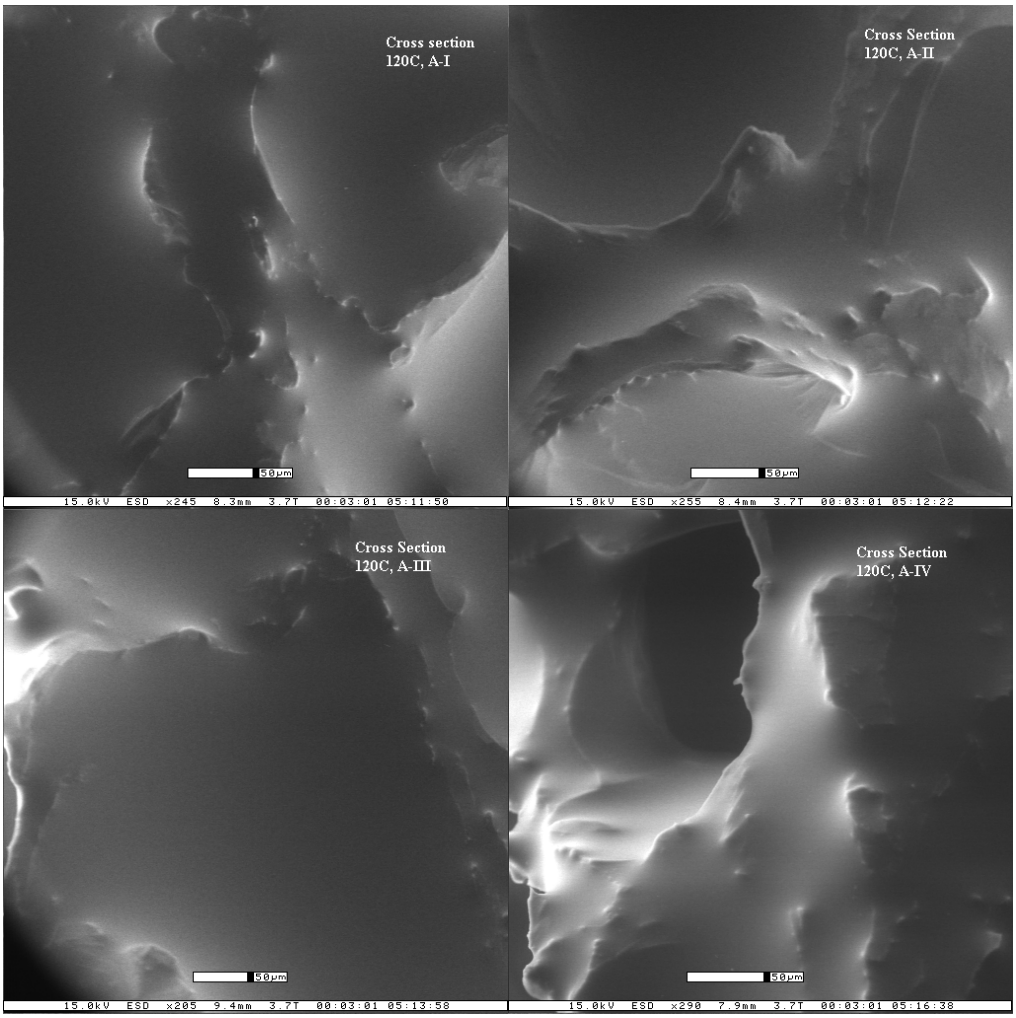

Figure 4-23.The ESEM cross-sectional view of potato chips fried at 120^{o}C oil temperature for 360 s in a vacuum fryer at 1.33kPa (15.0 kV power at 50 µm resolution).

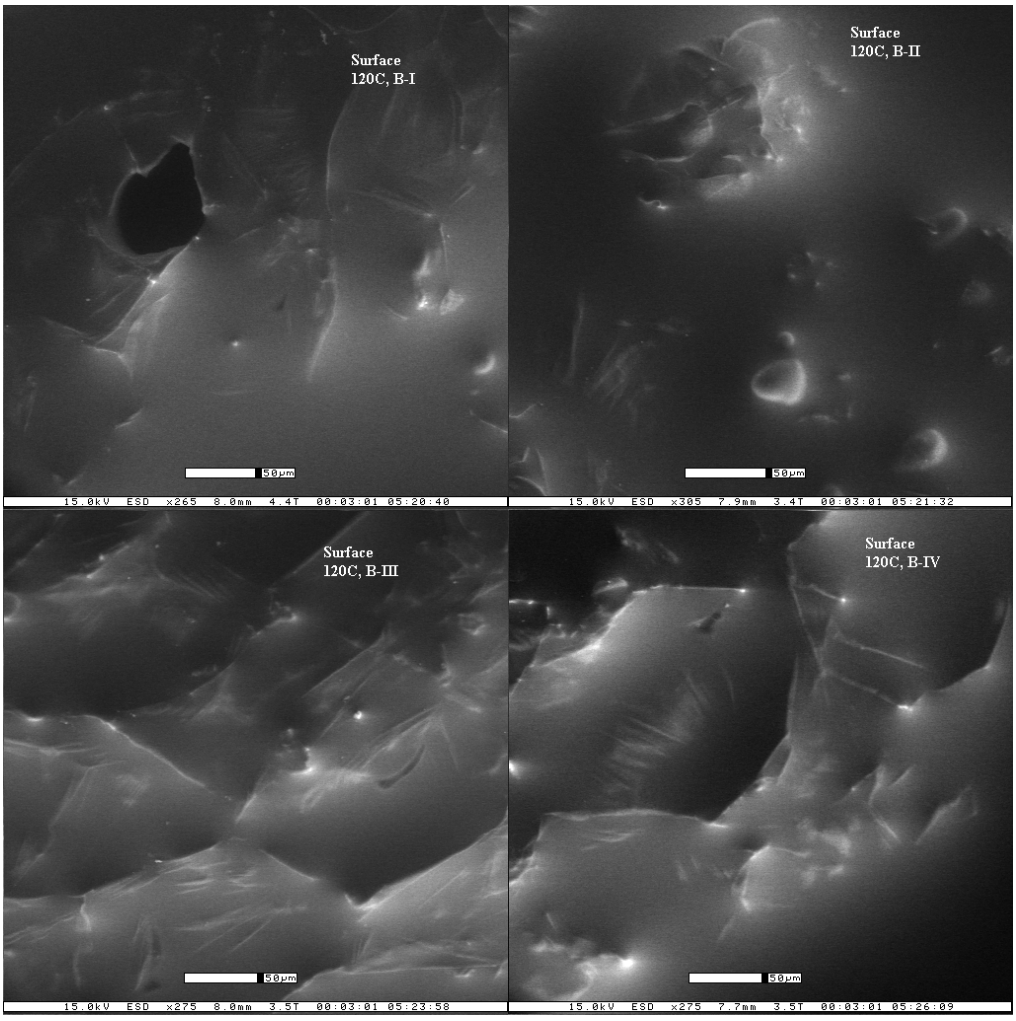

Figure 4-24.The ESEM surface view of potato chips fried at 120^{o}C oil temperature for 360 s in a vacuum fryer at 1.33kPa (15.0 kV power at 50 µm resolution).

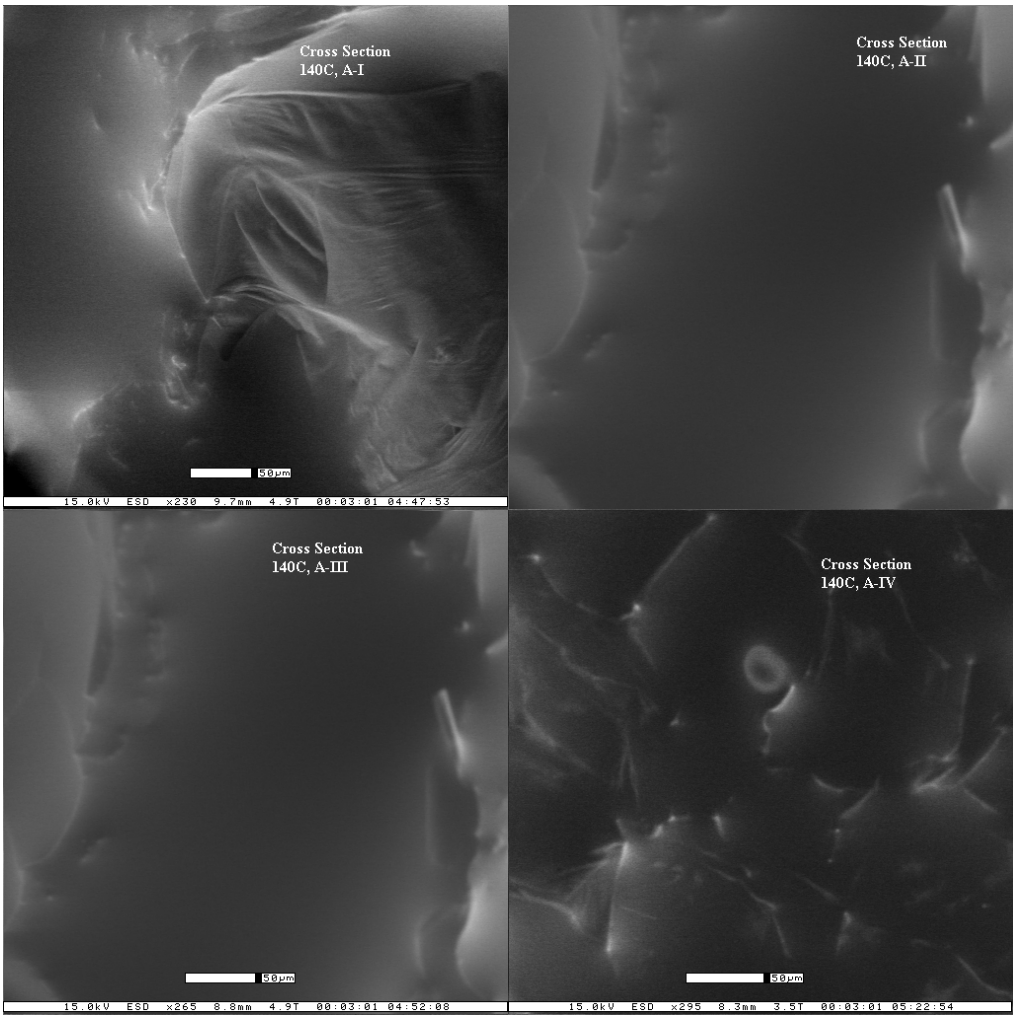

Figure 4-25.The ESEM cross-sectional view of potato chips fried at 140^{o}C oil temperature for 360 s in a vacuum fryer at 1.33 kPa (15.0 kV power at 50 µm resolution).

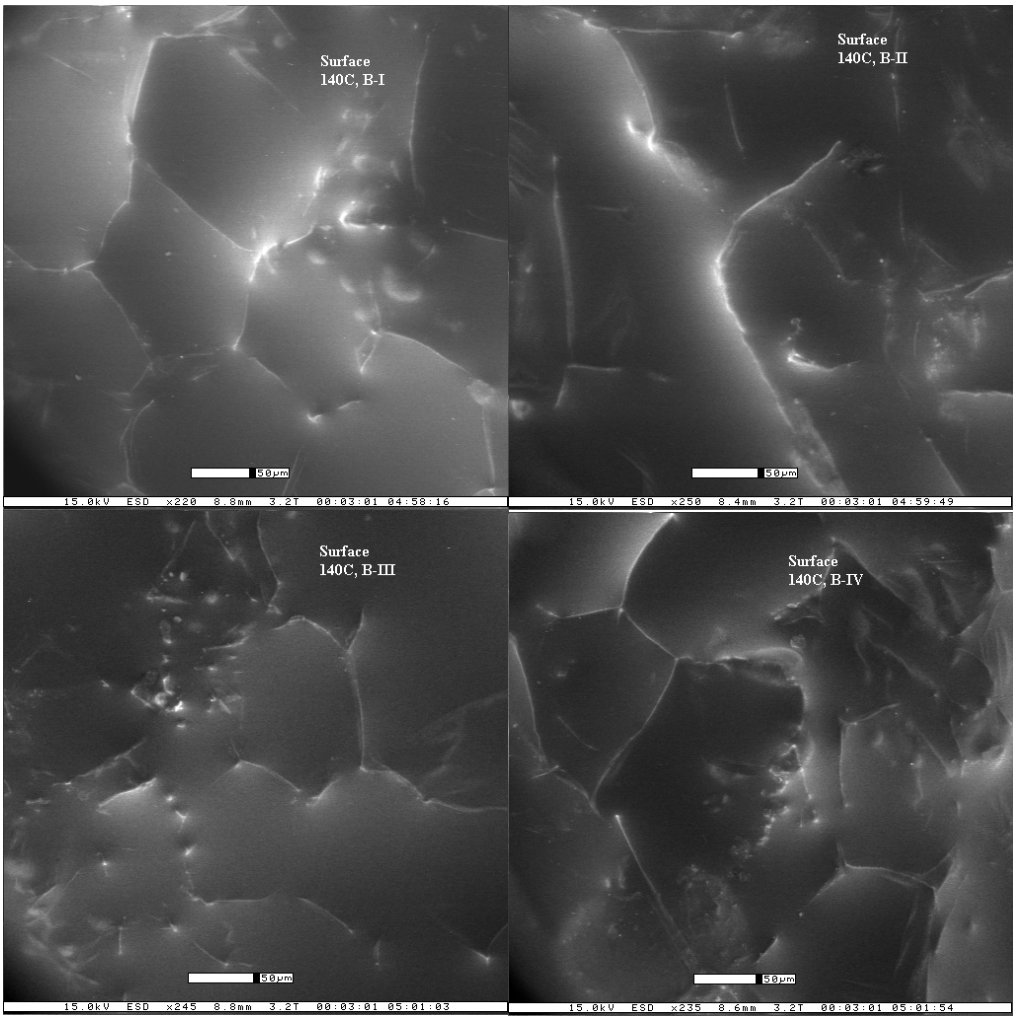

Figure 4-26.The ESEM surface view of potato chips fried at 140 ^{o}C oil temperature for 360 s in a vacuum fryer at 1.33 kPa (15.0 kV power at 50 µm resolution).

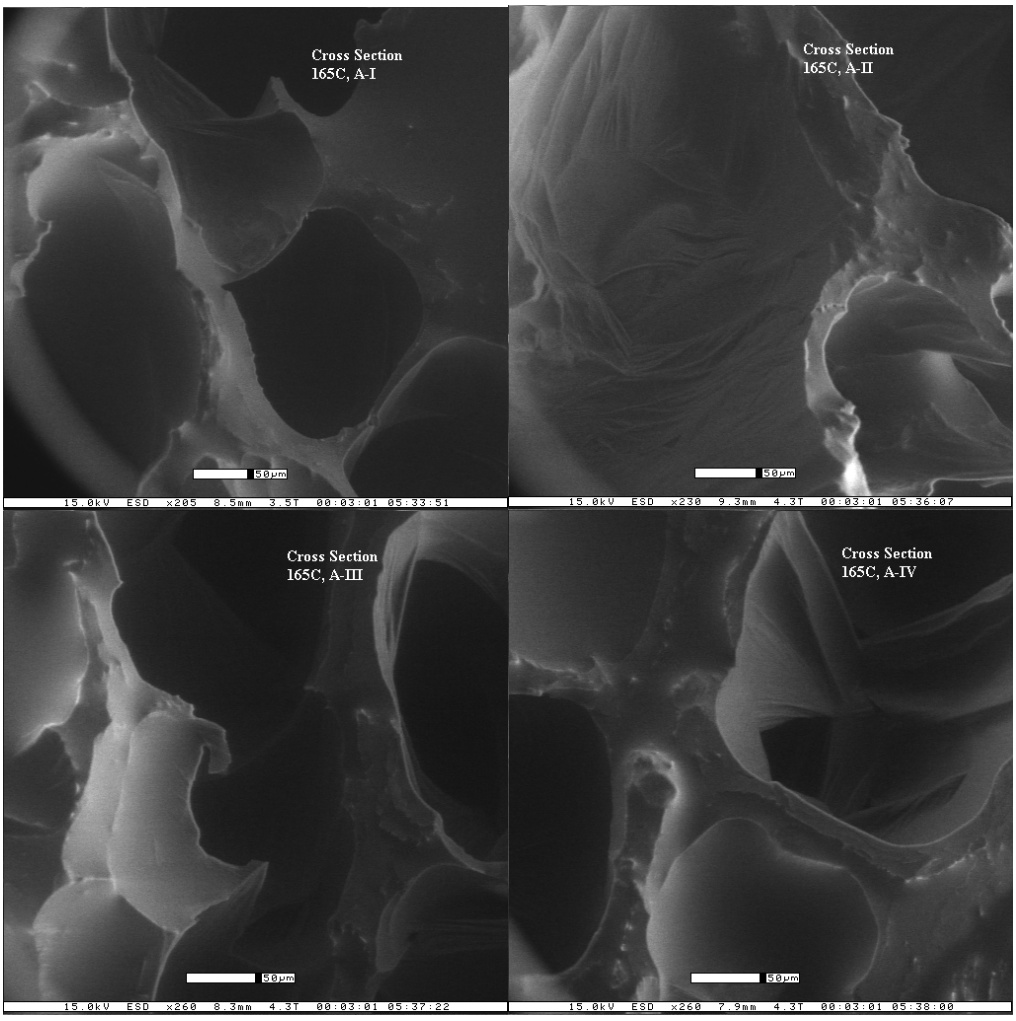

Figure 4-27.The ESEM cross-section view of potato chips fried at 165^{o}C oil temperature for 360 s in a (atmospheric) traditional fryer at 101.3325 kPa (15.0 kV power at 50 µm resolution).

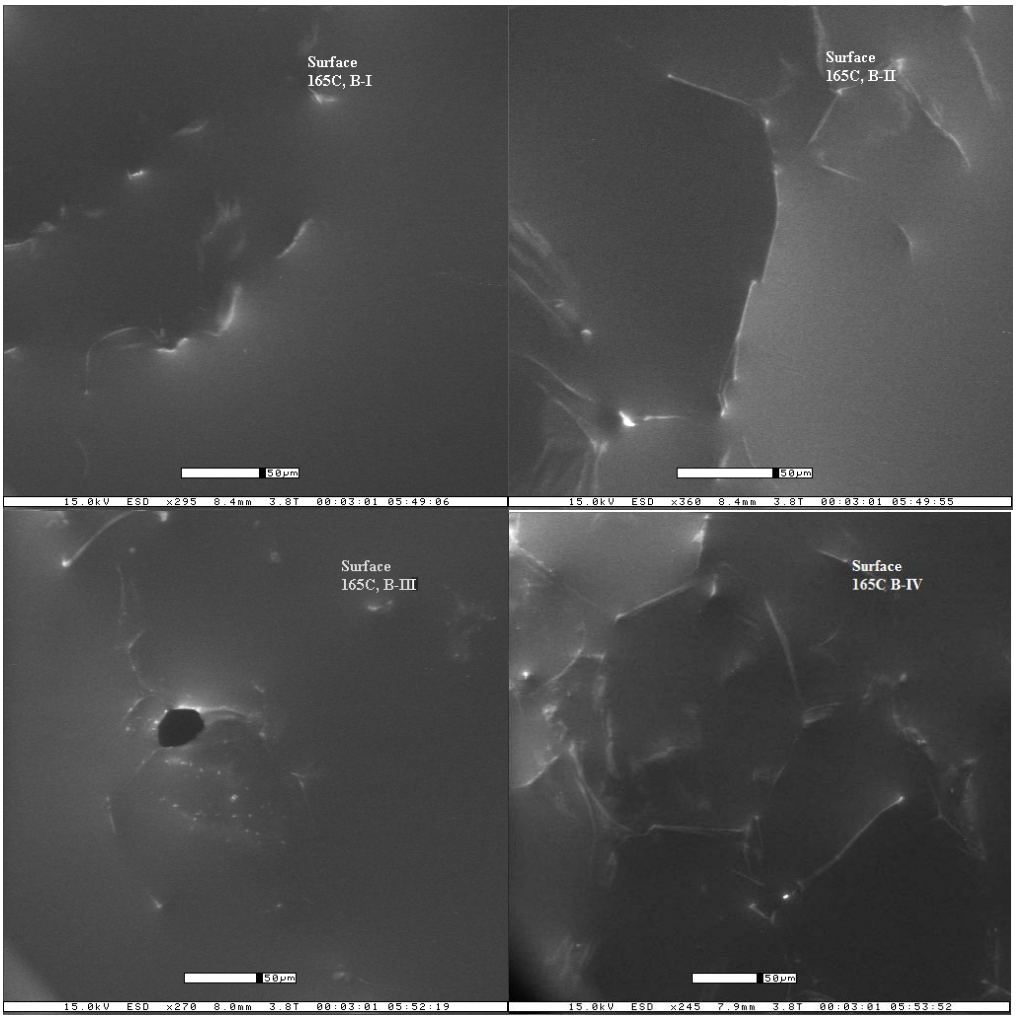

Figure 4-28.The ESEM surface view of potato chips fried at 165^{o}C oil temperature for 360 s in a (atmospheric) traditional fryer at 101.325 kPa (15.0 kV power at 50 µm resolution).

4.12. Optimization of vacuum fryer vessel with COMSOL™

The COMSOL simulation domain plot (Figure 4-29) depicts the heat transfer in a vacuum fryer without any product load inside it. The model was successful in showing the convection and radiation heat transfers inside a vacuum fryer. The temperature distribution in the vacuum fryer shows a large amount of heat flux leaking outside the fryer. An immersed coil heater at 120^{o}C heated up the oil through convection, this oil transferred heat through convective flux to the fryer walls. The mechanism of heat transfer in the walls was governed by conduction and between the walls and between the walls and ambient by radiation and convection.

The main purpose of this study was to design and use proper insulation to increase efficiency and optimize the performance of the vacuum frying vessel. The result shows the 2-D vacuum fryer model across $r = 0$ axial symmetry. The results were plotted by using a surface on contour plot for temperature profiling of the vacuum frying vessel.

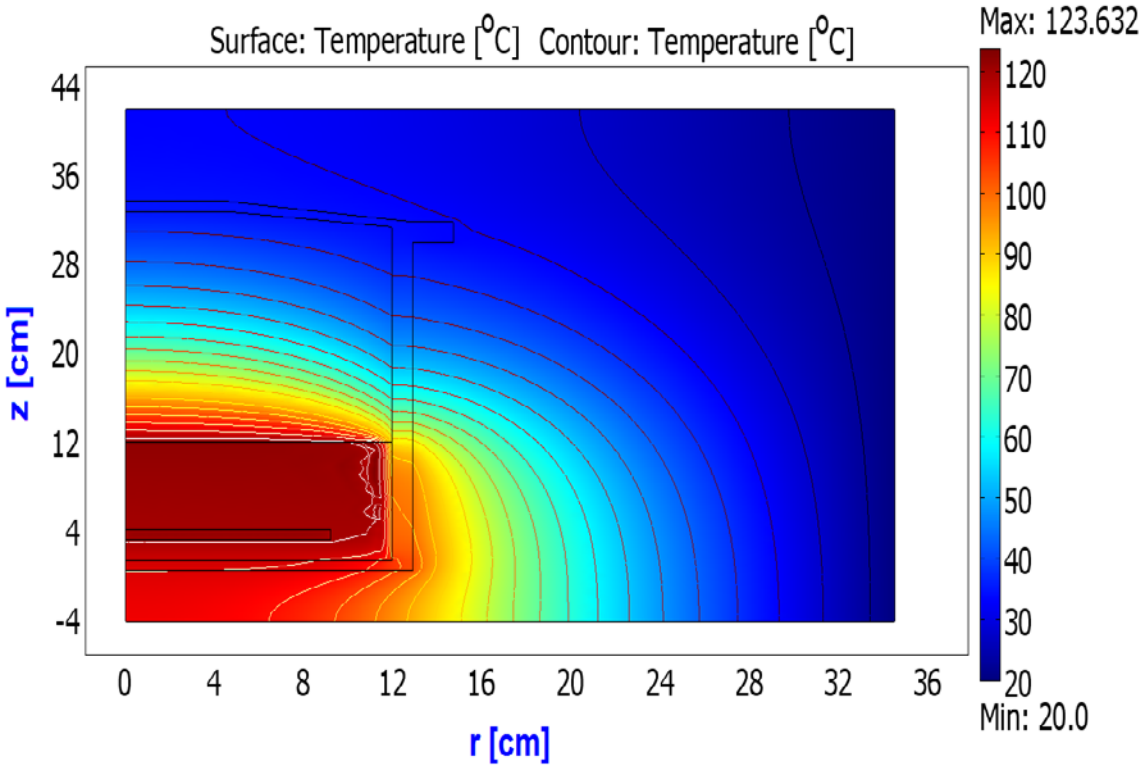

Figure 4-29.The 2-D axis symmetric domain plot for vacuum frying vessel within the control volume of air represented by surface and contour plot at oil temperature of 120°C and 1.33 kPa vacuum pressure without thermal insulation.

A plot between temperature and z-axis (cm) for the vertical fryer outer wall (Figure 4-30) showed a rapid drop in temperature across the boundary where the oil level ends around 12 cm from the total height of the fryer vessel. Therefore, maximum heat transfer takes place at the level of the oil.

The temperature started rapidly depleting up to 76^{o}C from 107^{o}C over the height of the fryer wall. This temperature drop in the aluminum wall was mainly due to natural convection of air on outer wall as well as by the resistive loss in aluminum.

The temperature distribution across the arc length of the axial symmetry (Figure 4-31) inside the fryer shows a drop in radiant heat inside the frying vessel. Figure 4-31 shows the uniform distribution of heat inside the vacuum fryer vessel in 3-D, where the results from 2-D axis symmetric model were revolved around the r-axis.

Finally, sensitivity analysis results proved that, using a 1.3 cm thick layer of insulating material (k = 0.04 W/m^{2}K) completely restrained heat loss from the fryer vessel.

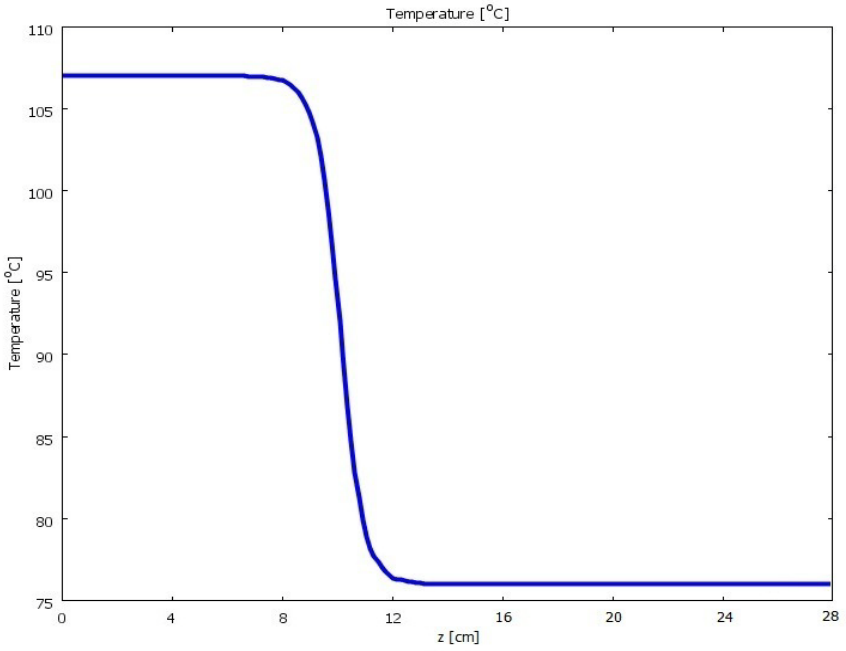

Figure 4-30.The loss in temperature across the length of vertical (z-component) aluminum vacuum fryer vessel wall.

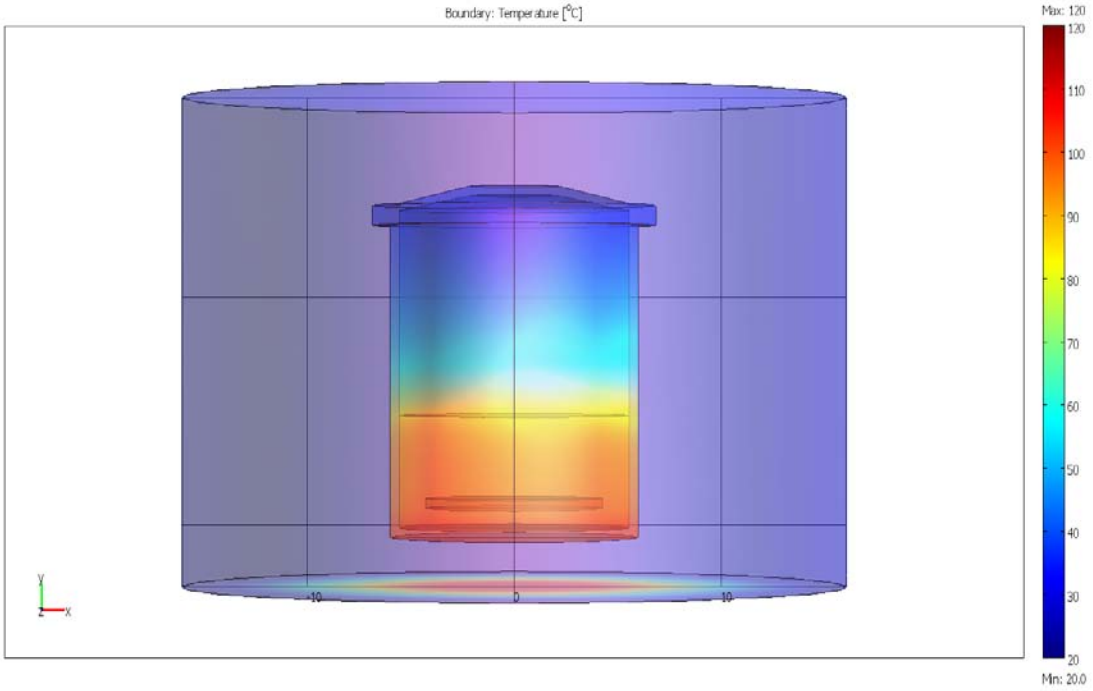

Figure 4-31. The 3-D domain plot for vacuum frying vessel within control volume of air represented by boundary plot at oil temperature of 120^{o}C.

4.13. Sensitivity analysis (vacuum fryer)

4.13.1. Effect of volume of oil in the fryer vessel (6.65 L, 10 L, and 12 L)

Sensitivity analysis was performed with change in domain size with respect to change of oil level inside the fryer vessel. The main idea was to understand the heat distribution inside the fryer vessel with different volumes of oil. The basic fryer model oil domain shows a model with 6.65 liters of oil at 10.16 cm height in the fryer vessel. The heat distribution across the fryer wall shows much less heat reaching the top lid of the fryer. The calculated and measured temperature was around 50 to 60^{o}C at the lid.

In the case of a 10 liter volume, the oil level is at 20.32 cm height (Figure 4-32). This shows a high increase in temperature at the oil boundary and higher temperatures in the fryer top space in range of 65 to 70^{o}C. At 12 liter oil volume (Figure 4-33), the depth of the oil was about 22.86 cm and the temperature of the head space was very close to the 90^{o}C mark. This temperature distribution model helped in understanding how the behavior of the fryer deviated from standard operating conditions.

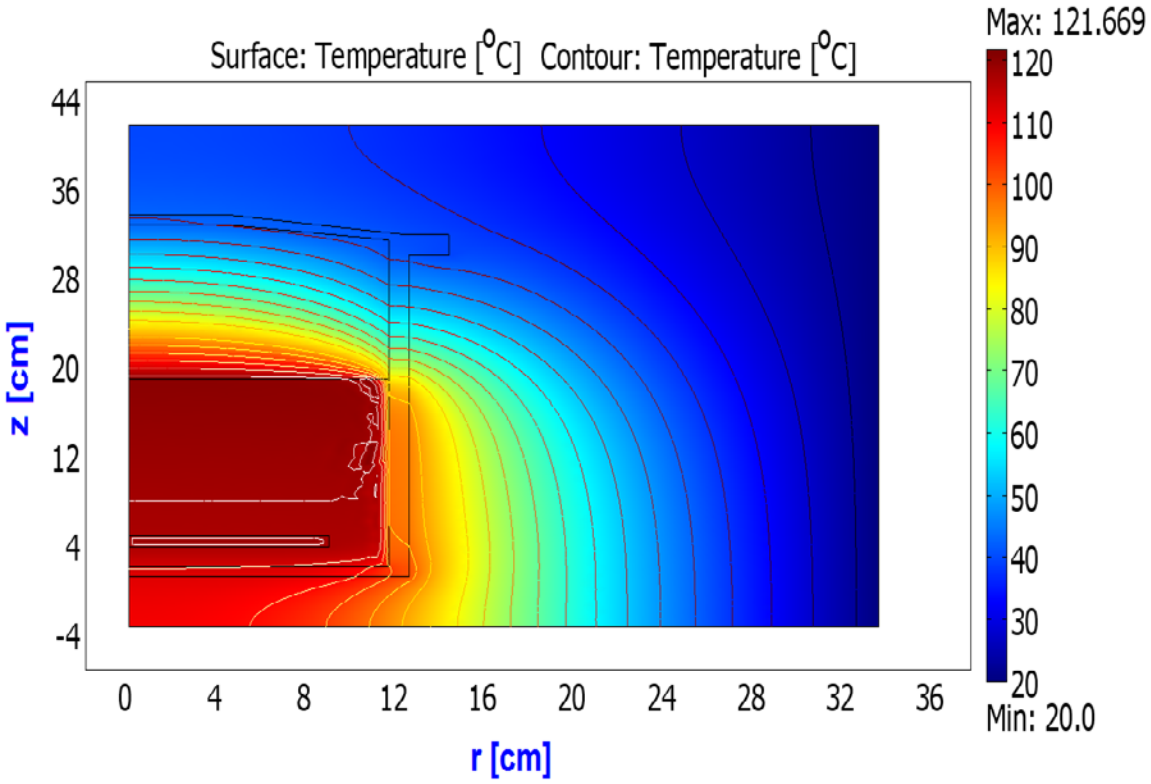

Figure 4-32.The 2-D axis symmetric domain plot for vacuum frying vessel within control volume of air represented by surface and contour plot at oil temperature of 120°C with 10 liter of oil at 0.2032 m height in the vessel.

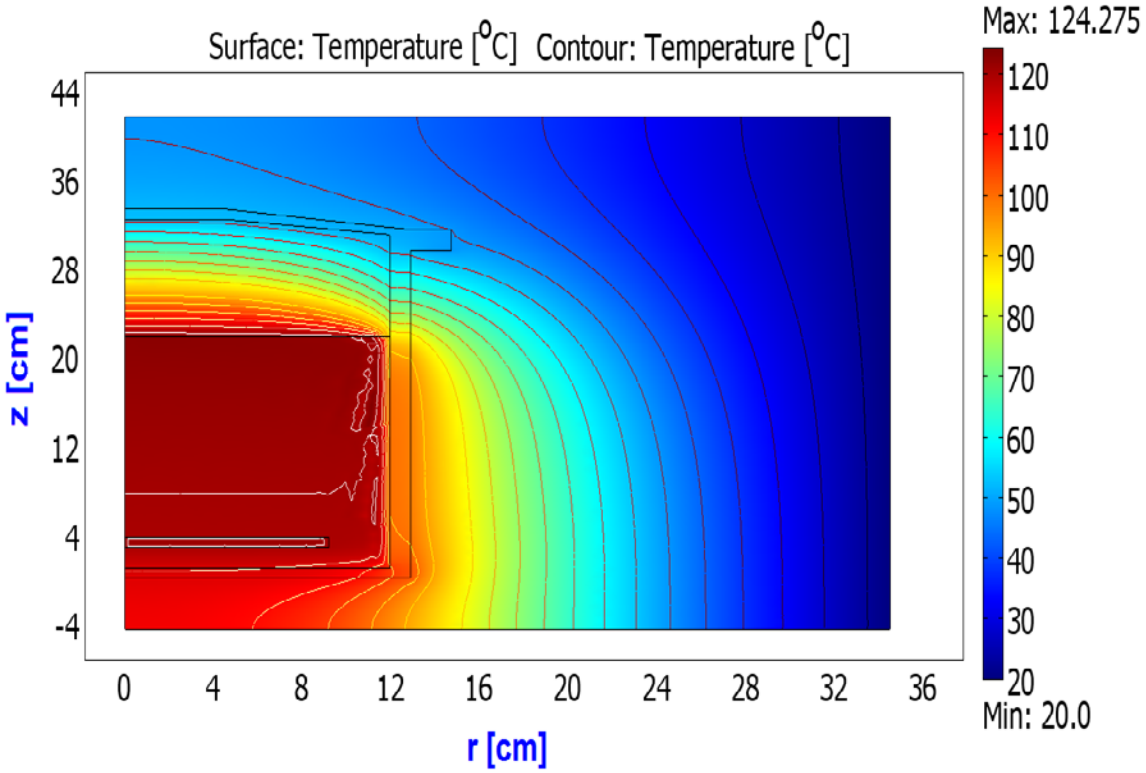

Figure 4-33.The 2-D axis symmetric domain plot for vacuum frying vessel within control volume of air represented by surface and contour plot at oil temperature of 120°C with 12 liter of oil at 0.2286 m height in the vessel.

4.13.2. Effect of vessel pressure 1.33kPa (vacuum), 101.325 kPa (atmospheric) and 200 kPa (pressure fryer)

In a vacuum space, the primary mode of heat transfer is radiation. The heat transfer is limited in a cavity only by surface to surface radiation. The temperature distributed across the farthest boundary at the top space of the fryer was 50 to 60^{o}C in standard vacuum frying conditions. The effect of change in pressure from vacuum to atmospheric and high pressure is shown in (Figures 4-34 and 4-35). At atmospheric pressure conduction, radiation, and convection increased heat transfer inside the top space of the fryer.

The temperature distribution due to conduction in the fryer's aluminum wall does not show a higher temperature rise, but slight temperature drop profiles (Figure 4-36). Increase in pressure is directly related to rise in temperature according to the ideal gas law for the air present inside the fryer vessel. The pressure increased the convective heat transfer from the oil. This increase was only noticed for the air inside the fryer, while the temperature drop on the aluminum wall was very little and can be seen for 1.33 kPa, 101.325 kPa, and 200 kPa (Figure 4-36).

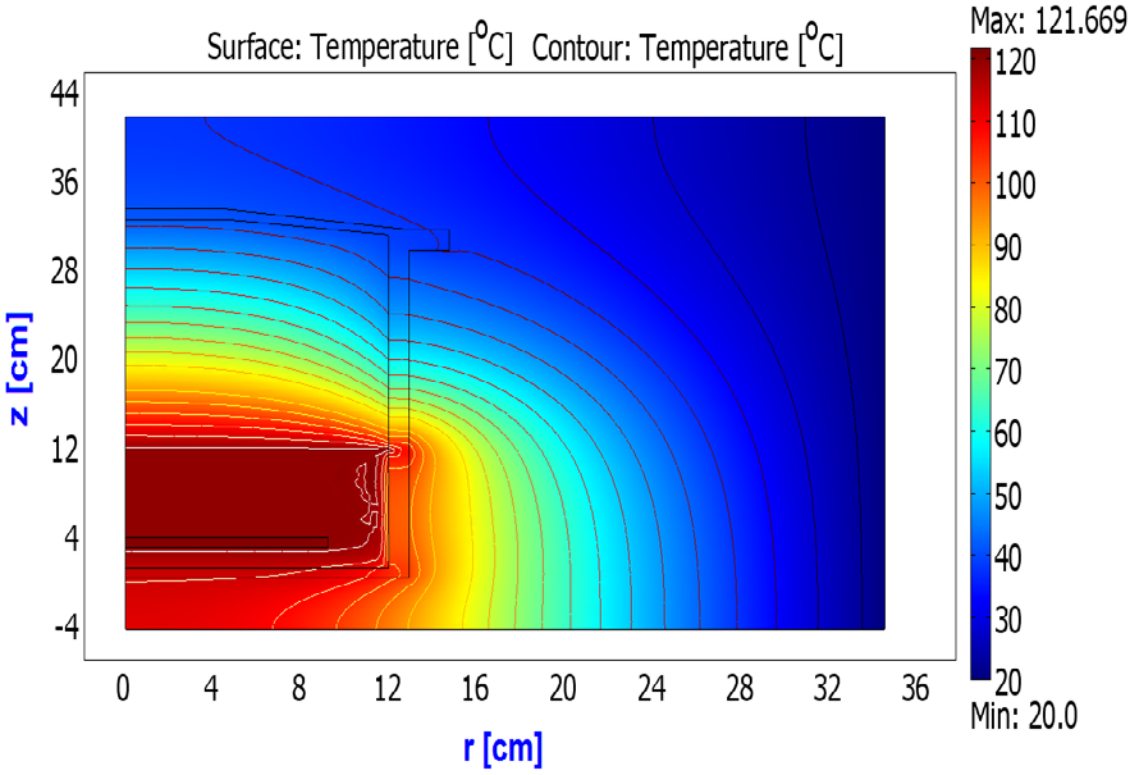

Figure 4-34. 2-D axis symmetric domain plot for vacuum frying vessel within control volume of air represented by surface and contour plot at oil temperature of 120°C at atmospheric head space pressure condition.

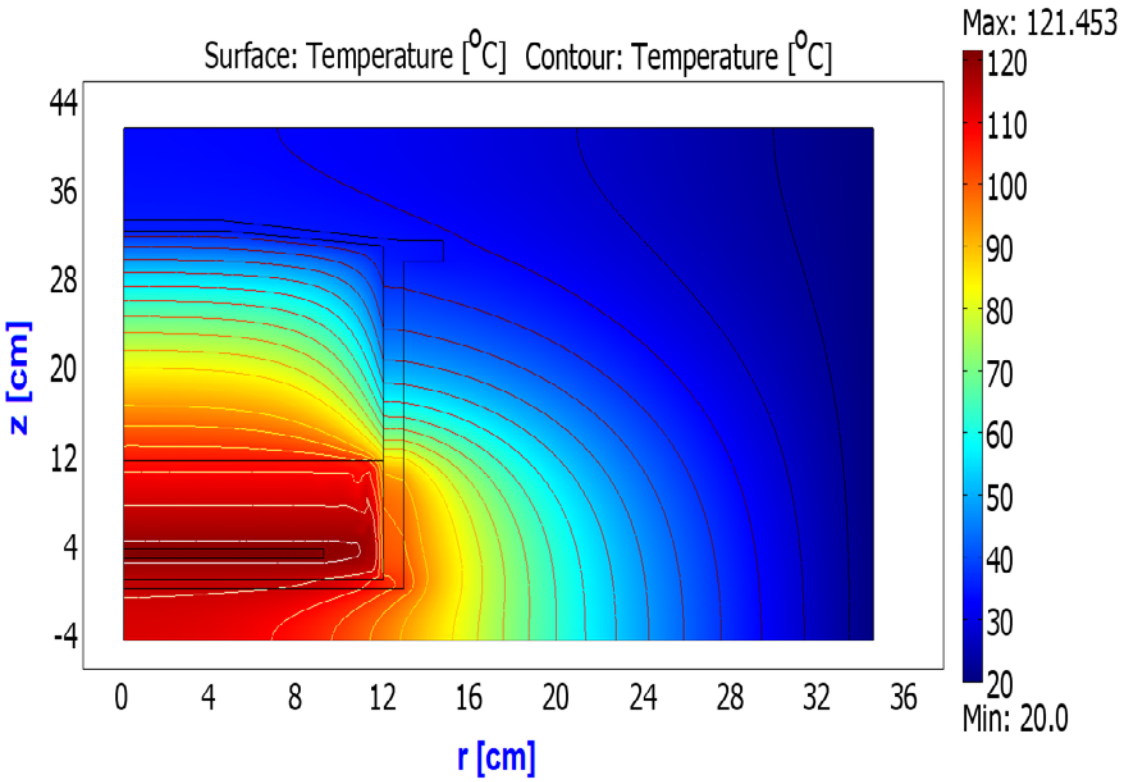

Figure 4-35. 2-D axis symmetric domain plot for vacuum frying vessel within control volume of air represented by surface and contour plot at oil temperature of 120°C at 200 kPa head space (high pressure) condition.

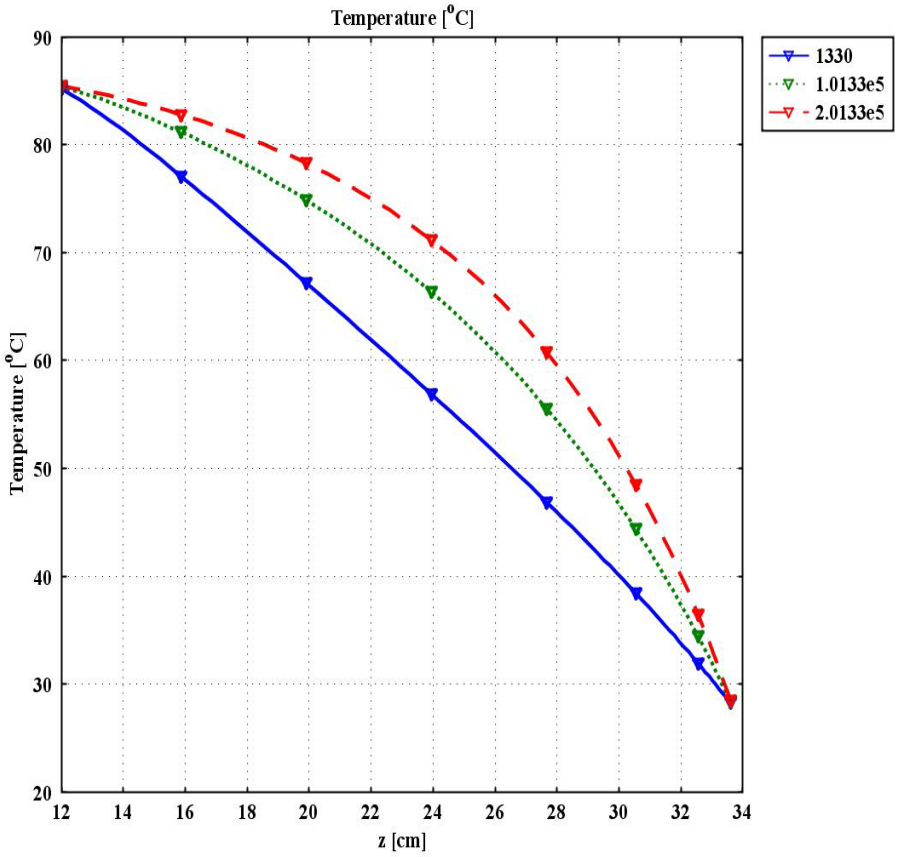

Figure 4-36. Loss in temperature across the length of vertical (z-component [cm]) aluminum vacuum fryer vessel wall with change in pressure at 1.33 kPa, 101.325 kPa, and 200 kPa.

4.13.3. Effect of insulation thickness (0.5 cm, 1.3 cm, and 2.54 cm thick layer)

The vacuum fryer heating element was controlled by a thermostat probe that sensed the temperature of the oil. Temperature loss of the fryer vessel and optimization of heat distribution inside the vessel led to a detailed sensitivity analysis. The modeling results were applied in the real condition to achieve better energy efficiency of the fryer. The effect of different thickness of insulation (k = 0.04 W/m^{2}K) was found through sensitivity analysis. It helped in finding the most suitable thickness of insulation that can be installed on the fryer.

Thickness of 0.5 cm showed a slight drop in heat loss from fryer walls and increased the temperature distribution inside the fryer vessel (Figure 4-37). The result was not optimum and the temperature loss was analyzed by further increasing the thickness to 1.3 cm and 2.54 cm (Figures 4-38 and 4-39) respectively. The graph between the different thickness of insulation and temperature drop at the bottom of the fryer vessel along the radius of the vessel is shown by Figure 4-40.

Using 1.3 cm and 2.54 cm thick insulation gave very close results, although using 2.54 cm thickness for the fryer vessel was not a feasible solution, because of the space covered due to an increase in the diameter of the fryer. Therefore, a 1.3 cm thickness was chosen as the most suitable thickness for reducing heat loss around the fryer walls. The observation of the fryer after installing the insulation showed a similar temperature drop in the T_{amb} thermocouple, and thermostat switching became more infrequent than in the previous design without insulation.

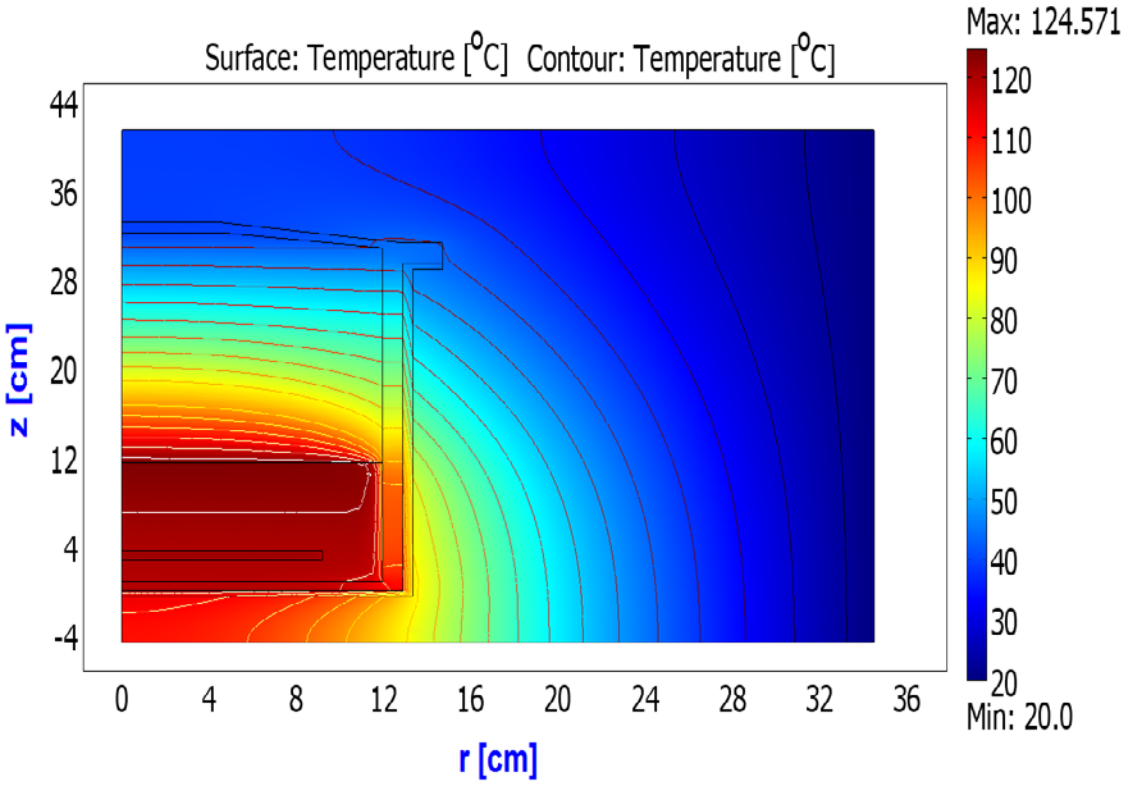

Figure 4-37. 2-D axis symmetric domain plot for vacuum frying vessel within control volume of air represented by surface and contour plot at oil temperature of 120°C at 1.33 kPa head space and insulation thickness 0.5 cm.

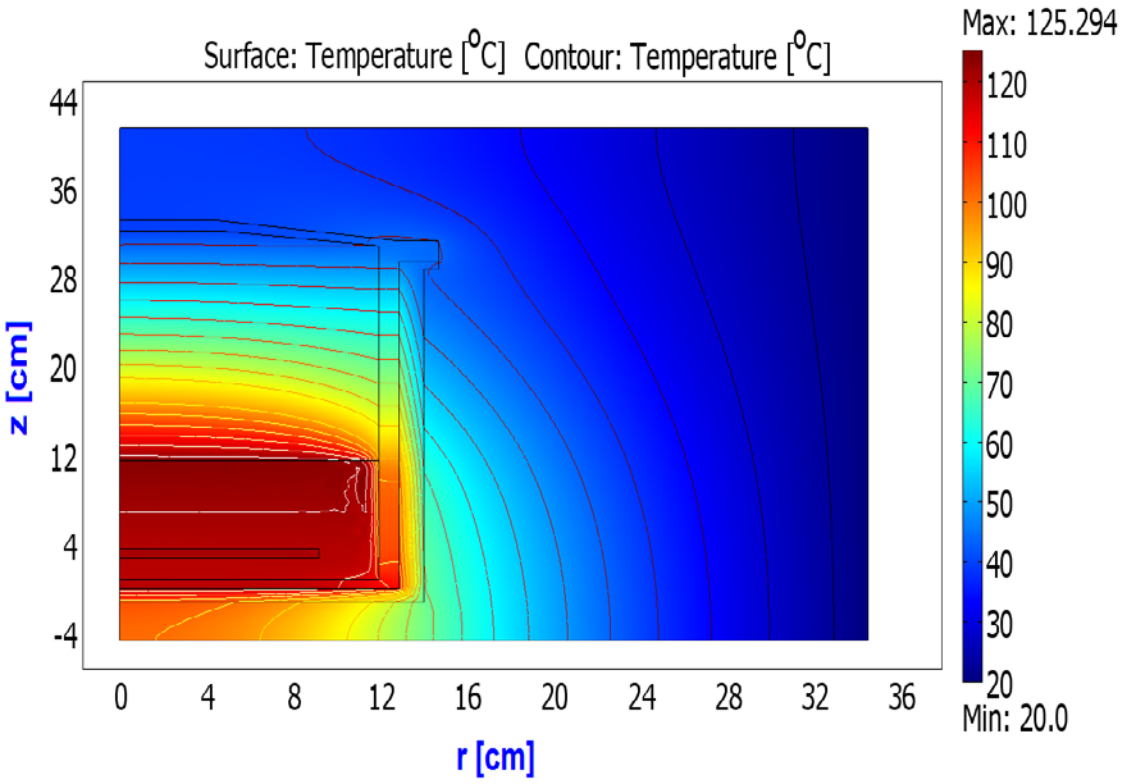

Figure 4-38. 2-D axis symmetric domain plot for vacuum frying vessel within control volume of air represented by surface and contour plot at oil temperature of 120°C at 1.33 kPa head space and insulation thickness 1.3 cm.

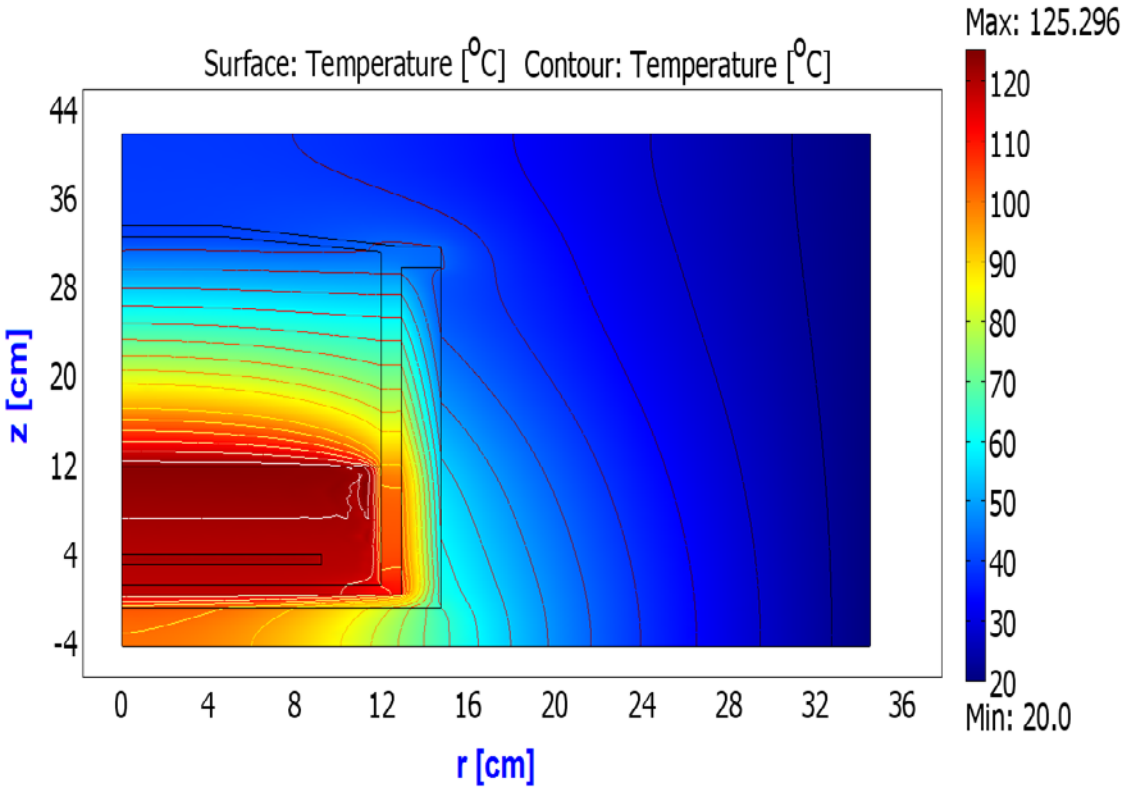

Figure 4-39. 2-D axis symmetric domain plot for vacuum frying vessel within control volume of air represented by surface and contour plot at oil temperature of 120°C at 1.33 kPa head space and insulation thickness 2.54 cm.

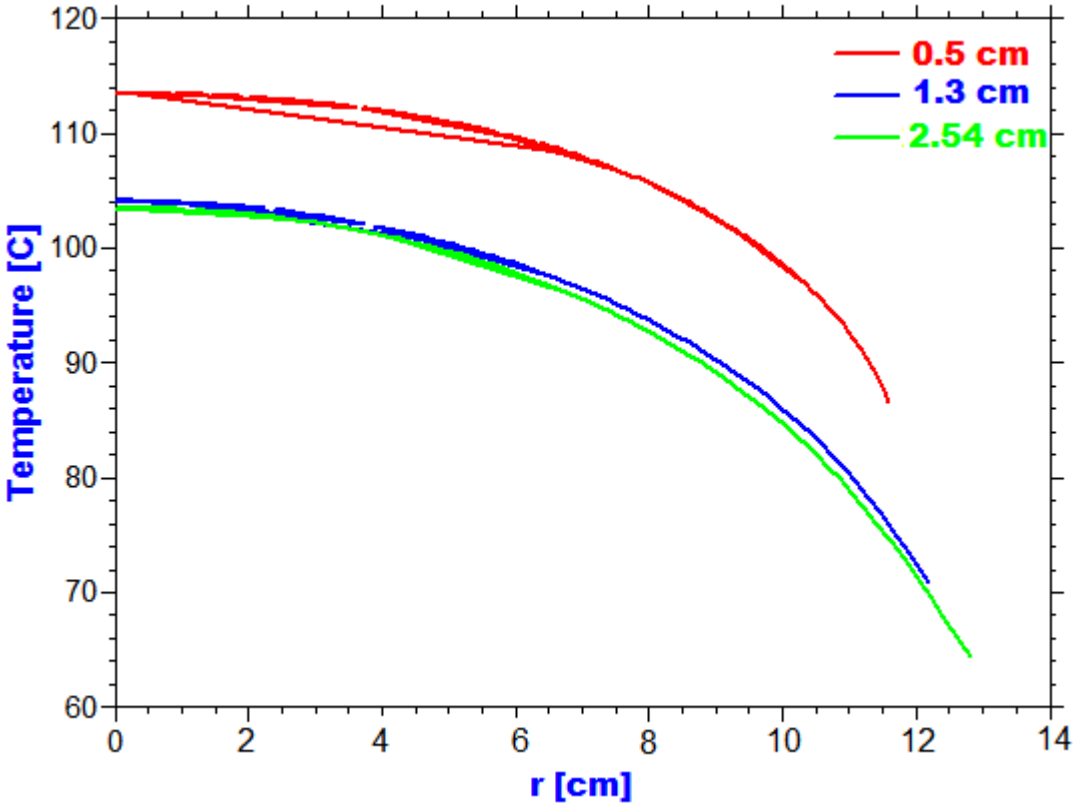

Figure 4-40. Loss in temperature across the radius of horizontal (*r*-component) aluminum vacuum fryer vessel bottom with change in thickness of insulation at 0.5 cm, 1.3 cm, and 2.54 cm.

4.14. Condenser simulation

A model was developed to optimize the spiral coiled tube heat exchanger (SHE) unit connected to a refrigeration system by using equipment and process data. Various theoretical equations were used to form a complete model for the heat and mass transfer taking place in the vacuum frying system (see Chapter III).

Experimental data were collected to identify the values of temperature at different location in the refrigeration system to determine the system performance. Figure 4-41 shows the locations of the thermocouples in the refrigeration system. About 30 g of potato slices were fried during the process. The experimental data were collected in triplicate.

The temperatures of the condenser (inlet, middle, and outlet) and capillary (inlet and outlet) remained almost constant during the process at 50^{o}C, 29^{o}C, 26^{o}C, 26^{o}C, -15^{o}C, respectively (Figure 4-42). The condenser inlet temperature varied slightly from 45-50^{o}C. For the compressor and evaporator units, the temperatures were recorded at the compressor in and out, at the evaporator in and out as well as after the capillary and before the compressor points. There was a larger variation in the temperatures at the compressor in and refrigerant out during the period of time when most of the water vaporized from the product (Figure 4-43).

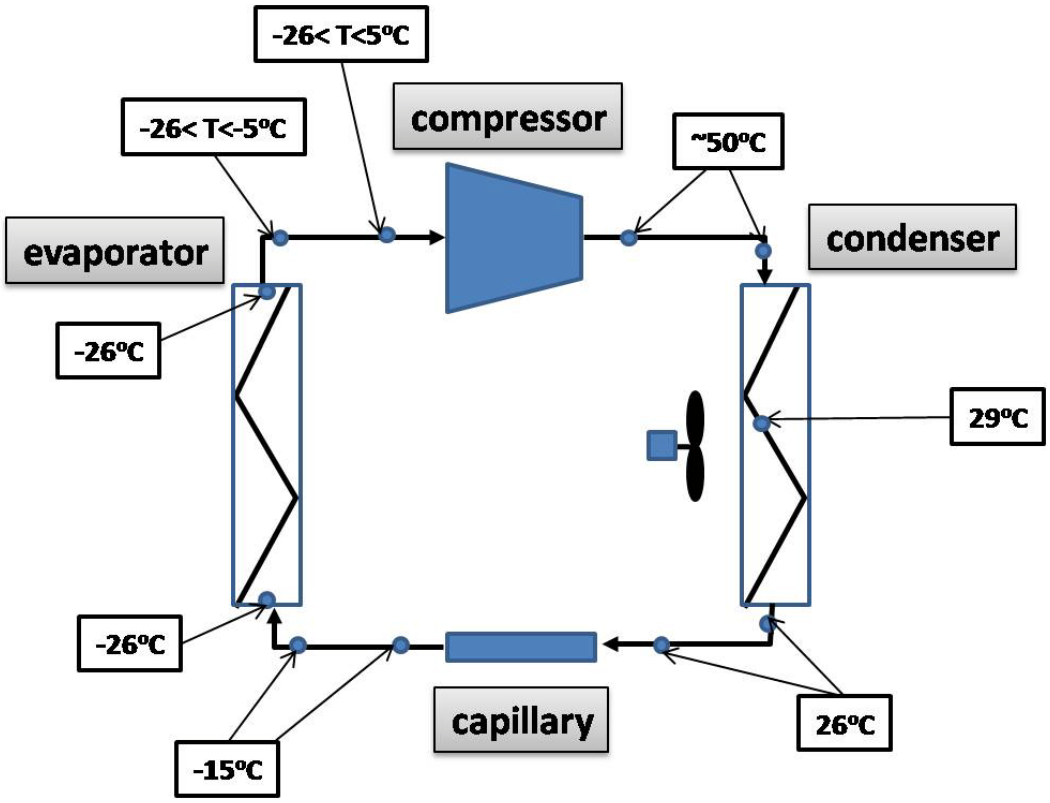

Figure 4-41. Location of the thermocouples (and their measured values) in the vapor-compression refrigeration cycle used in the vacuum frying system (P_{vac} = 1.33 kPa, T_{oil} = 120°C, 30 g of potato slices).

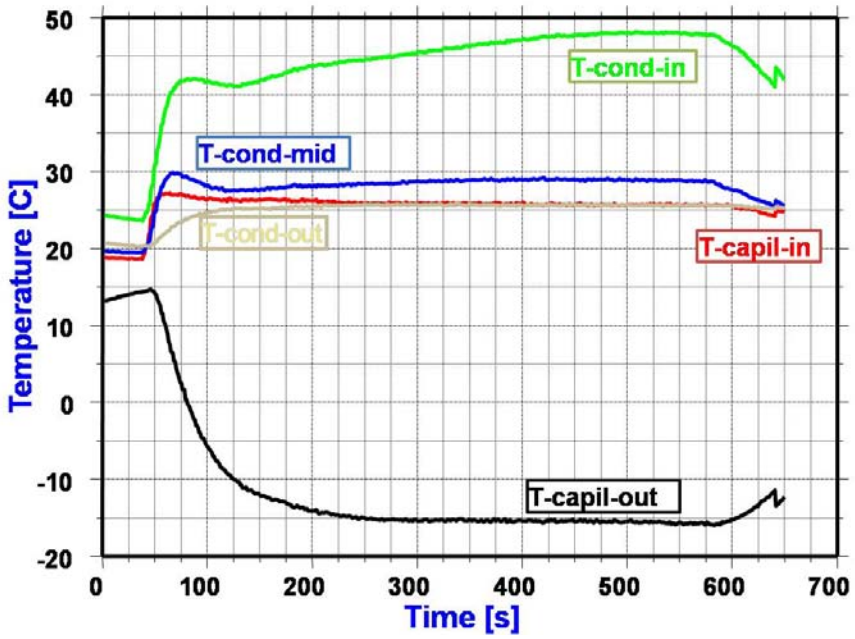

Figure 4-42. Temperature history of different locations in the refrigeration system at condenser and capillary tube.

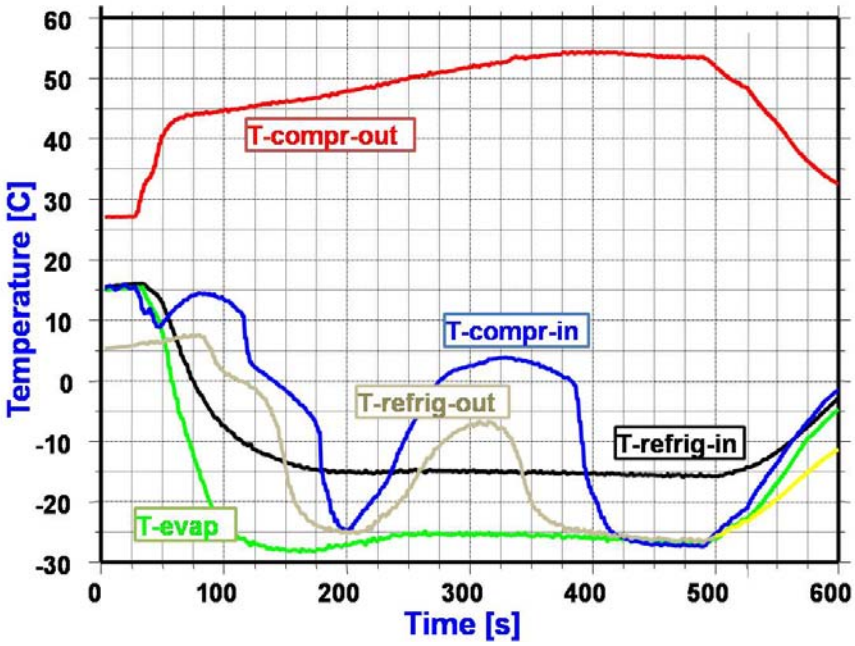

Figure 4-43. Temperature history of different locations in the refrigeration system at compressor and evaporator.

Drawing the temperature values in a *P-h* diagram for R-404A allowed for a better analysis of the operational aspect of the system. Figure 4-44 shows the lines drawn for each component in the refrigerant chart. From the diagram, the enthalpy values were obtained and used to calculate the system capacity. The results in Figure 4-44 clearly show that the system is operating at 26^{o}C sub-cooling temperature and maximum superheating (returning gas temperature) at 5^{o}C. The values of the enthalpies were the following (Figure 4-45): h_1 = 239.5 kJ/kg; h_2 = 355.8 kJ/kg; h_3 = 386.1 kJ/kg; h'_2 with 5^{o}C superheat = 378.4 kJ/kg and h'_3 = 440 kJ/kg.

The maximum cooling load is obtained at the beginning of frying and can be calculated from Equation [3-17] to be q = 1125 W. Therefore, the maximum mass flow rate of refrigerant can be determined as:

$q_{evap} = \dot{m}_{ref}(h_2 - h_1) \rightarrow \dot{m}_{ref} = 1125/[(355.8 - 239.5) \times 1000] = 0.0097 kg/s$ or

$\dot{m}_{ref} = 1125/[(378.4 - 239.5) \times 1000] = 0.0082 kg/s$ if considering the evaporator outlet has a 5^{o}C superheat. The average mass flow rate of the refrigerant was calculated as 0.0021 kg/s (average cooling load of 249 W) during the frying period (first 200 s).

Figure 4-45 shows the compressor power consumption data collected during the experiments. A voltmeter (Model P4400, kill-a-watt, NY, USA) was used to measure these values. The average power consumption values were 343.00±10.46 W before the basket was immersed in the oil ($t < 200s$).

During frying, the power consumption increased to 362.65±7.39 W ($200 s < t < 520 s$) and remaining around 360 W after most of the water evaporated from the product. The total average power consumption was 358.18±11.55 W. Based on the average power consumption, the system capacity was determined as 284 W with a mass flow rate of 0.0025 kg/s (close to the simulated results).

Table 4-5 shows the measured and calculated values used to analyze the system performance. The system will have a lower COP when operating under superheated conditions.

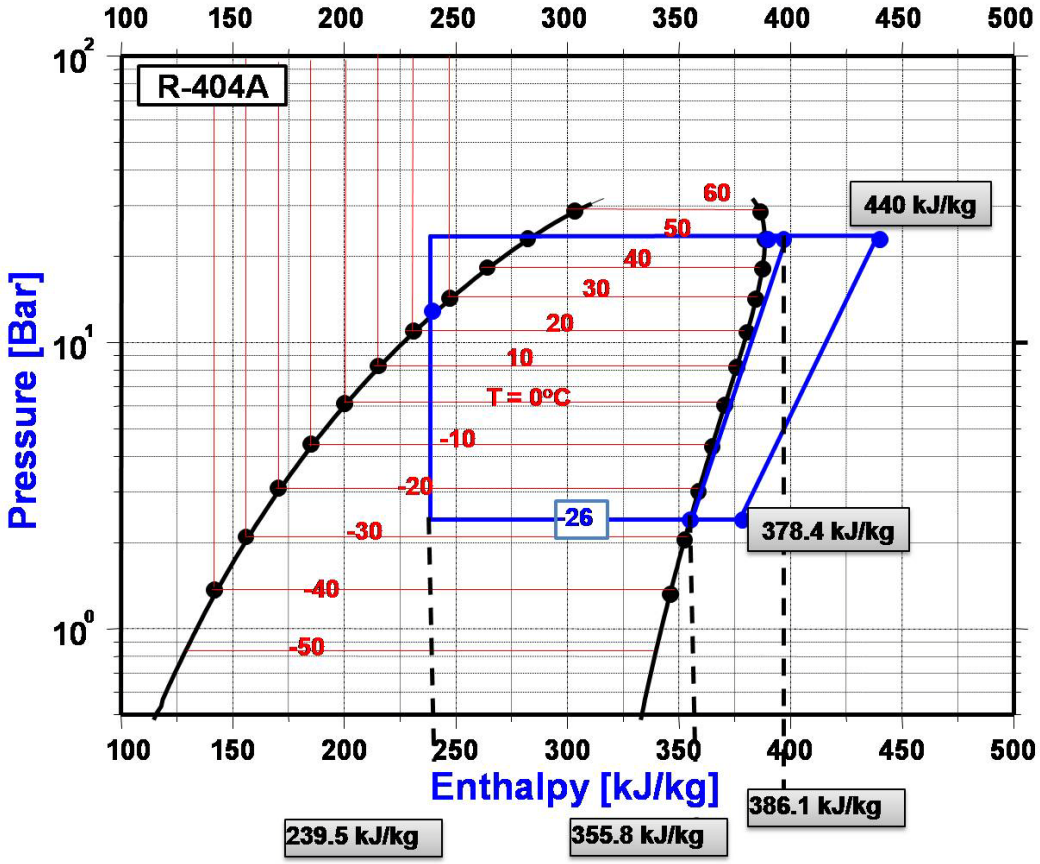

Figure 4-44. A pressure-enthalpy chart for the vapor-compression refrigeration cycle for the vacuum frying system (P_{vac} = 1.33 kPa, T_{oil} = 120°C, 30 g of potato slices).

Table 4-5. Average values for compressor power and evaporator capacity calculated based on the measured temperatures at different locations in the refrigeration system.

Evaporator *T* [°C]	-26	**Superheat *T* [°C]**	5
Condenser *T* [°C]	50	**Sub-cooling *T* [°C]**	26
Power [W]	358.2±11.6	**Current [A]**	5.9±0.2
Capacity [W] (measured)	249 (284)	**Mass flow rate [kg/s]**	0.0021(0.0025)
EER [kJ/W-h]	2.5	**COP (with superheat)**	3.87 (2.26)

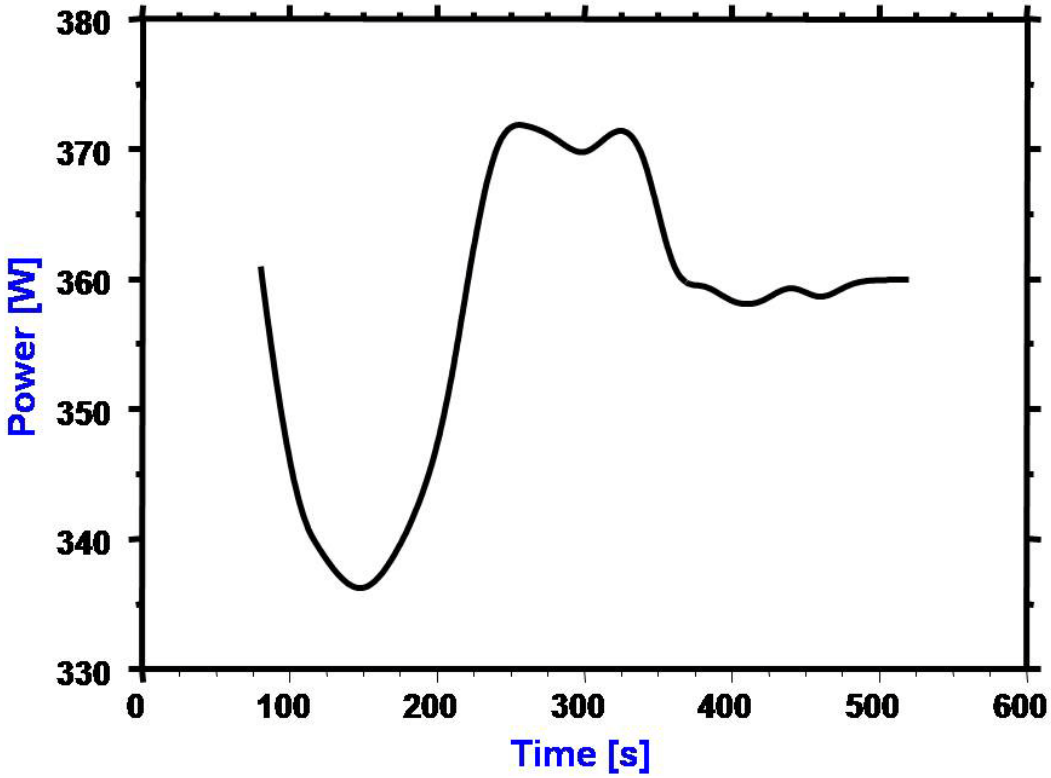

Figure 4-45. Power consumption curve for the vapor-compression refrigeration cycle for the vacuum frying system (P_{vac} = 1.33 kPa, T_{oil} = 120^{o}C, 30 g of potato slices).

This system was charged with 0.908 kg (2 lbs) of R-404A. The efficiency of all refrigeration systems suffers if the system has either too little or too much refrigerant charge. Also, the compressor may suffer damage if the system is overcharged. Some systems have only minimal reservoir capacity, making it important to charge the system precisely. Such systems are more vulnerable to loss of efficiency from small leaks (Farzad and O'Neal, 1988).

In direct-expansion chiller systems (which send the refrigerant directly into the cooling coils), low charge is indicated by high superheat in the gas leaving the evaporator, especially when the compressor is operating at full load. Superheat is the excess of the gas suction temperature above the gas saturation temperature. When the evaporator becomes "starved" for refrigerant, the available refrigerant boils off quickly and the unsatisfied heat load of the evaporator superheats the refrigerant gas excessively. In systems that use a thermostatic expansion valve, the valve is designed to maintain a fixed amount of superheat. The purpose of the superheat is to ensure that liquid refrigerant does not enter the compressor. If the superheat setting of the valve is unknown (it is typically 5°C to 11°C), the charge is probably not low if the superheat remains essentially the same at all loads (Farzad and O'Neal, 1988).

In systems with air-cooled condensers, excessive charge is indicated by excessive sub-cooling (cooling of the liquid refrigerant below its saturation temperature) of the refrigerant. When the system is overcharged, the condenser fills with liquid refrigerant and its capacity drops. The liquid lingers in the condenser long enough to become

excessively sub-cooled. The difference in temperature between normal and sub-cooled refrigerant from a condenser is small (Farzad and O'Neal, 1988).

4.15. Theoretical sensitivity analysis (evaporator/condenser units)

The effect of different parameters on the coefficient of performance (COP) were evaluated to determine the best operating conditions of the refrigeration system designed to condenser the water vapor coming from the vacuum fryer.

Table 4-6 shows the simulation results. The average values (during the frying process) as well as the minimum and maximum values are presented to illustrate the effect of steam flow rate (high during the first 200 s of frying).

4.15.1. Effect of frying load (30 g, 50 g, and 70 g)

In this case, the condenser surface area, the T_{comp} and T_{evap}, and the LMTD were maintained the same for all frying loads considered in the analysis (Table 4-6, columns 1-3). Increasing the frying load resulted in an increase in the average mass flow rate of refrigerant from 0.0021 kg/s (30 g) to 0.0032 kg/s (50 g) and 0.0050 kg/s (70 g). The overall heat transfer coefficient (U) in the condenser increased from 441 W/m^{2}K (30 g) to 774 W/m^{2}K (50 g) and 1031 W/m^{2}K (70 g) due to an increasing in the cooling load (CL) and thus the mass of water vapor. The compressor power requirement increased with the frying load from 0.074 kW (0.1 hp) (30 g) to 0.11 kW (0.15 hp) (50 g) and 0.18 kW (0.24 hp) (70 g). The maximum power requirements ranged from 0.33 to 0.81 kW (0.44 – 1.1 hp). The COP was 3.87 for all loads.

4.15.2. Effect of operating the system at sub-cooling and superheating conditions

For this analysis, the frying load was 30 g and the condenser dimensions and the LMTD were constant (Table 4-6, columns 1, 4, 5). Operating at the saturation conditions (Figure 4-46 – cycle abcd) with enthalpy values of h_1 = 282 kJ/kg, h_2 = 356 kJ/kg, and h_3 = 386 kJ/kg, resulted in a COP of 2.47, the average refrigerant mass flow rate was 0.0032 kg/s, and the average compressor power requirements of 0.11 kW (0.15 hp) (maximum at 0.49 kW (0.66 hp)). Operating the system at a sub-cooling ($T_{subcool}$ = 26^{o}C) conditions (Figure 4-46 - cycle a'b'cd) increased the COP to 3.87, reduced the refrigerant mass flow rate to 0.0021 kg/s, and diminished the power requirements to (0.11 kW (0.15 hp) (maximum at 0.33 kW (0.44 hp)). When operating at sub-cooling and superheating conditions ($T_{superheat}$ = 5^{o}C), the mass flow rate was reduced (0.0018 kg/s), the compressor power requirements increased (from 0.074 to 0.13 kW (0.099 - 0.18 hp)), and the COP decreased (from 3.87 to 2.23).

4.15.3. Effect of changing the evaporator temperatures (-26^{o}C to -10^{o}C)

The results of this study are shown in columns 2, 6, 8, and 9 (Table 4-6). Operating the system at an evaporator temperature of -10^{o}C (green lines in Figure 4-46) compared to running it at T_{evap} = -26^{o}C, reduced the LMTD (from 42 to 26^{o}C) and thus increased the overall heat transfer coefficient (441 to 702 W/m^{2}K) of the evaporator for the same frying load. The average refrigerant mass flow rate did not change significantly (and the compressor requirements), but the COP was reduced from 3.87 to 3.79. Comparing the results from columns 6 and 9, i.e., when operating the system at sub-cooling and superheating conditions showed that it would be more efficient if the

T_{evap} = -10°C (COP = 3.38) than if T_{evap} = -26°C (COP = 2.23). The mass flow rate of refrigerant is the same, but the compressor power requirements is reduced (from 0.13 kW to 0.085 kW (0.18 to 0.11 hp)) when the system is running at -10°C evaporator temperature compared to -26°C.

4.15.4. Effect of changing the condenser temperatures (50°C to 40°C)

In this analysis, the frying load was 30 g and the evaporator dimensions were the same for all cases. The results of this simulation are presented in columns 8-11 (Table 4-6). Changing the condenser temperature from 50 to 40°C (running at sub-cooling conditions) reduced the COP (columns 8 and 10 – Table 4-6) a little (from 3.78 to 3.68), but the compressor power requirement remained the same (pink lines in Figure 4-46). When the system operates at sub-cooling and superheating conditions and T_{evap} = 40°C compared to 50°C (columns 9 and 11 – Table 4-6), the COP increased (from 3.38 to 4.09) and the compressor power requirements lowered (from 0.085 kW to 0.070 kW (0.11 – 0.095 hp)).

Lower compression power requirements is obtained by running the system at T_{evap} = -10°C and T_{comp} = 40°C than at T_{evap} = -26°C and T_{comp} = 50°C.

4.15.5. Effect of changing the evaporator surface area (0.0129 m^2 and 0.0258 m^2)

If the evaporator surface area is doubled, but the cooling load is the same, the only thing that will be affected is the overall heat transfer coefficient (U) as shown in Table 4-6 (columns 2 and 7). It was reduced by half (441 to 221 W/m^2K).

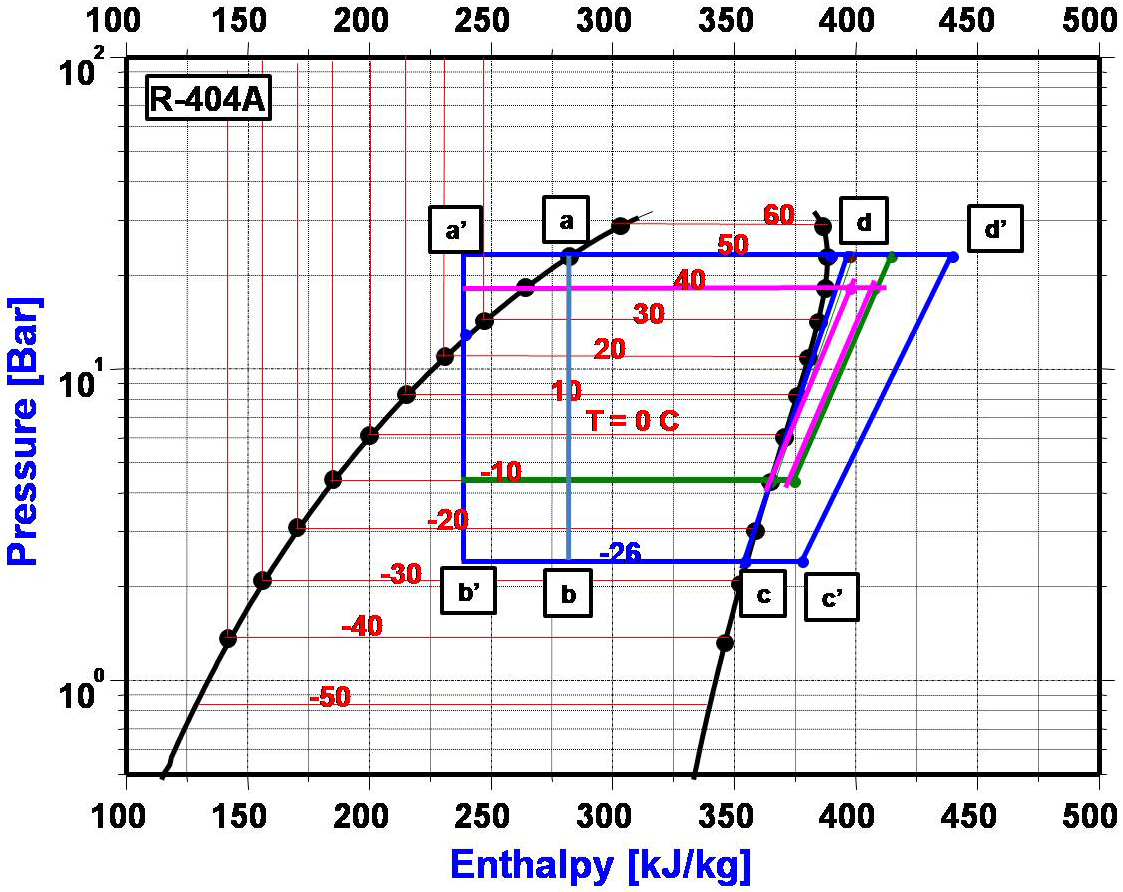

Figure 4-46. A pressure-enthalpy chart for the vapor-compression refrigeration cycle for different operating conditions (P_{vac} = 1.33 kPa, T_{oil} = 120°C, 30 g of potato slices).

Table 4-6. Results of sensitivity analysis for the vapor-compression refrigeration cycle.

Load	**30**	**50**	**70**	**30**	**30**	**30**	**30**	**30**	**30**	**30**
m_{ref} [kg/s] min max	0.0021 9.98e-5 0.0094	0.0032 0.00016 0.015	0.0050 0.00024 0.023	0.0032 0.00015 0.014	0.0018 8.67e-5 0.0082	0.0021 9.98e-5 0.0094	0.0020 9.58e-5 0.0090	0.0018 9.21e-5 0.0087	0.0020 9.58e-5 0.0090	0.0018 9.21e-5 0.0087
m_{water} [kg/s] min max	4.79e-5 4.41e-6 0.00043	8.09e-5 7.45e-6 0.00071	1.12e-4 1.03e-5 0.00099	4.79e-5 4.41e-6 0.00043	4.79e-5 4.41e-6 0.00043	4.79e-5 4.41e-6 0.00043	4.79e-5 4.41e-6 0.00043	4.79e-5 4.41e-6 0.00043	4.79e-5 4.41e-6 0.00043	4.79e-5 4.41e-6 0.00043
Mass water [g]	22	37	52	22	22	22	22	22	22	22
Cooling Load [W] min max	249 12 1125	420 20 1899	582 28 2630	249 12 1125	249 12 1125	249 12 1125	249 12 1125	249 12 1125	249 12 1125	249 12 1125
LMTD min max	42 41 48	42 41 48	42 41 48	42 41 48	42 41 48	42 41 48	26 25 32	26 25 32	26 25 32	26 25 32
UA [W/K] min max	5.71 0.29 23.25	9.63 0.49 39.25	13.00 0.69 54.00	5.71 0.29 23.25	5.71 0.29 23.25	5.71 0.29 23.25	9.1 0.49 25	9.1 0.49 25	9.1 0.49 25	9.1 0.49 25
A [m^2]	0.0129	0.0129	0.0129	0.0129	0.0129	0.0258	0.0129	0.0129	0.0129	0.0129
U [W/m^2K] min max	441 22 1798	744 38 3031	1031 53 4200	441 22 1798	441 22 1798	221 11 1028	702 38 2686	702 38 2686	702 38 2686	702 38 2686
h1 [kJ/kg] h2 [kJ/kg] h3 [kJ/kg]	240 356 386	240 356 386	240 356 386	282 356 386	240 378 440	240 356 386	240 365 398	240 375 415	240 365 399	240 375 408
COP	3.87	3.87	3.87	2.47	2.23	3.87	3.78	3.38	3.68	4.09
Compressor Power [W] $\eta = 85\%$	74.12	112.94	176.47	112.94	131.29	74.12	77.65	84.71	80.00	69.88
T_{evap} [°C]	-26	-26	-26	-26	-26	-26	-10	-10	-10	-10
T_{cond} [°C]	50	50	50	50	50	50	50	50	40	40
$T_{subcool}$[°C]	26	26	26	no	26	26	26	26	26	26
$T_{superheat}$[°C]	No	no	no	no	5	no	no	5	no	5

4.15.6. Effect of ice formation at the evaporator coil (vacuum frying system condenser)

During the experiments, it was noticed that ice formed at the surface of the heat exchanger coil. Ice behaves as an insulator and it can reduce the efficiency of heat transfer between the refrigerant and the steam. Thus, it is important to analyze the effect of ice formation on the heat transfer rate. A simplified heat transfer analysis was done to calculate the effect of ice formation at the surface of the evaporator coil. At steady state, it was assumed that the temperature of the steam entering the heat exchanger unit was 20°C, the temperature of the refrigerant -26°C, and the heat exchanger was simplified as a concentric cylinder as shown in Figure 3-14 (Chapter III). A resistance in series was used to model the heat transfer through the coil to the steam (Figure 4-47):

$$q = \frac{\Delta T}{\frac{1}{2\pi r_{steam} h_{steam} L} + \frac{\ln(r_{ice}/r_{cop2})}{2\pi k_{ice} L} + \frac{\ln(r_{cop2}/r_{cop1})}{2\pi k_{cop} L}} = \frac{(20-(-26))^{o}C}{\frac{1}{2\pi r_{steam} h_{steam} L} + \frac{\ln(r_{ice}/r_{cop2})}{2\pi k_{ice} L} + \frac{\ln(r_{cop2}/r_{cop1})}{2\pi k_{cop} L}} \quad [4\text{-}3]$$

where the h_{steam} is the convective heat transfer coefficient for condensation and convection (~10,000 W/m^{2}K) (Chapter III) and k_{cop} is the thermal conductivity for copper (~ 401 W/mK). Assuming that the copper wall is thin, the resistance term due to conduction in the copper wall can be considered negligible. The value of h_{ice} depends on the porosity of ice layer formed around the coil ($= (1 - porosity)^2 \times k_{ice} / \Delta x_{ice}$) (Chapter III). Figure 4-48 shows the effect of ice formation on the rate of heat transfer (q [W]) from the steam to the refrigerant.

As expected, the heat transfer rate decreases as the thickness of ice increases during the process. The heat transfer without an ice layer at the coil surface is around 41 kW because the only resistance term in Equation 4-3 is due to condensation of steam. Reducing the refrigerant temperature to -10°C, for example, may decrease the condensation rate ($\dot{m}_{cond} = q / h_{fg}^{'}$; see Equation 3-33) from 0.0164 kg/s (at 41 kW) to 0.011 kg/s.

Porosity of the ice affects the thermal conductivity of ice (k_{ice} ~ 2.2 W/mK). For a porosity value of 0.3, the k_{ice} = 1.1 W/mK; for 0.5 ice porosity the k_{ice} = 0.55 W/mK, and for an ice with a porosity of 0.8, the k_{ice} = 0.088 W/mK. Therefore, the higher the porosity of the ice layer, the lower the heat transfer rate (Figure 4-48).

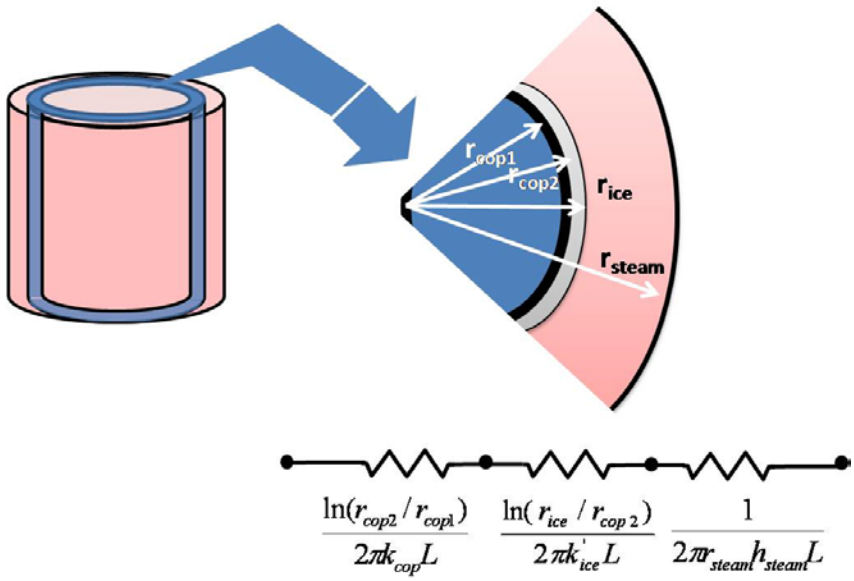

Figure 4-47. Resistance schematic in the condenser unit of the vacuum frying system.

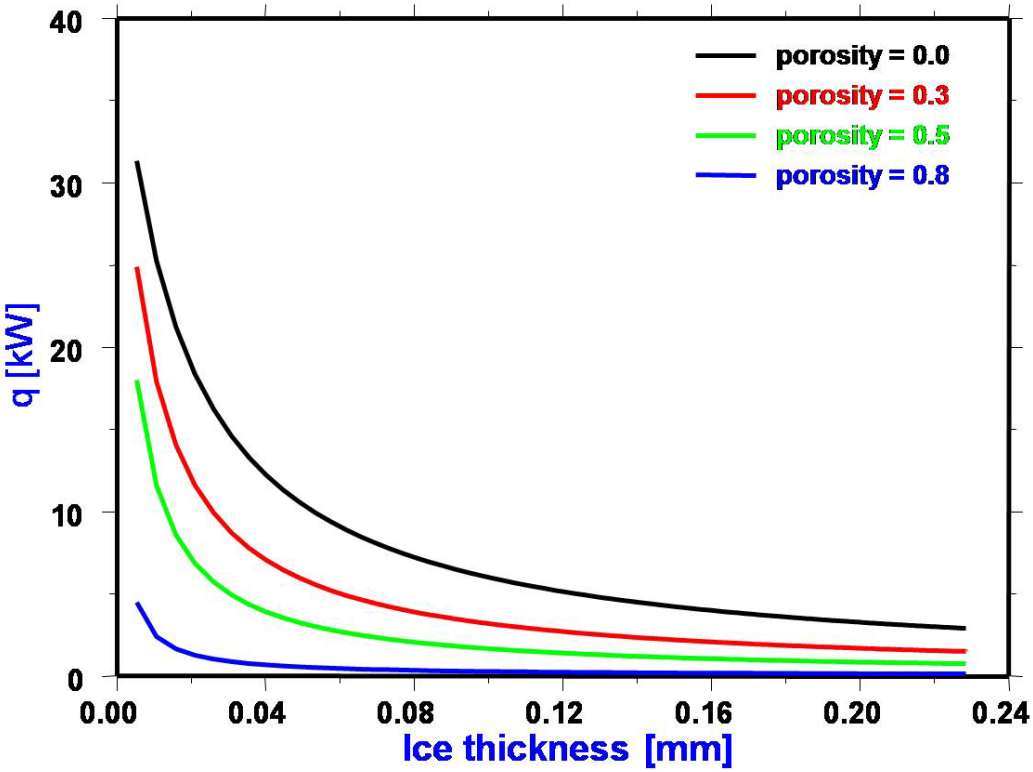

Figure 4-48. Effect of ice formation on the heat transfer rate to condense the steam from potato slices during frying (P_{vac} = 1.33 kPa, T_{oil} = 120^{o}C, 30 g of potato slices).

CHAPTER V

CONCLUSIONS

The centrifuge and condenser units were successfully designed, installed, and optimized through various experiments and modeling of the vacuum frying system. Potato chips were fried at 120^{o}C and 140^{o}C oil temperature and 1.33 kPa pressure. The corresponding results were used to improve the design and to gain more knowledge of the process operations in detail.

The following conclusions can be drawn from this work:

- During vacuum frying, the $T_{cond,\ out}$ temperature reached a value of 8^{o}C to 9^{o}C at 70 g load, while T_{sat} for water vapor at 1.33 kPa vacuum pressure is 9.14^{o}C. Therefore, the maximum load capacity of the condenser is 70 g of potato slices.
- The fryer head space and T_{amb} temperature showed a slight increase with the increase in potato slice load (30 g, 50 g, and 70 g); therefore temperature of the steam in the system is independent of potato slice frying load, but dependent on the vacuum pressure of the system.
- The amount of water collected in the condenser was very close (6 to 0.4 g differences) to the amount of water evaporated when frying potato slices; this shows that the efficiency of the system is more than 99% during vacuum frying of potato chips.
- The amount of water collected in the condenser after frying increased with the amount of potato slices fried: for 30 g of potato slices, ~ 16 g of moisture was

collected; for 50 g potato slices, about 33 g of moisture was collected; and for 70 g of potato slices ~ 52 g of moisture was collected.

- The de-oiling system removed up to 72% of the chip's surface oil when centrifuged for 40 s at 750 rpm (67% at 300 rpm). At 750 rpm, the oil content in the chips was reduced by 38%, 44%, and 51% when centrifuged for 10 s, 40 s, and 60 s, respectively.
- Less variability in oil content was found at pressurization after de-oiling at 750 RPM in comparison to 300 RPM.
- The heated oil convective heat transfer coefficients (h) for the vacuum frying process were 217$\pm$13 W/m^{2}K (120^{o}C) and 258$\pm$37 W/m^{2}K (140^{o}C). The h-values increased up to 3.6 times during the boiling period. For the atmospheric frying process, the h-value during boiling was 2.5 times larger than during heating.
- During frying (at 120^{o}C), the temperature at the center of chips increased at a faster rate showing a temperature spike just after submersion in frying oil. In less than 25 s, after that, the chip's temperature was reduced to 80^{o}C. This phenomenon can be explained by analogy with the Joule-Thompson effect, i.e, a cooling effect due to evaporation of gas (water vapor) in a porous media (potato slices). During this process, the enthalpy remains constant, while the water vaporizes through the pore space, from high pressure to lower pressure, to cover the place of already evaporated surface water at the pore's outlet.
- The vacuum process (1.33 kPa) may cause the center temperature of potato slices to drop down (evaporation cooling effect) to a maximum of about 9^{o}C (T_{sat}) inside the

vacuum fryer head space before the slice are immersed in the hot oil (200 s). During this period, about 0.8 g of water was removed from the potato slices.

- The microstructure of vacuum fried potato chips is very different from atmospheric fried chips. Vacuum fried ships show less pore rupture and a more uniform pore size distribution. Atmospheric frying cause higher starch gelatinization due to the higher frying temperature used in the process.
- The COMSOL^{TM} software helped in analyze the fryer system by showing the temperature distribution around the vessel. Large temperature gradients were observed at the head space of the vessel and around the wall. A sensitivity analysis showed that higher oil volume (12 L instead of 6.65 L) would reduce these temperature gradients in the head space thus increasing the process thermal efficiency. Atmospheric and higher pressure increased the convection heat transfer from the oil to the head space.
- A 2.54 cm layer of insulation showed to be very effective in stopping the heat leakage from the vacuum fryer walls. However, a 1.3 cm thick layer was most feasible for the fryer size, and it was chosen to be installed on the fryer wall. After installation of the insulation, the set temperature was maintained and the thermo-switch remained off for longer periods of time during frying.
- The spiral coiled tube heat exchanger (SHE) unit designed to condense the steam generated in the fryer was connected to a vapor-compression refrigeration system to use the refrigerant (R-404A) as the cooling medium. Experimental test showed that the refrigeration system operated at T_{evap} = -26^{o}C and T_{cond} = 50^{o}C with 26^{o}C sub-cooling.

- Sensitivity analysis using fundamental equations showed that the system COP was about 3.87 at these conditions with a compressor power requirement (CPR) of 74 W (85% efficiency) when frying 30 g of potatoes (control case). The CPR increased to 113 W and 176 W when the frying loads were 50 g and 70 g, respectively.
- Operating at the saturation conditions (compared with the control case) decreased the COP to 2.47 and increased the CPR to 113 W. Operating under superheating (5^{o}C) and sub-cooling conditions reduced further the COP to 2.23 while the CPR increased to 131 W.
- Operating the system T_{evap} = -10^{o}C and T_{cond} = 50^{o}C with 26^{o}C sub-cooling reduced slightly the COP to 3.78 and increased the CPR to 78 W in relation to the control case.
- The best results were obtained when operating the system at T_{evap} = -10^{o}C and T_{cond} = 40^{o}C with 26^{o}C sub-cooling and superheat of 5^{o}C. The predicted COP was 4 and the CRP 70 W.
- Fundamental calculations showed that ice formation at the surface of the evaporator coils can reduce substantially the condensation rate during the process. Also, reducing the refrigerant temperature to -10^{o}C (from -26^{o}C) can reduce the condensation rate by 30%.

CHAPTER VI

RECOMMENDATIONS FOR FUTURE WORK

- The effect of the pre-condenser and its further optimization must be carried out in future studies for increasing the performance of the vapor condenser system.
- A better methodology must be found for measuring surface temperature of thin potato slices during vacuum frying.
- Condensation of steam is a complex process that can be studied using both surface and drop-wise condensation approaches. A detailed study of condensation on the helical coil inside the main condenser must be developed in the future.
- Ice formation inside the condenser was ignored in this study, but it should also be analyzed in future work.
- The condensing unit can be further optimized with the help of a TXV thermal expansion throttle valve instead of the currently used capillary tube system.
- The vacuum fryer simulator needs further development by incorporating the refrigeration cycle, which may allow more detailed understanding of the process. However this may require mounting more thermocouples and upgrading the (OMB-DAQ 54) data acquisition system.
- The current centrifuge de-oiling system must be improved and overtaken by a new and more efficient design.

- A mathematical heat exchanger model must be developed using COMSOL™ or similar modeling tools like ANSYS™ for better understanding of turbulent steam flow and heat transfer inside the heat exchanger.
- The vacuum frying vessel design using COMSOL™ needs further verification and studies must be carried out by introduction of potato chips inside the currently designed 2-D axis symmetric and 3-D models of the vacuum fryer.
- New versions of the vacuum fryer simulator program must be released with addition of more features and compatibility with frying other products.

REFERENCES

AACC, 1986. Approved Methods of American Association of Cereal Chemists. Minneapolis, MN.

Anderson, M.H., Murphy, J.G., Corradini, M.L., Merrill, B.J., 2001. Review and analysis of condensation experiments at University of Wisconsin at Madison-Paper presented at the International Energy Agency Task 2 meeting, March 22, 2001, Idaho National Engineering and Environmental Laboratory, Idaho Falls, ID.

ASHRAE, 2006. Handbook of Refrigeration, (S-I Edition). American Society of Heating, Refrigerating and Air-Conditioning Engineers, Inc. Atlanta, GA.

Bai, B., Guo, L., Chen, X., Feng, Z., 1999. Turbulent heat transfer in a horizontal helically coiled tube. Heat Transfer-Asian Research 28 (5), 395-403.

Baker, J.E., Chandler, S.T., Cornwell, C.J., Johnson,T.A., McKay, H.R., 1997. Process of making reduced oil masa chips, Patent No.(WO/1997/040706). USA.

Banga, J.R., Alonso, A., Gallardo, J.M., Perez-Martin, R.I , 1993. Mathematical modelling and simulation of the thermal processing of anisotropic and non-homogeneous conduction-heated canned foods: Application to canned tuna. Journal of Food Engineering 18 (4) , 369-387.

Banks, D., 2007. Industrial frying, edible oil technology, deep frying: Chemistry, Nutrition, and Practical Applications, Urbana, IL: AOCS Press, 291-304.

Bloch H.P., 2006. A Practical Guide to Compressor Technology, Wiley-Interscience, Malden, MA.

Brooker, D.B., Bakker-Arkena, F.W., Hall, C.W., 1992. Drying and Storage of Grains and Oilseeds. Van Nostrand Reinhold, Inc., New York.

Caixeta, A.T., Moreira, R.G., Catell-Perez, E.M., 2002. Impingement drying of potato chips. Journal of Food Process Engineering 25, 63-90.

COMSOL™, 2005. COMSOL™ multiphysics: Model Library - Heat Transfer. COMSOL™ version 3.4a, Food Engineering Lab, Texas A&M University.

Coulson, J.M., Richardson, J.F., Sinnott, R.K., 1983. Chemical Engineering (6). Pergamon Press, New York.

Da Silva, P.F., Moreira, R.G., 2008. Vacuum frying of high-quality fruit and vegetable-based snacks. LWT- Food Science and Technology 10 (41), 1758-1767.

Da Silva, P.F., Moreira, R.G., Gomes, C.F., 2009. The effect of a de-oiling mechanism on the production of high quality vacuum fried potato chips. Journal of Food Engineering 3 (92), 297-304.

Dupont™, 2009. Transport Properties of DuPont™ Suva® refrigerants. Retrieved August 20, 2009, from http://refrigerants.dupont.com: http://refrigerants.dupont.com/Suva/en_US/pdf/h49740.pdf

Earle, R.L., Earle, M.D., 2004. Unit operations in food processing; web edition. The New Zealand Institute of Food Science & Technology, Inc., Palmerston North, New Zealand: Pergamon Press, web link: http://www.nzifst.org.nz/unitoperations/.

Farkas, B.E., Singh, R.P., Rumsey, T., 1996. Modeling heat and mass transfer in immersion frying I. Model development. Journal of Food Engineering 29, 211-226.

Farzad, M., O'Neal, D.L., 1988. An evaluation of improper refrigerant charge on the performance of a split system air conditioner with capillary tube expansion. Energy Systems Laboratory, Texas A&M University - Research Consortium - esl-tr-88/07-01.

Gamble, M.H., Rice, P., 1987. Effect of pre-fry drying on oil uptake and distribution in potato chip manufacture. International Journal of Food Science and Technology 22, 535-548.

Garayo, J., 2001. Production of low-fat potato chips using vacuum frying, Master Thesis, Biological and Agricultural Engineering Department, Texas A&M University, College Station, TX.

Garayo, J., Moreira, R.G., 2002. Vacuum frying of potato chips. Journal of Food Engineering 55 (2), 181-191.

Garcia, F.C., Bertola, N., Martino, M., Zartizky, N., 2002. Methylcellulose coatings applied to reduce oil uptake in fried products. Food Science and Technology International 10, 339–346.

Gould, W.A., 1995. Specific gravity-its measurement and use. In Gould W.A. (Ed.): Chipping Potato Handbook, pp. 18-21, The Snack Food Association, Arlington, VA.

Granda, C.E., 2005. Kinetics of acrylamide formation in potato chips, Master Thesis, Biological and Agricultural Engineering Department, Texas A&M University, College station, TX.

Gupta, M., 2009. Industrial frying. In S.G. Sahin (Ed.), Advances in Deep-Fat Frying of Foods, pp. 263-287, CRC Press, New York.

Halder, A., Dhall, A., Datta, A., 2006. Modeling of frying and related processes involving strong evaporation: a porous media approach. Excerpt from the Proceedings of the COMSOL Users Conference. Boston, MA.

Halder, A., Datta, A., 2008. Use of COMSOL multiphysics to develop a comprehensive, user-friendly predictive tool for food safety and quality. COMSOL Conference, Boston, MA.

Hewitt, G.F., Shires, G.L., Bott, T.R., 1994. Processs Heat Transfer, CRC Press. Ann Arbor, MI.

Incropera, F.P., Dewitt, D.P., Bergman, T.L., Lavine, A.S. 2006. Fundamentals of Heat Transfer, 6th edition, John Wiley & Sons Company, Hoboken, NJ.

Jones, C.F., Obrien, J., 1991. Mistakes That Worked. Doubleday Books, New York.

Khan, J.R, Zubair, S.M., 1999. Design and perfromance evaluation of reciprocating refrigeration system. International Journal of Refrigeration 22, 235-243.

Lucas, R., Rooney, L., 2001. Snack Food Processing. CRC Press Inc., Boca Raton, FL..

Lulai, P.H., Orr, E.C., 1979. Influence of potato specific gravity on yield and oil content of chips. American Journal of Potato Research 8 (56), 379-390.

Marisol, D., Franco, P., Moyano, P., Troncoso, E., 2007. Oil partition in pre-treated potato slices during frying and cooling. Journal of Food Engineering 1 (81), 257-265.

Minton, P.E., 1986. Handbook of Evaporation Technology. Noyes Publication, Park Ridge, NJ.

Moreira, R.G., Sun, X., Chen, Y., 1997. Factors affecting oil uptake in tortilla chips in deep-fat frying. Journal of Food Engineering 4 (31), 485-498.

Moreira, R.G., Castell-Perez, E.M., Barrufet, M.A., 1999. Deep-fat Frying: Fundamentals and Application. Aspen Publication, Gaithersburg, MD.

Oztopa, M.H., Sahin, S., Sumuna, G., 2007. Optimization of microwave frying of potato slices by using Taguchi technique. Journal of Food Engineering 1 (79), 83-91.

Pita, E.G., 1984. Refrigeration Principles and Systems-An Energy Approach. John Wiley and Sons Company, New York.

Pollock, D.D., 1991. Thermocouples: Theory and Properties. CRC Press Inc., Boca Raton, FL.

Przybylski, R., n.d.. Physical and chemical properties. Retrieved August 21/2009 from: http://www.canola-council.org: http://www.canola-council.org/uploads/technical/chemical1-6/chemical1-6_1.html

Reid, R.C., Prasunitz, J.M., Poling, B.E., 1987. The Properties of Gases and Liquids. McGraw-Hill Inc., New York.

Richard, E., Stier, F., Bluementhal, M., 1993. Quality control in deep-fat frying. Baking and Snacks 2 (15), 67–76.

Rimac-Brncic, S., Lelas, V., Rade, D., Simundic, B., 2004. Decreasing of oil absorption in potato strips during deep-fat frying. Journal of Food Engineering 2 (64), 237–241.

Serth, R.W., 2007. Process Heat Transfer, Princliples and aAplications. Academic Press, Burlington, MA.

Shyu, S.L., Hwang, L.S., 2001. Effects of processing conditions on the quality of vacuum fried apple chips. Food Research International 34, 133-142.

Singh, R.P., Heldman, D.R., 2001. Introduction to Food Engineering. (3rd edition) Academic Press, London, UK.

Skelton, K., 1999. Cavitation in Liquid Ring Vacuum Pumps Used in Condenser Venting Service. Graham Corporation, New York.

Smith, P.G., 2002. Introduction to Food Process Engineering. Kluwer Academic/Plenum Publishers, New York.

Snack Food Association., 1991. Potato Composition Guide, American Slide-Chart Corp., Wheaton, IL.

Steinmann, W.D., Eck, M., 2006. Buffer storage for direct steam generation. Solar Energy 80, 1277-1282.

Tseng, Y.C., Moreira, R.G., Sun, X., 1996. Total frying-use time effects on soybean-oil deterioration and on tortilla chip quality. International Journal of Food Science and Technology 31, 287–294.

Ufheil, G., Escher, F., 1996. Dynamics of oil uptake during deep-fat frying of potato slices. Lebensmittel-Wissenschaft und-Technologie 52, 640–644.

USDA/ARS, 2007. Nutrient database for standard reference. Retrieved March 29, 2009, from Nutrient Data Laboratory, web link: http://www.nal.usda.gov/fnic/foodcomp

Wile, D., 1977. Refrigerant Line Sizing. ASHRAE, Atlanta, GA.

Yildiza, A., Palazoğlu, T.K., Erdoğdua, F., 2007. Determination of heat and mass transfer parameters during frying of potato slices. Journal of Food Engineering 1 (79), 11-17.

APPENDIX A

OPERATION PROCEDURE AND TROUBLESHOOTING

A.1 Centrifuge unit

The centrifuge unit was designed for centrifugation of vacuum fried product inside the vacuum fryer vessel as a post frying operation. This allowed user to conduct de-oiling experiments without need of pressurizing the vacuum fryer.

The centrifuge unit motor was mounted across the motion feed-through shaft used for lowering the basket into the oil. An arrangement was made such that the basket is freely moving on the shaft which is rotated with the help of gears of transmission ratio of 2:1. The motor employed has a RPM of 90-1500 rotations per minute. Therefore by utilizing a 2:1 gear ratio the basket could achieve a RPM of 45-750 rotations per minute. The basket was designed for allowing product loading and evacuation from the bottom. This increased the ease of product loading and quick removal of the product after frying. The centrifuge unit was controlled by a custom-designed control box which consists of RPM control knob and an on/off switch. This helps the user to set the desired RPM and the time of de-oiling. A stepwise procedure for operating the centrifugation system is described below.

A.1.1. Operation procedure

1. Open the wing nut for removing the bottom of centrifuge basket.
2. Place the product eccentrically and evenly distributed on the basket bottom.
3. Re-align the bottom with the disk and tighten the wing nut.
4. Once the wing nut is tight to hold the basket firmly, commence with the regular frying procedure.
5. Set a timer for the time you want to centrifuge.

6. Once the frying is complete, pull the basket to the top.
7. Tighten the shaft with the tightening screws.
8. Set the RPM from 0-100% of 45-750 RPM before starting the centrifugation.
9. After the desired RPM is set, turn on the centrifugation on/off switch.
10. Start the timer along with the start of centrifugation.
11. Turn off the centrifugation switch as soon as the timer expires.
12. Open the frying chamber and place the fryer vessel lid back on its stand.
13. For next load, repeat step number 1.

A.1.2. Cautions

1. The bottom should not be loose before commencing centrifugation, tight the wing nut carefully, but avoid over tightening.
2. Ensure that the product is properly placed inside the basket, for more than 1 quantity of product place in opposite direction and equal distance from each other.
3. Properly pull up the basket and ensure that it is above the oil surface before centrifugation.
4. The level of oil inside the fryer should not exceed 10 to 12 cm from the base of the frying vessel or the basket will be contact with the oil.
5. The Motion feed through shaft should be held all time by the operator to lessen the vibrations and avoiding the basket to slip back into the oil.
6. The tightening screw for the shaft should be ensured for proper tightening.

7. Caution should be practiced while removing the product from the basket as hot oil and metal surface may cause burn injury.

A.1.3. Troubleshooting

1. In case of misaligned gears remove the gear from the motor shaft with a proper Allen wrench key.
2. Once the gear is removed properly align it back with the other gear and tighten the bolt located on the side of the gear with Allen wrench key.
3. In case the basket falls down or it is wobbling more than usual the center lock nut should be tightened up to proper extent.
4. Best tool for tightening the center bolt is to use nose pliers, caution must be practiced while tightening the lock nut.
5. The lock nut must be tight enough to let the central gear of the basket rotate freely on the central shaft.
6. If motor does not turn on the six pin wire connector must be checked for any broken wires that must be soldered back to the connector.
7. The wire should be checked right from the motor to the control box for any cuts or breaks.
8. The power unit should be checked for connections to the speed controller ES-02 unit and the motor.
9. There are two fuses in the system, one on the side of the power supply unit and other inside the control box.
10. If the fuses are damaged they should be replaced with correct spare parts.

11. If a need arises to replace a faulty part in the system. The following list of parts must only be purchased as the replacement.

Table A-1. BOM (Bill of Material) for future parts replacement of de-oiling unit.

Serial	**Part Name**	**Purchased from**	**Price [$]**
1.	2IK6RA-CWE Speed control motor	Oriental Motor Company, Torrance, CA	140.45
2.	ES-02 Speed Control Unit	Oriental Motor Company, Torrance, CA	117.50
3.	22 Tooth spur gear+ 44 Tooth spur gear+ Isostatic bushing	Purvis Bearing Service, College Station, TX	45.40
4.	Toggle Switch+ Utility Box+ Indicator Switch Plate+ Neon Indicator	Mid State Supply Inc., College Station, TX	67.81
5.	Power supply surge protector (120-240 volts converter)	Radio Shack, College Station, TX	129.89
6.	Plug Adapter 240 volts to 120 volts	Radio Shack, College Station, TX	10.81
7.	2” No-Hub Coupling	Lowes Home Center Inc., College Station, TX	3.76
8.	Power Supply Fuse (250 V, 3 Amp)	Radio Shack, College Station, TX	3.24
9.	Lock Nut+ Lock Washer	Lowes Home Center Inc., College Station, TX	1.06
10.	Motor Starter capacitor	Radio Shack	1.72
11.	Bolts and Nuts (8-32)”	The Home Depot, College Station, TX	2.12
	TOTAL		523.76

A.2. Condenser unit

The condenser unit works with the help of 1/3 hp Copeland™ low temperature, R-404a refrigeration condensing unit (M4FL-033-IAA, United Refrigeration, Houston, TX) and custom built shell and coil heat exchanger. This heat exchanger is a counter-flow type condenser that condenses water vapor and stores the condensate at the bottom until the operation is complete. The condensing unit provides the cooling effect in the condenser. A heat-exchange takes place between the steam (shell side) and the refrigerant (tube side). The system is an automatic system that defrosts after every use. It also has a super heater installed that must be turned on together with the condenser. The automatic system is designed to be controlled with a guarded relay bypass switch or a manual switch. The standard setting for the system does not require any user control to turn the refrigeration system on/off. The system automatically turns off with the help of a 12 VDC relay when user opens the fryer lid. When the lid is closed again the refrigeration system starts. This allows the coil in the heat exchanger to get cold enough and reach the desired temperature. However manual over-ride switch allows user to control the operation of the condenser system by over riding the auto switch.

The other advantage of having such a system is that it helps in defrosting the ice formed on the condenser coils. The condenser is actually a stainless steel full-nipple. The top and bottom flanges of the full nipple can be removed for cleaning the heat exchanger. Above the condensing unit lies the air cooled pre-condenser that is a spirally wound copper tube with a small fan at the center. This fan can be turned on /off for controlling the pre-condenser. All three controls of condenser are located on the control

box named as “refrigeration system Auto on/off switch”, “super heater on/off switch” and the “condenser manual on/off switch”. When the super heater switch is turned on it must always be operated with condenser switch. The super heater switch turns the stand by red light on. This shows that the heater is in stand by position but is not heating. It will start heating as soon as the refrigerant outlet temperature will reach 4^{o}C and a green light will turn on. The operating procedure for the condenser unit is discussed in stepwise manner below.

A.2.1. Operation procedure

1. Turn on the condenser manual and super heater switch on the control box.
2. Super heat stand by light and condensing unit power light on the front of condensing unit should turn on and must be checked for being operational before commencing each experiment.
3. A normal procedure for frying should be initiated, for new experimental mass loads the temperature of condenser outlet should be closely monitored during the process.
4. In case of temperature rise from the noted value of 9.14^{o}C, the basket should be immediately removed from the fryer to avoid water vapor from entering into the vacuum pump.
5. The temperature of heater should be checked during the experiment as heating will not be continuous and the green heating light should go off as the temperature of the refrigerant outlet rises to about 13^{o}C.

6. If a further rise in heater temperature is noted than the superheater switch can be manually turned off.
7. The coils and the inner wall of the condenser should be kept clean and washed with degreasing solution to avoid fouling of the heat exchanger in at least 6 month of time.
8. Any water deposited inside the heat exchanger should be evacuated by the end of each experiment or a set of three experiments to avoid condensate over flow.

A.2.2. Precautions

1. The condensate removal depends upon the amount of product being fried, to avoid any overflow complete discharge must be performed after every experiment or few.
2. Extreme caution must be taken as the condensate discharge may be at high temperature after removal.
3. If heater starts to operate irrespective of thermostat controls the thermostat must be checked for temperature dial and must be set at 40^{o}F or 4^{o}C.
4. Do not touch the heater, it may be very hot.
5. All lights must be checked during vacuum frying.
6. If heater does not turn off for long period they may get very hot and possibly damage the system or fire.
7. Always perform manual over-ride of the system when running for the first time in the day or after a gap between experiments.

8. Failing to check the pre-condenser fan may result in poor performance of the system and chances of vapor retrieval will be lessened by 10-15%. Therefore it is highly advisable to check if the condenser fan is operational.
9. Care must be taken to clean the refrigerated condenser tubes, any bending or tempering may result in refrigerant leak.
10. The flare nuts should never be loosened or removed. This may result in refrigerant leakage from the system.
11. The vacuum flanges must be handled with caution as it has very fragile knife edge to maintain vacuum tight seal, which may get scratched or broken.

A.2.3. Troubleshooting

1. If the system performance is reduced a complete cleaning of condenser by a good quality degreasing solvent must be carried out at least once in six months.
2. From continuous vibrations in the system flare nuts might get loose, they should be checked for tightness once in a 3 to 4 month of period. The flare nuts should never be loosened or removed. This may result in refrigerant leakage from the system.
3. If the vacuum is not sustaining by itself there may be few reasons as follows:
    a) The copper gasket fittings on the condenser flanges may be old and require replacement, refer Table A-2.

b) The vacuum hose must be checked at the joints for any leaks, rubber hoses which get cracked can be replaced with new ones.

c) The flanges might not be tight enough to provide proper airtight interlock.

d) The valve at the bottom of the condenser for water evacuation should be checked if it is properly closed.

e) The vacuum fryer lid should be checked for tight fitting.

f) All other point of pipes and hose connections in the system must be analyzed for leakage.

4. If the condenser unit does not turn on, cable connection between the fryer and the lid should be examined.
5. Faulty wires should be checked and replace with the help of multi-meter.
6. Relay and its power supply are crucial for automatic operation of the condensing unit; a fault in the connection must be checked and replaced in case condensing unit does not turn on.
7. Users cannot replace or work on condensing unit and its parts as it requires license authorization. Any problem beyond wires, switches and relay must be addressed by certified personnel only.
8. The condenser unit consists of parts listed in the Table A-2.

Table A-2.BOM (Bill of Material) for future parts replacement of condenser unit.

Serial	Part Name	Purchased from	Price($)
1	Copeland R-404a, 1/3 HP Condensing Unit	United Refrigeration, Houston, TX	395.00
2	Copper Tube, ¼" x 20'	The Home Depot, College Station, TX	20.00
3	Nipple, full, stainless steel,10.62" Oal,6"od uhv,4"od tube	Kurt J. Lesker, PA	220.50
4	Flange,UHV, stainless steel, Blank ,fixed,6"OD x 2	Kurt J. Lesker, PA	138.60
5	Gasket, annealed, copper for 6"OD UHV flange,5/pack	Kurt J. Lesker, PA	27.00
6	Hex B, N &W set,(25)5/1624 X 21/4 for 6R,63/4", 8"flanges	Kurt J. Lesker, PA	24.30
7	Tubing,304L Stainless Steel, rigid,1/2"od, .035"Wall, per inch x 2	Kurt J. Lesker, PA	2.16
8	Tubing,304L Stainless Steel, rigid,3/4"od, .035"wall, per polished OD & ID x2	Kurt J. Lesker, PA	3.51
9	Thermocouple Feed through, 2PR Type K,W/Connection Plug ½"MNPT	Kurt J. Lesker, PA	195.70
10	¾" Front Ferrule x 2, Back Ferrule x 2 & Nut x 2	Swagelok Inc., Houston, TX	22.16
11	Thermocouple Type K Beaded x 5	Omega Engineering Inc., Stamford, CT	55.00
12	Thermocouple Type K, 2"L x 0.032" Stainless Steel Insulated	Omega Engineering Inc. , Stamford, CT	27.00
13	Thermocouple Type K, 18"L x 0.010" W SS Insulated	Omega Engineering Inc. , Stamford, CT	56.00
14	OMB-DAQ 54 data acquisition system	Omega Engineering Inc. , Stamford, CT	649.00
15	Guarded on/off switch	Radio Shack Inc., College Station, TX	5.00
16	On/off switch	Radio Shack Inc. , College Station, TX	3.00
17	12 volt SPST relay	Radio Shack Inc. , College Station, TX	8.32
18	12 volt transformer	Midstate Supply Inc. , College Station, TX	11.96
	TOTAL		1864.21

A.3. The vacuum fryer simulator

The real-time simulator is the main P&ID program that is used to analyze various operation parameters while the vacuum frying process is being carried out. It is explained in detail in Chapter III of this thesis. The operation procedures for the Real Time Simulator program are as follows.

A.3.1. Operation procedure

1. Open the Microsoft Excel spreadsheet file name Vacuum Fryer Simulator.
2. Press the Start Simulator button on the excel sheet.
3. When prompted for user name and password enter "*admin*" as the user name and "*124*" is the password.
4. Once in the program's main window, users may open a pre-saved file or enter their own input parameters.
5. The PC monitor parameters must be filled out first by entering the data for the refrigeration condenser.
6. The default data for condenser unit parameters are evaporator temperature of -15^{o}C, Diameter of Tube 0.00635 m and Thickness of tube 0.000762 m.
7. Now user must select the temperature of oil from its drop down box. The available temperatures are 120^{o}C, 130^{o}C and 140^{o}C.
8. After both of the pc monitor parameters are set user must select an interval between the readings that is in seconds. The default interval is set to 1. The user may select minimum reading as 1 per second and maximum of 1 per min or 60 s.

9. The user must select the thermocouples to be operated by checking the boxes on different thermocouple lines.
10. Finally user can either select a choice of getting all the data obtained by the simulator by checking draw reference table box beside the “simulate now” button.
11. User can make graph of as many combinations between any two parameters as they desire. The draw graph button and selection of graphing parameter can be done after the process is complete. This data has to be separately saved by the user after closing the simulator and saving through the Microsoft excel file tab.

A.3.2. Precautions

1. The vacuum fryer simulator-program generated data should always be saved as a new file name, if saved on the existing file program may result in data permanently over written on the original file.
2. The program may only be run when the data acquisition unit OMB-DAQ 54 is connected. Any other data acquisition unit has not been tried to be compatible with the program.
3. The user saved file when opened should once be checked for any data accidently being missing for maintaining accuracy in the experiments.

A.3.3. Troubleshooting

1. If accidently the data is being saved on the master vacuum fryer simulator file any sheets must be deleted and generated data must be erased except the sheet named condenser main. Once the file is properly erased it can be saved as the vacuum fryer simulator master file.
2. If the program is unable to detect the Data acquisition system on the USB port, try changing the port and restart the program until it detects the hardware.
3. If problem persist in detection of hardware the system must be restarted while the data acquisition unit must be removed for once.
4. The program utilizes save files with *.aki extension. These files can be open and changed through notepad in case of any missing parameter.
5. Once user open a saved file the extension must not be changed for the program may not be able to detect and load the parameters of an unknown extension.
6. Check if the macro option in the excel file is enabled; security should be set to minimum.

APPENDIX B

TABLES

Table B-1. The percentage oil content in wet basis for potato chips fried at 120°C and 140°C oil temperature for 360 s during de-oiling at 300 RPM (10.08 g-force) and 750 RPM (63 g-force).

Sample Name	**Oil Content [%w.b.]**	**Sample Name**	**Oil Content [%w.b.]**
120°C		**140°C**	
Control 1-m	47.69857	Control 1-m	42.33058
Control 2-m	47.8028	Control 2-m	41.73223
Control 3-m	47.72787	Control 3-m	42.58349
300/40a-m	15.89224	300/40a-m	22.83459
300/40b-m	15.87504	300/40b-m	22.73577
300/40c-m	15.71245	300/40c-m	23.20067
750/40a-m	13.82876	750/40a-m	24.62696
750/40b-m	13.79164	750/40b-m	24.88417
750/40c-m	13.02752	750/40c-m	24.64766
Control 1-wm	40.46807	Control 1-wm	40.87075
Control 2-wm	39.79469	Control 2-wm	40.8711
Control 3-wm	39.28997	Control 3-wm	39.90615
300/40a-wm	22.62129	300/40a-wm	22.13768
300/40b-wm	21.69768	300/40b-wm	21.70434
300/40c-wm	21.38578	300/40c-wm	22.98765
750/40a-wm	18.34087	750/40a-wm	21.01669
750/40b-wm	17.87945	750/40b-wm	20.63397
750/40c-wm	17.93209	750/40c-wm	21.59055

Table B-2.Oil content in potato chips versus vacuum release valve as function of centrifuge speed of 300 RPM (8.89 g-force) and 750 RPM (63 g-force) for 40 s for chips fried at 120°C and 140°C for 360 s.

120°C oil temperature			**140°C oil temperature**		
Sample (RPM/centrifuge duration)Release %	**Oil Content**	**Standard Deviation**	**Sample (RPM/centrifuge duration)Release %**	**Oil Content**	**Standard Deviation**
Control/0s/100%	44.35985	0.345158	Control/0s/100%	44.86532	1.352398
300/ 40s/100%	22.4352	0.487539	300/ 40s/100%	27.32461	0.411017
300/40s/50%	12.09633	0.57037	300/40s/50%	15.57978	0.362062
300/40s/25%	11.36999	0.795486	300/40s/25%	13.22893	0.916128
750/ 40s/100%	13.5373	0.071892	750/ 40s/100%	22.9748	0.653429
750/40s/50%	13.63235	0.130667	750/40s/50%	23.07634	0.404368
750/40s/25%	13.99048	0.065204	750/40s/25%	19.73749	0.134575

Table B-3. Temperature history profile of 9 different thermocouples (Time [s], Temp [^{o}C])

Frying Time	$T_{ref,in}$	$T_{fryer, top}$	$T_{cond, out}$	$T_{cond, in}$	$T_{ref,out}$	$T_{steam\ hose}$	$T_{pre, cond}$	$T_{comp, cond}$	$T_{cond, cap}$
1	-14.9352	51.839	-5.9248	20.8097	-25.5412	28.2435	21.9079	39.5517	25.4141
2	-14.9352	51.839	-5.9248	20.8097	-25.5412	28.2435	21.9079	39.5517	25.4141
3	-14.9352	51.839	-5.9248	20.8097	-25.5412	28.2435	21.9079	39.5517	25.4141
4	-15.019	59.9445	-4.7482	20.6232	-25.6507	28.3036	21.8572	39.7099	25.2511
5	-15.019	59.9445	-4.7482	20.6232	-25.6507	28.3036	21.8572	39.7099	25.2511
6	-15.18	61.4925	-4.8145	21.3914	-25.6721	27.9538	21.9376	39.8601	25.5306
7	-15.18	61.4925	-4.8145	21.3914	-25.6721	27.9538	21.9376	39.8601	25.5306
8	-15.18	61.4925	-4.8145	21.3914	-25.6721	28.2033	21.8701	39.8935	25.4512
9	-15.1822	63.3052	-3.9009	21.2789	-25.9295	28.2033	21.8701	39.8935	25.4512
10	-15.1822	63.3052	-3.9009	21.2789	-25.9295	28.2033	21.8701	39.8935	25.4512
11	-15.1822	63.3052	-3.9009	21.2789	-25.9295	28.1193	21.8956	39.9777	25.5616
12	-15.224	67.2429	-3.0236	22.7073	-25.8713	28.1193	21.8956	39.9777	25.5616
13	-15.224	67.2429	-3.0236	22.7073	-25.8713	28.1029	21.8591	40.0454	25.5508
14	-15.2978	70.1011	-2.6842	22.6845	-25.9621	28.1029	21.8591	40.0454	25.5508
15	-15.2978	70.1011	-2.6842	22.6845	-25.9621	28.2321	21.8692	40.0927	25.4306
16	-15.2427	73.0776	-1.4604	23.0259	-25.9172	28.2321	21.8692	40.0927	25.4306
17	-15.2427	73.0776	-1.4604	23.0259	-25.9172	28.2321	21.8692	40.0927	25.4306
18	-15.2697	76.3172	-1.2848	24.96	-25.88	28.4157	21.844	40.2312	25.3851
19	-15.2697	76.3172	-1.2848	24.96	-25.88	28.4157	21.844	40.2312	25.3851
20	-15.3549	78.1413	-1.3443	25.1138	-25.9274	28.3348	21.8765	40.226	25.4411
21	-15.3549	78.1413	-1.3443	25.1138	-25.9274	28.3348	21.8765	40.226	25.4411
22	-15.3549	78.1413	-1.3443	25.1138	-25.9274	28.3764	21.8299	40.3299	25.4237
23	-15.3061	80.0768	-0.2046	24.5197	-25.7694	28.3764	21.8299	40.3299	25.4237
24	-15.3061	80.0768	-0.2046	24.5197	-25.7694	28.3764	21.8299	40.3299	25.4237
25	-15.3061	80.0768	-0.2046	24.5197	-25.7694	28.0299	21.87	40.3248	25.605
26	-15.3258	81.3914	-0.4896	25.5477	-25.237	28.0299	21.87	40.3248	25.605
27	-15.3258	81.3914	-0.4896	25.5477	-25.237	28.0299	21.87	40.3248	25.605
28	-15.3328	83.6129	0.1371	24.9882	-24.6112	28.3744	21.8969	40.5322	25.5437
29	-15.3328	83.6129	0.1371	24.9882	-24.6112	28.3744	21.8969	40.5322	25.5437
30	-15.2369	84.5301	0.7097	25.5679	-23.5841	28.3744	21.8969	40.5322	25.5437
31	-15.2369	84.5301	0.7097	25.5679	-23.5841	28.4433	21.8663	40.4814	25.4642
32	-15.2105	85.6924	0.2331	26.0619	-22.3042	28.4433	21.8663	40.4814	25.4642
33	-15.2105	85.6924	0.2331	26.0619	-22.3042	28.1657	22.7658	40.6187	25.6639
34	-15.1798	85.3779	0.5957	25.3443	-21.0255	28.1657	22.7658	40.6187	25.6639

Table B-3. Continued

Frying Time	$T_{ref,in}$	$T_{fryer, top}$	$T_{cond, out}$	$T_{cond, in}$	$T_{ref,out}$	$T_{steam\ hose}$	$T_{pre, cond}$	$T_{comp, cond}$	$T_{cond, cap}$
35	-15.1798	85.3779	0.5957	25.3443	-21.0255	28.1657	22.7658	40.6187	25.6639
36	-15.1798	85.3779	0.5957	25.3443	-21.0255	28.7075	27.1825	40.6576	25.4937
37	-15.0219	85.9944	1.6078	25.3821	-19.3681	28.7075	27.1825	40.6576	25.4937
38	-15.0219	85.9944	1.6078	25.3821	-19.3681	28.7075	27.1825	40.6576	25.4937
39	-15.0219	85.9944	1.6078	25.3821	-19.3681	28.6544	32.434	40.7487	25.5131
40	-14.9807	85.5154	1.0707	25.4384	-17.6444	28.6544	32.434	40.7487	25.5131
41	-14.9807	85.5154	1.0707	25.4384	-17.6444	29.0981	34.4185	40.72	25.4297
42	-14.9807	85.5154	1.0707	25.4384	-17.6444	29.0981	34.4185	40.72	25.4297
43	-14.9268	83.5408	1.2569	25.9575	-15.782	29.0981	34.4185	40.72	25.4297
44	-14.9268	83.5408	1.2569	25.9575	-15.782	28.94	35.5722	40.8309	25.6243
45	-14.9268	83.5408	1.2569	25.9575	-15.782	28.94	35.5722	40.8309	25.6243
46	-14.8977	82.1105	2.2026	25.055	-13.6151	29.1932	36.7533	40.8582	25.6511
47	-14.8977	82.1105	2.2026	25.055	-13.6151	29.1932	36.7533	40.8582	25.6511
48	-14.8977	82.1105	2.2026	25.055	-13.6151	29.1405	37.5916	40.9188	25.6944
49	-14.8939	80.9292	1.7659	25.3056	-11.8113	29.4733	38.4814	40.9691	25.5817
50	-14.8939	80.9292	1.7659	25.3056	-11.8113	29.3618	38.8943	41.105	25.7225
51	-14.8146	81.1253	2.4827	24.9759	-10.0373	29.3618	38.8943	41.105	25.7225
52	-14.8146	81.1253	2.4827	24.9759	-10.0373	29.5666	39.0948	41.1138	25.5826
53	-14.8146	81.1253	2.4827	24.9759	-10.0373	29.5666	39.0948	41.1138	25.5826
54	-14.6866	80.0902	1.9086	25.2305	-8.3442	29.4998	39.3597	41.1616	25.6197
55	-14.6866	80.0902	1.9086	25.2305	-8.3442	29.4998	39.3597	41.1616	25.6197
56	-14.6866	80.0902	1.9086	25.2305	-8.3442	29.4998	39.3597	41.1616	25.6197
57	-14.6685	78.4047	2.2894	25.483	-6.825	29.9121	39.2646	41.2344	25.5413
58	-14.6685	78.4047	2.2894	25.483	-6.825	29.9121	39.2646	41.2344	25.5413
59	-14.6179	77.9785	2.421	24.9365	-5.2905	29.7424	39.2248	41.3176	25.6708
60	-14.6179	77.9785	2.421	24.9365	-5.2905	29.7424	39.2248	41.3176	25.6708
61	-14.6179	77.9785	2.421	24.9365	-5.2905	29.5534	38.9917	41.3656	25.7375
62	-14.5259	77.197	2.8796	25.426	-3.8329	29.5534	38.9917	41.3656	25.7375
63	-14.5259	77.197	2.8796	25.426	-3.8329	29.5534	38.9917	41.3656	25.7375
64	-14.5117	77.5253	3.3901	24.2943	-2.2265	29.8924	38.4298	41.4853	25.6146
65	-14.5117	77.5253	3.3901	24.2943	-2.2265	29.8924	38.4298	41.4853	25.6146
66	-14.4622	76.9789	3.2324	24.9589	-1.3537	29.8924	38.4298	41.4853	25.6146
67	-14.4622	76.9789	3.2324	24.9589	-1.3537	29.8159	38.3899	41.5281	25.5998
68	-14.4622	76.9789	3.2324	24.9589	-1.3537	29.8159	38.3899	41.5281	25.5998
69	-14.5374	77.5964	3.8631	24.1295	0.1943	29.8159	38.3899	41.5281	25.5998
70	-14.5374	77.5964	3.8631	24.1295	0.1943	29.6209	38.2277	41.6343	25.7541
71	-14.4579	76.979	3.9006	24.9815	0.9267	29.6209	38.2277	41.6343	25.7541

Table B-3. Continued

Frying Time	$T_{ref,in}$	$T_{fryer, top}$	$T_{cond, out}$	$T_{cond, in}$	$T_{ref,out}$	$T_{steam\ hose}$	$T_{pre, cond}$	$T_{comp, cond}$	$T_{cond, cap}$
72	-14.4579	76.979	3.9006	24.9815	0.9267	29.6209	38.2277	41.6343	25.7541
73	-14.4579	76.979	3.9006	24.9815	0.9267	29.6904	37.8322	41.6749	25.6663
74	-14.4225	77.3744	3.4788	24.8007	1.786	29.6904	37.8322	41.6749	25.6663
75	-14.4225	77.3744	3.4788	24.8007	1.786	29.6904	37.8322	41.6749	25.6663
76	-14.4225	77.3744	3.4788	24.8007	1.786	29.6984	37.343	41.7983	25.8142
77	-14.3374	76.4313	4.2981	24.5477	2.8298	29.6984	37.343	41.7983	25.8142
78	-14.3374	76.4313	4.2981	24.5477	2.8298	29.5726	36.79	41.8451	25.7741
79	-14.3374	76.4313	4.2981	24.5477	2.8298	29.5726	36.79	41.8451	25.7741
80	-14.3911	76.6604	4.2899	23.8105	3.7281	29.5726	36.79	41.8451	25.7741
81	-14.3911	76.6604	4.2899	23.8105	3.7281	29.7535	36.4265	42.0073	25.7282
82	-14.3395	76.3663	4.4889	24.0357	4.4074	29.7535	36.4265	42.0073	25.7282
83	-14.3395	76.3663	4.4889	24.0357	4.4074	29.5192	35.8588	41.9727	25.8357
84	-14.3384	76.7076	4.0195	24.4979	4.7644	29.5192	35.8588	41.9727	25.8357
85	-14.3384	76.7076	4.0195	24.4979	4.7644	29.5192	35.8588	41.9727	25.8357
86	-14.4338	75.7358	3.996	24.0645	5.2673	29.8333	35.2446	42.097	25.641
87	-14.4338	75.7358	3.996	24.0645	5.2673	29.8333	35.2446	42.097	25.641
88	-14.4338	75.7358	3.996	24.0645	5.2673	29.5515	34.5981	42.1951	25.8446
89	-14.4128	75.8287	4.7143	24.1252	6.0644	29.5515	34.5981	42.1951	25.8446
90	-14.4128	75.8287	4.7143	24.1252	6.0644	29.5515	34.5981	42.1951	25.8446
91	-14.4128	75.8287	4.7143	24.1252	6.0644	29.7903	33.2595	42.2828	25.7073
92	-14.367	76.19	4.5553	23.353	6.6014	29.7903	33.2595	42.2828	25.7073
93	-14.367	76.19	4.5553	23.353	6.6014	29.7903	33.2595	42.2828	25.7073
94	-14.3704	77.4002	4.8796	23.3737	6.9729	29.4097	32.7377	42.2779	25.8535
95	-14.3704	77.4002	4.8796	23.3737	6.9729	29.4097	32.7377	42.2779	25.8535
96	-14.3704	77.4002	4.8796	23.3737	6.9729	29.4097	32.7377	42.2779	25.8535
97	-14.4055	77.3991	4.0425	23.5402	7.2356	29.6679	32.0794	42.4077	25.7653
98	-14.4055	77.3991	4.0425	23.5402	7.2356	29.6901	31.6178	42.5317	25.7045
99	-14.2798	77.5964	4.3874	23.7976	7.5125	29.6901	31.6178	42.5317	25.7045
100	-14.2798	77.5964	4.3874	23.7976	7.5125	29.2887	30.7446	42.5033	25.8579
101	-14.3882	79.2908	3.9847	23.8668	7.6049	29.2887	30.7446	42.5033	25.8579
102	-14.3882	79.2908	3.9847	23.8668	7.6049	29.2887	30.7446	42.5033	25.8579
103	-14.3882	79.2908	3.9847	23.8668	7.6049	29.7231	30.1848	42.6232	25.6676
104	-14.3332	79.4502	4.6567	22.9968	7.9359	29.7231	30.1848	42.6232	25.6676
105	-14.3332	79.4502	4.6567	22.9968	7.9359	29.7231	30.1848	42.6232	25.6676
106	-14.3332	79.4502	4.6567	22.9968	7.9359	29.3379	29.5603	42.6521	25.8559
107	-14.3701	79.0235	3.674	23.1833	7.7991	29.3379	29.5603	42.6521	25.8559
108	-14.3701	79.0235	3.674	23.1833	7.7991	29.3379	29.5603	42.6521	25.8559

Table B-3. Continued

Frying Time	$T_{ref,in}$	$T_{fryer, top}$	$T_{cond, out}$	$T_{cond, in}$	$T_{ref,out}$	$T_{steam\ hose}$	$T_{pre, cond}$	$T_{comp, cond}$	$T_{cond, cap}$
109	-14.2377	77.89	4.2276	23.1753	7.971	29.5594	29.026	42.7823	25.734
110	-14.2377	77.89	4.2276	23.1753	7.971	29.5594	29.026	42.7823	25.734
111	-14.2377	77.89	4.2276	23.1753	7.971	29.5594	29.026	42.7823	25.734
112	-14.4113	78.6055	3.7386	22.6511	7.915	29.5776	28.4916	42.756	25.7232
113	-14.4113	78.6055	3.7386	22.6511	7.915	29.5776	28.4916	42.756	25.7232
114	-14.4312	78.8909	4.0571	22.4117	7.9273	29.3318	28.4156	42.8841	25.8341
115	-14.4312	78.8909	4.0571	22.4117	7.9273	29.3318	28.4156	42.8841	25.8341
116	-14.3242	77.4887	3.9675	22.6624	7.8109	29.3318	28.4156	42.8841	25.8341
117	-14.3242	77.4887	3.9675	22.6624	7.8109	29.6727	28.0666	42.8756	25.7006
118	-14.3242	77.4887	3.9675	22.6624	7.8109	29.6727	28.0666	42.8756	25.7006
119	-14.3809	78.9513	2.9615	22.769	7.5706	29.6727	28.0666	42.8756	25.7006
120	-14.3809	78.9513	2.9615	22.769	7.5706	29.2522	27.7096	42.9801	25.8546
121	-14.4351	79.3043	2.9591	22.3238	7.3617	29.2522	27.7096	42.9801	25.8546
122	-14.4351	79.3043	2.9591	22.3238	7.3617	29.2522	27.7096	42.9801	25.8546
123	-14.4152	80.3678	3.0487	22.0453	7.2587	29.5762	27.442	43.0125	25.7184
124	-14.4152	80.3678	3.0487	22.0453	7.2587	29.5762	27.442	43.0125	25.7184
125	-14.3966	80.3237	2.9602	22.2568	7.0694	29.5762	27.442	43.0125	25.7184
126	-14.3966	80.3237	2.9602	22.2568	7.0694	29.3775	27.1021	43.0552	25.6717
127	-14.3593	80.3592	2.5972	22.4761	6.6682	29.3775	27.1021	43.0552	25.6717
128	-14.3593	80.3592	2.5972	22.4761	6.6682	29.3775	27.1021	43.0552	25.6717
129	-14.3593	80.3592	2.5972	22.4761	6.6682	29.3234	26.8853	43.118	25.8319
130	-14.3878	80.9377	2.0582	22.7591	6.2048	29.3234	26.8853	43.118	25.8319
131	-14.3878	80.9377	2.0582	22.7591	6.2048	29.5766	26.6397	43.1515	25.6871
132	-14.3878	80.9377	2.0582	22.7591	6.2048	29.5766	26.6397	43.1515	25.6871
133	-14.4731	81.176	2.3056	21.8486	5.983	29.5766	26.6397	43.1515	25.6871
134	-14.4731	81.176	2.3056	21.8486	5.983	29.1486	26.4833	43.2872	25.8837
135	-14.4739	81.3668	2.6988	21.7229	5.4384	29.1486	26.4833	43.2872	25.8837
136	-14.4739	81.3668	2.6988	21.7229	5.4384	29.1486	26.4833	43.2872	25.8837
137	-14.319	81.5045	2.6932	21.9357	4.9706	29.5583	26.3045	43.2513	25.6614
138	-14.319	81.5045	2.6932	21.9357	4.9706	29.5583	26.3045	43.2513	25.6614
139	-14.3856	81.2289	2.3407	22.2676	4.3031	29.5583	26.3045	43.2513	25.6614
140	-14.3856	81.2289	2.3407	22.2676	4.3031	29.1924	26.1102	43.3448	25.8018
141	-14.4459	81.3201	2.0345	21.8248	3.7079	29.1924	26.1102	43.3448	25.8018
142	-14.4459	81.3201	2.0345	21.8248	3.7079	29.1924	26.1102	43.3448	25.8018
143	-14.4459	81.3201	2.0345	21.8248	3.7079	29.4127	25.9964	43.4052	25.779
144	-14.5238	81.6817	2.502	22.0324	3.0145	29.4127	25.9964	43.4052	25.779
145	-14.5002	82.0235	2.29	22.2633	2.0623	29.5783	25.684	43.3948	25.6657

Table B-3. Continued

Frying Time	$T_{ref,in}$	$T_{fryer, top}$	$T_{cond, out}$	$T_{cond, in}$	$T_{ref,out}$	$T_{steam\ hose}$	$T_{pre, cond}$	$T_{comp, cond}$	$T_{cond, cap}$
146	-14.5002	82.0235	2.29	22.2633	2.0623	29.5783	25.684	43.3948	25.6657
147	-14.5599	82.4031	1.8718	22.2157	1.287	29.5783	25.684	43.3948	25.6657
148	-14.5599	82.4031	1.8718	22.2157	1.287	29.2254	25.4684	43.4773	25.7068
149	-14.4938	83.3641	1.8569	21.8809	0.2123	29.2254	25.4684	43.4773	25.7068
150	-14.4938	83.3641	1.8569	21.8809	0.2123	29.2254	25.4684	43.4773	25.7068
151	-14.4938	83.3641	1.8569	21.8809	0.2123	29.2957	25.319	43.5544	25.8112
152	-14.6215	84.2071	2.7078	21.4202	-0.8614	29.2957	25.319	43.5544	25.8112
153	-14.6215	84.2071	2.7078	21.4202	-0.8614	29.5479	25.1519	43.5808	25.6306
154	-14.5237	84.4974	2.5833	21.6701	-2.4319	29.5479	25.1519	43.5808	25.6306
155	-14.5237	84.4974	2.5833	21.6701	-2.4319	29.4927	25.0492	43.6631	25.7147
156	-14.6357	84.9779	2.1819	22.0514	-4.1991	29.4927	25.0492	43.6631	25.7147
157	-14.6357	84.9779	2.1819	22.0514	-4.1991	29.4927	25.0492	43.6631	25.7147
158	-14.5154	85.2352	1.838	21.9802	-6.3856	29.3218	24.8048	43.6772	25.6219
159	-14.5154	85.2352	1.838	21.9802	-6.3856	29.3218	24.8048	43.6772	25.6219
160	-14.6081	85.4193	1.8766	21.6269	-9.1284	29.3218	24.8048	43.6772	25.6219
161	-14.6081	85.4193	1.8766	21.6269	-9.1284	29.3539	24.6773	43.7212	25.748
162	-14.6081	85.4193	1.8766	21.6269	-9.1284	29.3539	24.6773	43.7212	25.748
163	-14.512	85.7423	2.4683	21.1565	-11.9711	29.2212	24.4406	43.7587	25.7522
164	-14.512	85.7423	2.4683	21.1565	-11.9711	29.2212	24.4406	43.7587	25.7522
165	-14.512	85.7423	2.4683	21.1565	-11.9711	29.2212	24.4406	43.7587	25.7522
166	-14.6385	85.7198	1.65	21.6075	-14.4952	29.4347	24.2714	43.7285	25.6653
167	-14.6385	85.7198	1.65	21.6075	-14.4952	29.4347	24.2714	43.7285	25.6653
168	-14.6736	85.4977	1.7798	21.201	-15.9802	29.4347	24.2714	43.7285	25.6653
169	-14.6736	85.4977	1.7798	21.201	-15.9802	29.4208	23.9952	43.7971	25.6891
170	-14.6736	85.4977	1.7798	21.201	-15.9802	29.4208	23.9952	43.7971	25.6891
171	-14.6714	85.5914	2.3336	21.1535	-17.2354	29.4208	23.9952	43.7971	25.6891
172	-14.6714	85.5914	2.3336	21.1535	-17.2354	29.2205	23.8747	43.8283	25.7652
173	-14.6714	85.5914	2.3336	21.1535	-17.2354	29.2205	23.8747	43.8283	25.7652
174	-14.6099	85.2715	1.5264	21.3482	-18.3808	29.2205	23.8747	43.8283	25.7652
175	-14.6099	85.2715	1.5264	21.3482	-18.3808	29.6179	23.7435	43.8673	25.6231
176	-14.6839	85.422	1.8141	20.9342	-18.9675	29.6179	23.7435	43.8673	25.6231
177	-14.6839	85.422	1.8141	20.9342	-18.9675	29.4276	23.5092	43.9232	25.7374
178	-14.6631	85.3372	2.1117	20.6925	-19.557	29.4276	23.5092	43.9232	25.7374
179	-14.6631	85.3372	2.1117	20.6925	-19.557	29.4276	23.5092	43.9232	25.7374
180	-14.6631	85.3372	2.1117	20.6925	-19.557	29.6134	23.3299	44.0049	25.5486
181	-14.6647	85.0666	1.4603	21.6332	-20.242	29.6134	23.3299	44.0049	25.5486
182	-14.6647	85.0666	1.4603	21.6332	-20.242	29.6134	23.3299	44.0049	25.5486

Table B-3. Continued

Frying Time	$T_{ref,in}$	$T_{fryer, top}$	$T_{cond, out}$	$T_{cond, in}$	$T_{ref,out}$	$T_{steam\ hose}$	$T_{pre, cond}$	$T_{comp, cond}$	$T_{cond, cap}$
183	-14.8272	84.9861	0.9228	21.2912	-20.7378	29.3002	23.1167	43.9895	25.7911
184	-14.8272	84.9861	0.9228	21.2912	-20.7378	29.3002	23.1167	43.9895	25.7911
185	-14.6224	84.7769	0.8573	20.7385	-21.0258	29.6005	22.9913	44.0359	25.6334
186	-14.6224	84.7769	0.8573	20.7385	-21.0258	29.6005	22.9913	44.0359	25.6334
187	-14.6224	84.7769	0.8573	20.7385	-21.0258	29.3243	22.8185	44.0784	25.729
188	-14.7347	84.4557	0.4655	21.3256	-21.3738	29.3243	22.8185	44.0784	25.729
189	-14.7347	84.4557	0.4655	21.3256	-21.3738	29.3243	22.8185	44.0784	25.729
190	-14.7347	84.4557	0.4655	21.3256	-21.3738	29.4342	22.6631	44.0544	25.7223
191	-14.7115	84.0877	-0.1212	20.4927	-21.7294	29.4342	22.6631	44.0544	25.7223
192	-14.7115	84.0877	-0.1212	20.4927	-21.7294	29.2958	22.4783	44.081	25.7648
193	-14.7476	83.9487	0.2023	20.5125	-21.9086	29.4647	22.3544	44.1244	25.6731
194	-14.7948	83.5687	0.1469	20.93	-22.2441	29.4647	22.3544	44.1244	25.6731
195	-14.7948	83.5687	0.1469	20.93	-22.2441	29.643	22.2373	44.0627	25.5918
196	-14.7774	83.3043	-0.2349	21.3071	-22.4257	29.643	22.2373	44.0627	25.5918
197	-14.7774	83.3043	-0.2349	21.3071	-22.4257	29.4185	22.1428	44.2155	25.7409
198	-14.7774	83.3043	-0.2349	21.3071	-22.4257	29.4185	22.1428	44.2155	25.7409
199	-14.8687	83.2993	0.4113	20.4196	-22.6665	29.4185	22.1428	44.2155	25.7409
200	-14.8687	83.2993	0.4113	20.4196	-22.6665	29.2479	21.9491	44.1918	25.8069
201	-14.8687	83.2993	0.4113	20.4196	-22.6665	29.2479	21.9491	44.1918	25.8069
202	-14.7804	82.9424	-0.1196	21.1818	-22.8995	29.6071	21.7565	44.1937	25.5715
203	-14.7804	82.9424	-0.1196	21.1818	-22.8995	29.6071	21.7565	44.1937	25.5715
204	-14.8739	82.7529	0.0741	20.6778	-23.1276	29.3113	21.632	44.2143	25.7375
205	-14.8739	82.7529	0.0741	20.6778	-23.1276	29.3113	21.632	44.2143	25.7375
206	-14.8739	82.7529	0.0741	20.6778	-23.1276	29.6515	21.4437	44.1978	25.6174
207	-14.8576	82.3582	0.5989	21.1542	-23.1075	29.6515	21.4437	44.1978	25.6174
208	-14.8576	82.3582	0.5989	21.1542	-23.1075	29.4003	21.204	44.2419	25.6437
209	-14.8576	82.3582	0.5989	21.1542	-23.1075	29.4003	21.204	44.2419	25.6437
210	-14.9352	82.1469	0.6257	20.3381	-23.4199	29.6978	21.1127	44.2615	25.5875
211	-14.8145	82.1469	0.6257	20.3381	-23.4199	29.6978	21.1127	44.2615	25.5875
212	-14.8145	82.1469	0.6257	20.3381	-23.4199	29.302	20.8469	44.3083	25.7734
213	-14.7921	82.0591	0.2472	21.1449	-23.4405	29.302	20.8469	44.3083	25.7734
214	-14.7921	82.0591	0.2472	21.1449	-23.4405	29.5904	20.6231	44.2526	25.6901
215	-14.7921	82.0591	0.2472	21.1449	-23.4405	29.5904	20.6231	44.2526	25.6901
216	-14.8116	82.3382	1.0525	20.4473	-23.5941	29.6251	20.5424	44.3459	25.5927
217	-14.8116	82.3382	1.0525	20.4473	-23.5941	29.6251	20.5424	44.3459	25.5927
218	-14.8615	82.3741	0.5496	21.1272	-23.7175	29.2968	20.3085	44.2719	25.7485
219	-14.8615	82.3741	0.5496	21.1272	-23.7175	29.2968	20.3085	44.2719	25.7485

Table B-3. Continued

Frying Time	$T_{ref,in}$	$T_{fryer, top}$	$T_{cond, out}$	$T_{cond, in}$	$T_{ref,out}$	$T_{steam\ hose}$	$T_{pre, cond}$	$T_{comp, cond}$	$T_{cond, cap}$
220	-14.8615	82.3741	0.5496	21.1272	-23.7175	29.2968	20.3085	44.2719	25.7485
221	-14.9506	82.4873	-0.0835	21.0834	-23.896	29.696	20.1443	44.3619	25.6102
222	-14.9506	82.4873	-0.0835	21.0834	-23.896	29.696	20.1443	44.3619	25.6102
223	-14.9227	82.5233	-0.1323	20.4678	-23.9267	29.4452	19.9669	44.3161	25.7619
224	-14.9227	82.5233	-0.1323	20.4678	-23.9267	29.4452	19.9669	44.3161	25.7619
225	-14.9227	82.5233	-0.1323	20.4678	-23.9267	29.7228	19.7425	44.402	25.6218
226	-14.8511	82.5984	0.0671	21.0288	-23.9747	29.7228	19.7425	44.402	25.6218
227	-14.8511	82.5984	0.0671	21.0288	-23.9747	29.639	19.6092	44.3129	25.7243
228	-14.9489	82.5599	-0.7036	20.9353	-24.1895	29.639	19.6092	44.3129	25.7243
229	-14.9489	82.5599	-0.7036	20.9353	-24.1895	29.5799	19.5606	44.3941	25.637
230	-15.0396	82.5375	-0.8261	20.3825	-24.312	29.5799	19.5606	44.3941	25.637
231	-15.0396	82.5375	-0.8261	20.3825	-24.312	29.5799	19.5606	44.3941	25.637
232	-14.965	82.5895	-0.5214	20.0877	-24.349	29.3691	19.5794	44.343	25.7164
233	-14.965	82.5895	-0.5214	20.0877	-24.349	29.3691	19.5794	44.343	25.7164
234	-14.965	82.5895	-0.5214	20.0877	-24.349	29.6005	19.7054	44.3451	25.6828
235	-14.9152	82.4575	-1.2669	20.9052	-24.4653	29.6005	19.7054	44.3451	25.6828
236	-14.9152	82.4575	-1.2669	20.9052	-24.4653	29.6005	19.7054	44.3451	25.6828
237	-14.9152	82.4575	-1.2669	20.9052	-24.4653	29.7688	19.7225	44.3462	25.5923
238	-14.9222	82.7281	0.0058	20.2108	-24.5279	29.7688	19.7225	44.3462	25.5923
239	-14.9222	82.7281	0.0058	20.2108	-24.5279	29.7688	19.7225	44.3462	25.5923
240	-14.9389	82.4873	0.1299	20.6644	-24.6895	29.6987	19.8556	44.3552	25.6794
241	-14.9389	82.4873	0.1299	20.6644	-24.6895	29.6987	19.8556	44.3552	25.6794
242	-15.026	82.2744	-0.3562	20.2555	-24.8113	29.6987	19.8556	44.3552	25.6794
243	-15.026	82.2744	-0.3562	20.2555	-24.8113	29.7557	19.9365	44.3932	25.7035
244	-15.026	82.2744	-0.3562	20.2555	-24.8113	29.7557	19.9365	44.3932	25.7035
245	-15.1105	81.9551	-0.3577	20.7855	-24.7372	29.7557	19.9365	44.3932	25.7035
246	-15.1105	81.9551	-0.3577	20.7855	-24.7372	29.8501	19.9457	44.3891	25.5227
247	-15.0975	81.663	-0.4603	20.0626	-24.9171	29.8501	19.9457	44.3891	25.5227
248	-15.0975	81.663	-0.4603	20.0626	-24.9171	29.7117	19.9882	44.3444	25.7238
249	-15.0975	81.663	-0.4603	20.0626	-24.9171	29.7117	19.9882	44.3444	25.7238
250	-15.1163	81.4874	-1.0238	20.8775	-24.8026	29.4323	19.9958	44.3229	25.7787
251	-15.1163	81.4874	-1.0238	20.8775	-24.8026	29.4323	19.9958	44.3229	25.7787
252	-15.0436	81.595	-1.5097	20.5997	-25.0149	29.4978	20.0248	44.4105	25.8012
253	-15.0436	81.595	-1.5097	20.5997	-25.0149	29.4978	20.0248	44.4105	25.8012
254	-15.0971	81.7149	-1.4088	19.9626	-25.0738	29.4978	20.0248	44.4105	25.8012
255	-15.0971	81.7149	-1.4088	19.9626	-25.0738	29.6655	19.9793	44.3216	25.7212
256	-15.0971	81.7149	-1.4088	19.9626	-25.0738	29.6655	19.9793	44.3216	25.7212

Table B-3. Continued

Frying Time	$T_{ref,in}$	$T_{fryer, top}$	$T_{cond, out}$	$T_{cond, in}$	$T_{ref,out}$	$T_{steam\ hose}$	$T_{pre, cond}$	$T_{comp, cond}$	$T_{cond, cap}$
257	-15.0925	82.0238	-1.5941	20.7267	-25.0504	29.6655	19.9793	44.3216	25.7212
258	-15.0925	82.0238	-1.5941	20.7267	-25.0504	29.8419	20.0957	44.3746	25.6512
259	-15.1116	82.4537	-2.1824	20.6212	-25.2309	29.8419	20.0957	44.3746	25.6512
260	-15.1116	82.4537	-2.1824	20.6212	-25.2309	29.8419	20.0957	44.3746	25.6512
261	-15.1026	82.7657	-2.2679	20.132	-25.2515	29.4696	20.066	44.3628	25.7533
262	-15.1026	82.7657	-2.2679	20.132	-25.2515	29.4696	20.066	44.3628	25.7533
263	-15.059	83.3039	-1.9698	19.7857	-25.2647	29.5414	20.0296	44.3598	25.7311
264	-15.059	83.3039	-1.9698	19.7857	-25.2647	29.5414	20.0296	44.3598	25.7311
265	-15.0551	83.8494	-1.8445	19.7649	-25.3483	29.5414	20.0296	44.3598	25.7311
266	-15.0551	83.8494	-1.8445	19.7649	-25.3483	29.6811	20.0442	44.3677	25.6781
267	-15.1031	84.3086	-2.0098	20.1198	-25.2797	29.6811	20.0442	44.3677	25.6781
268	-15.1031	84.3086	-2.0098	20.1198	-25.2797	29.4225	20.0421	44.3215	25.7626
269	-15.1031	84.3086	-2.0098	20.1198	-25.2797	29.4225	20.0421	44.3215	25.7626
270	-15.1983	84.2567	-3.0763	20.1925	-25.2969	29.4225	20.0421	44.3215	25.7626
271	-15.1983	84.2567	-3.0763	20.1925	-25.2969	29.8919	20.0545	44.3565	25.6279
272	-15.142	84.0189	-2.9001	19.7037	-25.4523	29.8919	20.0545	44.3565	25.6279
273	-15.142	84.0189	-2.9001	19.7037	-25.4523	29.8919	20.0545	44.3565	25.6279
274	-15.0307	84.0038	-2.6851	19.5218	-25.5259	29.6363	20.0222	44.3977	25.6684
275	-15.0307	84.0038	-2.6851	19.5218	-25.5259	29.6363	20.0222	44.3977	25.6684
276	-15.1951	84.3859	-2.6304	19.7691	-25.5351	29.6363	20.0222	44.3977	25.6684
277	-15.1951	84.3859	-2.6304	19.7691	-25.5351	29.7122	20.022	44.3308	25.7768
278	-15.1466	84.611	-3.6245	19.9111	-25.4259	29.7122	20.022	44.3308	25.7768
279	-15.1466	84.611	-3.6245	19.9111	-25.4259	29.5035	20.0725	44.388	25.8246
280	-15.1466	84.611	-3.6245	19.9111	-25.4259	29.5035	20.0725	44.388	25.8246
281	-15.1287	84.8981	-2.8856	19.8051	-25.5089	29.9053	19.9928	44.3791	25.6058
282	-15.1287	84.8981	-2.8856	19.8051	-25.5089	29.9053	19.9928	44.3791	25.6058
283	-15.2109	85.007	-3.6558	20.0288	-25.5728	29.6026	20.0116	44.3412	25.7345
284	-15.2109	85.007	-3.6558	20.0288	-25.5728	29.6026	20.0116	44.3412	25.7345
285	-15.2461	85.1766	-4.2099	19.8372	-25.6536	29.5068	19.9225	44.37	25.761
286	-15.2461	85.1766	-4.2099	19.8372	-25.6536	29.5068	19.9225	44.37	25.761
287	-15.224	85.4921	-4.2474	19.1469	-25.7455	29.5068	19.9225	44.37	25.761
288	-15.224	85.4921	-4.2474	19.1469	-25.7455	29.7891	19.9943	44.3805	25.6152
289	-15.1313	85.8476	-4.3691	19.8125	-25.7074	29.7891	19.9943	44.3805	25.6152
290	-15.1313	85.8476	-4.3691	19.8125	-25.7074	29.9947	19.9413	44.3546	25.5584
291	-15.2903	86.0827	-4.8961	19.6598	-25.7286	29.9947	19.9413	44.3546	25.5584
292	-15.2903	86.0827	-4.8961	19.6598	-25.7286	29.9947	19.9413	44.3546	25.5584
293	-15.1554	86.3813	-4.7503	18.9013	-25.748	29.5864	19.9483	44.4093	25.8624

Table B-3. Continued

Frying Time	$T_{ref,in}$	$T_{fryer, top}$	$T_{cond, out}$	$T_{cond, in}$	$T_{ref,out}$	$T_{steam\ hose}$	$T_{pre, cond}$	$T_{comp, cond}$	$T_{cond, cap}$
294	-15.1554	86.3813	-4.7503	18.9013	-25.748	29.5864	19.9483	44.4093	25.8624
295	-15.2735	86.7105	-4.3553	18.9791	-25.8044	29.5864	19.9483	44.4093	25.8624
296	-15.2735	86.7105	-4.3553	18.9791	-25.8044	29.8108	20.0173	44.4059	25.6662
297	-15.1459	86.7702	-4.9772	19.4704	-25.9144	29.8108	20.0173	44.4059	25.6662
298	-15.1459	86.7702	-4.9772	19.4704	-25.9144	29.8108	20.0173	44.4059	25.6662
299	-15.2553	87.1666	-5.5934	19.4436	-25.9126	29.6172	19.9455	44.4039	25.8123
300	-15.2553	87.1666	-5.5934	19.4436	-25.9126	29.6172	19.9455	44.4039	25.8123
301	-15.2553	87.1666	-5.5934	19.4436	-25.9126	29.6566	19.9315	44.3895	25.8028
302	-15.232	87.1902	-4.8339	19.1055	-25.8754	29.6566	19.9315	44.3895	25.8028
303	-15.232	87.1902	-4.8339	19.1055	-25.8754	29.6566	19.9315	44.3895	25.8028
304	-15.2323	87.4776	-5.743	18.8078	-25.9395	29.945	19.9632	44.3456	25.7202
305	-15.2323	87.4776	-5.743	18.8078	-25.9395	29.945	19.9632	44.3456	25.7202
306	-15.2323	87.4776	-5.743	18.8078	-25.9395	29.945	19.9632	44.3456	25.7202
307	-15.2066	87.7903	-5.5384	19.368	-25.8929	29.8111	19.8856	44.3733	25.7018
308	-15.2066	87.7903	-5.5384	19.368	-25.8929	29.8111	19.8856	44.3733	25.7018
309	-15.2066	87.7903	-5.5384	19.368	-25.8929	29.8111	19.8856	44.3733	25.7018
310	-15.2103	87.6784	-5.2692	18.4943	-26.067	29.7873	19.9051	44.347	25.7484
311	-15.2103	87.6784	-5.2692	18.4943	-26.067	29.7873	19.9051	44.347	25.7484
312	-15.1955	87.9079	-5.3026	19.0262	-25.9591	29.7873	19.9051	44.347	25.7484
313	-15.1955	87.9079	-5.3026	19.0262	-25.9591	29.9957	19.8853	44.3537	25.5455
314	-15.1955	87.9079	-5.3026	19.0262	-25.9591	29.9957	19.8853	44.3537	25.5455
315	-15.2562	87.8475	-5.68	18.4179	-26.049	30.1011	19.9437	44.3099	25.6912
316	-15.2562	87.8475	-5.68	18.4179	-26.049	30.1011	19.9437	44.3099	25.6912
317	-15.2562	87.8475	-5.68	18.4179	-26.049	30.1011	19.9437	44.3099	25.6912
318	-15.311	87.8967	-6.1101	19.2573	-26.1156	29.654	19.861	44.3339	25.702
319	-15.311	87.8967	-6.1101	19.2573	-26.1156	29.654	19.861	44.3339	25.702
320	-15.3252	87.6563	-5.9475	18.434	-26.1557	30.0061	19.8975	44.3329	25.6991
321	-15.3252	87.6563	-5.9475	18.434	-26.1557	30.0061	19.8975	44.3329	25.6991
322	-15.3252	87.6563	-5.9475	18.434	-26.1557	29.9558	19.9418	44.3707	25.6769
323	-15.2831	86.2132	-5.3683	18.447	-26.1066	29.9558	19.9418	44.3707	25.6769
324	-15.2831	86.2132	-5.3683	18.447	-26.1066	29.9558	19.9418	44.3707	25.6769
325	-15.2831	86.2132	-5.3683	18.447	-26.1066	29.9126	19.9141	44.3291	25.7995
326	-15.3167	85.0226	-6.1465	18.3921	-26.0817	29.9126	19.9141	44.3291	25.7995
327	-15.3167	85.0226	-6.1465	18.3921	-26.0817	29.9126	19.9141	44.3291	25.7995
328	-15.3239	84.4873	-5.4212	18.2402	-26.2108	30.1218	19.9272	44.3146	25.5671
329	-15.3239	84.4873	-5.4212	18.2402	-26.2108	30.1218	19.9272	44.3146	25.5671
330	-15.3239	84.4873	-5.4212	18.2402	-26.2108	30.1218	19.9272	44.3146	25.5671

Table B-3. Continued

Frying Time	$T_{ref,in}$	$T_{fryer, top}$	$T_{cond, out}$	$T_{cond, in}$	$T_{ref,out}$	$T_{steam\ hose}$	$T_{pre, cond}$	$T_{comp, cond}$	$T_{cond, cap}$
331	-15.4076	83.5959	-6.3689	18.5591	-26.1991	29.7647	19.9146	44.3395	25.8624
332	-15.4076	83.5959	-6.3689	18.5591	-26.1991	29.7647	19.9146	44.3395	25.8624
333	-15.4076	83.5959	-6.3689	18.5591	-26.1991	29.7647	19.9146	44.3395	25.8624
334	-15.4432	82.687	-5.9594	18.9281	-26.1889	30.1793	19.9876	44.2652	25.6074
335	-15.4432	82.687	-5.9594	18.9281	-26.1889	30.1793	19.9876	44.2652	25.6074
336	-15.3158	82.0105	-6.4866	18.7565	-26.3086	29.9967	19.9511	44.3091	25.7566
337	-15.3158	82.0105	-6.4866	18.7565	-26.3086	29.9967	19.9511	44.3091	25.7566
338	-15.2664	81.7979	-5.7986	18.5815	-26.2179	29.9967	19.9511	44.3091	25.7566
339	-15.2664	81.7979	-5.7986	18.5815	-26.2179	30.1621	19.8558	44.271	25.5403
340	-15.2664	81.7979	-5.7986	18.5815	-26.2179	30.1621	19.8558	44.271	25.5403
341	-15.4135	81.592	-6.1673	17.9521	-26.2598	30.224	19.9059	44.2217	25.6156
342	-15.4135	81.592	-6.1673	17.9521	-26.2598	30.224	19.9059	44.2217	25.6156
343	-15.3692	81.432	-5.7099	18.2341	-26.2635	30.224	19.9059	44.2217	25.6156
344	-15.3692	81.432	-5.7099	18.2341	-26.2635	29.9779	19.9865	44.3166	25.6929
345	-15.3692	81.432	-5.7099	18.2341	-26.2635	29.9779	19.9865	44.3166	25.6929
346	-15.326	80.9308	-6.6191	18.1721	-26.369	29.9779	19.9865	44.3166	25.6929
347	-15.326	80.9308	-6.6191	18.1721	-26.369	30.0281	19.9688	44.2493	25.7646
348	-15.326	80.9308	-6.6191	18.1721	-26.369	30.0281	19.9688	44.2493	25.7646
349	-15.3716	80.4089	-6.1589	18.6618	-26.2995	29.8314	19.9951	44.2527	25.7221
350	-15.3716	80.4089	-6.1589	18.6618	-26.2995	29.8314	19.9951	44.2527	25.7221
351	-15.3676	79.9882	-6.5722	18.5444	-26.4264	29.8314	19.9951	44.2527	25.7221
352	-15.3676	79.9882	-6.5722	18.5444	-26.4264	30.0094	19.9679	44.2505	25.7383
353	-15.4766	79.6072	-6.3394	17.8682	-26.3691	30.0094	19.9679	44.2505	25.7383

APPENDIX C

PROGRAM CODE FOR VACUUM FRYER SIMULATOR

```
Dim handle&                                          ' Device handle returned by VBdaqOpen
Dim ret&                                             ' Function return value
Dim errorString$                                     ' String to hold formatted error message
Const ChanCount& = 5                                 ' 5 channels
Const ScanCount& = 1                                 ' 1 Scans
Const TotalCount& = (ScanCount& * ChanCount&)        ' Buffer size
Const startChan = 1                                  ' First channel in sequence
Dim deviceIndex&                                     ' Device index counter
Dim deviceList() As String                           ' Device list array
Dim deviceCount&                                     ' Number of devices
Dim deviceProps As DaqDevicePropsT                   ' Device properties structure
Dim i&, j&, k&                                       ' Counter/loop variables
Dim buf!(TotalCount&)                                ' Data buffer
Dim chans&(ChanCount&)                               ' Channel sequence array
Dim flags&(ChanCount&)                               ' Flag sequence array
Dim gains&(ChanCount&)                               ' Gain sequence array
Dim trgSrc&(ChanCount&)                              ' Trigger sources
Dim adcRanges&(ChanCount&)                           ' A/D ranges
Dim trigSense&(ChanCount&)                           ' Trigger sensitivity
Dim levels!(ChanCount&)                              ' Trigger levels
Dim hysteresis!(ChanCount&)                          ' Hysteresis values
Dim active&                                          ' Acquisition active flag
Dim retCount&                                        ' Transfer return count
Dim errCode&                                         ' Error code
Dim actualRate!                                      ' Used by daqAdcSetRate
Dim optString As String                              ' Used by daqAdcSetTrigEnhanced
Dim Buffer() As String                               ' Array to store Values of Simulation
Dim blDimensioned As Boolean                         ' For first array variable
Dim TimeCount As String                              ' Time Counter
Dim ThermoVal As String                              ' Time Counter
Dim StVal As String                                  ' Time Counter

Public Function openSIM()

' Obtain the device list

ret& = VBdaqGetDeviceList(deviceList, deviceCount)


' Find the first PersonalDaq device in the device list by retrieving the device properties
one device at a time and then checking to see if each device is a PersonalDaq

handle& = -1
For deviceIndex& = 0 To deviceCount - 1
```

```
ret& = VBdaqGetDeviceProperties(deviceList(deviceIndex), deviceProps)
If deviceProps.DeviceType = PersonalDaq55 Or _
deviceProps.DeviceType = PersonalDaq56 Then
' Initialize the PersonalDaq and obtain a handle to the opened
' device that can be used with all of the other function calls
handle& = VBdaqOpen&(deviceList(deviceIndex))
Exit For
End If
Next deviceIndex&

' Exit if no PersonalDaq devices were found

If handle& = -1 Then
MsgBox "daqErrno& : " & Hex$(daqErrno&) & ". No hardware Found."
Exit Function
End If

' Initialize the scan sequence arrays

For i& = 0 To ChanCount& - 1
chans&(i&) = i& + startChan
gains&(i&) = PGainX1&
flags&(i&) = DafAnalog& + DafDifferential& + DafMeasDuration40 + DafTcTypeK
Next i&

' Set the error handler

ret& = VBdaqSetErrorHandler&(handle&, 100)
On Error GoTo ErrorHandlerADC1

' Set the data format to floating point

ret& = VBdaqAdcSetDataFormat(handle&, DardfFloat, DappdfRaw)

' Configure A/D scan group using the scan sequence arrays

ret& = VBdaqAdcSetScan&(handle&, chans&(), gains&(), flags&(), ChanCount&)


' Set and arm the trigger of the A/D converter;  the acquisition will be triggered
immediately upon issuance of the VBdaqAdcArm command

For i = 0 To ChanCount - 1
trgSrc&(i) = DatsImmediate&
```

```
adcRanges&(i) = DarBiMinus5to5V
trigSense&(i) = DetsRisingEdge&
levels!(i) = 0
hysteresis!(i) = 0
Next i
ret& = VBdaqAdcSetTrigEnhanced&(handle&, trgSrc&(), gains&(), adcRanges&(), _
            trigSense&(), levels!(), hysteresis!(), _
            chans&(), ChanCount& - 1, optString)

' Characterize the acquisition mode and pre/post trigger durations so that once
' triggered, the acquisition will continue until the specified post trigger count
' (ScanCount&) is satisfied, at which point the acquisition will be automatically
' disarmed.

ret& = VBdaqAdcSetAcq&(handle&, DaamNShot&, 0, ScanCount&)

' Set the frequency to 3Hz

ret& = VBdaqAdcSetRate&(handle&, DarmFrequency, DaasPostTrig, 8!, actualRate!)

' Configure the user-allocated buffer (buf!) with cycling disabled and single
' sample updating

ret& = VBdaqAdcTransferSetBufferSingle&(handle&, buf!(), ScanCount&, DatmWait)

Exit Function
ErrorHandlerADC1:
errorString$ = "ERROR in ADC1"
errorString$ = errorString$ & Chr(10) & "BASIC Error :" + Str$(Err)
If Err = 100 Then errorString$ = errorString$ & Chr(10) & "PersonalDaq Error : " +
Hex$(daqErrno&)
MsgBox errorString$, , "Error!"
closeSIM   'Close the device
End Function

Public Function readSIM()



' Set the error handler

ret& = VBdaqSetErrorHandler&(handle&, 100)
On Error GoTo ErrorHandlerADC1
```

```
' Setup and start the data transfer

ret& = VBdaqAdcTransferStart&(handle&)

' Arm the acquisition
ret& = VBdaqAdcArm&(handle&)

' Retrieve the transfer status information

Do
ret& = VBdaqAdcTransferGetStat&(handle&, active&, retCount&)
Loop While (active& And DaafAcqActive&)

' Print the acquired data

If CheckBox1.value = True Then
Thermo1.Caption = Round(Format$(buf!(0), "#0.0###"), 8)
ThermoVal = Round(Format$(buf!(0), "#0.0###"), 8)
Else
If CheckBox1.Enabled = False Then
Label97.Caption = Round(Format$(buf!(0), "#0.0###"), 8)
ThermoVal = Round(Format$(buf!(0), "#0.0###"), 8)
End If
End If
If CheckBox2.value = True Then
Thermo2.Caption = Round(Format$(buf!(1), "#0.0###"), 8)
End If
If CheckBox3.value = True Then
Thermo3.Caption = Round(Format$(buf!(2), "#0.0###"), 8)
End If
If CheckBox4.value = True Then
Thermo4.Caption = Round(Format$(buf!(3), "#0.0###"), 8)
End If
If CheckBox5.value = True Then
Thermo5.Caption = Round(Format$(buf!(4), "#0.0###"), 8)
End If
If Thermo2.Caption > 20 And Thermo2.Caption < 30 Then
Sbar.Caption = "Simulation Started : " & StVal & " Current Process : Chips Outside
Fryer/ Depressurizing"
End If
If Thermo2.Caption > 30 And Thermo2.Caption < 50 Then
Sbar.Caption = "Simulation Started : " & StVal & " Current Process : Chips Inside
Fryer"
End If
```

```
If Thermo2.Caption > 50 And Thermo2.Caption < 150 Then
Sbar.Caption = "Simulation Started : " & StVal & " Current Process : Chips Frying"
End If
Exit Function
ErrorHandlerADC1:
errorString$ = "ERROR in ADC1"
errorString$ = errorString$ & Chr(10) & "BASIC Error :" + Str$(Err)
If Err = 100 Then errorString$ = errorString$ & Chr(10) & "PersonalDaq Error : " +
Hex$(daqErrno&)
MsgBox errorString$, , "Error!"
closeSIM   'Close the device
End Function

Public Function closeSIM()

' Close the device

VBdaqAdcDisarm (handle&)
ret& = VBdaqClose&(handle&)
End Function

Public Function Initiative() As Integer
If TextBox1 = "" Or TextBox1 = 0 Then Initiative = 1
'If TextBox2 = "" Or TextBox2 = 0 Then Initiative = 1
If TextBox3 = "" Or TextBox3 = 0 Then Initiative = 1
'If TextBox5 = "" Or TextBox5 = 0 Then Initiative = 1
If TextBox6 = "" Or TextBox6 = 0 Then Initiative = 1
End Function

Public Function Calc()
On Error Resume Next

'0=Time[Sec]
'1=Tref,in
'2=Tamb
'3=Tcond,out
'4=Tcond,in
'5=Tref,out
'6=Moisture Content [db]
'7=Mass Flow Rate [Kg/sec]
'8=Total heat rate of steam to condense (watt)
'9=Thickness of liquid film[m]
'10=Thickness of Ice[m]
'11=Thickness of tube+ice[m]
```

```
'12=Change in Area of tube with ice formation [m^2]
'13=Condenser capacity [watt]
'14=Mass flow rate of R-404a required Sensible [kg/s]
'15=mass flow rate of R-404a Latent [kg/s]
'16=Total Mass Flow Rate Required (Kg/s)
'17=Evaporator Coil Capacity
'18=Condenser heat Qc
'19=Compressor power q comp

' Check for the Initial Values

If Initiative() Then MsgBox "Please Provide the Initial Values.", vbInformation: Exit
Function

'Initialization of the Master Values

If blDimensioned = True Then
ReDim Preserve Buffer(19, UBound(Buffer, 2) + 1) As String
Else
ReDim Buffer(19, 0) As String
blDimensioned = True
End If
Dim curRow As Integer
curRow = UBound(Buffer, 2)
TimeCount = Val(TimeCount) + 1
Label92.Caption = TimeCount
Buffer(0, curRow) = TimeCount * Val(TextBox123.Text)
Buffer(1, curRow) = ThermoVal
Buffer(2, curRow) = Thermo2.Caption
Buffer(3, curRow) = Thermo3.Caption
Buffer(4, curRow) = Thermo4.Caption
Buffer(5, curRow) = Thermo5.Caption
TextBox10.Caption = Round(3.14 * Val(TextBox1.Text) * 6.096, 8)
TextBox26.Caption = Round(((Val(Buffer(5, curRow)) - Val(Buffer(4, curRow))) -
(Val(Buffer(3, curRow)) - Val(Thermo1.Caption))) / Log((Val(Buffer(5, curRow)) -
Val(Buffer(4, curRow))) / (Val(Buffer(3, curRow)) - Val(Thermo1.Caption))), 8)
TextBox23.Caption = Round((1.345 + (4.435 * (10 ^ -3) * (Thermo1.Caption)) + (6.914
* 10 ^ (-5) * (Thermo1.Caption ^ 2)) + (2.113 * 10 ^ (-6) * (Thermo1.Caption ^ 3))), 8)
TextBox16.Caption = Round(Val(TextBox3.Text) * (1 - 0.85), 8)
Select Case ComboBox3.ListIndex
Case 0 '120 C
Buffer(6, curRow) = Round((3.147 * Exp((-0.01686) * Val(Buffer(0, curRow))) +
0.01496), 8)
Case 1 '130 C
```

```
Buffer(6, curRow) = Round((3.147 * Exp((-0.02573) * Val(Buffer(0, curRow))) +
0.01496), 8)
Case 2 '140 C
Buffer(6, curRow) = Round((3.147 * Exp((-0.02992) * Val(Buffer(0, curRow))) +
0.01496), 8)
End Select

'Cumulative Mass Flow Rate

If curRow = 0 Then
Buffer(7, curRow) = 0 'First Mass Flow Rate[Kg/sec]=0
Else
Buffer(7, curRow) = Round((Val(Buffer(6, curRow - 1)) - Val(Buffer(6, curRow))) *
Val(TextBox16.Caption), 8)
End If

'Average Mass Flow Rate

AverageMassFlowRate = 0
For Row = 0 To curRow + 1
AverageMassFlowRate = Val(AverageMassFlowRate) + Val(Buffer(7, Row))
Next Row
TextBox24.Caption = Round((Val(AverageMassFlowRate) / Val(Buffer(0, curRow))),
8)
TextBox120.Caption = Buffer(6, curRow)
TextBox7.Caption = Buffer(7, curRow)
'Total heat rate of steam to condense (watt)
If curRow = 0 Then
Buffer(8, curRow) = 0 'First Total heat rate of steam to condense (watt)=0
Else
Buffer(8, curRow) = Round(((Val(Buffer(7, curRow)) * 4.1855 * (Val(Buffer(4, curRow
- 1)) - Val(Thermo1.Caption))) + Val(Buffer(7, curRow)) * Val(TextBox8.Caption) +
Val(Buffer(7, curRow)) * 333.15 + Val(Buffer(7, curRow)) * 2110 * (9.968 -
Val(Thermo1.Caption))), 8)
End If
If curRow = 0 Then
Buffer(9, curRow) = 0 'First Thickness of liquid film[m]=0
Else
Buffer(9, curRow) = Round(((Val(TextBox10.Caption)) * Val(TextBox22.Caption)) *
(Val(Buffer(3, curRow - 1)) - (Val(Thermo1.Caption))) / Val(Buffer(8, curRow)), 8)
End If
TextBox11.Caption = (0.943) * (((Val(TextBox14.Caption) * 9.8 * (999.35 - 0.011157)
* (Val(TextBox22.Caption) ^ 3)) / (Val(Buffer(9, curRow)) * (Val(Buffer(3, curRow)) -
Val(Thermo1.Caption)) * 0.00000855)) ^ (1 / 4))
```

```
If curRow = 0 Then
Buffer(10, curRow) = 0 'First Thickness of Ice[m]=0
Else
Buffer(10, curRow) = Round(Val(Buffer(9, curRow)) / 5, 8)
End If
Buffer(11, curRow) = Round(Val(TextBox1.Text) + Val(Buffer(9, curRow)), 8)
If Not curRow = 0 Then
TextBox13.Caption = Round(1 / ((Val(Buffer(9, curRow)) / Val(TextBox22.Caption)) +
(1 / Val(TextBox11.Caption)) + (Val(TextBox1.Text) / Val(TextBox21.Caption)) +
(Val(Buffer(9, curRow)) / Val(TextBox28.Caption))), 8)
TextBox15 = Round(Val(Buffer(8, curRow)) / Val(3.14 * Val(TextBox1.Text) *
Val(TextBox13.Caption) * Val(Val(Buffer(3, curRow)) - Val(Thermo1.Caption))), 8)
TextBox17.Caption = Round(3.14 * Val(TextBox15.Caption) * Val(TextBox1.Text),
10)
End If
Buffer(12, curRow) = 3.14 * Val(Buffer(11, curRow)) * Val(TextBox13.Caption)
Buffer(13, curRow) = Val(TextBox13.Caption) * Val(Buffer(12, curRow)) *
Val(TextBox26.Caption)
Buffer(14, curRow) = (Val(Buffer(13, curRow)) / (Val(TextBox21.Caption) *
Val(TextBox28.Caption))) / 1000
Buffer(15, curRow) = (Val(Buffer(13, curRow)) / 180200)
Buffer(16, curRow) = Val(Buffer(14, curRow)) + Val(Buffer(15, curRow))
Buffer(17, curRow) = (Val(Buffer(16, curRow)) * (367.2 - 359.6))
Buffer(18, curRow) = (Val(Buffer(16, curRow)) * (382.9 - 367.2))
Buffer(19, curRow) = (Val(Buffer(16, curRow)) * (382.9 - 359.6))
TextBox25 = Buffer(8, curRow)
TextBox19 = Buffer(13, curRow)
End Function

Private Sub ComboBox4_Change()
If ComboBox4.ListIndex = 0 Then
Thermo1.Caption = "-15.0000"
CheckBox1.Enabled = False
CheckBox1.value = 0
Label97.Visible = True
Else
CheckBox1.Enabled = True
Label97.Visible = False
Thermo1.Caption = "00.0000"
End If
End Sub

Private Sub CommandButton10_Click()
'Draw Reference Table
```

```
On Error GoTo Err:
a2 = Val(UBound(Buffer, 2))
Dim TableSIM As Worksheet
Set TableSIM = Sheets.Add
TableSIM.Cells(1, 1).value = "Time[Sec]"
If CheckBox1.Enabled = False Then
TableSIM.Cells(1, 2).value = "Tpc"
Else
TableSIM.Cells(1, 2).value = "Tref,in"
End If
TableSIM.Cells(1, 3).value = "Tamb"
TableSIM.Cells(1, 8).value = "Tcond,out"
TableSIM.Cells(1, 5).value = "Tcond,in"
TableSIM.Cells(1, 6).value = "Tref,out"
TableSIM.Cells(1, 7).value = "Moisture Content[db]"
TableSIM.Cells(1, 8).value = "Mass Flow Rate of Steam[Kg/s]"
TableSIM.Cells(1, 9).value = "Heat Transfer Rate of Steam[Watt]"
TableSIM.Cells(1, 10).value = "Thickness of liquid film[m]"
TableSIM.Cells(1, 11).value = "Thickness of Ice[m]"
TableSIM.Cells(1, 12).value = "Thickness of tube+ice[m]"
TableSIM.Cells(1, 13).value = "Change in Area of tube with ice formation [m^2]"
TableSIM.Cells(1, 14).value = "Condenser capacity[watt]"
TableSIM.Cells(1, 15).value = "Mass flow rate of R-404a required Sensible[Kg/s]"
TableSIM.Cells(1, 16).value = "Mass flow rate of R-404a Latent[Kg/s]"
TableSIM.Cells(1, 17).value = "Total Mass Flow Rate Required [Kg/s]"
TableSIM.Cells(1, 18).value = "Evaporator Coil Capacity"
TableSIM.Cells(1, 19).value = "Condenser heat Qc"
TableSIM.Cells(1, 20).value = "Compressor power q comp"
For Row = 2 To Val(UBound(Buffer, 2)) + 1
For Col = 0 To 19
TableSIM.Cells(Row, Col + 1).value = Buffer(Col, Row - 2)
Next Col
Next Row
Exit Sub
Err:
MsgBox "No Table in Reference. Please Simulate to get the output table.",
vbInformation, "Simulator Request"
End Sub

Private Sub CommandButton11_Click()
If CommandButton11.Caption = "Compact Mode" Then
CommandButton11.Caption = "Full Mode"
Frame3.Top = -50
Me.Height = 55
```

```
Else
CommandButton11.Caption = "Compact Mode"
Frame3.Top = 336
Me.Height = 539.25
End If
End Sub

Private Sub CommandButton6_Click()
If Initiative() Then MsgBox "Please Provide the Initial Values. Before Enabling Auto -
Simulation", vbInformation: CheckBox1.value = False: Exit Sub
If CommandButton6.Caption = "SIMULATE" Then
CommandButton6.Caption = "HALT NOW"
CommandButton6.BackColor = &HFF&
Label92.Caption = "00"
ReDim Buffer(19, 0) As String
openSIM
StVal = Now

' Exit if no PersonalDaq devices were found

If handle& = -1 Or Len(errorString$) > 1 Then
MsgBox "daqErrno& : " & Hex$(daqErrno&) & " + " & errorString$
CommandButton6.Caption = "SIMULATE"
CommandButton6.BackColor = &H80FF80
Timer1.Enabled = False
Timer2.Enabled = False
Exit Sub
End If

'If everything goes OK then Start Reading Values

Timer1.Enabled = True
Timer2.interval = TextBox123.Text * 290
Timer2.Enabled = True
Sbar.Caption = "Simulation Started : " & StVal & " Current Process : Chips Outside
Fryer/ Depressurizing"
TimeCount = 0
Else
CommandButton6.Caption = "SIMULATE"
CommandButton6.BackColor = &H80FF80
Timer1.Enabled = False
Timer2.Enabled = False
Sbar.Caption = "Simulation Started : " & StVal & " Simulation Stopped : " & Now
TimeCount = 0
```

```
closeSIM
End If
End Sub

Private Sub CommandButton7_Click()
End
End Sub

Private Sub CommandButton9_Click()

'Variale Declaration

Dim xMin As Double
Dim xMax As Double
Dim yMin As Double
Dim yMax As Double
Set TableSIM2 = Worksheets("CondenserSIM")
Sheets("CondenserSIM").Select


'Cleaning Previous

TableSIM2.range("M7:M1007").ClearContents
TableSIM2.range("N7:N1007").ClearContents

'Labelling Chart

Set chMain = TableSIM2.ChartObjects("Chart 1")
chMain.Chart.HasTitle = True
chMain.Chart.ChartTitle.Text = UCase(ComboBox1.Text) & " vs. " &
UCase(ComboBox2.Text)
chMain.Chart.Axes(xlCategory, xlPrimary).HasTitle = True
chMain.Chart.Axes(xlCategory, xlPrimary).AxisTitle.Characters.Text =
UCase(ComboBox1.Text)
chMain.Chart.Axes(xlValue, xlPrimary).HasTitle = True
chMain.Chart.Axes(xlValue, xlPrimary).AxisTitle.Characters.Text =
UCase(ComboBox2.Text)

'Chart Prepration - Min & Max Retrival

For Row = 1 To Val(UBound(Buffer, 2))
If Buffer(Val(ComboBox1.ListIndex), Row) < xMin Then xMin =
Buffer(Val(ComboBox1.ListIndex), Row)
```

```
If Buffer(Val(ComboBox1.ListIndex), Row) > xMax Then xMax =
Buffer(Val(ComboBox1.ListIndex), Row)
If Buffer(Val(ComboBox2.ListIndex), Row) < yMin Then yMin =
Buffer(Val(ComboBox2.ListIndex), Row)
If Buffer(Val(ComboBox2.ListIndex), Row) > yMax Then yMax =
Buffer(Val(ComboBox2.ListIndex), Row)
TableSIM2.Cells(Row + 6, 13).value = Buffer(Val(ComboBox1.ListIndex), Row)
TableSIM2.Cells(Row + 6, 14).value = Buffer(Val(ComboBox2.ListIndex), Row)
Next Row
chMain.Chart.Axes(1).MinimumScale = xMin
chMain.Chart.Axes(1).MaximumScale = xMax
chMain.Chart.Axes(2).MinimumScale = yMin
chMain.Chart.Axes(2).MaximumScale = yMax
End Sub

Private Sub ScrollBar2_Change()
TextBox123.Text = ScrollBar2.value
End Sub

Private Sub Timer1_Timer()
readSIM
If Len(errorString$) > 1 Then
CommandButton6.Caption = "SIMULATE"
Timer1.Enabled = False
closeSIM
Exit Sub
End If
End Sub

Private Sub Timer2_Timer()
Calc
End Sub

Private Sub UserForm_Initialize()

'Set A

ComboBox1.AddItem "Time[Sec]"
ComboBox1.AddItem "Tref,in[celsius]"
ComboBox1.AddItem "Tamb[celsius]"
ComboBox1.AddItem "Tcond,out[celsius]"
ComboBox1.AddItem "Tcond,in[celsius]"
ComboBox1.AddItem "Tref,out[celsius]"
ComboBox1.AddItem "Moisture Content[db]"
```

```
ComboBox1.AddItem "Mass Flow Rate[Kg/sec]"
ComboBox1.AddItem "Total heat rate of steam to condense (watts)"
ComboBox1.AddItem "Thickness of liquid film[m]"
ComboBox1.AddItem "Thickness of Ice[m]"
ComboBox1.AddItem "Thickness of tube+ice[m]"
ComboBox1.AddItem "Change in Area of tube with ice formation [m^2]"
ComboBox1.AddItem "Condenser capacity[watts]"
ComboBox1.AddItem "Mass flow rate of R-404a required Sensible[kg/s]"
ComboBox1.AddItem "mass flow rate of R-404a Latent[kg/s]"
ComboBox1.AddItem "Total Mass Flow Rate Required (Kg/s)"
ComboBox1.AddItem "Evaporator Coil Capacity"
ComboBox1.AddItem "Condenser heat Qc"
ComboBox1.AddItem "Compressor power q comp"
ComboBox1.ListIndex = 0

'Set B

ComboBox2.AddItem "Time[Sec]"
ComboBox2.AddItem "Tref,in[celsius]"
ComboBox2.AddItem "Tamb[celsius]"
ComboBox2.AddItem "Tcond,out[celsius]"
ComboBox2.AddItem "Tcond,in[celsius]"
ComboBox2.AddItem "Tref,out[celsius]"
ComboBox2.AddItem "Moisture Content[db]"
ComboBox2.AddItem "Mass Flow Rate[Kg/sec]"
ComboBox2.AddItem "Total heat rate of steam to condense (watt)"
ComboBox2.AddItem "Thickness of liquid film[m]"
ComboBox2.AddItem "Thickness of Ice[m]"
ComboBox2.AddItem "Thickness of tube+ice[m]"
ComboBox2.AddItem "Change in Area of tube with ice formation [m^2]"
ComboBox2.AddItem "Condenser capacity[watt]"
ComboBox2.AddItem "Mass flow rate of R-404a required Sensible[kg/s]"
ComboBox2.AddItem "mass flow rate of R-404a Latent[kg/s]"
ComboBox2.AddItem "Total Mass Flow Rate Required (Kg/s)"
ComboBox2.AddItem "Evaporator Coil Capacity"
ComboBox2.AddItem "Condenser heat Qc"
ComboBox2.AddItem "Compressor power q comp"
ComboBox2.ListIndex = 0

'T-oil

ComboBox3.AddItem "120"
ComboBox3.AddItem "130"
ComboBox3.AddItem "140"
```

```
ComboBox3.ListIndex = 0

'Tpc/Tref

ComboBox4.AddItem "Tpc"
ComboBox4.AddItem "Tref,in"
ComboBox4.ListIndex = 1
End Sub

Private Sub CommandButton8_Click()
With CommonDialog
   .DialogTitle = "Save"
   .CancelError = False
   'ToDo: set the flags and attributes of the common dialog control
   .Filter = "Aki Files (*.Aki)|*.Aki"
   .ShowSave
   If Len(.filename) = 0 Then
      Exit Sub
   End If
   sFile = .filename
End With
SaveToFile (sFile)
End Sub

Private Sub CommandButton4_Click()
With CommonDialog
  .DialogTitle = "Open"
  .CancelError = False

  'ToDo: set the flags and attributes of the common dialog control

  .Filter = "Aki Files (*.Aki)|*.Aki|All Files (*.*)|*.*"
  .ShowOpen
  If Len(.filename) = 0 Then
     Exit Sub
  End If
  oFile = .filename
End With
LoadFromFile (oFile)

'Calculate

End Sub
```

APPENDIX D

VACUUM PUMP

Model 1402 Welch Scientific Co., Skokie, Illinois

SPECIFICATIONS - Single Phase[1,2]

2-stages Vacuum Pump[3]			
Welch Model	**1400**	**1405**	**1402**
Free Air Displacement			
CFM	0.9	3.2	5.6
L/min	25	91	160
Ultimate Pressure (Torr)	1×10^{-4}	1×10^{-4}	1×10^{-4}
Gas Ballast	Yes	Yes	Yes
Pump RPM	580	525	525
Motor Horsepower	1/3	1/2	1/2
Oil Capacity, qt. (liters)	0.62 (0.59)	2.25 (2.1)	2.25(2.1)
Tubing Needed, I.D. in	7/16	7/16	13/16
Intake, Nipple Thread	3/4-20	1-20	1-20
Exhaust, Thread Type	3/4-20	1-20	1-20
Weight, lbs (kg)	58(26)	112(51)	112(51)
Dimensions L x W x H in (cm)	17.8 x 9 x 12.6 (45.1 x 22.9 x 32.1)	20 x 12 x 15 (51 x 30.5 x 38.1)	20 x 12 x 15 (51 x 30.5 x 38.1)
Ship Weight, lbs (kg)	68 (31)	128 (58)	128 (58)
Shipping Carton Dimensions L x W x H in (cm)	20.6 x 13.8 x 14.4 (52.3 x 35 x 36.5)	22.6 x 15 x 18.3 (57.5 x 38 x 46.5)	22.6 x 15 x 18.3 (57.5 x 38 x 46.5)

1. CSA approved models available. Explosion Proof, TEFC. 3-Phase motors available. Consult product list.
2. All 115 and 230V single phase motors include thermal overload protection. Models 1400C-02, 1405C-02 and 1402C-02 provided with CE marking.

3. Two-stage pumps should not be operated continuously at pressures above 10 Torr.

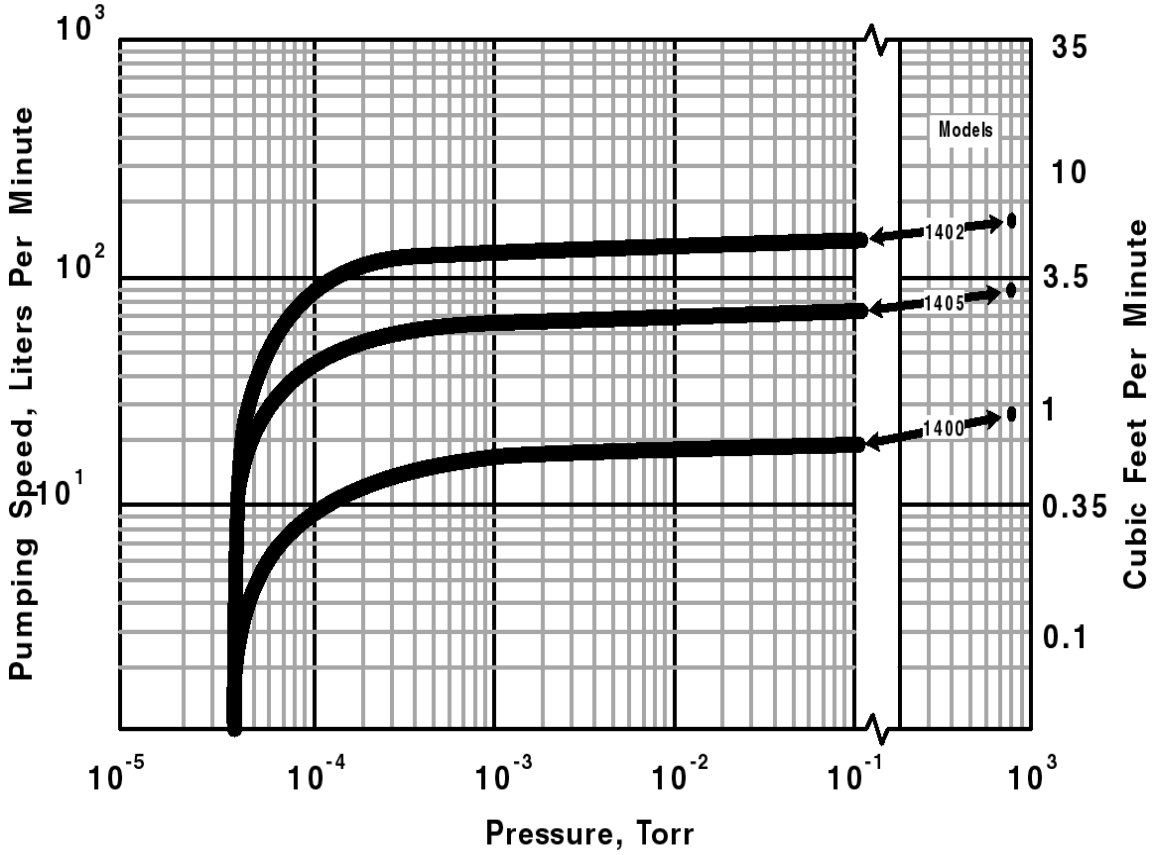

APPENDIX E

REFRIGERANT R404A

Product Description

- Substitute for R 502
- Near azeotropic refrigerant containing R 125, R 143a and R 134a
- (44/52/4% by weight)
- Refrigerant must be charged from liquid phase
- Physical and thermodynamical properties comparable to R 502
- Non-flammable
- Compressors must be charged with polyolester oils

Applications

- Cold-storage cells
- Supermarket display cases
- Ice machines
- Replacement for R 502 in transport refrigeration
- Retrofit of existing R502-installations with R 404A is possible

Environmental Aspects

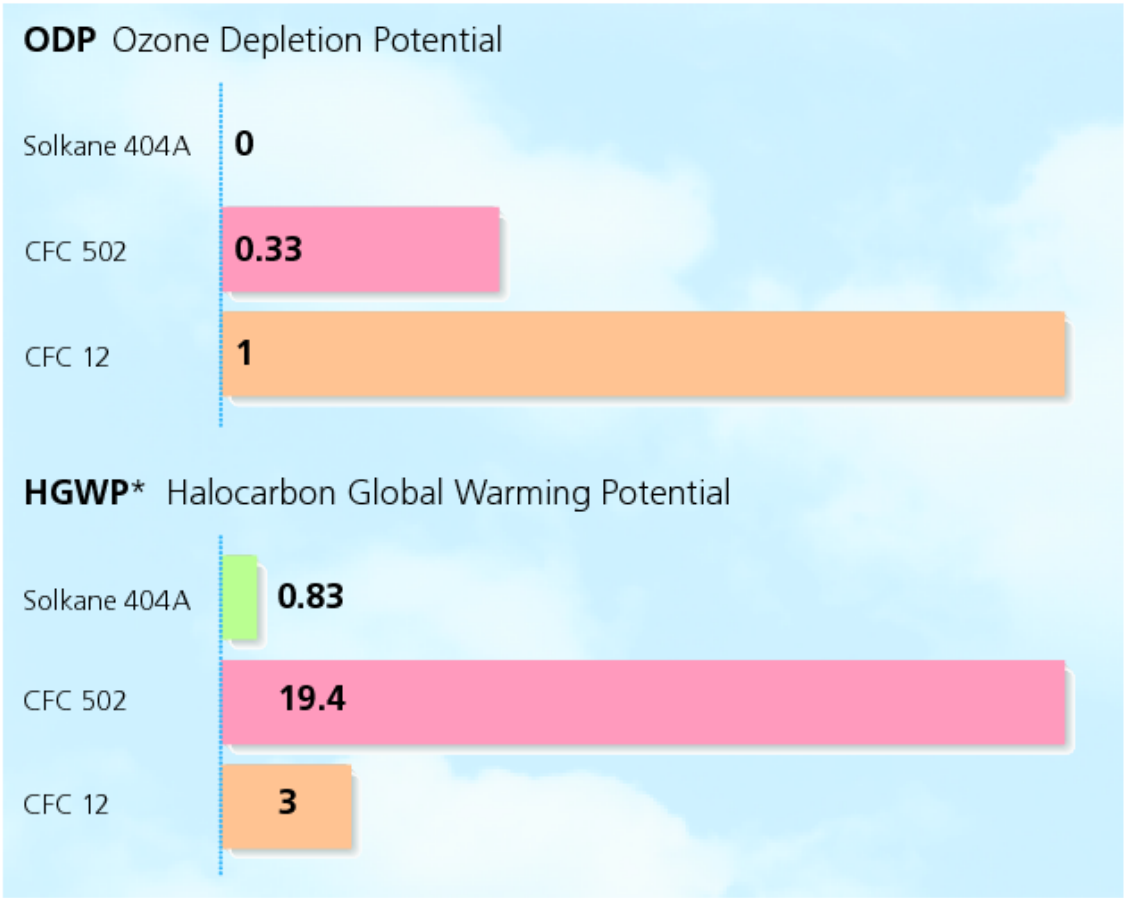

*The HGWP is related to R11 for an infinitive time horizon.

Range of Application

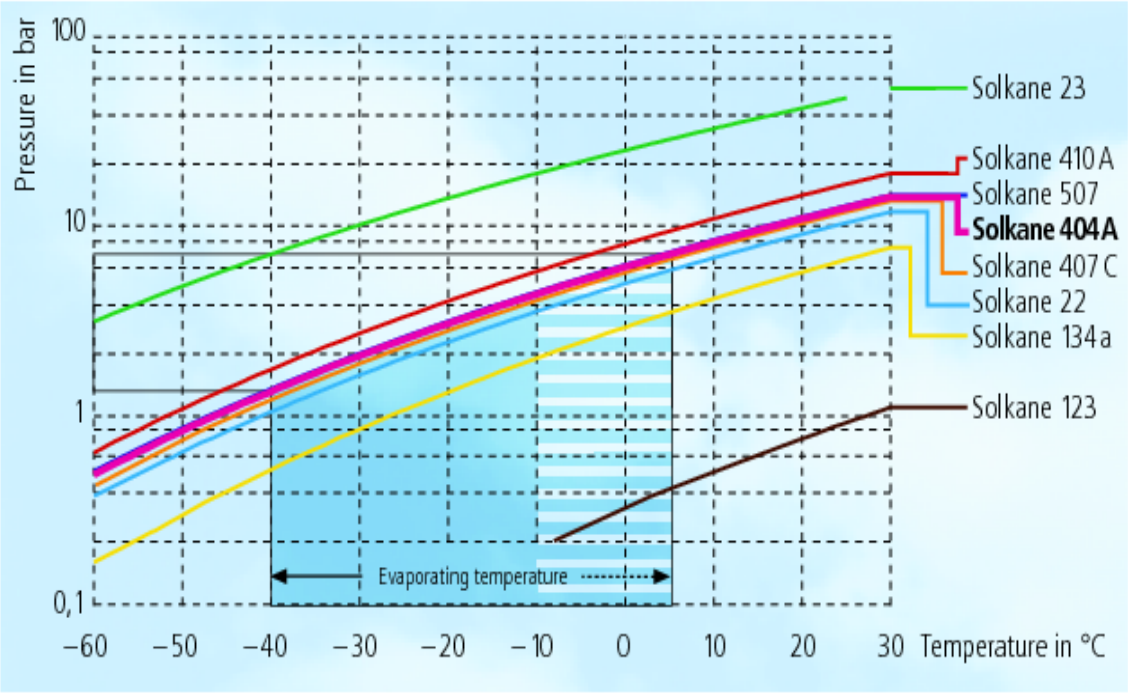

*Average pressure

Performance

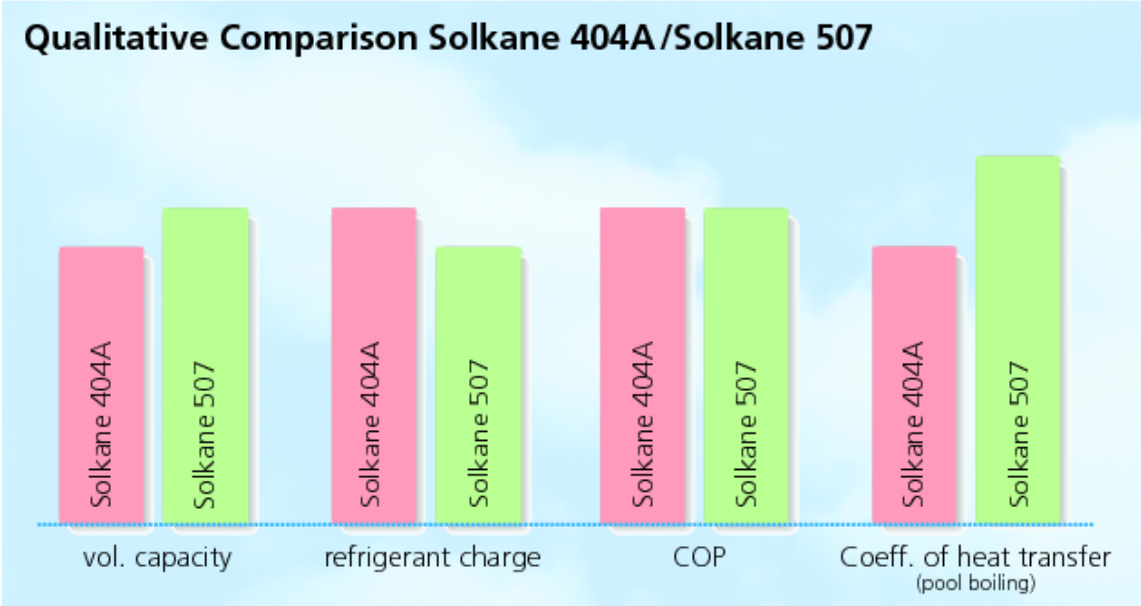

Specifications

Chemical Name		Pentafluoroethane/ 1,1,1-Trifluoroethane/ 1,1,1-Tetrafluoroethane
Chemical Formula		$CHF_2–CF_3/CH_3–CF_3/CF_3–CH_2F$
Molecular Weight	kg/kmol	97.60
Boiling Point at 1.013 bar bubble point/dew point	°C	–46.5/–45.8
Critical Temperature	°C	72.10
Critical Pressure	bar	37.30
Critical Density	kg/m^3	484.5
Critical Volume	m^3/kg	2.064×10^{-3}
Density Liquid[1)]	kg/m^3	1045
Density Saturated Vapour[1)]	kg/m^3	65.36
Heat of Vaporization[1)]	kJ/kg	140.03
Specific Heat Capacity[1)] (Liquid)	kJ/kgK	1.5301
Specific Heat Capacity[2)] (Vapour)	kJ/kgK	0.876

[1)] at 25°C
[2)] at 25°C and 1.013 bar

Table E-1. R404a refrigerant property table.

T	p-f	p-g	v-f	v-g	den-f	den-g	h-f	h-g	hfg	s-f	s-g
°C	bar	bar	dm^3/kg	dm^3/kg	kg/dm^3	kg/m^3	kJ/kg	kJ/kg	kJ/kg	kJ/kgK	kJ/kgK
-60	0.504	0.482	0.745	369.44	1.342	2.707	114.52	333.07	218.55	0.6456	1.671
-59	0.532	0.509	0.746	350.75	1.34	2.851	115.87	333.72	217.85	0.6521	1.6694
-58	0.562	0.538	0.748	333.18	1.337	3.001	117.92	334.38	217.15	0.6585	1.6678
-57	0.593	0.568	0.75	316.67	1.334	3.158	118.58	335.03	216.45	0.6649	1.6663
-56	0.625	0.6	0.751	301.14	1.331	3.321	119.93	335.68	215.75	0.6713	1.6649
-55	0.659	0.633	0.753	286.51	1.329	3.49	121.29	336.34	215.05	0.6777	1.6634
-54	0.694	0.667	0.754	272.74	1.326	3.667	122.65	336.99	214.34	0.684	1.6621
-53	0.731	0.703	0.756	259.75	1.323	3.85	124.01	337.65	213.64	0.6903	1.6607
-52	0.769	0.74	0.757	247.51	1.32	4.04	125.37	338.3	212.93	0.6966	1.6594
-51	0.809	0.779	0.759	235.96	1.317	4.238	126.74	338.96	212.22	0.7028	1.6581
-50	0.851	0.819	0.761	225.06	1.315	4.443	128.11	339.61	211.51	0.709	1.6569
-49	0.894	0.861	0.762	214.76	1.312	4.656	129.48	340.26	210.79	0.7153	1.6556
-48	0.938	0.905	0.764	205.02	1.309	4.877	130.85	340.92	210.07	0.7214	1.6545
-47	0.985	0.95	0.766	195.82	1.306	5.107	132.22	341.57	209.35	0.7276	1.6533
-46	1.033	0.998	0.767	187.11	1.303	5.344	133.6	342.22	208.63	0.7338	1.6522
-45	1.084	1.047	0.769	178.87	1.3	5.591	134.97	342.87	207.9	0.7399	1.6511
-44	1.136	1.098	0.771	171.06	1.297	5.846	136.36	343.53	207.17	0.746	1.6501
-43	1.19	1.151	0.773	163.67	1.294	6.11	137.74	344.18	206.44	0.7521	1.649
-42	1.246	1.206	0.774	156.66	1.291	6.383	139.12	344.83	205.7	0.7581	1.648
-41	1.304	1.263	0.776	150.01	1.288	6.666	140.51	345.47	204.96	0.7642	1.6471
-40	1.364	1.322	0.778	143.69	1.285	6.959	141.9	346.12	204.22	0.7702	1.6461
-39	1.427	1.383	0.78	137.7	1.282	7.262	143.3	346.77	203.47	0.7762	1.6452
-38	1.491	1.446	0.782	132.01	1.279	7.575	144.69	347.42	202.72	0.7822	1.6443
-37	1.558	1.512	0.784	126.61	1.276	7.898	146.09	348.06	201.97	0.7882	1.6435
-36	1.627	1.58	0.785	121.47	1.273	8.233	147.5	348.7	201.21	0.7942	1.6426
-35	1.699	1.65	0.787	116.58	1.27	8.578	148.9	349.35	200.45	0.8002	1.6418
-34	1.773	1.723	0.789	111.93	1.267	8.934	150.31	349.99	199.68	0.8061	1.6411
-33	1.849	1.798	0.791	107.5	1.264	9.303	151.72	350.63	198.91	0.812	1.6403
-32	1.928	1.875	0.793	103.28	1.261	9.682	153.14	351.27	198.14	0.8179	1.6396
-31	2.009	1.955	0.795	99.26	1.258	10.074	154.55	351.91	197.36	0.8238	1.6388
-30	2.093	2.038	0.797	95.43	1.255	10.479	155.99	352.56	196.57	0.8297	1.6382
-29	2.18	2.124	0.799	91.78	1.251	10.896	157.41	353.2	195.79	0.8356	1.6375
-28	2.27	2.212	0.801	88.29	1.248	11.326	158.84	353.83	194.99	0.8415	1.6369
-27	2.362	2.303	0.803	84.97	1.245	11.769	160.26	354.46	194.2	0.8473	1.6362
-26	2.457	2.397	0.805	81.79	1.242	12.226	161.7	355.09	193.39	0.8531	1.6356
-25	2.555	2.493	0.807	78.76	1.239	12.696	163.13	355.72	192.59	0.8589	1.635

Table E-1. Continued

T	p-f	p-g	v-f	v-g	den-f	den-g	h-f	h-g	hfg	s-f	s-g
°C	bar	bar	dm^3/kg	dm^3/kg	kg/dm^3	kg/m^3	kJ/kg	kJ/kg	kJ/kg	kJ/kgK	kJ/kgK
-24	2.656	2.593	0.809	75.87	1.235	13.181	164.57	356.34	191.77	0.8647	1.6344
-23	2.76	2.696	0.812	73.1	1.232	13.681	166.01	356.97	190.96	0.8705	1.6339
-22	2.867	2.801	0.814	70.45	1.229	14.195	167.45	357.59	190.13	0.8763	1.6333
-21	2.978	2.91	0.816	67.92	1.225	14.724	168.9	358.21	189.31	0.882	1.6328
-20	3.091	3.022	0.818	65.49	1.222	15.269	170.35	358.82	188.47	0.8877	1.6323
-19	3.208	3.138	0.82	63.17	1.219	15.83	171.8	359.44	187.64	0.8935	1.6318
-18	3.328	3.256	0.823	60.95	1.215	16.407	173.26	360.05	186.79	0.8992	1.6313
-17	3.452	3.378	0.825	58.82	1.212	17.001	174.72	360.66	185.94	0.9049	1.6308
-16	3.578	3.504	0.827	56.78	1.209	17.612	176.18	361.27	185.09	0.9106	1.6304
-15	3.709	3.633	0.83	54.83	1.205	18.24	177.65	361.88	184.23	0.9163	1.6299
-14	3.843	3.765	0.832	52.95	1.202	18.886	179.12	362.48	183.36	0.9219	1.6295
-13	3.98	3.901	0.834	51.15	1.198	19.55	180.59	363.08	182.49	0.9276	1.6291
-12	4.122	4.041	0.837	49.42	1.195	20.233	182.06	363.67	181.61	0.9332	1.6286
-11	4.267	4.185	0.839	47.77	1.191	20.935	183.54	364.27	180.73	0.9388	1.6283
-10	4.416	4.332	0.842	46.18	1.188	21.656	185.02	364.86	179.84	0.9445	1.6279
-9	4.568	4.483	0.844	44.65	1.184	22.398	186.5	365.45	178.94	0.9501	1.6275
-8	4.725	4.639	0.847	43.18	1.181	23.159	187.99	366.03	178.04	0.9557	1.6271
-7	4.885	4.798	0.85	41.77	1.177	23.942	189.48	366.61	177.13	0.9612	1.6268
-6	5.05	4.961	0.852	40.41	1.173	24.746	190.97	367.19	176.21	0.9668	1.6264
-5	5.219	5.128	0.855	39.1	1.17	25.573	192.47	367.76	175.29	0.9724	1.6261
-4	5.392	5.3	0.858	37.85	1.166	26.421	193.97	368.33	174.36	0.9779	1.6257
-3	5.569	5.476	0.86	36.64	1.162	27.293	195.47	368.9	173.43	0.9835	1.6254
-2	5.751	5.656	0.863	35.48	1.159	28.188	196.98	369.46	172.48	0.989	1.6251
-1	5.937	5.84	0.866	34.36	1.155	29.108	198.49	370.02	171.53	0.9945	1.6248
0	6.127	6.029	0.869	33.28	1.151	30.052	200	370.58	170.58	1	1.6245
1	6.322	6.223	0.872	32.24	1.147	31.022	201.52	371.13	169.61	1.0055	1.6242
2	6.522	6.421	0.875	31.23	1.144	32.017	203.03	371.67	168.64	1.011	1.6239
3	6.726	6.623	0.877	30.27	1.14	33.04	204.56	372.21	167.66	1.0165	1.6236
4	6.935	6.831	0.88	29.33	1.136	34.089	206.08	372.75	166.67	1.0219	1.6233
5	7.149	7.043	0.884	28.44	1.132	35.167	207.61	373.28	165.67	1.0274	1.623
6	7.367	7.26	0.887	27.57	1.128	36.274	209.14	373.81	164.67	1.0328	1.6227
7	7.591	7.483	0.89	26.73	1.124	37.411	210.68	374.33	163.65	1.0382	1.6224
8	7.82	7.71	0.893	25.92	1.12	38.577	212.22	374.85	162.63	1.0437	1.6221
9	8.053	7.942	0.896	25.14	1.116	39.776	213.76	375.36	161.6	1.0491	1.6218
10	8.292	8.179	0.9	24.39	1.112	41.006	215.31	375.87	160.56	1.0545	1.6216
11	8.536	8.422	0.903	23.66	1.108	42.269	216.86	376.37	159.51	1.0599	1.6213
12	8.785	8.67	0.906	22.95	1.103	43.566	218.41	376.87	158.45	1.0653	1.621
13	9.04	8.923	0.91	22.27	1.099	44.898	219.97	377.36	157.39	1.0707	1.6207
14	9.3	9.182	0.913	21.61	1.095	46.267	221.53	377.84	156.31	1.0761	1.6204
15	9.566	9.447	0.917	20.98	1.091	47.672	223.1	378.32	155.22	1.0814	1.6201

Table E-1. Continued

T	p-f	p-g	v-f	v-g	den-f	den-g	h-f	h-g	hfg	s-f	s-g
°C	bar	bar	dm^3/kg	dm^3/kg	kg/dm^3	kg/m^3	kJ/kg	kJ/kg	kJ/kg	kJ/kgK	kJ/kgK
16	9.838	9.717	0.921	20.36	1.086	49.115	224.67	378.79	154.12	1.0868	1.6198
17	10.115	9.992	0.924	19.76	1.082	50.598	226.24	379.25	153.01	1.0921	1.6195
18	10.397	10.274	0.928	19.19	1.078	52.121	227.82	379.71	151.89	1.0975	1.6192
19	10.686	10.561	0.932	18.63	1.073	53.686	229.41	380.16	150.75	1.1028	1.6188
20	10.981	10.855	0.936	18.09	1.069	55.294	230.99	380.6	149.61	1.1082	1.6185
21	11.281	11.154	0.94	17.56	1.064	56.946	232.59	381.03	148.45	1.1135	1.6182
22	11.588	11.46	0.944	17.05	1.059	58.645	234.18	381.46	147.28	1.1188	1.6178
23	11.901	11.771	0.948	16.56	1.055	60.391	235.79	381.88	146.09	1.1242	1.6175
24	12.22	12.089	0.952	16.08	1.05	62.186	237.39	382.29	144.9	1.1295	1.6171
25	12.546	12.414	0.957	15.62	1.045	64.033	239.01	382.69	143.68	1.1348	1.6167
26	12.877	12.745	0.961	15.17	1.04	65.932	240.63	383.08	142.46	1.1401	1.6163
27	13.216	13.082	0.966	14.73	1.036	67.885	242.25	383.47	141.21	1.1455	1.6159
28	13.561	13.426	0.97	14.31	1.031	69.895	243.89	383.84	139.95	1.1508	1.6155
29	13.913	13.777	0.975	13.9	1.026	71.964	245.52	384.2	138.68	1.1561	1.6151
30	14.272	14.135	0.98	13.5	1.02	74.094	247.17	384.56	137.39	1.1614	1.6146
31	14.637	14.5	0.985	13.11	1.015	76.288	248.82	384.9	136.08	1.1668	1.6142
32	15.01	14.871	0.99	12.73	1.01	78.547	250.48	385.23	134.75	1.1721	1.6137
33	15.389	15.25	0.995	12.36	1.005	80.876	252.15	385.55	133.4	1.1774	1.6132
34	15.776	15.636	1.001	12.01	0.999	83.276	253.83	385.85	132.03	1.1828	1.6126
35	16.17	16.03	1.006	11.66	0.994	85.75	255.51	386.15	130.64	1.1881	1.6121
36	16.572	16.431	1.012	11.32	0.988	88.303	257.2	386.43	129.23	1.1935	1.6115
37	16.981	16.839	1.018	11	0.982	90.937	258.91	386.7	127.79	1.1988	1.6109
38	17.398	17.256	1.024	10.68	0.977	93.657	260.62	386.95	126.33	1.2042	1.6102
39	17.822	17.68	1.03	10.37	0.971	96.466	262.35	387.19	124.84	1.2096	1.6096
40	18.255	18.112	1.037	10.06	0.965	99.369	264.08	387.41	123.33	1.215	1.6089
41	18.695	18.552	1.043	9.77	0.958	102.371	265.83	387.61	121.78	1.2205	1.6081
42	19.143	19	1.05	9.48	0.952	105.477	267.59	387.8	120.21	1.2259	1.6073
43	19.6	19.457	1.057	9.2	0.946	108.692	269.36	387.97	118.6	1.2314	1.6065
44	20.065	19.922	1.065	8.93	0.939	112.023	271.15	388.12	116.96	1.2369	1.6057
45	20.538	20.395	1.073	8.66	0.932	115.476	272.96	388.25	115.29	1.2424	1.6048
46	21.02	20.877	1.081	8.4	0.925	119.058	274.78	388.35	113.57	1.2479	1.6038
47	21.511	21.368	1.089	8.14	0.918	122.778	276.62	388.44	111.81	1.2535	1.6028
48	22.01	21.868	1.098	7.9	0.911	126.644	278.48	388.5	110.01	1.2592	1.6017
49	22.518	22.377	1.107	7.65	0.903	130.666	280.36	388.53	108.17	1.2648	1.6006
50	23.036	22.896	1.117	7.42	0.895	134.855	282.27	388.54	106.27	1.2706	1.5994
51	23.563	23.423	1.127	7.18	0.887	139.223	284.19	388.51	104.32	1.2763	1.5982
52	24.099	23.96	1.138	6.95	0.879	143.783	286.15	388.46	102.31	1.2822	1.5968
53	24.645	24.507	1.15	6.73	0.87	148.551	288.13	388.37	100.23	1.2881	1.5954
54	25.2	25.064	1.162	6.51	0.861	153.545	290.15	388.24	98.09	1.294	1.5939
55	25.765	25.631	1.175	6.3	0.851	158.784	292.21	388.07	95.87	1.3001	1.5923

Table E-1. Continued

T	p-f	p-g	v-f	v-g	den-f	den-g	h-f	h-g	hfg	s-f	s-g
°C	bar	bar	dm^3/kg	dm^3/kg	kg/dm^3	kg/m^3	kJ/kg	kJ/kg	kJ/kg	kJ/kgK	kJ/kgK
56	26.341	26.208	1.189	6.09	0.841	164.29	294.3	387.86	93.56	1.3063	1.5905
57	26.926	26.795	1.204	5.88	0.831	170.092	296.44	387.6	91.16	1.3126	1.5887
58	27.522	27.393	1.22	5.67	0.819	176.219	298.64	387.29	88.66	1.319	1.5867
59	28.128	28.001	1.238	5.47	0.808	182.709	300.89	386.92	86.03	1.3255	1.5846
60	28.745	28.62	1.258	5.27	0.795	189.606	303.21	386.49	83.28	1.3323	1.5822
61	29.373	29.251	1.28	5.08	0.781	196.965	305.61	385.98	80.37	1.3392	1.5797
62	30.012	29.893	1.304	4.88	0.767	204.853	308.11	385.38	77.27	1.3464	1.577
63	30.662	30.546	1.332	4.69	0.751	213.356	310.72	384.69	73.97	1.354	1.574
64	31.324	31.211	1.364	4.49	0.733	222.586	313.48	383.88	70.4	1.3619	1.5707
65	31.997	31.888	1.401	4.3	0.714	232.692	316.42	382.93	66.51	1.3703	1.567

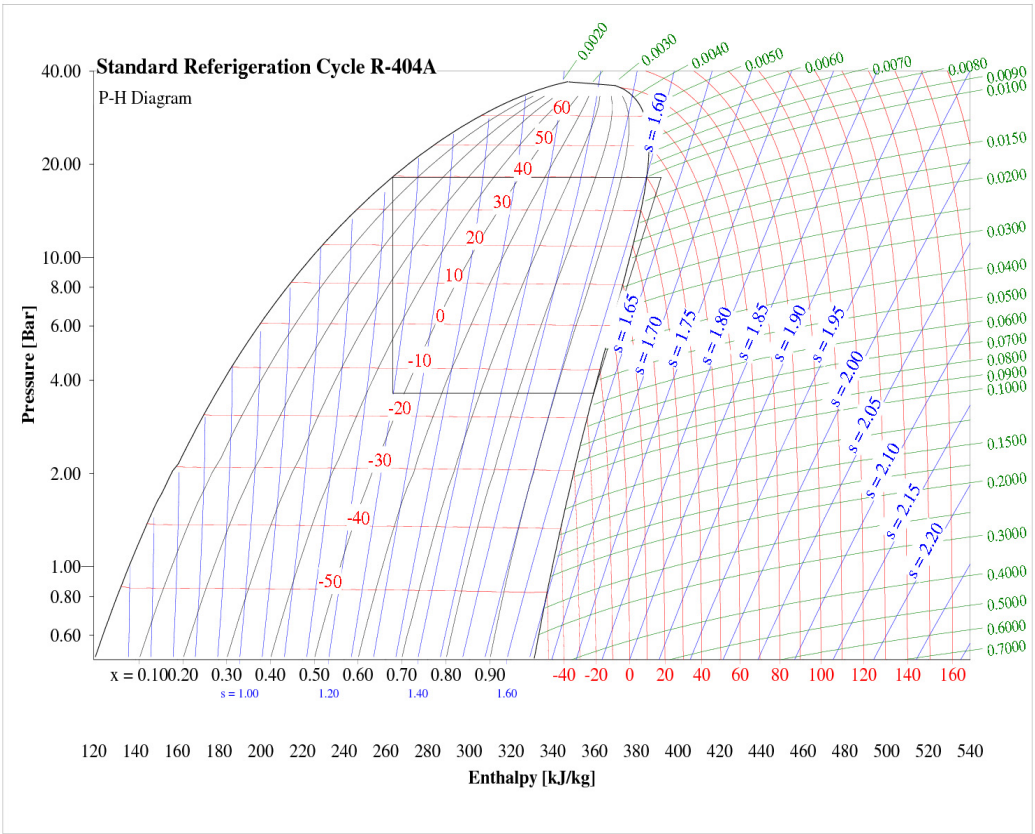
Standard Referigeration Cycle R-404A
P-H Diagram
Pressure [Bar]
Enthalpy [kJ/kg]
40.00
20.00
10.00
8.00
6.00
4.00
2.00
1.00
0.80
0.60
x = 0.10 0.20 0.30 0.40 0.50 0.60 0.70 0.80 0.90
s = 1.00 1.20 1.40 1.60
-40 -20 0 20 40 60 80 100 120 140 160
120 140 160 180 200 220 240 260 280 300 320 340 360 380 400 420 440 460 480 500 520 540
60
50
40
30
20
10
0
-10
-20
-30
-40
-50
0.0020
0.0030
0.0040
0.0050
0.0060
0.0070
0.0080
0.0090
0.0100
0.0150
0.0200
0.0300
0.0400
0.0500
0.0600
0.0700
0.0800
0.0900
0.1000
0.1500
0.2000
0.3000
0.4000
0.5000
0.6000
0.7000
s = 1.60
s = 1.65
s = 1.70
s = 1.75
s = 1.80
s = 1.85
s = 1.90
s = 1.95
s = 2.00
s = 2.05
s = 2.10
s = 2.15
s = 2.20

VITA

Akhilesh Pandey was born in Indore, India, the son of Kiran and Suresh Pandey. After completing schooling from Emerald Heights International, Indore, he went to Mahatma Gandhi University in India where he received his Bachelor of Technology degree in Food Science and Technology in August 2005. In December 2009 he completed his Master of Science program in Food Engineering at Texas A&M University.

His permanent address is:

Akhilesh Pandey

Department of Biological and Agricultural Engineering

2117 TAMU, 201 Scoates Hall, Texas A&M University

College Station, Texas 77843-2117